Advancing therapeutic and preventive strategies for combating coronaviruses: Small molecule antiviral drug discovery and development of methods to identify substandard/falsified vaccines

Yohan Arman

University of Oxford

Department of Biochemistry

St. Hugh's College

Submitted in partial fulfilment of the requirements for the degree of Doctor of Philosophy

Trinity Term 2025

Advancing therapeutic and preventive strategies for combating coronaviruses: Small molecule antiviral drug discovery and development of methods to identify substandard/falsified vaccines

Yohan Arman

Supervisors:

Prof. Nicole Zitzmann

Dr. Annette von Delft

Word count: 42,414 words

Abstract

An integrated approach combining both preventive and therapeutic strategies is essential for combating viral infections, including diseases caused by coronaviruses. The discovery of potent and specific antiviral drugs can significantly complement COVID-19 vaccine efforts but novel approaches are also needed to strengthen and safeguard both strategies. These include the development of small molecule inhibitors and innovative methods to detect substandard/falsified (SF) vaccines.

Currently, there is a shortage of potent oral antiviral drugs against SARS-CoV-2. Drug discovery efforts described in this study have led to the identification of three novel directly acting antivirals targeting the viral main protease, all showing strong inhibition of SARS-CoV-2 replication. In addition, the host-targeting antiviral iminosugar MON-DNJ demonstrated broad-spectrum activity against both SARS-CoV-2 variants and human coronavirus OC43.

To address the threat of SF vaccines, new analytical methods have been developed to assist key shareholders in the future, including national regulatory authorities. Mass spectrometry (MS)-based techniques successfully distinguish genuine vaccines from counterfeit versions by analysing excipients. Furthermore, MALDI-ToF MS analysis of vaccine vial labels offers a non-invasive means of verifying authenticity. Simple low-cost assays also prove effective for detecting ethylene glycol and diethylene glycol contamination in raw materials and medicinal syrups, as well as for assessing heat-induced degradation in sucrose-containing vaccines via glucose detection.

Together, the advances in antiviral drug discovery and SF vaccine detection presented in this thesis provide critical tools to reinforce both therapeutic and preventive responses

against corona- and other viruses. Their implementation could strengthen pandemic preparedness and improve future public health resilience.

Keywords: antiviral, drug discovery, coronavirus, COVID-19, SARS-CoV-2, vaccine, substandard/falsified, supply chain, MALDI-ToF, mass spectrometry

Abstract word count: 250 words

Statement of Contributions

The completion of this thesis involved research that would not have been possible without collaboration. I certify that the work detailed here is my own unless explicitly stated below.

My two supervisors, Prof. Nicole Zitzmann and Dr. Annette von Delft, discussed various aspects of this work with me throughout my DPhil study. My thesis committee, Profs. Peter Simmonds and James S.O. McCullagh provided advice and input for my study progress.

Chapter 2: Michelle L. Hill and Juliane Brun developed and helped with the antiviral screening assay. Michelle L. Hill supervised and helped with the CL-3 work in the Peter Medawar Building. Lizbe Koekemoer helped with Moonshot antiviral compound sample preparation.

Chapter 3: Michelle L. Hill helped with testing MON-DNJ as a SARS-CoV-2 antiviral, including work done in CL-3. Matteo N. Barbaglia helped with the exploration of MON-DNJ antiviral activity and its mechanistic action against HCoV 229E. Snezana Vasiljevic advised on iminosugar activity in the calnexin cycle.

Chapter 4: I acknowledge the help from Rebecca Clarke, Tehmina Bharucha, Laura Gomez Fernandez, and Bevin Gangadharan in the development of MALDI-ToF mass spectrometry and multivariate analysis to detect substandard/falsified vaccines. The laboratory work presented in my thesis was performed jointly with Rebecca Clarke and

Laura Gomez Fernandez. I acknowledge the help from the rest of the Vaccine Identity Evaluation (VIE) team: Paul N. Newton, Céline Caillet, Pavel Matousek, James McCullagh, John Walsby-Tickle, Isabelle Legge, Michael Deats, Sara Mosca, Qianqi Lin, Sneha Banerjee, Susanna Dunachie, Hamid A. Merchant, and Robert Stokes. Fay Probert and Anshul Thakur helped with the machine learning analysis of the study. The support from the World Health Organization staff, Rutendo Kuwana, Alexandrine Maes, Pernette Bourdillon Esteve, and Anita Sands, was acknowledged.

Chapter 5: Tim James and Jennifer Brook at the Biochemistry Department, John Radcliffe Hospital, University of Oxford, helped with the vaccine analysis using an automated urine analyser. Andrea Magri, Matteo N. Barbaglia, and Lawrence Petherbridge from the Clinical BioManufacturing Facility, University of Oxford, helped perform the vaccine potency assay.

Chapter 6: Isabelle Legge from the Department of Chemistry, University of Oxford helped prepare the DEG- and EG-containing propylene glycol and syrup samples.

Acknowledgements

My greatest appreciation goes to my supervisors, Nicole Zitzmann and Annette von Delft, for their immense mentorship provided with endless care and support, making the completion of my study possible. Nicole is always ready for a consultation with her open-door policy, for matters related to science, administration, and most importantly, personal well-being. The weekly DPhil meeting keeps me motivated to expand my knowledge and broaden my point of view. Annette supported me with optimism and support, as well as pushed me to think out of the box. I am grateful for Annette's straightforward and critical input while preparing my thesis and manuscripts. I also want to thank my thesis committee members, Peter Simmonds and James S.O. McCullagh, for their guidance, advice, and encouragement during the completion of each milestone of my DPhil study endeavour.

Members of the Zitzmann group provided a family atmosphere that made my whole study life enjoyable. I would like to express my gratitude to Bevin Gangadharan, Snezana Vasiljević, Matteo N. Barbaglia, Konstantina (Dina) Foteinou, and Priyadarshini Chatterjee. My special thanks to Bevin, Snez, and Dina, who are always ready to share their thoughts and help solve problems in science, as well as personal matters. My gratitude is extended also to former members of the Zitzmann group, Michelle L. Hill, Juliane Brun, Fergus Bremner, Tehmina Bharucha, Laura Gomez Fernandez, Anu V. Chandran, and Mario Hensen. The kind and generous attention from the former Director of the Oxford Glycobiology Institute, Raymond A. Dwek, is highly appreciated.

This study would not be possible without the help of many people supporting me from the background. I would like to thank the staff of the Department of Biochemistry, especially the amazing support and help from the Graduate Study Office, Matthew

Whitby and Dawn Gibbons. The kind support and help from the staff of the KAVLI Institute for Nanotechnology are greatly acknowledged. I am also grateful to the staff of St. Hugh's College, the College Office, the Accommodation team, and the Bursary team, especially the Dining Hall staff who take care of me as their family member.

I am greatly helped by colleagues and mentors from the Vaccine Identity Evaluation (VIE) collaboration. My gratitude to Paul N. Newton, Céline Caillet, Pavel Matousek, James S.O. McCullagh, Susanna Dunachie, Hamid A. Merchant, Rebecca Clarke, Isabelle Legge, John Walsby-Tickle, Michael Deats, Sara Mosca, Qianqi Lin, Sneha Banerjee, Robert Stokes, Fay Probert, Anshul Thakur, David Clifton, Cathrin Hauk, Gesa Gnegel, Kerlijn Van Assche, and Julia Gabel. I would also like to thank the World Health Organization (WHO) team, Rutendo Kuwana, Alexandrine Maes, and Anita Sands, for their support through VIE.

This research would not have been possible without generous funding for my study. My DPhil study was funded by the Indonesian Education Scholarship (Beasiswa Pendidikan Indonesia) from the Ministry of Higher Education, Science and Technology of the Republic of Indonesia (Kemendiktisaintek) within a funding scheme from Indonesia Endowment Fund for Education (LPDP). The laboratory work of my study was supported by the Oxford Glycobiology Endowment. The VIE project was funded by two anonymous philanthropic families and the Oak Foundation via the University of Oxford, the WHO, and the Bill & Melinda Gates Foundation.

My love and gratitude to my beloved family, to my wife Maria Jovita Dauna, my daughter Anna Margaret (Maggie) Yohan, my parents, and my extended family. My forever adoration to Jovita, who has always been my "rock", giving strong support and endless love, especially when we as a family needed to be temporarily separated and struggled a lot during my DPhil study. I will not be able to do this without Jovita and Maggie. I also

thank the Fathers and brothers at Grandpont House, the Oxford Oratory, and Griya Semeru Study Center, Indonesia, who gave me loving and untiring spiritual formation while I was studying. My gratitude to the family of Luis Carlos and Mariana Valdes, and all 'Chilenos' in Oxford, for their warmth and friendship. Thank you to the Indonesian Students' Association in Oxford (PPI Oxford) and the Doctoral Epistemic of Indonesia in the United Kingdom (DOCTRINE UK) for their friendship and companionship in an Indonesian family atmosphere. And to others whom I cannot mention one by one and who have helped me during my stay in Oxford.

Deo Omnis Gloria

Oxford, 6 June 2025

Yohan Arman

For Jovita and Maggie

Table of Contents

List of Figures

List of Tables

List of Formulas

List of Appendices

Abbreviations

Abbreviation	Definition
$3Cl^{pro}$	3-chymotrypsin-like protease
ACE2	Angiotensin-converting enzyme 2
APCI	Atmospheric chemical ionisation
API	Active pharmaceutical ingredient
BPOM RI	Badan Pengawas Obat dan Makanan Republik Indonesia
CC_{10}	10% cell cytotoxicity concentration
CC_{50}	Half-maximum cell cytotoxicity concentration
CHCA	α-cyano-4-hydroxycinnamic acid
CI	Chemical ionisation
CMC	Carboxymethylcellulose
CME	Clathrin-mediated endocytosis
CNX	Calnexin
COVID-19	Coronavirus disease 2019
CPE	Cytopathic effect
CPZ	Chlorpromazine
CRT	Calreticulin
CsA	Cyclosporin A
CV	Cross-validation (in multivariate analysis) or column volume (in protein purification)
CypA	Cyclophilin A
DAA	Directly acting antiviral
DEG	Diethylene glycol
DENV	Dengue virus
E	Envelope protein
EBOV	Ebola virus
EC_{50}	Half-maximum effective concentration
EG	Ethylene glycol
EI	Electron ionisation
ELISA	Enzyme-linked immunosorbent assay
ER	Endoplasmic reticulum

ERAD	Endoplasmic reticulum-associated degradation
ERGIC	ER-to-Golgi intermediate compartment
ESI	Electrospray ionisation
EUA	Emergency use authorisation
FDA	Food and Drug Administration
FFU	Focus forming unit
FIASMA	Functional inhibitors of acid sphingomyelinase
FOS	Free ologosaccharide
FTICR	Fourier-transform ion cyclotron resonance
GC	Gas chromatography
GC-MS	Gas chromatography-mass spectrometry
GMP	Good manufacturing practices
HAdV-5	Human Adenovirus type 5
HBV	Hepatitis B virus
HCoV	Human coronavirus
HCV	Hepatitis C virus
HIV	Human immunodeficiency virus
HPLC	High-performance liquid chromatography
HRP	Horseradish peroxidase
HTA	Host-targeting antiviral
IC_{50}	Half-maximum inhibitory concentration
ICP	Inductively coupled plasma ionisation
IFN	Interferon
Ifu/mL	Infectious unit per milliliter
IL	Interleukin
IQR	Interquartile range
JAK	Janus kinase
LMIC	Low- and middle-income country
LOWESS	Locally weighted scatterplot smoothing
M	Membrane protein
m.o.i	Multiplicity of infection
m/z	mass-to-charge ratio
mAb	Monoclonal antibody

MALDI-ToF	Matrix-assisted Laser Desorption Ionisation – Time of Flight
MERS-CoV	Middle East respiratory syndrome coronavirus
M^{pro}	Main protease
MS	Mass spectrometry
N	Nucleocapsid protein
NRA	National Regulatory Authority
NSP	Non-structural protein
ORF	Open reading frame
OTC	Over-the-counter
PBS	Phosphate-buffered saline
PCA	Principal component analysis
PEG	Polyethylene glycol
Pfu/mL	Plaque forming unit per milliliter
PG	Propylene glycol
pIC_{50}	The negative logarithm of IC_{50} in molar concentration
PK	Pharmacokinetic
PL^{pro}	Papain-like protease
PLS-DA	Partial least squares-discriminant analysis
PQN	Probabilistic quotient normalisation
QC	Quality control
RBD	Receptor binding domain
RCT	Randomised controlled trial
RdRp	RNA-dependent RNA polymerase
RFU	Relative fluorescence unit
RNA	Ribonucleic acid
RSD	Relative standard deviation
RT	Room temperature
RT-PCR	Reverse transcription-Polymerase chain reaction
S	Spike protein
SARS-CoV-1	Severe acute respiratory syndrome coronavirus 1
SARS-CoV-2	Severe acute respiratory syndrome coronavirus 2
SF	Substandard/falsified
SNR	Signal to noise ratio

SORS	Spatially-offset Raman spectroscopy
$TCID_{50}$	Half-maximum tissue culture infectious dose
TFA	Trifluoroacetic acid
TIC	Total ion count
TLC	Thin layer chromatography
TMPRSS2	Transmembrane protease, serine 2
TNF-α	Tumour necrosis factor alpha
UGGT	UDP-glucose:glycoprotein glucosyltransferase
v/v	Volume per volume
VIE	Vaccine Identity Evaluation
w/v	Weight per volume
w/w	Weight per weight
WHO	World Health Organization

Publications arising from this thesis

1. Brun J, **Arman BY**, Hill ML, Kiappes JL, Alonzi DS, Makower LL, *et al*. Assessment of repurposed compounds against coronaviruses highlights the antiviral broad-spectrum activity of host-targeting iminosugars and confirms the activity of potent directly acting antivirals. *Antiviral Res*. 2025 Feb 23;237:106123.
2. **Arman BY**, Clarke R, Bharucha T, Fernandez LG, Walsby-Tickle J, Deats M, *et al*. Identifying falsified COVID-19 vaccines by analysing vaccine vial label and excipient profiles using MALDI-ToF mass spectrometry. *npj Vaccines*. 2025 Jan 30;10(1):1–14.
3. Clarke R, Bharucha T, **Arman BY**, Gangadharan B, Gomez Fernandez L, Mosca S, *et al*. Using matrix assisted laser desorption ionisation mass spectrometry combined with machine learning for vaccine authenticity screening. *npj Vaccines*. 2024 Aug 28;9(1):1–14.
4. **Arman BY**, Brun J, Hill ML, Zitzmann N, von Delft A. An Update on SARS-CoV-2 Clinical Trial Results-What We Can Learn for the Next Pandemic. *Int J Mol Sci*. 2023 Dec 26;25(1):354.

1

Advancing therapeutic and preventive strategies to combat coronavirus

Viruses are everywhere around us, and historical viral epidemics and pandemics should have become constant reminders that we need to continue to advance strategies for combating them. Past pandemics revealed multiple factors that influenced their outcomes, including virus detection, diagnostic testing, contact tracing, social distancing, isolation, therapeutics, vaccines, transparent communication, healthcare authorities, and pandemic decision-making (1). Both therapeutic and preventive strategies have been considered amongst the most important aspects of combating viral diseases, including coronavirus disease 2019 (COVID-19) (2). The rapid development of vaccines in response to the COVID-19 pandemic was admirable. However, attempts to develop new therapeutics have not paralleled this success with regard to speed and efficacy, and the pandemic has highlighted the lack of specific antiviral drugs that can prevent an epidemic from turning into a catastrophic pandemic, causing a global emergency (3). Both strategies, vaccination and antiviral drug treatment together, proved to be synergistic in preventing mortality and disease progression in COVID-19 patients, as documented, *e.g.* for molnupiravir and nirmatrelvir/ritonavir and two vaccines,

CoronaVac and COMIRNATY, in Hong Kong (4). This desirable synergistic effect can also be aimed for future pandemics as long as both avenues are available. In addition, antivirals will always still be needed even if vaccines are available as they offer some additional advantages: they can be used to treat new coronavirus variants that existing vaccines may have lost their potency for, cover immunocompromised individuals and those who do not develop a sufficient level of immunity post-vaccination or unvaccinated people with high-risk of exposure, to reduce viral load and the spread of infection (5).

Previous coronavirus epidemics highlighted the need to identify therapeutic drugs that could work against all coronaviruses (6). Early on in the COVID-19 pandemic, potentially repurposable drugs were evaluated against severe acute respiratory syndrome coronavirus 2 (SARS-CoV-2), the causative agent of COVID-19 (7); developments of new specific drugs were initiated at the same time, during which some drugs showed early promise to be developed into therapeutics against coronaviruses (8,9). To date, several drugs have been approved for clinical use or are under emergency use authorisation (EUA), *e.g.* remdesivir (Veklury), nirmatrelvir/ritonavir (Paxlovid), molnupiravir (Lagrevio), and ensitrelvir (Xocova) (10,11).

The rapid development of COVID-19 vaccines was a great success in biomedical research (12), and billions of vaccine doses have been distributed and administered worldwide within the two years (2020-2022) of the pandemic (13). However, supply chains of COVID-19 therapeutics and vaccines, along with those of other medical products, are at risk once these products leave the manufacturers' sites, as there is a lack of appropriate quality assurance systems. Irresponsible and criminal counterfeit activities put the wider world at risk, as evidenced by the global surge of substandard/falsified (SF) vaccines and medical products (14).

In this thesis, the development of methods to advance therapeutic and preventive strategies for combating coronaviruses, amongst other indications, is investigated. To advance the development of a potential broad-spectrum antiviral, I investigated the potency of small molecule antiviral compounds, which is described in Chapters 2 and 3. Chapter 2 focuses on directly acting antivirals (DAAs) while Chapter 3 describes the host-targeting antiviral (HTA) approach. In Chapters 4 and 5, I investigate the development of methods to identify SF vaccines, including COVID-19 vaccines. In Chapter 4, the development of a matrix-assisted laser desorption/ionisation time of flight (MALDI-ToF) mass spectrometry (MS) method and its proposed use for detecting falsified COVID-19 vaccines in near real-life situations is discussed. Chapter 5 describes methods to detect substandard vaccines by detecting the degradation of an excipient in the vaccine formulation due to high-temperature exposure. The developed MALDI-ToF MS method was then adapted to also successfully detect the harmful contaminants ethylene glycol (EG) and diethylene glycol (DEG) in raw materials and medicinal syrups, which is presented in Chapter 6. Chapter 7 summarises the thesis and points out future directions in the fields of preventive and therapeutic pandemic preparedness.

1.1. Coronavirus and human disease

Coronaviruses (family *Coronaviridae*, subfamily *Orthocoronavirinae)* are the cause of respiratory and intestinal infections in animals and humans. The family *Coronaviridae* is divided into four genera. Alphacoronaviruses and betacoronaviruses exclusively infect mammalian species, while gammacoronaviruses and deltacoronaviruses have a wider host range, including avian species (15). Coronaviruses that are important human pathogens have been recorded in history; these include the alphacoronaviruses, Human

Coronavirus (HCoV) 229E and HCoV NL63. Amongst the betacoronaviruses, some viruses cause mild to severe respiratory symptoms, including HCoV OC43, HCoV HKU1, severe acute respiratory syndrome coronavirus 1 (SARS-CoV-1), Middle East respiratory syndrome coronavirus (MERS-CoV), and SARS-CoV-2 (16). In the last two decades, the world has seen the emergence of *Coronaviridae,* causing a significant impact on public health. The pathogenic human coronaviruses are thought to be a spillover of an animal coronavirus (specifically a bat coronavirus) developing into strains capable of human-to-human transmission with rapid spread and continuous evolution in the human population (17). For SARS-CoV-1 in 2002, MERS-CoV in 2012, and SARS-CoV-2 in 2019/2020, the estimated human mortality rates reached 10%, 34.4% and 3.6%, respectively (18). SARS-CoV-2 has caused a global pandemic with more than 777.37 million cases and 7.09 million confirmed deaths (Our World in Data, https://ourworldindata.org/grapher/ cumulative-deaths-and-cases-covid-19, as of 02 February 2025). SARS-CoV-2 is characterised as highly transmissible between humans and causes more asymptomatic cases or cases with undifferentiated mild symptoms than symptomatic ones, generating problems in containing the infection and preventing its spread (19–21). From an evolutionary perspective, new variants of SARS-CoV-2 are continuously emerging, *e.g.* the Omicron variant, which was estimated to be up to 70% more transmissible than the previously circulating virus variants (22,23). In terms of total infection numbers, both SARS-CoV-1 and MERS-CoV infections combined did not reach even 1% of the world's infections caused by SARS-CoV-2 (19).

Coronaviruses are enveloped viruses with a genome of positive-sense single-stranded ribonucleic acid (RNA) molecules (16). The coronavirus genome is unusually large for an RNA genome, ranging from 27.3 to 31.3 kb in length, with a typical order of the gene for the replicase followed by genes encoding structural proteins Spike (S),

Envelope (E), Membrane (M), and Nucleocapsid (N) (24,25). The replicase gene occupies the largest part of the genome and encodes non-structural proteins (NSPs), such as 3-chymotrypsin-like protease $3CL^{pro}$ or main protease (M^{pro}), papain-like protease (PL^{pro}), and RNA-dependent RNA polymerase (RdRp) (25,26).

The typical morphological characteristic of coronaviruses is the fringe on their surface forming a 'spike' formation resembling the solar corona when observed in negative-stained electron microscopy, from which the name coronavirus is derived (16,24). The binding of the S protein to the host cellular receptor angiotensin-converting enzyme 2 (ACE2), together with the action of the cell surface transmembrane protease, serine 2 (TMPRSS2), induces virus-cell membrane fusion, which mediates viral entry that plays a vital role in virus invasion (15) (Figure 1.1).

After virus entry, the release of the viral genome is followed by the immediate translation of viral proteins through two large open reading frames (ORFs), namely ORF1a and ORF1b, generating viral proteins that form the viral replication and transcription complex. The CL^{pro}/M^{pro} and PL^{pro} proteases cleave the virus polypeptide into 16 NSPs. Structural glycoproteins are synthesised in the endoplasmic reticulum (ER) membrane for transit through the ER-to-Golgi intermediate compartment (ERGIC). Newly synthesised genomic RNA is encapsulated and buds into the ERGIC to form a virion. The new virions leave the cell via lysosomes and can infect other susceptible cells (15,27). SARS-CoV-2 infection also activates the acid sphingomyelinase/ceramide system, resulting in the formation of ceramide-enriched membrane domains that serve viral entry and infection by clustering ACE2 (28). Therefore, both the S protein and some NSPs have become the key targets of antiviral drug discovery efforts (29) (Figure 1.1).

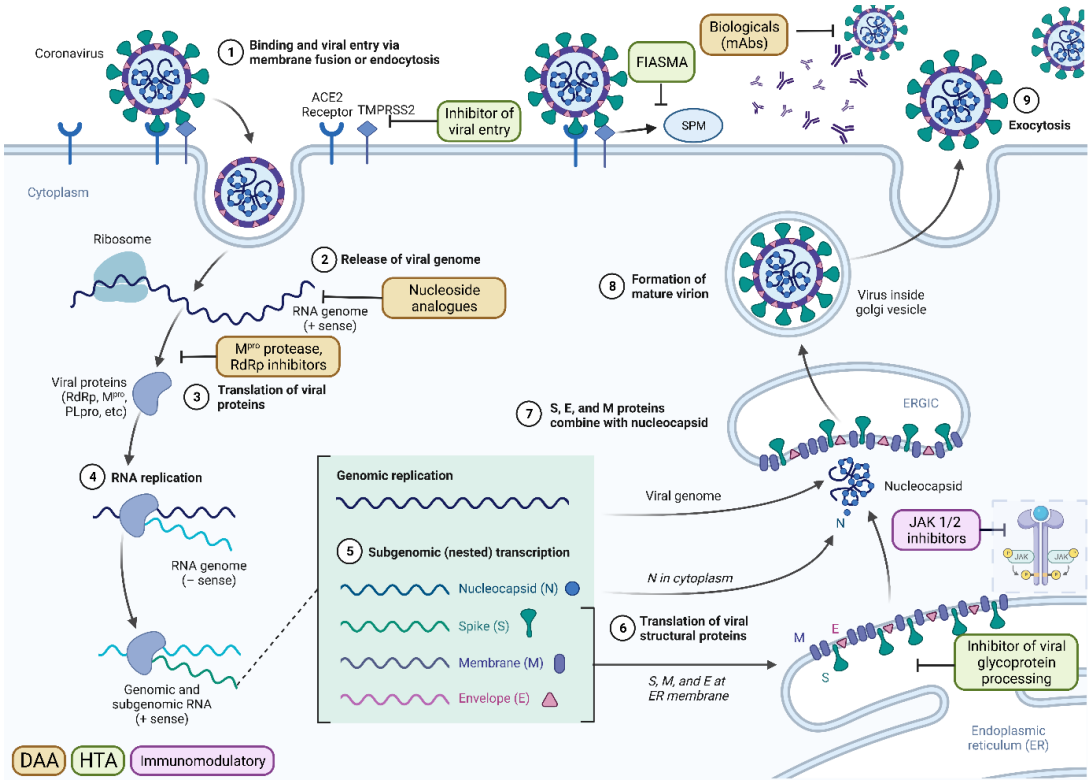

Figure 1.1. Coronavirus life cycle and the mechanistic actions of antiviral drugs within the viral replication process, using SARS-CoV-2 as an example. Directly acting antivirals (DAAs) target viral proteins and include the monoclonal antibody (mAb) biologicals against the Spike (S) protein of the virus, the main protease (M^{pro}) inhibitors, nucleoside analogues, and RNA-dependent RNA polymerase (RdRp) inhibitors. Host-targeting antivirals (HTAs) target human proteins involved in viral replication and include inhibitors of viral entry, functional inhibitors of acid sphingomyelinase activity (FIASMA), and inhibitors of viral glycoprotein processing. Immunomodulatory drugs modify the negative effects of an overreacting immune system, such as the interleukins and JAK 1/2 inhibitors. Image reproduced from Arman BY, *et al*. 2023 (9).

1.2. Antiviral drug discovery against coronavirus

COVID-19 was an unprecedented pandemic where specific therapeutics in the form of antiviral drugs were not available at the outset (3). Initial efforts to search for new drugs against COVID-19 were focused more on the development of repurposed small molecule drugs and monoclonal antibodies (mAbs) to deliver treatments quickly, given the long drug discovery timelines (30). Lessons learned from COVID-19 highlight the need to

develop and stockpile drugs for emerging viruses, and such pandemic preparedness will be vital to better combat pandemic threats of the future (6).

Small molecule antivirals may offer advantages in the fight against COVID-19 as they can offer cross-reactivity against new virus variants and are able to reduce viral load and thereby also the risk of spreading infection. They can also be used by immunocompromised individuals and those who do not develop a sufficient level of immunity post-vaccination or unvaccinated people with high risks of exposure (5). Even when some useful drugs were identified and approved (*e.g.* remdesivir), their availability was often limited by supply constraints, and there was a need to prioritise their use for patients at higher risks of clinical progression (11).

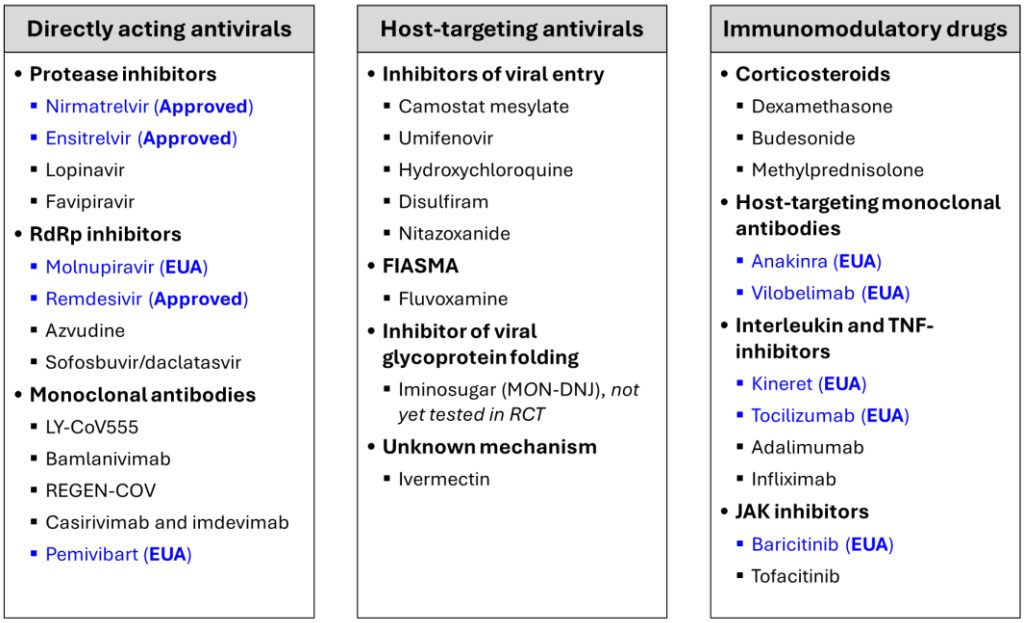

Figure 1.2. Drugs in development or approved against SARS-CoV-2 based on their mechanism of action. Drugs investigated in randomised controlled trials (RCTs) fall into three major categories: directly acting antivirals, host-targeting antivirals, and immunomodulatory drugs. Examples of drugs tested in RCTs at the time of writing this thesis are shown. Drugs granted emergency use authorisation (EUA) and full approval are printed in blue. FIASMA, Functional inhibitors of acid sphingomyelinase activity. Image was modified and updated from Arman BY, *et al*. 2023 (9).

Drugs that were investigated for their potential use against SARS-CoV-2 in *in vitro* studies as well as in COVID-19 randomised controlled trials (RCTs) generally fall into three categories based on their proposed mechanism of action: directly acting antivirals, host-targeting antivirals, and immunomodulatory drugs (Figure 1.2) (9). Among current COVID-19 therapeutics, many are repurposed drugs being evaluated in line with past investigations as SARS-CoV-1 and MERS-CoV therapeutics (7).

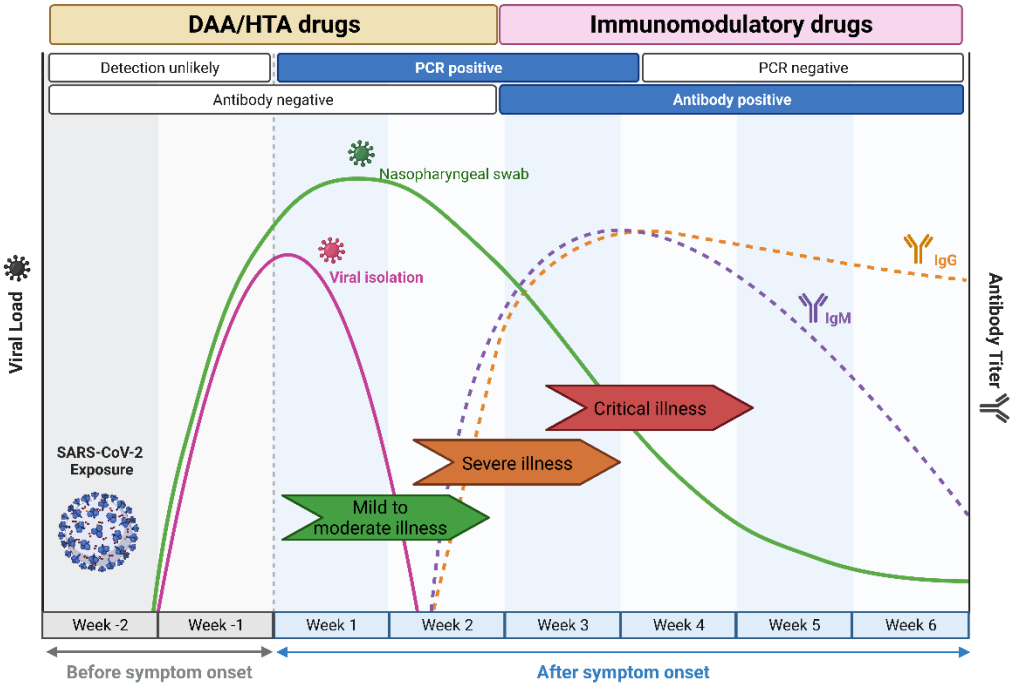

Figure 1.3. COVID-19 disease progression and the windows of opportunity for antiviral drugs. DAAs and HTAs are most effective for an intervention in the earlier stages of disease in mild to moderate cases when the viral load is increasing and detectable by RT-PCR. Immunomodulatory drugs are more potent in later disease phases when the host immune system responds to the infection, and clinical manifestations in severe to critical cases may include a cytokine storm. Image reproduced from Arman BY, *et al*. 2023 (9).

In parallel, industry efforts have come up with new antiviral drugs that are effective against SARS-CoV-2, such as nirmatrelvir/ritonavir and ensitrelvir (31–33). Collaborative open science efforts from people with collective trust, combined with sufficiently

diverse expertise and perspectives that avoided bureaucracy, proved to be effective in rapidly reaching and implementing strategic decisions in coronavirus drug discovery, such as in the COVID Moonshot project (30,34).

With the diverse range of clinical manifestations, from mild to severe disease, accompanied by high mortality caused by the COVID-19 disease progression (35), the window of opportunity for deploying antiviral drugs is crucial, with antivirals being more effective when administered early in the course of the disease (36) (Figure 1.3). Both DAAs and HTAs can potentially be used within the first week of disease symptoms when the viral load is high. In the later stages of the disease, the virus no longer drives the disease. At this point, virus-targeting drugs will be less effective, and immunomodulatory drugs have the potential to control the excessive immune response that can lead to organ damage. Some DAAs and immunomodulatory drugs used against COVID-19 have been listed in the Food and Drug Administration (FDA) list of Drugs and Non-Vaccine Biological Products (Table 1.1).

1.3. Therapeutic approaches

1.3.1. Directly acting antivirals (DAAs)

Directly acting antivirals are expected to efficiently suppress viral replication *in vivo* since these drugs specifically target the virus (57). Hence, they will be most effective if administered early in infection, before or as the virus reaches the peak of its replicative phase, thus preventing the progression to severe disease (58) (Figure 1.3).

Table 1.1. Biologicals and small molecule antiviral drugs granted Food and Drug Administration (FDA) full approval or emergency use authorisation (EUA) for the treatment of COVID-19*.

Drug Name	Approval Status	Drug Description	Mechanism of Action	References
Remdesivir (brand name Veklury)	Full approval	RdRp inhibitor	DAA	(37,38)
Pemivibart (brand name Pemgarda)	EUA	Recombinant human monoclonal IgG1λ antibody against S protein	DAA	(39)
Vilobelimab (brand name Gohibic)	EUA	Recombinant chimeric monoclonal IgG4 antibody that binds to the soluble human complement split product C5a	Immunomodulatory drug	(40,41)
Kineret (brand name Anakinra)	EUA	Interleukin-1 (IL-1) receptor antagonist	Immunomodulatory drug	(42,43)
Molnupiravir (brand name Lagevrio)	EUA	Nucleoside analogue incorporating mutations in the RNA elongation process	DAA, RdRp inhibitor	(44,45)
Nirmatrelvir/ritonavir (brand name Paxlovid)	Full approval	SARS-CoV-2 main protease (M^{pro}) inhibitor	DAA, M^{pro} inhibitor	(46,47)
Baricitinib	Full approval	JAK 1/2 inhibitor	Immunomodulatory drug	(48–51)
Tocilizumab (brand name Actemra)	Full approval	IL-6 inhibitor	Immunomodulatory drug	(52–55)

DAA, directly acting antiviral; JAK, Janus kinases; M^{pro}, main protease; RdRp, RNA-dependent RNA polymerase. *Extracted and expanded from the FDA EUA list for Drugs and Non-Vaccine Biological Products at https://www.fda.gov/drugs/emergency-preparedness-drugs/emergency-use-authorizations-drugs-and-non-vaccine-biological-products (56) and the NIH COVID-19 treatment guidelines (11) (both accessed 3 April 2025).

This small window of opportunity limits the use of DAAs (58). If the viral targets are sufficiently different from any related host cell off-targets, DAAs with limited toxicity could be developed (5). However, a drawback of DAAs is the generation of resistance mutations in the targeted viral proteins that may lead to reduced efficacy (59,60), as observed in many viruses, including herpesviruses, varicella-zoster virus, cytomegalovirus, and hepatitis B virus (HBV) (61).

1.3.2. Host-targeting antivirals (HTAs)

Host-targeting antivirals are drugs that target host cell mechanisms required for viral replication (58). This class of drugs includes small molecule agents that modulate virus-host interactions by inhibiting human proteins used by the virus in its life cycle. HTAs are considered the next frontier of coronavirus drug discovery with the potential for broad-spectrum activity and a smaller likelihood of generating drug resistance. They can be used as a prompt response even before detailed information about a newly emerging virus becomes available (8,59,60,62). However, since HTAs target host proteins, there are also higher risks of unintended off-target effects (63).

1.3.3. Immunomodulatory drugs

Immunomodulatory drugs are a class of drugs used to modify the negative effects of overreacting immune systems that target the inflammatory reaction happening in patients and the potential cytokine storm in some severe cases (64). Recent investigations focused on agents commonly used in inflammatory conditions, including corticosteroids, hydroxychloroquinone, inhibitors of Interleukin (IL)-1 and IL-6, Tumor Necrosis Factor-alpha (TNF-α) inhibitors, Janus kinases (JAK) inhibitors, and mAbs (with

named examples shown in Figure 1.2) (65,66). To date, emerging data show the protective effect of immunomodulatory drugs in reducing COVID-19 features and the improvement of patient recovery (64,67).

1.4. Safeguarding vaccines and medical products from substandard and falsified conditions

The rapid development of vaccines against COVID-19 was a remarkable success in biomedical research marked by the supply, distribution, and administration of billions of vaccine doses worldwide (13). However, inequitable global distribution of COVID-19 vaccines has been associated with increasing concerns about the occurrence and impact of SF vaccines (14,68,69). According to the World Health Organization (WHO), approximately 10.5% of all medical products distributed in low- and middle-income countries (LMICs) are either substandard or falsified (70,71). This estimate is deeply concerning and suggests a significant but neglected risk, potentially leading to higher rates of illness and death, as well as eroding public trust in healthcare systems and causing economic harm (72).

Substandard or 'out of specification' medical products are products that have already been authorised for marketing yet fail to meet either their quality standards or specifications, or both (71). For example, if the vaccine cold chain is not maintained in the supply chain, this is likely to result in a poor-quality substandard vaccine. In contrast, falsified products refer to products that deliberately or fraudulently misrepresent their identity, composition, or source (71).

SF medical products pose a significant threat to health as they are of poor quality, unsafe and/or ineffective (73). Moreover, the scale of the problem is often

underestimated due to the lack of monitoring and intervention systems (14). In the public domain, between 12th March 2020 and 31st March 2022, there have been 184 incident reports of diverted and SF COVID-19 vaccines from 48 countries, and most cases of vaccine falsification have been in LMICs (74).

To date, there are no devices or protocols for the National Regulatory Authority (NRA) inspectors to screen for SF vaccines in supply chains. This highlights the failure to meet the critical role of NRAs to prevent, detect and remove SF medical products (75). The monitoring of SF medical products should also be an intrinsic part of disease surveillance programs (76).

There is a dire need for innovative, accurate, affordable, rapid and user-friendly screening devices that can be effectively implemented to rapidly detect SF vaccines at different levels of supply chains (77). For effective application, devices are needed to cover all levels of the supply chain. Of note, a single device will not ever be able to cover all required levels. The developed devices must be adapted to the circumstances encountered and must be accurate, affordable and effective for those levels (78). The developed tools will empower inspectors, regulators and vaccine manufacturers as the key end users and could be integrated into the national regulatory standards and WHO's Prevent, Detect, and Respond strategy (14).

During the early phase of the COVID-19 pandemic, a consortium of scientists assembled to perform urgent research to develop tools for detecting SF vaccines. The Vaccine Identity Evaluation (VIE) team includes virologists, biochemists, chemists, physicists, pharmacists and clinicians from the Nuffield Department of Medicine, the Biochemistry Department and the Chemistry Department of the University of Oxford, the Rutherford-Appleton Laboratory of UK Research and Innovation (UKRI), the University of

East London, and Agilent Technologies. The VIE team is actively collaborating with the WHO, NRAs, vaccine manufacturers, and other stakeholders.

During the course of my thesis work, the VIE team extended its scope to also include method development for the detection of harmful and potentially lethal DEG and EG contamination in medical products. These alcohols have mostly and tragically been found in children's medicinal syrups, and in 2022, more than 300 children died due to syrups contaminated with DEG and/or EG (79,80). Contamination may result from either the substitution or adulteration of the ingredients during the pharmaceutical manufacturing process, a failure to adhere to manufacturing quality control (QC) procedures (81,82), or both. The ingestion of toxic alcohols DEG and EG can cause severe metabolic acidosis, acute renal failure, and death (83). Both DEG and EG are legitimately used in industrial production of, *e.g.* brake fluid, antifreeze and glues, and most intoxications result from accidental oral ingestion of products containing these alcohols, or in sporadic cases from suicide attempts (81).

1.5. Multi-pronged efforts to tackle coronavirus disease

From the recent COVID-19 pandemic, we learned that a comprehensive, multipronged approach is needed to combat coronaviruses (1). Both therapeutic and preventive measures are crucial and need to be supported by continuous research for pandemic preparedness. Accelerated drug discovery efforts during the pandemic yielded multiple novel DAAs with clinical efficacy, including small molecule inhibitors and mAbs (Figure 1.2 and Table 1.1) (9). To prepare for future pandemics, this needs to be supported by a large-scale investment, developing an arsenal of broad-spectrum antivirals beyond

coronaviruses and building worldwide clinical trial networks that can be rapidly utilised. In addition, more research is needed to generate vaccines with long-term and broad immunity profiles (1), with sufficient and equal worldwide distribution and effective safeguarding measures to prevent the surge of SF vaccines. The open and consistent QC measures would improve the trust in vaccination strategies.

1.6. Study aims

The aims of this study are twofold: 1) To evaluate existing and novel directly acting and host-targeting antivirals for their broad-spectrum activity against multiple coronaviruses, and 2) To develop new tools for safeguarding vaccines and medicinal syrups, in the face of increased risks from substandard and falsified products.

Publication arising from this chapter

The substance of this chapter has now been published in the following paper:

Arman BY, Brun J, Hill ML, Zitzmann N, von Delft A. An Update on SARS-CoV-2 Clinical Trial Results-What We Can Learn for the Next Pandemic. *Int J Mol Sci*. 2023 Dec 26;25(1):354.

2

Cellular screening of small molecule main protease (M^{pro}) inhibitors as antiviral drugs against coronavirus

An important lesson learned from the COVID-19 pandemic is the need to develop and stockpile specific antiviral drugs to prevent an epidemic from becoming a global emergency (3). Despite the theory that drug repurposing makes existing drugs with antiviral effects rapidly available, recent RCTs revealed that repurposed drugs failed to reach the expected clinical benefits (9). For COVID-19, novel drug development yielded promising DAAs that are now approved for use against SARS-CoV-2 or authorised for emergency use (described in Chapter 1).

This chapter describes my involvement in research to discover novel DAA drugs against coronaviruses. Using cell-based antiviral assays, small molecule antivirals targeting the M^{pro} were screened to identify drug candidates with antiviral properties against SARS-CoV-2 and other human coronaviruses. I joined the Zitzmann group whilst cellular screening of SARS-CoV-2 antiviral compounds was ongoing. The compounds screened include those developed by the COVID Moonshot consortium, a global multi-disciplinary collaboration aiming to develop SARS-CoV-2 protease inhibitors that are potent and specific against SARS-CoV-2. I also modified the focus forming unit (FFU)

assay, initially developed for SARS-CoV-2, for use in HCoVs. Together, this work may aid the discovery of potent antiviral drugs against coronaviruses.

2.1. Introduction

Early on during the COVID-19 pandemic, repurposed drugs were evaluated against SARS-CoV-2 (7). Although initial promising results were obtained (8), RCTs revealed that repurposed drugs failed to reach clinical benefits (9,84,85) or were likely linked to insufficient exposure at the approved concentration (86). Many compounds progressed to clinical trials based only on their *in vitro* efficacy without modelling and addressing pharmacokinetic (PK) and bioavailability profiles (86). This highlights the urgent need for the development of new specific antiviral drugs against coronaviruses, with good PK and bioavailability, and ideally showing activity against a broad range of coronaviruses (pan-coronavirus drugs).

Recent drug development yielded promising DAAs already approved for use against SARS-CoV-2 or authorised for emergency use only (Figure 1.2 and Table 1.1 of Chapter 1). DAA targets virally encoded proteins directly and efficiently suppresses viral replication *in vivo* (8,57,87). This class of drugs includes small molecules and antibodies, and common targets include key enzymes like viral polymerases and proteases, such as the SARS-CoV-2 $3CL^{pro}$, also known as M^{pro}, and PL^{pro}, or viral entry and fusion proteins (8,57). Some DAAs target M^{pro} as the critical enzyme that cleaves SARS-CoV-2 polyproteins and is essential for viral replication (47). The enzyme has an active site that is distinct from known human proteases, and thus inhibitors to M^{pro} are unlikely to have prohibitive toxic side effects in humans. M^{pro} also shares a high degree

of conservation across different coronaviruses and is considered one of the best-characterised viral drug targets (88–91).

2.1.1. Protease inhibitors

The coronavirus replication depends on the role of virus proteases encoded by the virus genome that cleave the translated polypeptide into virus NSPs. Two major conserved enzymes, the CL^{pro}/M^{pro} and PL^{pro}, cleave the virus's polypeptide into 16 NSPs, where M^{pro} alone processes 11 NSPs, making this enzyme one of the major targets for antiviral drug discovery (92) and protease inhibitors are considered excellent drug targets for COVID-19 treatment (87). Compounds classified as M^{pro} inhibitors have been the focus of drug discovery that targets binding to SARS-CoV-2 M^{pro} either covalently or non-covalently (93), and both drug repurposing and novel development strategies have been pursued in M^{pro} inhibitor development.

2.1.2. Repurposed protease inhibitors

Early in the pandemic, many RCTs focused on repurposed drugs, including protease inhibitors with known safety profiles and efficacy against other viruses (84,94). Examples of repurposed drugs with *in vitro* activity against SARS-CoV-2 protease are lopinavir, ritonavir, darunavir, and danoprevir, with the lopinavir/ritonavir combination (brand name Kaletra or Aluvia) as the most investigated (87). Lopinavir was originally developed as a human immunodeficiency virus (HIV) protease inhibitor. It showed potential for the treatment of SARS-CoV-1 with a moderate half-maximum inhibitory concentration (IC_{50})

of 26 µM *in vitro* (95,96). However, lopinavir may still have a beneficial effect in combination with a so-called "PK enhancer". Ritonavir has often been used as a PK enhancer in HIV therapy, based on its potent inhibition of the metabolising enzyme cytochrome P450 3A, increasing the exposure and half-life of the co-dosed compound (95,97,98). The inhibition of cytochrome P450, however, has the negative effect of increasing the risk of drug interaction and side effects, preventing its use in patients with severe renal or hepatic impairment (31,99,100). The use of the lopinavir/ritonavir combination has been assessed in RCTs where a limited efficacy was observed from its use in severe and hospitalised patients with COVID-19 (101–103). Due to this failure to show any clinical benefit, lopinavir/ritonavir is therefore not recommended as COVID-19 standard care for hospitalised patients in the NIH guidelines (11,104,105). A summary of RCT results is presented in Appendix 1, as published in Arman BY, *et. al*. 2023 (9).

Darunavir is another HIV protease inhibitor in clinical use in combination with the PK enhancer cobicistat (106). Darunavir was not active against SARS-CoV-2 *in vitro* at clinically relevant concentrations (107) and, in line with these results, did not show clinical efficacy in COVID-19 RCTs (Appendix 1).

Danoprevir, a hepatitis C virus (HCV) protease (NS3/4A) inhibitor that is used in combination with ritonavir (108), showed cellular activity against SARS-CoV-2 with a half-maximum effective concentration (EC_{50}) of 87 µM in Vero E6 cells (109). In hospitalised patients infected with SARS-CoV-2, danoprevir with ritonavir shows a good safety profile (108) with shorter times to PCR negativity and shorter hospital stays compared to the lopinavir/ritonavir group (110). The efficacy of danoprevir needs to be assessed in further large-scale clinical trials.

Disulfiram, a potent anti-inflammatory agent and hepatic aldehyde dehydrogenase inhibitor, has been repositioned from its use as a drug to treat alcohol

use disorder due to its properties as an inhibitor of viral proteases (111,112). Disulfiram has been reported to inhibit PL^{pro} protease enzymes of MERS-CoV and SARS-CoV-1 *in vitro* and thus inhibit coronavirus infection (113). Disulfiram also targets M^{pro} of SARS-CoV-2, although in a non-specific fashion (114). Disulfiram reduces the incidence and severity of COVID-19 (111) and significantly reduces the risk of COVID-19 symptoms in patients, although it does not significantly reduce the number of Reverse Transcription-Polymerase Chain Reaction (RT-PCR)-confirmed cases (112). Further large-scale clinical trials are needed to assess the findings.

2.1.3. Novel development of protease inhibitors

SARS-CoV-2 M^{pro} has been a drug development target from early on in the pandemic, with numerous novel SARS-CoV-2 inhibitors in the clinical and preclinical pipeline (Appendix 1). Two SARS-CoV-2 MPro inhibitors are now under EUA, including nirmatrelvir/ritonavir (brand name Paxlovid) and ensitrelvir (brand name Xocova) (9).

The M^{pro} inhibitor nirmatrelvir (or PF-07321332) protects from severe COVID-19 and events of patient hospitalisation when given during the first days of symptom onset (47). The orally administered drug inhibits not only SARS-CoV-2 but also SARS-CoV-1 and MERS-CoV and thus has potential as a pan-coronavirus antiviral drug (46,47). Nirmatrelvir in combination with ritonavir (brand name Paxlovid) has been tested in an RCT and reported to reduce the incidence of COVID-19-related hospitalisation or death by day 28 and contribute to the lower viral load on day five of treatment when treatment was initiated within three days of symptoms onset, significantly reducing the risk of severe COVID-19 (46). The drawback of the nirmatrelvir-ritonavir combination is the

possible serious and life-threatening drug interactions from the use of the PK-enhancer ritonavir (31).

The therapeutic drug S-217622 or ensitrelvir was developed by Hokkaido University and Shionogi as an oral noncovalent nonpeptidic M^{pro} inhibitor of SARS-CoV-2 (115,116). Ensitrelvir was reported to overcome the challenges faced by nirmatrelvir-ritonavir with its improved target selectivity, optimised PK profiles, and favourable drug metabolism (115). The compound displays antiviral activity against SARS-CoV-2 variants of concern, including the delta and Omicron variants (117), although the status of these variants has been de-escalated as of 3 Mar 2023. Ensitrelvir has progressed to complete its phase II/III clinical trial, where results disclosed from the phase IIa trial showed a significant reduction in viral titer and viral RNA on day four, the median time of negative RT-PCR conversion of two days, and acceptable adverse events (32). Ensitrelvir received emergency regulatory approval in 2022 and full approval in March 2024 for its use in Japan and Singapore (118). Ensitrelvir has been tested in a phase III trial named SCORPIO-PEP that includes approximately 2,400 participants aged 12 years and older across the United States of America as well as several countries in South America, Africa and Asia (ClinicalTrials.gov ID NCT05897541). Ensitrelvir demonstrated a 67% reduction in the risk of COVID-19, meeting its primary endpoint and key secondary endpoint, in uninfected individuals treated after exposure, compared to placebo at day 10 (119). Other oral protease inhibitor clinical candidates in clinical trials are compound PBI-0451 from Pardes Biosciences and EDP-235 from Enanta Pharmaceuticals (120).

In addition, many academic efforts have explored novel M^{pro} inhibitors as therapeutic agents against SARS-CoV-2. The search for potent M^{pro} inhibitors has brought together academic and industrial partners from across the world in an international effort to combine experimental and computational expertise to further develop antiviral

compounds within the COVID Moonshot project (34,121). In this consortium, more than 2,400 molecules have been synthesised and shared rapidly in an open environment to create a rich, open, and intellectual property-free knowledge base for anti-coronavirus drug discovery (34). The project has now proposed its clinical leads for M^{pro} inhibitor that will be continued in human clinical trials for use as oral small molecule antiviral drugs.

In this Chapter, I describe my work on screening M^{pro} inhibitor compounds generated by the Moonshot collaborative project as potential DAAs against SARS-CoV-2. I also extended the scope of the antiviral activity to other HCoVs OC43 and 229E. I used an *in vitro* cell-based antiviral assay in human lung epithelial Calu-3 and hepatocellular carcinoma HuH-7 cells that represent more physiologically relevant tissues for testing therapeutics for COVID-19, compared to other cell lines used in early drug discovery screens, *e.g.* the monkey kidney epithelial Vero cells (122).

2.2. Materials and Methods

2.2.1. Cell lines and culture

The human lung cancer cell line Calu-3 (ATCC HTB-55) was a gift from Anderson Ryan, Department of Oncology, Medical Science Division, University of Oxford and cultured in a 1:1 mixture of DMEM with GlutaMAX (Gibco) and Ham's F-12 nutrient mix medium (Gibco), supplemented with 100 U/mL penicillin, 100 µg/mL streptomycin (penicillin-streptomycin, Sigma-Aldrich), 10% volume per volume (*v/v*) of heat-inactivated foetal bovine serum (FBS, Gibco), 1× MEM non-essential amino acid (Gibco), and 1 mM sodium pyruvate (Gibco). African green monkey Vero E6 cell line (ATCC CRL-1586) was cultured

in DMEM with GlutaMAX supplemented with penicillin-streptomycin, and 10% *v/v* of FBS.

Vero E6 cells expressing human transmembrane protease, serine 2 (Vero-TMPRSS2) were a gift from William James at Sir William Dunn of Pathology, University of Oxford, and cultured in DMEM-10% FBS supplemented with penicillin-streptomycin and 200 µg/mL of G418 geneticin (Gibco).

Human hepatocellular carcinoma HuH-7 cells (JCRB0403) were a gift from Dr. Narayan Ramamurthy (Peter Medawar Building/Nuffield Department of Medicine) and maintained in DMEM with GlutaMAX supplemented with penicillin-streptomycin, 10% *v/v* of FBS and 1× MEM non-essential amino acid. Cells were grown in standard T75 and T175 flasks (Greiner) in a humidified incubator (Heracell-Heraeus) with 5% CO_2 supplementation, until reaching confluency.

Subculture was performed by decanting the supernatant of confluent flasks and washing the cell monolayer using 1× Dulbecco's Phosphate-buffered saline (D-PBS, Gibco). The monolayer of cells was dislodged from the flask using 1× Trypsin-EDTA solution (Sigma-Aldrich) and incubated at 37°C for approximately two minutes or after initial signs of dislodged cells. Without delay, cells were completely dislodged from the flask by banging the side of the flask. Cells were resuspended in their appropriate culture medium and split in a ratio of 1:6 to 1:10 depending on further use of the cells.

Cells were maintained as mycoplasma-free, with regular testing coordinated by the Zitzmann laboratory. Cells are carefully monitored for any possible bacterial or yeast contamination and infected cells are directly disinfected and discarded, followed by deep cleaning of the incubators.

2.2.2. Virus propagation and stock

Viruses that were used in the study are listed in Table 2.1. SARS-CoV-2 ENG2/20 strain was received from Public Health England, Porton Down, UK. SARS-CoV-2 variants alpha (B.1.1.7), beta (B.1.351), gamma (P.1), delta (B.1.617.2), and Omicron (B.1.1.529), as well as human coronavirus (HCoV) OC43 were gifts from William James (Sir William Dunn School of Pathology, University of Oxford). HCoV 229E was a gift from Narayan Ramamurthy (Peter Medawar Building/Nuffield Department of Medicine).

Virus working stocks were produced by infecting Vero E6 (SARS-CoV-2), Vero-TMPRSS2 (HCoV OC43), or HuH-7 (HCoV 229E) cells at a multiplicity of infection (m.o.i) of 0.01 in a virus propagation medium (DMEM with GlutaMAX supplemented with 2% of FBS) and incubating until a cytopathic effect (CPE) was visible.

Table 2.1. Coronaviruses from different genera used in the study.

No.	Virus	Variant/strain	Genus	Passage (P)[a]	Titer (Pfu/mL)
1.	SARS-CoV-2	ENG2/20 (wild type)	betacoronavirus	P3	2.6×10^6
2.	SARS-CoV-2	Alpha (B.1.1.7)	betacoronavirus	P3	2.0×10^6
3.	SARS-CoV-2	Beta (B.1.351)	betacoronavirus	P3	2.3×10^6
4.	SARS-CoV-2	Gamma (P.1)	betacoronavirus	P3	8.0×10^6
5.	SARS-CoV-2	Delta (B.1.617.2)	betacoronavirus	P3	1.5×10^6
6.	SARS-CoV-2	Omicron (B.1.1.529)	betacoronavirus	P3	1.4×10^6
7.	HCoV	OC43	betacoronavirus	P3	$3.0 \times 10^{6\,b}$
8.	HCoV	229E	alphacoronavirus	P3	$6.1 \times 10^{6\,b}$

[a] Number of virus propagation passages from the original virus stock to generate virus working stocks.

[b] Converted to Pfu/mL by dividing the $TCID_{50}$/mL result with a constant value of 0.69.

The cell supernatant was then centrifuged at 500 × *g* for 5 minutes, aliquoted and stored at -70°C. The titer of SARS-CoV-2 viral stocks was determined by plaque assay. All work involving SARS-CoV-2 and the risk group 3 viruses was performed in the Category Level 3 (CL-3) Laboratory at the Peter Medawar Building, University of Oxford. The titer of HCoV OC43 and 229E virus stocks was determined by the half-maximum tissue culture infectious dose ($TCID_{50}$).

2.2.3. Cell viability assay

Cell viability after treatment with compound was measured using CellTiter 96 AQueous One Solution Cell Proliferation MTA (3-(4,5-dimethylthiazol-2-yl)-5-(3-carboxymethoxy phenyl)-2-(4-sulfophenyl)-2H-15 tetrazolium, inner salt; MTS) Assay (Promega, Madison, WI, USA) according to the manufacturer's instruction (the schematic of the steps is shown in Figure 2.1).

Briefly, Calu-3 cells were seeded into 96 well plates (Nunc, Thermo Scientific) at a cell density of 6 × 10^4 cells/well in the Calu-3 medium. After 48 hours of incubation at 37°C, 5% CO_2, cells were treated with serially diluted compounds in Calu-3 medium, in triplicate, followed by incubation at 37°C, 5% CO_2 for 3 days. Wells with 200 µL of growth medium with and without cells were included as controls, in triplicate. After the incubation, 100 µL of growth medium was removed and 20 µL of MTA reagent was added to the remaining medium in each well. The half-maximum cell cytotoxicity concentration (CC_{50}) is determined as the concentration of compound that generates 50% inhibition of cell viability compared to the no-compound control. Likewise, CC_{10} is the concentration that results in a 10% inhibition of cell viability.

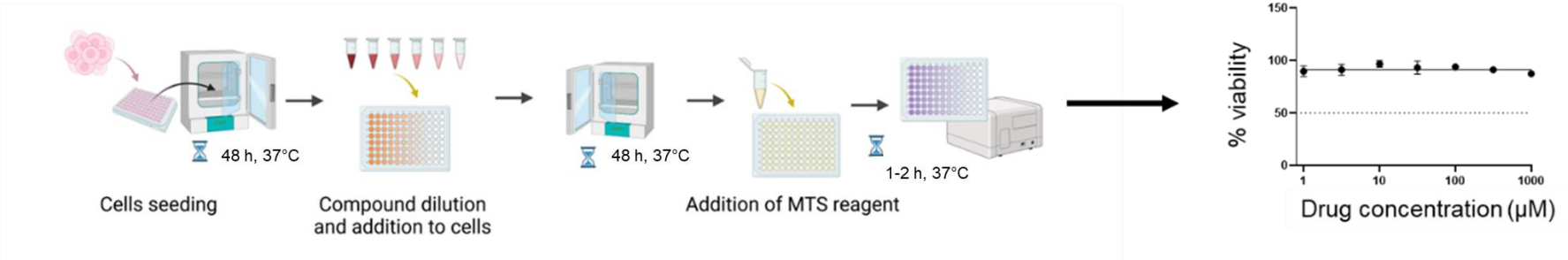

Figure 2.1. Steps performed in a cell cytotoxicity assay screening compounds in Calu-3 cells. The figure was prepared using BioRender.

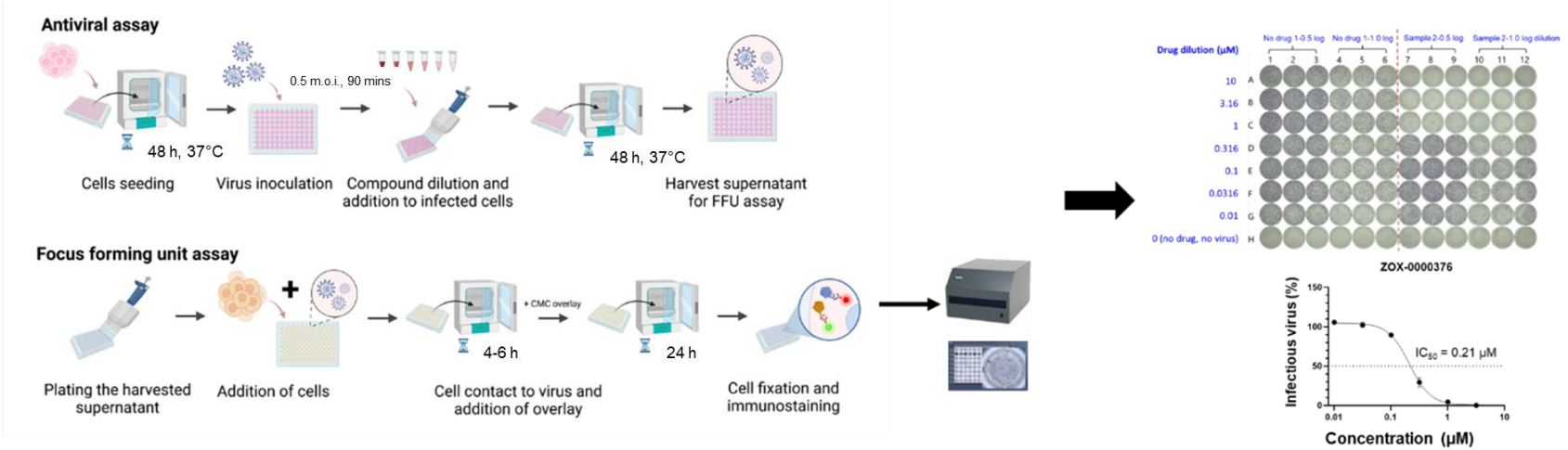

Figure 2.2. A summary of the steps performed in determining the compounds' antiviral activities, including the antiviral assay where the infected cells are treated with the diluted compound and further visualisation step using the focus forming unit (FFU) assay. The figure was prepared using BioRender.

After a further one-hour incubation in a humidified 37°C incubator with 5% CO_2, the absorbance at 490 nm was measured on a Clariostar Plus microplate reader (BMG Labtech, Ortenberg, Germany). Readouts from the medium-only wells were subtracted from the compound-treated wells which were then compared to the untreated control wells and plotted as a compound concentration vs cell viability curve.

2.2.4. Plaque assay

SARS-CoV-2 virus stock was 10-fold serially diluted in six 1.5-mL centrifuge tubes resulting in 10^{-1} to 10^{-6} diluted virus stock. A volume of 100 µL of each diluted virus concentration was added to wells of 24-well plates (Nunc), in quadruplicate, starting from the most diluted stock. A medium-only control was included. To all wells, 500 µL of Vero E6 cell suspension (5×10^5 cells/mL) was then added. Without delay, plates were incubated at 37°C, 5% CO_2 for at least two hours, allowing the virus infection to cells. Following the incubation step, 500 µL of 1% carboxymethylcellulose (CMC) overlay (mixture of the same amount of sterile 2% weight per volume (*w/v*) CMC in dH_2O and DMEM-2% medium) was added to the wells and plates were incubated at 37°C, 5% CO_2 for three to four days until CPE detected.

Following the incubation period, overlay and medium were removed from wells, rinsed with 500 µL of D-PBS, and cells stained with 1 mL of amido black staining solution (0.1% *w/v* amido black, 6% *v/v* glacial acetic acid, 0.16 M sodium acetate anhydrous, all from Merck). Cell fixation and staining were allowed to proceed for at least 30 minutes prior to aspiration and rinsing the wells with tap water. Visible plaques were counted by eye at the dilution factor where plaques can be identified easily as discreet entities and

calculated using the formula 2.1 to yield the virus titer in plaque forming unit per mL (Pfu/mL).

Formula 2.1. Titer determination in plaque assay.

$$Titer\ in\ Pfu/mL = \frac{average\ plaque\ count}{starting\ virus\ volume\ (0.1\ mL)} \times dilution\ factor$$

2.2.5. Tissue culture infectious dose ($TCID_{50}$) assay

The $TCID_{50}$ assay was performed by seeding Vero-TMPRSS2 (for OC43) or HuH-7 (for 229E) cells at a density of 1×10^5 cells/well in wells of 96-well plates. The plates were incubated in a humidified 37°C, 5% CO_2 incubator for 48 hours until a cell monolayer was formed. Virus stock was 10-fold serially diluted by adding 20 µL of virus stock into 180 µL of DMEM-2% FBS to generate 10^{-1} to 10^{-8} dilutions in rows of 96-well plates. Two well columns were used as medium-only controls, and the other 10 well columns as virus titration wells. Following the serial dilution, the medium was aspirated from plates containing a monolayer of cells and then, without delay, inoculated with 100 µL of diluted virus or control, following the same plate configuration as the dilution plate. The plates were then incubated at 37°C, 5% CO_2 in an incubator for 6 days, with daily checking for cell death.

Following the incubation period, the medium was aspirated from all wells and 100 µL of amido black staining solution was added. Cell fixation and staining were allowed for 30 minutes, followed by rinsing the wells with tap water. Cell death was observed in the 10 wells of virus-infected cells, and the $TCID_{50}$ was determined by first calculating

the proportionate distance (PD) using formula 2.2. The 50% TCID is monitored where there are five out of ten wells with cell death (clear wells).

Formula 2.2. Titer determination in TCID50 assay.

$$PD = \frac{(\%\ next\ above\ 50\%) - 50\%}{(\%\ next\ above\ 50\%) - (\%\ next\ below\ 50\%)}$$

$TCID_{50}$ was then calculated by adding PD with the log lower dilution (dilution in which position is next above 50%, for example, -6 for 10^{-6} dilution).

$$Log\ TCID50 = Log\ (PD + \log lower\ dilution)$$

$$TCID50/mL = \frac{10^{-(PD+\log lower\ dilution)}}{initial\ volume\ of\ viral\ stock\ (0.02\ mL)}$$

The titer in PFU/mL can be calculated by dividing the $TCID_{50}$/mL with a constant value of 0.69.

2.2.6. SARS-CoV-2 antiviral assay

The steps performed to determine the antiviral activities of compounds against SARS-CoV-2 are summarised in Figure 2.2. Calu-3 cells were seeded into 96-well plates (Nunc, Thermo Scientific) at a cell density of 6 × 10^4 cells/well in the Calu-3 medium. After 48 hours of incubation at 37°C, 5% CO_2, the wells were inoculated with 50 µL of the challenge virus at the m.o.i of 0.5, in triplicate. Cell infection was allowed for 90 minutes. Following the incubation period, the inoculum was replaced with 200 µL of growth medium containing the appropriate compound dilutions or vehicle control (DMSO or D-PBS, according to the compound) and incubated for three days. The supernatant was harvested and stored at -70°C prior to analysis by FFU assay.

A SARS-CoV-2 FFU assay was performed based on the method described elsewhere (34). Briefly, two half-log dilutions of each supernatant to be analysed were prepared in virus propagation medium. An amount of 20 µL of each dilution was inoculated into wells of a 96-well plate, in triplicate, followed by the addition of 100 µL of Vero E6 cells at 4.5 × 10^5 cells/mL in virus propagation medium. The plates were incubated for two hours at 37°C, 5% CO_2, before the addition of 100 µL of 2% CMC overlay to each well. The plates were incubated for a further 24 hours prior to the removal of the overlay. The cells were washed once with PBS before a fixation step with 50 µL of 4% paraformaldehyde in PBS (Thermo Scientific). The fixation step was allowed to proceed for 30 minutes, then the fixation reagent was aspirated from the wells, and 100 µL of 1% ethanolamine in PBS (Sigma) was added. The plates were stored at 4°C prior to the immunostaining step.

2.2.7. Human coronavirus antiviral assay

The antiviral assay for HCoVs was established based on the SARS-CoV-2 antiviral assay (Section 2.2.6). Changes were made in the choosing of the most appropriate cell line used to support the growth of both HCoVs OC43 and 229E. The human cell line HuH-7 was seeded into 96-well plates (Nunc) at a cell density of 5 × 10^4 cells/well in the HuH-7 medium (DMEM-10% FBS supplemented with 1× MEM non-essential amino acids). Following the 48 hours of incubation at 37°C, 5% CO_2, the wells were inoculated with 50 µL of the challenge virus at the m.o.i of 0.5, in triplicate. Cell infection was allowed for 90 minutes, then the inoculum was replaced with 200 µL of growth medium containing the appropriate compound dilutions or vehicle control and incubated for three days. The supernatant was harvested and stored at -70°C prior to analysis by FFU assays,

performed in Vero-TMPRSS2 cells for HCoV OC43 and HuH-7 for HCoV 229E and according to the SARS-CoV-2 FFU assay described in section 2.2.6 with an adjustment in cell number to 5×10^4 cells/well seeded.

2.2.8. Immunostaining of FFU assay

Cells were permeabilised by replacing the ethanolamine with 2% *v/v* Triton X100 in PBS (Sigma) and incubating at 37°C for 30 minutes. The plates were then washed three times with 100 µL of wash buffer (0.1% v/v Tween 20 in PBS, Sigma), inverted, and gently tapped onto tissue to dry before the addition of 50 µL of the appropriate primary antibody solution, prepared in wash buffer (Table 2.2).

Table 2.2. Primary antibodies used in the immunostaining of the FFU assay.

Antibody	**Species**	**Reactivity**	**Stock Concentration (mg/mL)**	**Working concentration (µg/mL)**
EY2A	Human	SARS-CoV-2 variants ENG2/20, Gamma, Delta	2.5	15.0
FB9B	Human	SARS-CoV-2 variants Alpha, Beta, Delta, Omicron	1.0	15.0
FD6D	Human	SARS-CoV-2 variants Alpha, Beta, Gamma	1.1	15.0
FB1E	Human	SARS-CoV-2 variants, HCoV OC43	1.9	15.0
Anti-OC43 (R&D Systems)	Mouse	HCoV OC43	0.5	2.5
Anti-229E (R&D Systems)	Mouse	HCoV 229E	0.5	2.5

The plates were rocked at room temperature (RT) for one hour. Wells were then washed three times, blotted, and added 100 µL of goat anti-Human IgG (Fc-specific)-peroxidase-conjugate secondary antibody (Thermo Fisher) or goat anti-mouse IgG (Fab specific)-peroxidase-conjugate secondary antibody (Sigma), diluted 1:5,000, and incubated at RT for an hour on the rocker. Following three washes, 50 µL of KPL TrueBlue peroxidase substrate (SeraCare) was added to the wells and incubated at RT for 10 minutes on the rocker, after 10 minutes the substrate was removed, and the plates were washed with distilled water for 10 minutes. The water was removed, and the plates were allowed to air-dry. The foci (dark blue spots) were counted using an ELISPOT classic reader system (AID GmbH). The IC_{50} is determined as the concentration of the compound that generates 50% inhibition of viral replication (as the reduction of viral FFU number) compared to the untreated control wells. GraphPad Prism v.9.0 (GraphPad Software, San Diego, CA, USA) was used to generate curves and calculate the IC_{50} values using non-linear logistic regression analysis (dose-response). The antiviral potency was inferred by the calculated pIC_{50}, the negative logarithm of IC_{50} in molar concentration (123).

2.2.9. Human monoclonal antibody (mAb) production

The human mAbs used as primary antibodies in the FFU assay were gifts from the Weatherall Institute of Molecular Medicine, Oxford and received as DNA plasmids. The antibodies were produced in HEK-293 mammalian expression system using a transient transfection method. Two plasmid DNAs consisting of kappa (light chain) and heavy chain genes of human mAb directed to SARS-CoV-2 N protein or receptor-binding domain (RBD) were transformed into *E. coli* DH5α and stored as glycerol stock. The

bacterial stock was grown overnight in 500 mL of LB medium containing 100 µg/mL of carbenicillin at 37°C in an incubator with 180 rpm shaking. The bacterial cells were harvested by centrifugation at 5,000 x *g* for 10 minutes using a fixed-angle rotor. Plasmid DNA extraction was then performed using the Qiagen Maxiprep kit, according to the manufacturer's protocol. The bacterial pellet was resuspended using 20 mL of Buffer P1 and moved into a 50 mL centrifuge tube. Without delay, 20 mL of Buffer P2 was added, and the tube was inverted six times to mix. The suspension was neutralised using 10 mL of Buffer N3 with six-times tube inversions to mix. The tube was then centrifuged at 3,000 x *g* for 30 minutes at RT. The cleared supernatant was carefully loaded into a Maxi column and allowed to bind the DNA using a gravity flow technique. The column was washed two times using wash buffer by filling the column and letting the wash buffer go through the column by gravity. The plasmid DNA was eluted using 5 mL of elution buffer. DNA was then precipitated using 10 mL isopropanol (Merck) and centrifugation at 3,000 rpm for 60 minutes at 4°C. Isopropanol was discarded, and the DNA pellet was washed with 10 mL of ethanol (Merck) with centrifugation at 3,000 rpm for 60 minutes. The DNA pellet was reconstituted in 350 µL of nuclease-free water.

For antibody production in human HEK-293 cells, DNA was transfected into HEK-293 cells using the heavy:light chain DNA ratio of 1:2. A flask containing 400 mL of 1 x 10^6 cells/mL was prepared by seeding 5×10^5 cells/mL a day before the transfection in 293 medium without antibiotic (Gibco). A mixture of DNA containing heavy and light chains plasmids was prepared by calculating the amount of plasmid DNA to supply 1 µg of DNA per mL of cells in a 1:2 ratio of heavy: light. For a 400 mL culture, a total of 400 µg of DNA mixture is needed. The correct amount of DNA was then dissolved in 10 mL of OptiMEM reduced serum medium (Gibco). Another tube was prepared containing 10 mL of OptiMEM reduced serum and 400 µL of transfection reagent from ExpiFectamine 293

transfection kit (Gibco). Both tubes were mixed well and incubated for 10 minutes. Transfection was performed by adding the transfection mixture gently to the cells with swirling. Transfected cells were incubated at 37°C, supplemented with 5% CO_2 with 180 rpm shaking for seven days. Following the incubation period, cells were harvested by centrifugation at 4,000 rpm for 10 minutes at 4°C. The supernatant was collected, pooled, and filtered using the 0.45 µm cut-off bottle-top filter. The mAb was purified from the supernatant using a protein A column on an AKTA system (Cytiva, UK). Prior to sample loading, the tubing and column were washed with 0.2 µm-filtered ddH_2O using 10× the column volume (CV). The column was then equilibrated with 10× CV of D-PBS and the sample containing supernatant was loaded. The supernatant was loaded into the protein A column (1 ml bed volume, Cytiva), and left overnight with a 1 ml/minute flow rate at 4°C. The column was washed with 10× CV of D-PBS to remove the unbound fraction. The antibody was then eluted with citric acid-sodium tricitrate buffer pH 3.0 (prepared freshly by mixing 73 ml of 0.1M citric acid and 27 ml of 0.1 M sodium tricitrate (Sigma)) at a 1 mL/minute flow rate. The eluted fraction of 1 mL was collected in collection tubes containing 500 µl of 1M Tris-HCl pH 9.0 to neutralize the pH of the antibody fraction. The antibody-containing fractions were pooled, and the pH was adjusted to approximately 7.0 with 1 M Tris HCl pH 9.0. The eluted antibody was concentrated and simultaneously buffer-exchanged to D-PBS using an Amicon concentrator with a 50 kDa cut-off. The antibody was collected in the retentate, and its concentration was measured as total protein using 280 nm spectrophotometer absorbance in NanoDrop system (Thermo Fisher Scientific).

2.2.10. The M^{pro} inhibitor clinical compounds and controls

The Moonshot consortium synthesised and rapidly shared more than 2,400 molecules in an open environment to create an open and intellectual property-free knowledge base for anti-coronavirus drug discovery (34). The compounds were then selected based on synthetic tractability and alchemical free-energy calculations, where every compound was profiled through crystal soaking and x-ray diffraction, totalling 587 structures, available on Fragalysis (https://fragalysis.diamond.ac.uk/viewer/react/ preview/target/ CoV-Mpro), along with the evaluation by biochemical assays using protease assays performed within the Moonshot collaboration.

The analysis of a subset of this structural data (n = 367, up to July 2021) reveals the hotspots for ligand engagement and plasticity of each binding pocket, and among them, a total of 333 compounds were synthesised by Enamine Ltd. (Kyiv, Ukraine) and received by the Oxford University Biochemistry Department for antiviral testing against SARS-CoV-2.

The Moonshot compounds were designed as potent ligand-efficient and geometrically compact inhibitors that fit tightly in the substrate binding pocket as an active site (34). The chemical structures of the Moonshot compounds are not shown in this thesis, due to a non-disclosure agreement, and will be made available to the public along with the publication by the Moonshot collaboration. The approved M^{pro} inhibitors nirmatrelvir and ensitrelvir, as well as the RdRp inhibitor remdesivir, were used as positive controls (Figure 2.3).

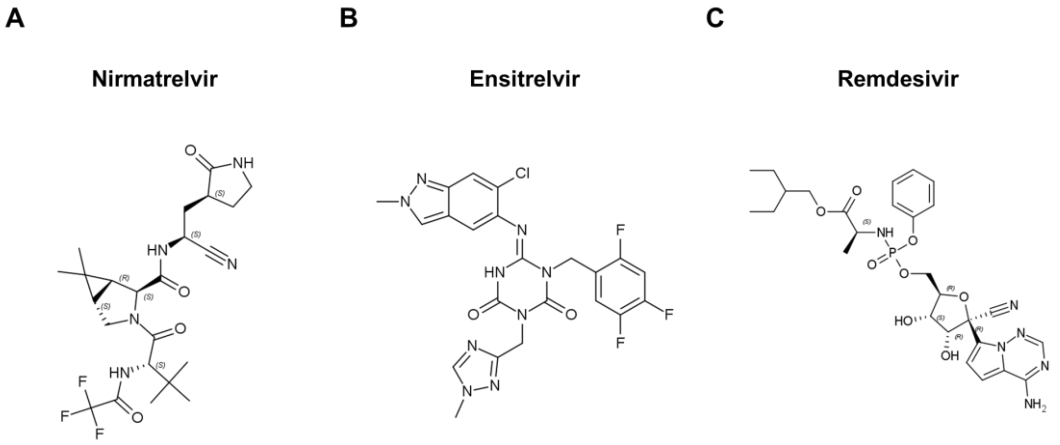

Figure 2.3. The chemical structure of three currently approved drugs used as positive controls. The structure of M^{pro} inhibitors nirmatrelvir (A) and ensitrelvir (B) are shown, along with the RdRp inhibitor remdesivir (C).

2.3. Results

2.3.1. The COVID Moonshot compounds

From a total of 333 COVID Moonshot compounds received by the Zitzmann laboratory and tested against SARS-CoV-2, I was involved in the screening of 60 compounds, with results from one biological replicate, in technical triplicate, are shown in Table 2.3. After completion of the cellular antiviral assay screening, antiviral drug candidates coded ZOX-0000376, ZOX-0000396, ZOX-0000415, and ZOX-0000436 were chosen as preclinical lead compounds based on the combination of their high CC_{10} and low IC_{50} values. Compound ZOX-0000396 is the racemate (mixture of two enantiomers, *i.e.* mirror image stereoisomers of a chiral molecule) of ZOX-0000436. Further testing of these selected compounds was performed with three biological replicates (N=3), in technical triplicate, against SARS-CoV-2 ENG2/20 and the Omicron variant.

Table 2.3. Moonshot compounds tested for cell cytotoxicity and antiviral activities against SARS-CoV-2 Eng2/20 strain. Compounds highlighted in bold were selected as the preclinical leads. Results are from one biological replicate (N=1) performed in triplicate, using the 10% maximum cell cytotoxicity concentration (CC_{10}) as the indicator of cell cytotoxicity.

No.	Compound	CC_{10} (μM)[a]	IC_{50} (μM)[b]
1.	ZOX-0000210	27.40	1.01
2.	ZOX-0000211	13.40	0.34
3.	ZOX-0000227	11.20	0.99
4.	ZOX-0000228	56.05	0.43
5.	ZOX-0000288	9.86	11.94
6.	ZOX-0000312	>100	2.11
7.	ZOX-0000331	>100	1.00
8.	**ZOX-0000376**	**35.80**	**0.34**
9.	ZOX-0000378	59.00	>10
10.	ZOX-0000379	41.20	>10
11.	ZOX-0000380	51.60	>10
12.	ZOX-0000381	63.70	>10
13.	ZOX-0000382	35.80	51.80
14.	ZOX-0000383	6.64	2.96
15.	ZOX-0000384	7.62	0.40
16.	ZOX-0000385	12.10	>100
17.	ZOX-0000386	14.80	5.15
18.	ZOX-0000387	83.30	9.81
19.	ZOX-0000388	21.80	5.52
20.	ZOX-0000389	13.10	0.62
21.	ZOX-0000390	>100	18.75
22.	ZOX-0000391	>100	>100
23.	ZOX-0000392	41.45	5.70
24.	ZOX-0000393	90.10	0.91
25.	ZOX-0000394	91.60	2.99
26.	ZOX-0000395	61.00	0.50
27.	**ZOX-0000396**	**89.10**	**1.71**
28.	ZOX-0000397	18.90	4.99
29.	ZOX-0000398	11.30	4.12
30.	ZOX-0000399	20.00	0.06
31.	ZOX-0000400	16.80	>10
32.	ZOX-0000401	9.31	0.94
33.	ZOX-0000402	10.30	0.27
34.	ZOX-0000403	19.50	0.08
35.	ZOX-0000404	10.90	0.11
36.	ZOX-0000405	3.11	>100
37.	ZOX-0000406	8.88	>10
38.	ZOX-0000407	>100	0.02
39.	ZOX-0000408	12.00	9.44
40.	ZOX-0000409	>10	0.40
41.	ZOX-0000410	11.30	0.09
42.	ZOX-0000411	54.20	>100
43.	ZOX-0000412	14.40	0.09
44.	ZOX-0000413	>100	>100
45.	ZOX-0000414	14.80	>100
46.	**ZOX-0000415**	**57.10**	**1.04**
47.	ZOX-0000416	13.40	2.58
48.	ZOX-0000417	10.90	0.34
49.	ZOX-0000418	79.60	>100
50.	ZOX-0000419	>100	0.16
51.	ZOX-0000420	>100	1.61
52.	ZOX-0000426	>100	32.64
53.	ZOX-0000427	8.87	>10
54.	ZOX-0000428	54.60	0.38
55.	ZOX-0000429	14.50	2.23
56.	ZOX-0000430	>100	4.44
57.	ZOX-0000432	>100	0.93
58.	ZOX-0000434	10.30	0.24
59.	**ZOX-0000436**	**>100**	**1.03**
60.	ZOX-0000443	>100	67.56

[a]Measured using MTS assay in Calu-3 cells, in triplicate

[b]The half-maximum virus inhibitory concentration in SARS-CoV-2-infected Calu-3 cells, Eng2/20 strain (N=1), in triplicate

Table 2.4. The cell cytotoxicity and virus inhibitory concentrations of Moonshot compounds compared to currently approved drugs against SARS-CoV-2 ENG2/20 strain and Omicron variants. The IC_{50} values were generated from three biological replicates (N=3) with three technical replicates each. pIC_{50} was calculated as the negative logarithm of IC_{50} in molar concentration, and the higher the pIC_{50} value, the higher the potency.

Compound	Drug mechanism	CC_{50} (μM)[a]	IC_{50} (95% CI) vs ENG2/20 (μM)	IC_{50} (95% CI) vs Omicron B.1.1.529 (μM)	pIC_{50} vs ENG2/20	pIC_{50} vs Omicron B.1.1.529
ZOX-0000376 (MAT-POS-c7726e07-5)	M^{pro} inhibitor	>100	0.40 (0.38 – 0.42)	0.21 (0.20 – 0.22)	6.40	6.68
ZOX-0000396 (EDG-MED-b1ef7fe3-1)[b]	M^{pro} inhibitor	>100	1.46 (1.38 – 1.54)	0.94 (0.88 – 1.00)	5.83	6.03
ZOX-0000415 (MAT-POS-e48723dc-2)	M^{pro} inhibitor	>100	1.12 (1.12 – 1.26)	0.64 (0.60 – 0.67)	5.95	6.19
ZOX-0000436 (LUO-POS-8c3e556a-1)	M^{pro} inhibitor	>100	0.60 (0.53 – 0.68)	0.39 (0.34 – 0.43)	6.22	6.41
Nirmatrelvir (part of Paxlovid)	M^{pro} inhibitor	>100	0.78 (0.68 – 0.89)	0.32 (0.10 – 0.68)	6.11	6.49
Ensitrelvir (Xocova)	M^{pro} inhibitor	>100	0.11 (0.10 – 0.11)	0.03 (0.02 – 0.04)	6.96	7.52
Remdesivir (Veklury)	RdRp inhibitor	>100	0.49 (0.44 – 0.53)	0.10 (0.09 – 0.12)	6.31	7.00

[a] The half maximum cell cytotoxicity concentration as measured using MTS assays in Calu-3 cells, in triplicate

[b] Racemate of ZOX-0000436

M^{pro}, main protease; RdRp, RNA-dependent RNA polymerase; CI, confidence intervals

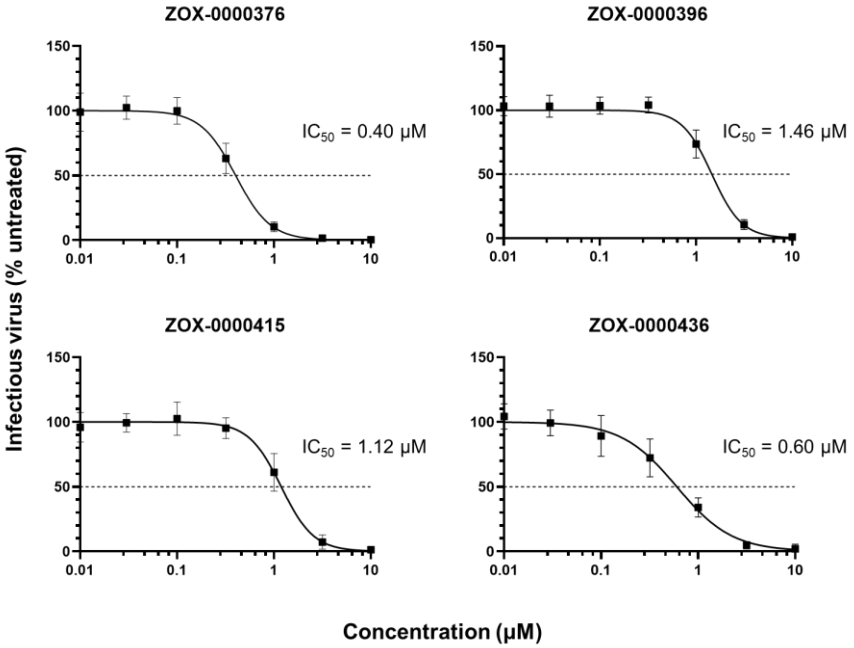

Figure 2.4. Antiviral activity of COVID Moonshot preclinical leads against the SARS-CoV-2 Eng2/20 strain. The inhibitory curve for each compound is displayed as a measurement result of FFU antiviral assays from three biological replicates (N=3) and three technical replicates with error bars showing the standard deviation of the mean.

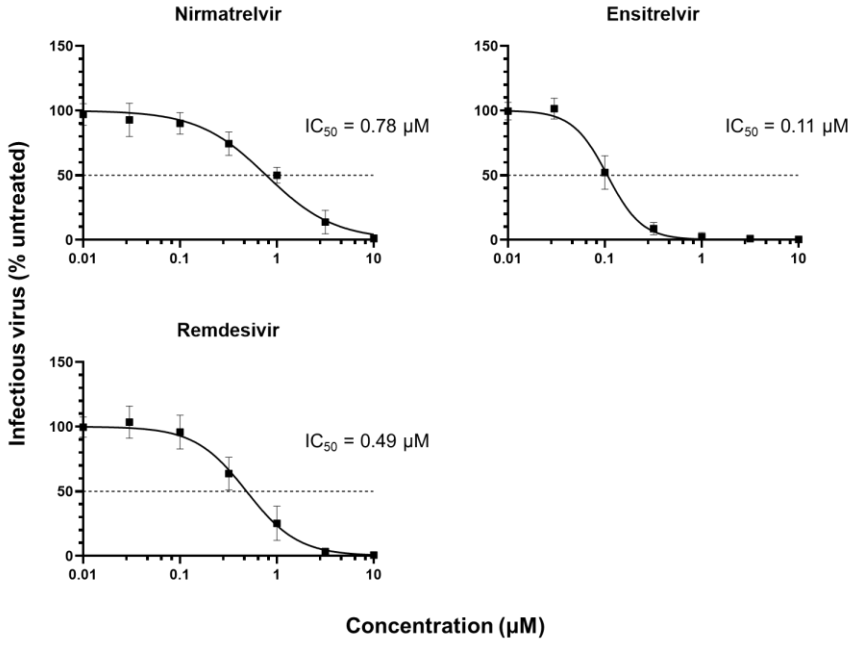

Figure 2.5. Antiviral activity of currently approved drugs against the SARS-CoV-2 ENG2/20 strain. The inhibitory curve for each compound is displayed as a measurement result of FFU antiviral assays from three biological replicates (N=3) and three technical replicates with error bars showing the standard deviation of the mean.

2.3.2. Antiviral activities of COVID Moonshot compounds and currently approved drugs against the SARS-CoV-2 ENG2/20 strain

COVID Moonshot clinical lead compounds demonstrated antiviral properties against the SARS-CoV-2 ENG2/20 strain with varying IC_{50} values (Figure 2.4). All preclinical leads showed cell cytotoxicity values of greater than 100 μM, reflecting good *in vitro* potency with low cytotoxicity (Table 2.4). The compound ZOX-0000376 has the lowest IC_{50} value (0.40 μM) among the Moonshot preclinical leads, making it the most potent of them. Ensitrelvir showed the highest potency among the approved drugs with an IC_{50} of 0.11 μM (Figure 2.5).

2.3.3. Antiviral activities of COVID Moonshot compounds and currently approved drugs against the SARS-CoV-2 Omicron B.1.1.529 variant

COVID Moonshot preclinical leads were tested against the SARS-CoV-2 Omicron B.1.1.529 variant. All compounds are active against the Omicron variant with IC_{50}s below 1 μM (Figure 2.6 and Table 2.4). Overall, the activity of these compounds against the Omicron variant was higher than against the ENG2/20 strain (Table 2.4).

Similar to the result against the ENG2/20 strain, compound ZOX-0000376 and the currently approved drug ensitrelvir yielded the lowest IC_{50} values against the Omicron variant, reaching nanomolar concentrations (210 and 30 nM for ZOX-0000376 and ensitrelvir, respectively) (Figures 2.6 – 2.7 and Table 2.4). Similar findings were observed for the potency inferred by the pIC_{50} values (Table 2.4).

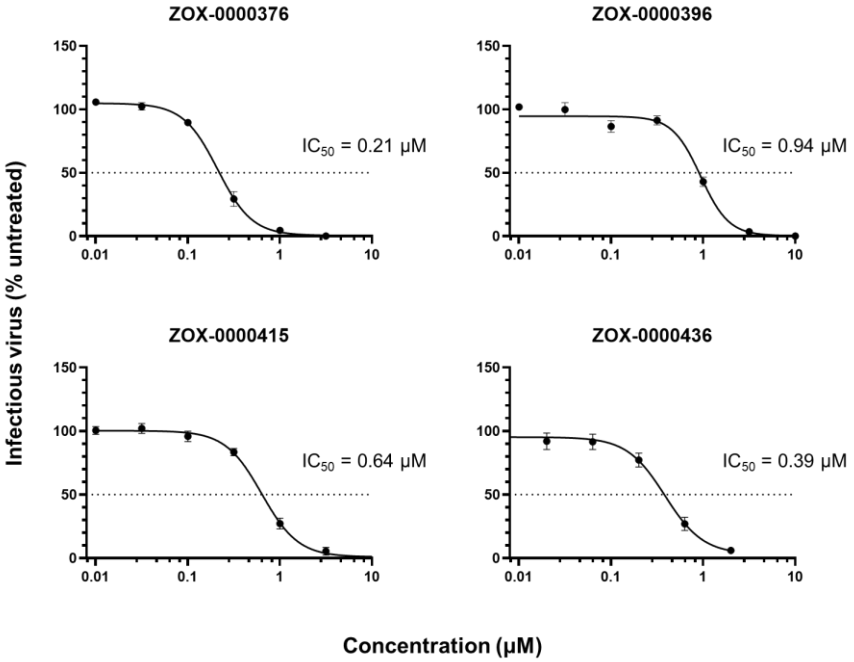

Figure 2.6. Antiviral activity of COVID Moonshot preclinical leads against the SARS-CoV-2 Omicron B.1.1.529 variant. The inhibitory curve for each compound is displayed as a measurement result of FFU antiviral assays from three biological replicates (N=3) and three technical replicates with error bars showing the standard deviation of the mean.

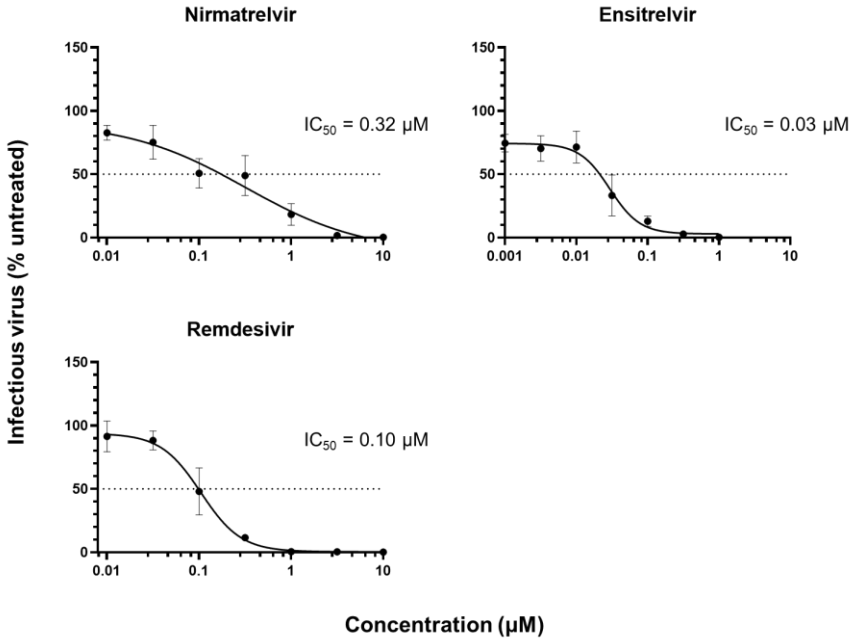

Figure 2.7. Antiviral activity of currently approved drugs against the SARS-CoV-2 Omicron B.1.1.529 variant. The inhibitory curve for each compound is displayed as a measurement result of FFU antiviral assays from three biological replicates (N=3) and three technical replicates with error bars showing the standard deviation of the mean.

2.3.4. The development of human coronavirus antiviral and FFU assays

To develop a human coronavirus FFU for the visualisation of compounds' antiviral activities, different combinations of cell lines for the FFU antiviral assay, as well as antibodies for immunostaining, were assessed.

The cell tropism of HCoV OC43 and 229E was assessed using Vero-TMPRSS2, Calu-3, and HuH-7 cell lines (Figure 2.8). The HuH-7 cell line was chosen as the host cell for the HCoV OC43 and 229E antiviral assays since both HCoVs grew well in this human cell line, as shown by the successful infection of the cell line by both HCoVs (Figure 2.8). HCoV OC43 also showed good infection of Vero-TMPRSS2 cells, though the human hepatoma liver cell line HuH-7 was still preferred over this modified monkey epithelial cell line.

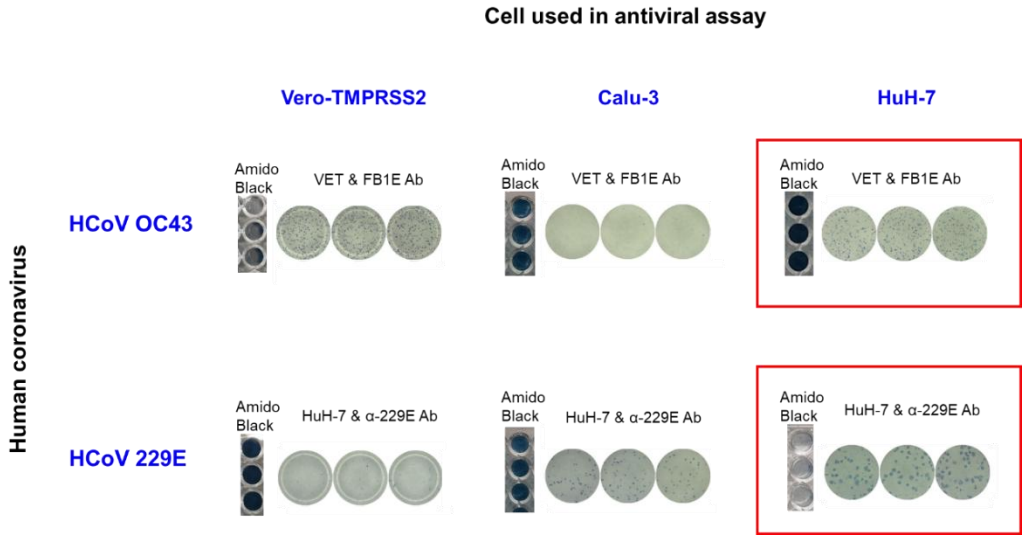

Figure 2.8. The optimised FFU antiviral assays for HCoVs OC43 and 229E. HuH-7 cells were selected for the antiviral assays for both HCoVs (red boxes) and continued with FFU assays in Vero-TMPRSS2 and HuH-7 for HCoV OC43 and 229E, respectively. Virus infection was performed at a m.o.i of 0.5 followed by a 48-hour infection period. Amido black staining of cells post incubation time shows cell viability after virus infection, where infected cells die and detach from the well, resulting in clear wells.

The use of the antibodies in the FFU assay mentioned above was based on mAb screening results (Figure 2.9). The FB1E mAb worked best for HCoV OC43, while HCoV 229E staining required a specific anti-229E antibody from a commercial source (R&D systems).

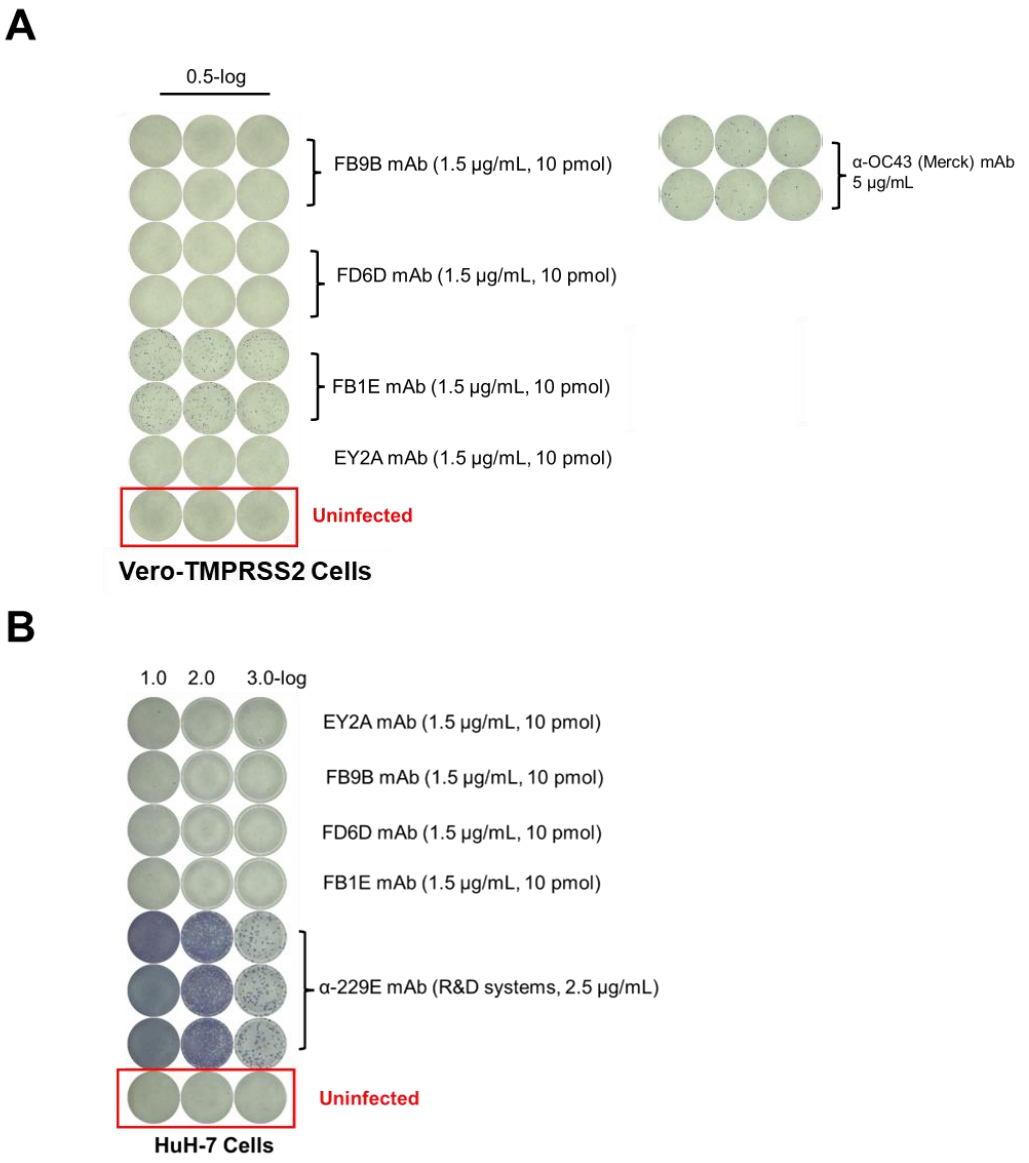

Figure 2.9. The optimised use of antibodies in HCoVs OC43 and 229E FFU assays. A. The human anti-SARS-CoV-2 FB1E was used for HCoV OC43 in FFU assays in Vero-TMPRSS2 cells. B. The mouse anti-229E monoclonal antibody was used for HCoV 229E. mAb, monoclonal antibody used in the FFU assay in HuH-7 cells

2.3.5. Antiviral activities of Moonshot compounds and currently approved drugs against HCoV OC43 and 229E

The Moonshot preclinical lead compounds were also tested against HCoVs OC43 and 229E to evaluate their potential as broad-spectrum antivirals. Moonshot preclinical leads showed good antiviral activity and potency against HCoV OC43 (Figure 2.10 and Table 2.5) with low IC_{50} values in micromolar concentrations. However, the results were inferior to the currently approved drugs, which showed even better potencies with IC_{50} values in nanomolar concentrations (Figure 2.11 and Table 2.5).

In contrast, Moonshot preclinical leads did not show antiviral activity against HCoV 229E, with only one compound yielding an IC_{50} value of 5.39 μM (Figure 2.12 and Table 2.5). A similar result was observed for ensitrelvir with no reduction in virus detected up to 10 μM (Figure 2.13 and Table 2.5). Nirmatrelvir and remdesivir showed superior antiviral activity in comparison to the COVID Moonshot compounds against HCoV 229E with IC_{50} values in nanomolar concentrations (Figure 2.13 and Table 2.5). An overview of IC_{50} and pIC_{50} values is shown in Table 2.5. Both Moonshot preclinical leads and clinical reference compounds show higher antiviral activity against betacoronaviruses than alphacoronaviruses.

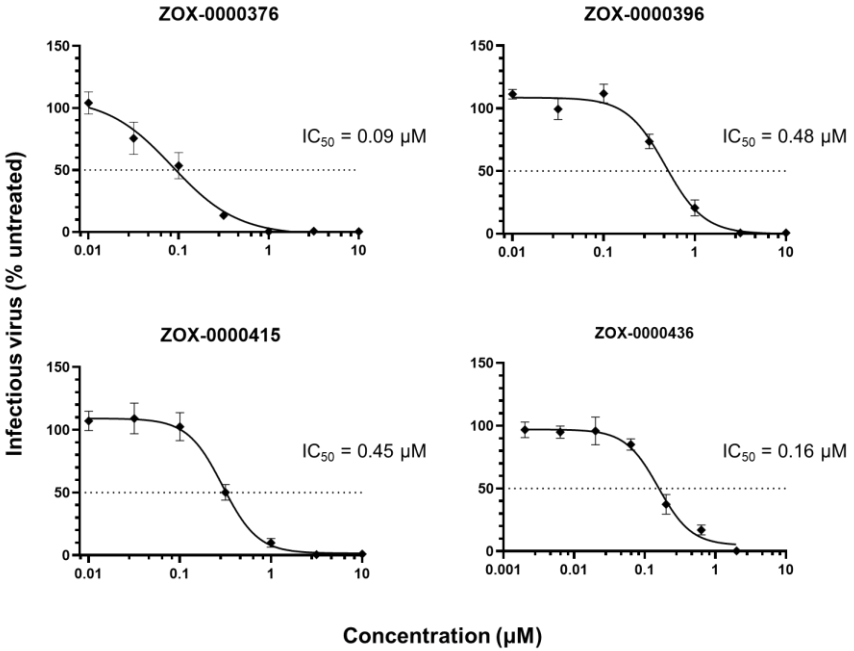

Figure 2.10. Antiviral activity of COVID Moonshot preclinical leads against HCoV OC43. The inhibitory curve for each compound is displayed as a measurement result of FFU antiviral assays from two biological replicates (N=2) and three technical replicates with error bars showing the standard deviation of the mean.

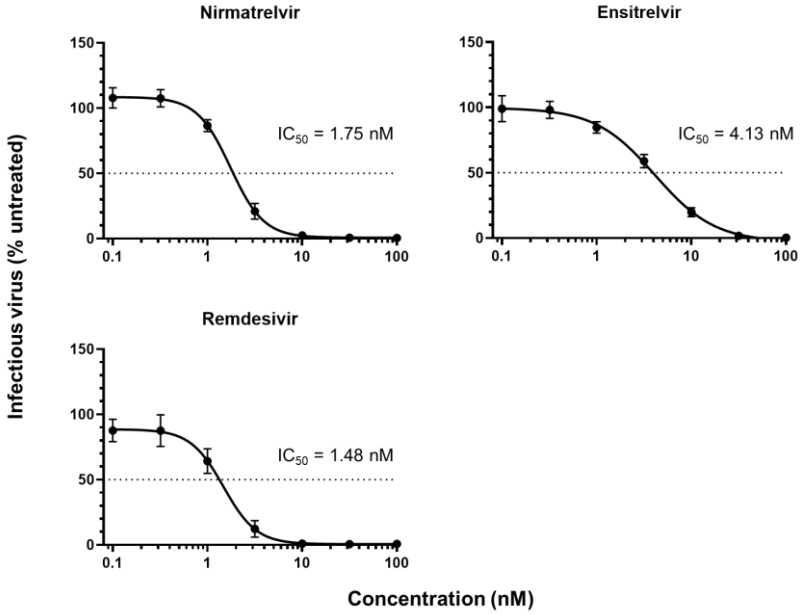

Figure 2.11. Antiviral activity of currently approved drugs against HCoV OC43. The inhibitory curve for each compound is displayed as a measurement result of FFU antiviral assays from two biological replicates (N=2) and three technical replicates with error bars showing the standard deviation of the mean.

Table 2.5. The antiviral activities of Moonshot preclinical leads and currently approved drugs against HCoV OC43 and 229E, calculated as their IC_{50} values in HuH-7 cells. pIC_{50} was calculated as the negative logarithm of IC_{50} in molar concentration and the higher the pIC_{50} value, the higher the potency.

Compound	Drug mechanism	IC_{50} vs HCoV OC43 (95%CI, μM)	IC_{50} vs HCoV 229E (μM)	pIC_{50} vs HCoV OC43	pIC_{50} vs HCoV 229E
ZOX-0000376 (MAT-POS-c7726e07-5)	M^{pro} inhibitor	0.09 (0.055 – 0.114)	5.39	7.05	5.27
ZOX-0000396 (EDG-MED-b1ef7fe3-1)	M^{pro} inhibitor	0.48 (0.424 – 0.535)	>10	6.32	<5.0
ZOX-0000415 (MAT-POS-e48723dc-2)	M^{pro} inhibitor	0.30 (0.267 – 0.323)	>10	6.52	<5.0
ZOX-0000436 (LUO-POS-8c3e556a-1)	M^{pro} inhibitor	0.16 (0.131 – 0.190)	>10	6.80	<5.0
Nirmatrelvir (part of Paxlovid)	M^{pro} inhibitor	1.75 (1.588 – 1.922) nM	0.1	8.76	7.01
Ensitrelvir (Xocova)	M^{pro} inhibitor	4.13 (3.533 – 4.845) nM	>10	8.38	<5.0
Remdesivir (Veklury)	RdRp inhibitor	1.48 (1.280 – 1.722) nM	2.78 nM	8.83	8.56

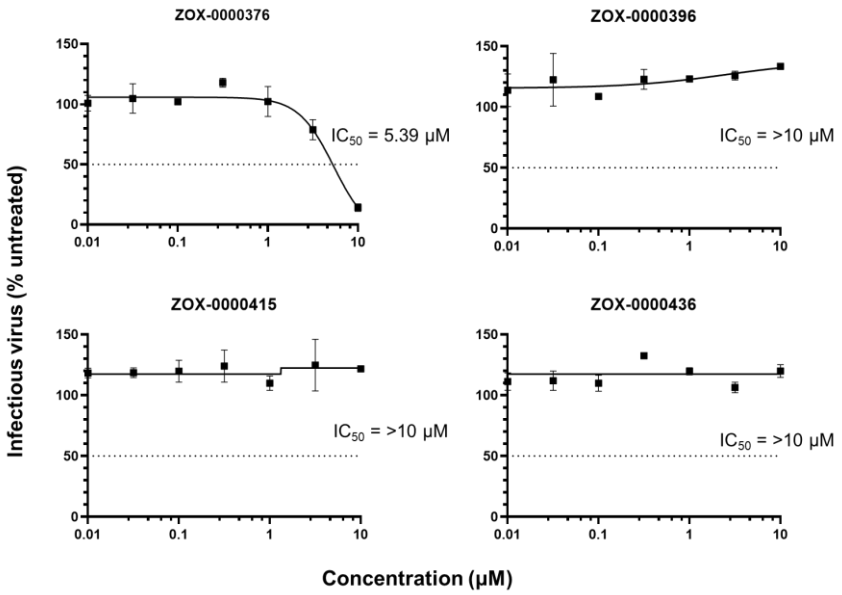

Figure 2.12. Antiviral activity of COVID Moonshot preclinical leads against HCoV 229E. The inhibitory curve for each compound is displayed as a measurement result of FFU antiviral assays from two biological replicates (N=2) and three technical replicates with error bars showing the standard deviation of the mean.

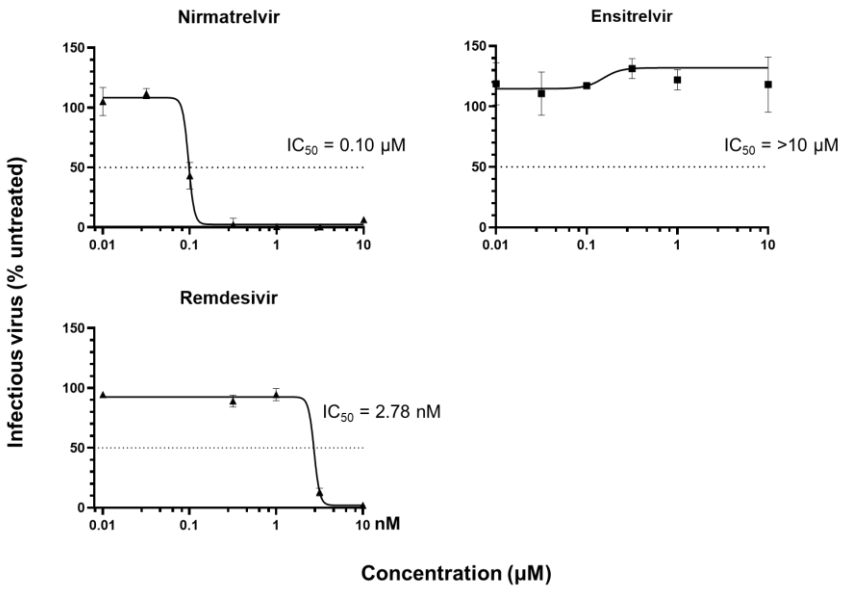

Figure 2.13. Antiviral activity of currently approved drugs against HCoV 229E. The inhibitory curve for each compound is displayed as a measurement result of FFU antiviral assays from two biological replicates (N=2) and three technical replicates with error bars showing the standard deviation of the mean.

2.3.6. Comparison of the in vitro *antiviral activity data of currently approved drugs with published data*

The *in vitro* antiviral activity data of currently approved drugs generated from this study were compared to previously published data (Table 2.6). Comparable profiles were observed between this study's results and other groups' data published between 2020–2023.

Table 2.6. The comparison of *in vitro* cellular assay data of currently approved drugs nirmatrelvir, ensitrelvir, and remdesivir obtained from this study with published data.

Drug tested	**Mode of action**	**Cell line**	**IC_{50}** values	**Reference(s)**
Nirmatrelvir	M^{pro} inhibitor	Calu-3	0.2 μM (vs wild type) 0.025 μM (vs Omicron)	(124)
Nirmatrelvir	M^{pro} inhibitor	Calu-3	0.78 μM (vs ENG2/20) 0.32 μM (vs Omicron)	This study
Ensitrelvir	M^{pro} inhibitor	Vero E6	13.2 nM (vs wild type)	(115,125)
Ensitrelvir	M^{pro} inhibitor	Calu-3	110 nM (vs ENG2/20) 30 nM (vs Omicron)	This study
Remdesivir	RdRp inhibitor	Calu-3	0.28 μM (EC_{50})	(126)
Remdesivir	RdRp inhibitor	Vero E6	1.65 μM	(126,127)
Remdesivir	RdRp inhibitor	HAE	10 nM	(126,127)
Remdesivir	RdRp inhibitor	Calu-3	0.49 μM (vs ENG2/20) 0.10 μM (vs Omicron)	This study

HAE, primary human airway epithelial

2.4. Discussion

Small molecule inhibitors are important for the pandemic preparedness toolbox (128). In this chapter, I present the antiviral *in vitro* efficacy of Moonshot preclinical lead compounds against SARS-CoV-2 and other HCoVs and compare their activity to other approved and authorised drugs for the treatment of COVID-19.

SARS-CoV-2 targets the human respiratory system and gastrointestinal tract as the primary target sites of infection, with cell tropism for the nasal epithelial cells, the alveolar macrophages, and the gastrointestinal tract enterocytes (129,130). The respiratory tract has been identified as one of the major sites of SARS-CoV-2 viral replication, in particular, the upper and lower airways. This includes nasal and bronchial epithelial cells, as well as pneumocytes like Calu-3 or A549 cells (131). Viral replication has also been detected in other tissues, including liver, brain, intestine, and kidney (132–134). However, for SARS-CoV-2, the lung represents the main site of human pathogenesis (135), and it is therefore crucial that therapeutics are tested in this tissue compartment (122). In addition, proteomics data have shown that Calu-3 cells are more representative of the target cells infected *in vivo* in the human respiratory tract in terms of both transcription and proteomic features, which resemble more closely those of primary airway cells (137–139).

The interpretation of cellular assay screening results is complicated by the varying IC_{50}/EC_{50} results published across different laboratories. This may be linked to the different cell types used, as well as a multitude of protocols ranging from CPE assays to plaque assays, that may have impacts on the reliability or comparability of data (122). Concerning cell type, variations in cellular antiviral screening data may be associated with differences in viral cell entry mechanisms, *e.g.* SARS-CoV-2 entry in Vero cells

requires a low pH and is triggered by acid-dependent endosomal proteases, but is pH-independent and requires TMPRSS2 in Calu-3 cells (136). In this study, I propose the TMPRSS2-bearing Calu-3 human lung cells as the more physiologically relevant cells to be used for coronavirus antiviral screening. Throughout, a SARS-CoV-2 microneutralisation assay was adapted for use as an FFU assay, as described elsewhere (140,141). The assay was further developed and extended for use in HCoVs OC43 and 229E antiviral assays (Figures 2.10 – 2.13).

COVID Moonshot compounds are highly specific and selective non-covalent inhibitors designed based on a structure-based fragment screen through fragment merging and growing approaches (34). Moonshot compounds offer advantages in drug specificity and selectivity compared to other drugs developed as drug combinations, such as Paxlovid (nirmatrelvir and ritonavir) (34,121). Pfizer has initiated a phase III clinical trial to evaluate the safety and efficacy of a new oral antiviral ibuzatrelvir, designed to be taken alone to reduce the risk of drug-drug interactions associated with ritonavir. The trial was commenced based on the phase IIb RCT results showing robust antiviral activity and an acceptable safety profile of ibuzatrelvir (142).

COVID Moonshot preclinical leads were active against both the SARS-CoV-2 ENG2/20 strain and the more recent Omicron variant with good cell cytotoxicity indicators (Table 2.4). Their antiviral activity was comparable to the clinical reference compounds nirmatrelvir, ensitrelvir, and remdesivir, demonstrating their potential to be used in future clinical trials and administration against SARS-CoV-2 (Table 2.6).

The Moonshot preclinical leads profiled here had a wider spectrum of activity against betacoronaviruses. This was observed when tested against SARS-CoV-2 and HCoV OC43, which are from the same genus of betacoronavirus (Table 2.5). The results were less promising when tested against the alphacoronavirus HCoV 229E, where only

one Moonshot compound showed detectable antiviral activity, and with lower potency. The tested clinical reference compounds nirmatrelvir, ensitrelvir, and remdesivir seem to have a broader pan-coronavirus activity and work better on betacoronaviruses (SARS-CoV-2 and HCoV OC43). Nevertheless, all tested compounds showed less efficacy against HCoV 229E (Figure 2.12 – 2.13 and Table 2.5). The RdRp inhibitor remdesivir was the drug with the broadest pan-coronavirus activity. This may be supported by the RdRp gene being highly conserved among coronaviruses (65,66), making it one of the most intriguing and promising drug targets for coronavirus drug development, with available biochemical enzyme and cell-based assays (143). Similar to COVID Moonshot preclinical leads, ensitrelvir also showed a narrow antiviral spectrum, being effective against betacoronaviruses and not alphacoronaviruses (Table 2.5). Compared to nirmatrelvir, ensitrelvir was not effective against HCoV 229E. This may reflect the difference in drug design between these drugs and their specific binding to the viral M^{pro} enzyme. There is only 52% conservation/sequence identity in the catalytic domain of the alpha- and betacoronaviruses M^{pro} enzyme, and mutation at catalytic site P168 is the only mutation that is predicted to potentially negatively impact the inhibitor binding (144). Future drug design may benefit from this information.

Drug resistance has always been a major challenge in antiviral drug development, including for coronaviruses (145). Newly evolving viral strains are linked to recurring waves, with partial immune escape and waning immunity within the population (146–148). Drug-induced viral mutations have been described for SARS-CoV-2 therapeutics, however, so far mostly in immunosuppressed individuals. Further, circulating viruses may harbour variants that are resistant to DAA, such as G15S and T21I that confer resistance to the M^{Pro} inhibitor Paxlovid (149–151). Emerging virus mutants with amino acid substitutions in their M^{pro} gene were detected in ensitrelvir-treated COVID-19

patients in the SCORPIO-SR phase III trial, although reductions in viral titer were unaffected by these mutations (152). Remdesivir treatment in patients with a prolonged course of infection caused intra-host viral genomic diversity that leads to the emergence of SARS-CoV-2 variants harbouring fixed mutations (153). The ongoing identification and characterisation of drug-resistant signatures within the SARS-CoV-2 genome will be crucial for clinical management and virus surveillance (154), and the efficacy of the developed compounds against new virus mutants or variants always needs to be monitored.

Access to effective treatment is crucial. As for the case of Paxlovid (nirmatrelvir/ritonavir), Pfizer and the Medicines Patent Pool have reached a voluntary licensing agreement for 95 LMICs to access affordable biosimilars or the generic forms of the drug. However, the generic production of Paxlovid is currently delayed by regulatory bioequivalence clinical trial testing to determine if the generic drug is therapeutically equivalent to the patented drug before it can be used in clinical settings (155). The Moonshot clinical leads are currently undergoing preclinical toxicology and *in vivo* efficacy studies in preparation for phase I readiness. The patent-free development of the Moonshot compounds aims to ensure equitable access, especially for LMICs.

Limitations of this study include the condition that the antiviral assay was only performed in one human lung cancer cell line, Calu-3. Additional testing utilising other human cell lines, such as Caco-2 and A549 cells, would have added greater depth to the dataset. In addition, the final leg of the study was hampered by the closure of the CL-3 laboratory at the Peter Medawar Building, preventing further confirmatory experiments involving SARS-CoV-2 strains.

In conclusion, I have performed a cellular screening experiment utilising both novel small molecule inhibitors targeting SARS-CoV-2 and clinical reference

compounds. Three preclinical leads from the COVID Moonshot project with potent antiviral activity and good PK (not shown, due to a non-disclosure agreement) were proposed for follow-on preclinical development. In terms of future pandemic preparedness, antiviral drug discovery efforts need to be backed by large-scale investment with dual goals to develop an arsenal of broad-spectrum antivirals for coronaviruses and other viruses of pandemic concern (11), as well as building worldwide clinical trial networks that can be rapidly utilised.

Acknowledgement

I would like to acknowledge the work and help from former members of the Zitzmann group: Michelle L. Hill, Juliane Brun, JL Kiappes, and Dominic S. Alonzi in the early setup of the cellular screening assay during lockdown. Michelle L. Hill was the bench supervisor for my study related to antiviral drug discovery before she left the Zitzmann group, and Juliane Brun took over mentoring. I acknowledge the help from Lizbé Koekemoer with COVID Moonshot compound logistics, preparation, and sharing.

Publication arising from this chapter

The substance of this chapter has been published in the following paper:

Brun J[#], **Arman BY**[#], Hill ML[#], Kiappes JL[#], Alonzi DS, Makower LL, Witt KD, Gileadi C, Rangel V, Dwek RA, von Delft A, Zitzmann N. Assessment of repurposed compounds against coronaviruses highlights the antiviral broad-spectrum activity of host-targeting iminosugars and confirms the activity of potent directly acting antivirals. *Antiviral Res*. 2025 Feb 23;237:106123.

[#]Equal contributions

3

Assessment of the iminosugar MON-DNJ as a host-targeting antiviral drug with broad-spectrum activity

Host-targeting antivirals target host cell factors essential for viral replication (59,156). HTAs can interfere with various stages of the viral life cycle, *e.g.* by modulating host pathways that interfere with viral entry, intracellular trafficking and uncoating, protein translation and replication machinery, lipid metabolism, and the induction of the host's immune response (156). HTAs offer several advantages over DAAs, such as a lower risk of developing viral drug resistance by not targeting the virus directly which encourages the development of viral escape mutants; their potential broad-spectrum activity by targeting host proteins that are used by multiple viruses in their replication cycle, and therefore also the potential for rapid repurposing when facing newly emerging unknown viruses that depend on the same host proteins (62). Because of these conceptual advantages, research interest in HTAs has increased over recent years, sparked by the COVID-19 pandemic, with numerous HTAs demonstrating antiviral efficacy against SARS-CoV-2 in cellular assays (122). Despite this data, only a limited number of HTAs have progressed to clinical trial phases (156), and no HTAs are included in current SARS-

COV-2 treatment guidelines (11). Inherent challenges of HTAs include the identification of safe, druggable host targets that are essential for viral replication, and the risk of unintended side effects (157,158).

3.1. Introduction

Drugs classified as HTAs target human proteins that are utilised by viruses for their replication cycle (Figure 1.1 of Chapter 1) (58,59,122,156,159). HTAs can interfere with several key host factors associated with various stages of the viral life cycle (159), including viral attachment and entry, interferon and lipid pathways, as well as viral glycoprotein folding in the endoplasmic reticulum (ER).

3.1.1. Inhibitors of viral attachment and entry

Virus entry into cells employs viral attachment to and penetration into the host target cell as critical steps of the virus life cycle (160,161). Targeting these steps may result in the blockage of viral entry (160). An example of an entry inhibitor is maraviroc, an FDA-approved CCR5 antagonist, that inhibits HIV-1 entry by blocking the interaction of the viral envelope glycoprotein gp120 with the CCR5 cellular co-receptor (162).

SARS-CoV-2 S protein consists of subunits S1 and S2, responsible for viral attachment and subsequent fusion with the host cell membrane, respectively (163,164). The S protein binds to the ACE2 receptor in the cell membrane via the S1 subunit which carries the receptor binding domain (RBD), while the host cell's TMPRSS2 and ADAM metallopeptidase domain 17 (ADAM17) are required for priming the S protein to allow fusion of the viral and host membranes through the S2 subunit promoting cellular entry

(163). Blocking the interaction between the S protein and the host's ACE2 and/or TMPRSS2 proteins can interrupt virus entry into the cell (165,166). Camostat mesylate, a clinically approved inhibitor of TMPRSS2, blocks SARS-CoV-2 infection *in vitro* (165).

SARS-CoV-2 S protein also interacts with human cyclophilin A (CypA), and their interaction increases S protein-mediated membrane fusion and viral infectivity (167). CypA has isomerase activity and chaperone-like function and plays an important role in the replication of several human viruses, including HIV, HBV, and coronaviruses *in vitro* (167–169). CypA is a cellular receptor of cyclosporin A (CsA), making CsA a potential inhibitor of SARS-CoV-2 viral entry (167). However, the immunosuppressive effect of CsA limits the use of this drug and non-immunosuppressive cyclosporin analogues have been developed, such as alisporivir (Debio 025), NIM811, SCY-635, sangliferins, and STG-175 (168,170). Another molecule that can interact with CypA is the extracellular matrix metalloproteinase inducer CD147. The interaction between CD147 and virus-associated CypA can promote virus infection into host cells. The anti-CD147 receptor antibody meplazumab is effective in blocking virus entry into cells *in vitro* (171). In an RCT study, meplazumab had a good safety profile and reduced mortality, viral load, and cytokine levels in a severe COVID-19 patient population (172).

Other virus entry inhibitors, like arbidol, are drugs that inhibit the membrane fusion of the viral envelope with the host's cytoplasmic membrane. Such inhibition is based on the intercalation of the drug into membrane lipids that modifies the physicochemical properties of the phospholipids in the membrane, leading to the inhibition of membrane fusion between virus particles and host membranes (173,174). Arbidol (umifenovir) reduces SARS-CoV-2 viral loads and efficiently inhibits SARS-CoV-2 infection *in vitro* (175,176). However, results from RCTs suggested a limited efficacy of arbidol in treating COVID-19 (175,177) (Appendix 1).

The internalisation of SARS-CoV-2 into host cells is mediated by endocytosis, especially clathrin-mediated endocytosis (CME) (178). In the absence of TMPRSS2, the virus enters via CME and is delivered to endosomes, where cathepsin L activates the fusogenic properties of the S protein, allowing the release of virus genetic material into the cytosol (164). Clathrin plays a key role in the initial stages of CME, forming a coat on the plasma membrane to initiate vesicle formation, while dynamin, a GTPase, is essential for the final step of vesicle scission (179). CME inhibitors target clathrin and dynamin, which are essential for coronaviruses to enter the cell via endocytic pathways (180). Chlorpromazine (CPZ), an antipsychotic medication, has been repurposed as a COVID-19 therapeutic as it affects the assembly of clathrin-coated pits at the plasma membrane and was reported for its antiviral activity against MERS-CoV and SARS-CoV-1, *in vitro* (181,182). The findings led to a clinical trial study of CPZ repurposing, which revealed a lower incidence of symptomatic forms of COVID-19 among patients treated with CPZ (183).

3.1.2. Interferon and lipid pathways modulators

As part of the host's innate immunity, the interferon (IFN) response is crucial in providing a first line of defence against virus infection (184,185). Different types of IFN inhibit SARS-CoV-2 *in vitro*; these include type I IFN α and β, type II IFN γ and type III IFN λ (186). However, whether the IFN response has a protective or pathogenic effect in viral infection seems to be dependent on which IFN signalling pathway is induced (187). The contradictory results of IFN therapy in handling COVID-19 infection underline that the time from the beginning of the treatment and the route of administration are two central factors to be considered (188).

Nitazoxanide (and its active form tizoxanide), an FDA-approved drug for parasitic diarrhoea, modulates host interferon signalling in response to viral infection and has been repurposed for influenza virus (189) and Ebola virus (EBOV) (190), with promising antiviral activities when tested *in vitro*. Nitazoxanide has been tested in a phase IIb/III clinical trial (clinicaltrials.gov ID NCT01227421), showing a reduction of the duration of symptoms in participants with acute, uncomplicated influenza after five days (191). Nitazoxanide has also been tested *in vitro* for coronaviruses (192,193) and various RCTs support its use for the treatment of COVID-19 with good safety profiles and efficacy in reducing SARS-CoV-2 viral load within 7 days, improving clinical outcomes, symptom resolution, a shorter duration for oxygen supplement, with lowered levels of CRP, D-dimer, and ferritin levels after 7 days (193–195).

The increase in lipid metabolism following viral infection indicated the utilisation of host lipids by the virus to replicate (196). In SARS-CoV-2 infection, the acid sphingomyelinase activity is triggered by SARS-CoV-2 binding to host cells, which in turn leads to the formation of ceramide-enriched membrane domains (197). The lipophilic ceramide forms large gel-like rafts/platforms in the plasma membrane that help viral entry by clustering the ACE2 receptor (28,197). Fluvoxamine inhibits the sphingomyelinase activity-prompted formation of the membrane rafts (28,197). Fluvoxamine and other functional inhibitors of acid sphingomyelinase activity (FIASMA) drugs were associated with reduced mortality in COVID-19 patients (198), although clinical evidence was deemed insufficient to issue a treatment recommendation in the National Institutes of Health treatment guidelines (11).

3.1.3. Inhibitor of viral glycoprotein folding

Viruses hijack cellular machinery to produce and traffic their proteins, processes that involve the exploitation of cellular factors, organelles, and intracellular pathways (199). Protein glycosylation is a ubiquitous modification of newly synthesised proteins in the ER, which is crucial for protein folding, QC, and proper trafficking within the secretory pathway. Depending on the linkage of the oligosaccharide to the amino acid side chain of the protein, there are two major types of protein glycosylation: N- and O-glycosylation. N-glycosylation and early N-glycan processing steps are highly conserved in all eukaryotes. The preassembled triglucosylated N-glycan precursors are transferred *en bloc* to nascent polypeptide chains where they undergo further trimming by ER alpha-glucosidase I and II in the calnexin (CNX)/calreticulin (CRT) cycle (Figure 3.1) (200,201).

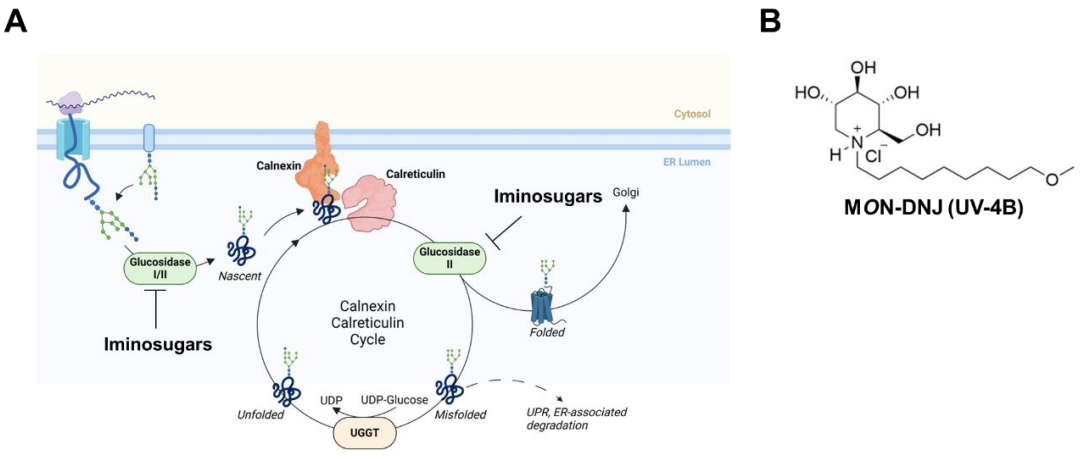

Figure 3.1. The calnexin/calreticulin cycle within the host cell's endoplasmic reticulum involved in the proper folding of secreted glycoproteins. A. MON-DNJ is an example of the iminosugars that inhibit glucosidase enzymes. B. The chemical structure of the hydrochloride salt form of MON-DNJ, also known as UV-4B

The resulting monoglucosylated N-linked glycan can interact with the ER-resident lectin chaperones CNX and CRT, which promote protein folding. These first steps of N-linked glycan processing within the CNX/CRT cycle are essential for the proper folding and function of many glycoproteins (200). After the final glucose residue has been removed by ER alpha-glucosidase II, re-addition of the single glucose unit by the folding sensor UDP-glucose:glycoprotein glucosyltransferase (UGGT) facilitates prolonged interaction with CNX/CRT for proteins not yet correctly folded (202). Several rounds of glucose trimming, re-glucosylation and interaction with CNX/CRT are possible until proteins achieve their final conformation and are released from this glycan-dependent QC process (200). Misfolded proteins failing this QC check are sent for ER-associated degradation (ERAD) processing that involves retro-translocating of misfolded proteins from the ER to the cytosol, followed by ubiquitination, and then degradation by the proteasome (203,204). Many enveloped viruses require the protein-folding machinery in the host ER to correctly fold their glycoproteins (205). Drugs that partially inhibit the enzymes involved in this QC pathway prevent such viruses from folding properly, and they either cannot be secreted at all or are secreted in a non-infectious form (59). The glucose stereochemistry of iminosugars, in which the cyclic oxygen is replaced with nitrogen, targets the ER alpha-glucosidase enzymes and prevents proper folding and incorporation of viral glycoproteins (205–208). Iminosugars are antiviral for many different enveloped viruses *in vitro* and *in vivo*, such as dengue virus (DENV) and other flaviviruses, influenza virus, HBV and HCV, as well as hemorrhagic fever viruses like Marburg and EBOV (201,209–214), making them interesting HTAs with potential broad-spectrum activities.

3.1.4. Glycoprotein folding inhibitors as broad-spectrum antivirals against coronaviruses

The extensively glycosylated SARS-CoV-2 S protein is essential for viral entry, and its proper folding in the ER may be dependent on the CNX/CRT cycle (215). Therefore, inhibiting the CNX/CRT cycle may lead to improper folding of the S protein, which may lead to an antiviral effect, such as observed in SARS-CoV-1, where the iminosugar IHVR-19029 disrupts the interaction of the S protein and CNX, and produces SARS virions with significantly lower infectivity than untreated virions (215,216). With that in mind, celgosivir, the oral prodrug of castanospermine, a naturally occurring bicyclic iminosugar and alpha-glucosidase inhibitor, was tested against SARS-CoV-2 and inhibited viral replication *in vitro* (158,215,217).

Miglustat, another iminosugar and clinically approved drug for Gaucher's disease, is also active *in vitro* against a variety of enveloped viruses, including SARS-CoV-2 (218). The treatment with miglustat led to a marked decrease in the level of RBD protein, both inside the cells and expressed on the cell surface, implying the role of miglustat as an inhibitor of the proper folding and/or release of functional S protein (218). In the study, Rajasekharan *et al.* used an expression vector for SARS-CoV-2 Spike RBD to assess the effect of miglustat treatment on protein release from transfected HEK-293T cells. The expressed RBD protein was detected by immunoblot for the His-tag and RBD protein, both in supernatant and cell extracts, with β-actin as the loading control. The released RBD protein was highly abundant in the cell supernatant under normal conditions; however, upon treatment with 200 μM of miglustat, the release of RBD protein to the supernatant was impaired. Conversely, RBD was more abundant in the intracellular

extracts of miglustat-treated cells, and this could be consistent with misfolded proteins being retained inside the cell (218).

Early on during the COVID-19 pandemic, the Zitzmann laboratory screened 100 FDA-approved and experimental compounds, all small molecules, in a human lung epithelial Calu-3 cell line infected with SARS-CoV-2, and identified iminosugars as potential antiviral inhibitors of coronaviruses, among them is MON-DNJ (122). The monocyclic MON-DNJ (N-(9-methoxynonyl)-1-deoxynojirimycin, also known as UV-4) is the furthest clinically developed antiviral iminosugar from the Zitzmann laboratory, with a proven clinical safety profile in humans (63).

A key mechanism by which iminosugars act as antivirals is their ability to disrupt glycoprotein folding, arising from the inhibition of ER alpha-glucosidase I and II. The iminosugar MON-DNJ interacts with the active site of these alpha-glucosidases (219), which control entry to the calnexin cycle (Figure 3.1). The calnexin cycle is required for the correct folding of many glycoproteins, including viral glycoproteins (205,220). MON-DNJ is a derivative of the naturally occurring iminosugar 1-Deoxynojirimycin (DNJ) from mulberry (*Morus spp*.) leaves and silkworm (221), showing inhibition of alpha-glucosidase activity, and modified to increase antiviral efficacy (205).

MON-DNJ was developed through alkyl chain elongation and oxygenation to be a more potent yet similarly non-toxic derivative of *N*B-DNJ (209,222). MON-DNJ has been tested against a range of viruses *in vitro* and shows *in vivo* efficacy in animal models against DENV and influenza A virus. The primary antiviral mechanism of action of MON-DNJ is the inhibition of alpha-glucosidases, which leads to a reduced release of virus from infected cells (reviewed in (209)).

The inhibition of alpha-glucosidase I and II and the resulting accumulation of misfolded proteins will trigger ERAD (205). This leads to the presence of glucosylated

free oligosaccharides (FOS), which are products of glycoprotein degradation where the glycan portion is released prior to the proteasomal destruction in the cytosol by a peptide: N-glycanase (PNGase). For example, the inhibition of alpha-glucosidase II results in a monoglucosylated glycoprotein. After trimming of the glycan precursor by mannosidases and recognition of the glycoprotein as terminally misfolded, a $Glc_1Man_4GlcNAc_1$ FOS species is generated during ERAD. Alpha-glucosidase I inhibition leads to the accummulation of $Glc_3Man_5GlcNAc_1$ FOS species (209).

FOS are considered a marker of the ERAD, and analysis of FOS derived from degraded glycoproteins provides both qualitative and quantitative insight into glycoprotein degradation in the ER on a cellular level (223). The presence and levels of cytosolic FOS can be measured (*e.g.* by high-performance liquid chromatography (HPLC)) to monitor ERAD activity, glycoprotein misfolding, and degradation pathways. In order to measure FOS, cells are treated with inhibitors of ER degradation or glycan-processing (using an iminosugar, *e.g. N*B-DNJ) or by overexpression/silencing of ERAD components such as EDEM1 (a mannosidase). The cytosolic and lumenal cell extracts are collected, and FOS are isolated and fluorescently labelled. HPLC is then used to separate and quantify oligosaccharides based on their structure (*e.g.* $Glc_1Man_4GlcNAc_1$ or $Glc_3Man_5GlcNAc_1$). Changes in FOS profiles or their quantities serve as indirect measures of misfolded glycoprotein processing and ERAD pathway engagement (223). The analysis of the level of glucosylated FOS in the cytosol is a valuable test for the efficacy of novel iminosugars in a cellular context (205,224).

MON-DNJ has been tested for its safety and PK profiles in both multiple ascending doses (clinicaltrials.gov ID NCT02696291) and single ascending doses (clinicaltrials.gov ID NCT02061358). The results from these phase I clinical trials showed that the drug could be administered at a comparably low concentration three times daily for seven

days or as long as required in acute infection. At the drug serum levels achieved at such low doses, MON-DNJ mostly inhibits ER alpha-glucosidase II (59). A single higher dose of MON-DNJ prevents death in mice infected with lethal doses of influenza or DENV, even if administered days after infection, and in this case, protection correlated with inhibition of ER alpha-glucosidase I (211). This raised the possibility of developing MON-DNJ as a single high-dose treatment that could be given even after infection (though before symptoms develop), *e.g.* after a known high-risk encounter. The advent of the COVID-19 pandemic around the time these data were published for dengue and influenza meant it was important and urgent to test the performance of MON-DNJ also against SARS-CoV-2 (59,215).

In this chapter, I investigated the antiviral activity of MON-DNJ against SARS-CoV-2 variants and HCoVs through cell-based antiviral assays in human cell lines combined with an FFU assay as a readout to measure viral replication *in vitro*.

3.2. Materials and Methods

3.2.1. Cell lines and viruses

The maintenance of the human lung cancer cell line Calu-3 (ATCC HTB-55), the African green monkey Vero E6 cell line (ATCC CRL-1586), Vero-TMPRSS2, and the human hepatocyte cell line HuH-7 (JCRB0403) was described in Chapter 2. SARS-CoV-2 wild-type strain ENG2/20 was provided as a passage 1 stock and passaged in Vero E6 cells to generate the passage 2 sub-master and passage 3 working stocks. SARS-CoV-2 variants alpha (B.1.1.7), beta (B.1.351), gamma (P.1), delta (B.1.617.2), and Omicron (B.1.1.529),

as well as HCoV OC43 were gifts from William James (Sir William Dunn School of Pathology, University of Oxford). HCoV 229E was a gift from Narayan Ramamurthy (Nuffield Department of Medicine, University of Oxford). Virus propagation, stock generation, and titer determination were described in Chapter 2.

3.2.2. MON-DNJ antiviral assay

Calu-3 cells were seeded into Nunc Edge 2.0 96 well plates (Nunc, Merck) at a cell density of 8×10^4 cells/well in 200 µL of growth medium (section 2.2.1. of Chapter 2). After 36 to 48 hours of incubation, the supernatant was removed, and the wells were inoculated for two hours with 50 µL of the challenge virus (*e.g.* SARS-CoV-2 ENG2/20) at a m.o.i of 0.5, in triplicate, in growth medium. The inoculum was removed and replaced with 200 µL of growth medium containing the appropriate MON-DNJ dilutions or D-PBS as the matched vehicle control. The infected cells were then incubated with the drug for two days (48 hours). The supernatant was harvested and stored at -70°C prior to analysis by FFU assay. The cell monolayer was stained with naphthol blue black to inspect cell death.

The antiviral assay for HCoVs was established based on the SARS-CoV-2 antiviral assay. Changes were made in the choice of the most appropriate cell line used to support the growth of both HCoVs OC43 and 229E. The human cell line HuH-7 was seeded into 96-well plates (Nunc) at a cell density of 5×10^4 cells/well in HuH-7 medium (DMEM-10% FBS supplemented with 1× MEM non-essential amino acids). Following the 48 hours of incubation at 37°C, 5% CO_2, the cells were inoculated with 50 µL of the challenge virus at a m.o.i of 0.5, in triplicate. Infection was allowed to proceed for 90 minutes, then the inoculum was replaced with 200 µL of growth medium containing

MON-DNJ dilutions or D-PBS control and incubated for 72 hours. The supernatant was harvested and stored at -70°C prior to analysis by FFU assays, performed in Vero-TMPRSS2 cells for HCoV OC43 and HuH-7 for HCoV 229E, and according to the SARS-CoV-2 FFU assay described in the following section.

3.2.3. MON-DNJ FFU assay

To increase throughput, the SARS-CoV-2 microneutralisation assay was adapted for use as an FFU assay, as described in detail in Chapter 2 and elsewhere (140,141). Briefly, three half-log dilutions of each supernatant to be analysed were prepared in virus propagation medium. A volume of 20 µL of each dilution was added to wells of a 96-well plate (Greiner Bio-One) in quadruplicate, followed by the addition of 100 µL of Vero E6 cells at 4.5×10^5 cells/mL in virus propagation medium. For HCoVs, the cell number of 5×10^4 cells/well was used. The plates were incubated for two hours prior to the addition of 100 µL of 1.8% CMC overlay. The plates were incubated for a further 24 hours. After 24 hours, the overlay was carefully removed, and the cells were washed once with PBS (Gibco) before fixing with 50 µL of 4% paraformaldehyde (Thermo). After 30 minutes of incubation, the paraformaldehyde was removed and replaced with 100 µL of 1% ethanolamine in PBS (Merck). The cells were permeabilised by replacing the ethanolamine with 2% Triton X100 in PBS (Merck) and incubating at 37°C for 30 minutes. The plates were then washed three times with wash buffer (PBS-0.1% Tween 20 (Merck)), inverted, and gently tapped onto a stack of tissue to dry before the addition of 50 µL of primary antibody specific for the tested virus (gift from Arthur Huang (Taiwan) via Alain Townsend and Jack Tan (Weatherall Institute of Molecular Medicine, University of Oxford)) at 10 pmol concentration in wash buffer. A summary of the optimal FFU assay

conditions for antiviral drug testing against coronaviruses is presented in Table 3.1. The plates were rocked at RT for one hour and subsequently washed six times with 100 µL of wash buffer, tapping to dry after every three washes. Then, 100 µL of secondary antibody anti-human IgG (Fc-specific)-peroxidase-conjugate produced in goat (Merck) diluted 1:5,000 or anti-mouse IgG-peroxidase conjugate diluted 1:1,000 (Merck) in wash buffer was added to the wells according to the species of the primary antibody and the plates were rocked at RT for one hour. The plates were rinsed six times with wash buffer, with tapping to dry after every three washes. Finally, 50 µL of TrueBlue peroxidase substrate (Insight Biotechnology Ltd.) was added to the wells and incubated at RT on the rocker for 10 minutes; the substrate was removed, and plates were washed with 100 µL of ddH_2O followed by a 10-minute incubation. The water was removed, and the plates were allowed to air dry. The foci (dark blue spots) were then counted using an ELISPOT classic reader system (AID GmbH).

3.2.4. Compound preparation and cell cytotoxicity assay

The hydrochloride salt form of MON-DNJ, also known as UV-4B, was dissolved in PBS (Gibco). For the antiviral assay, eight half-log dilutions in Calu-3 medium were prepared in triplicate from the highest non-toxic concentration determined (1,000 µM). Appropriate matched controls of the PBS solvent were also generated. Cell viability after treatment with MON-DNJ was measured using the CellTiter 96 AQueous One Solution Cell Proliferation MTA Assay (Promega), according to the manufacturer's instructions (described in detail in Chapter 2, section 2.2.3).

Table 3.1. Summary of the optimal FFU assay conditions for testing MON-DNJ against SARS-CoV-2 variants and human coronaviruses

Challenge virus	Cell line used in antiviral assay	m.o.i	Virus challenge incubation time	Cell line used in FFU assay	Optimised dilution factor of samples from antiviral assay	Optimised dilution factor for FFU readout	Primary antibody
SARS-CoV-2 strain ENG 2/20	Calu-3	0.5	48 hrs	Vero E6	1.0 & 1.5-log	1.5-log	EY 2A mAb (Human)
SARS-CoV-2 Alpha (B.1.1.7) variant	Calu-3	0.5	48 hrs	Vero E6	0.5 & 1.0-log	1.0-log	FB 9B mAb (Human)
SARS-CoV-2 Beta (B.1.351) variant	Calu-3	0.5	48 hrs	Vero E6	1.5 & 2.0-log	1.5-log	FB 9B mAb (Human)
SARS-CoV-2 Gamma (P1) variant	Calu-3	0.5	48 hrs	Vero E6	1.5 & 2.0-log	1.5-log	EY 2A mAb (Human)
SARS-CoV-2 Delta (B.1.617.2) variant	Calu-3	0.5	48 hrs	Vero E6	1.0 & 1.5-log	1.5-log	EY 2A mAb (Human)
SARS-CoV-2 Omicron (B.1.1.529) variant	Calu-3	0.5	48 hrs	Vero E6	0.5 & 1.0-log	1.0-log	FB 9B mAb (Human)
HCoV OC43	HuH-7	0.5	48 hrs	Vero-TMPRSS2	1.0 & 1.5-log	1.0-log	FB 1E mAb (Human)
HCoV 229E	HuH-7	0.5	48 hrs	HuH-7	2.0 & 3.0-log	3.0-log	α-229E mAb (Mouse)

3.3. Results

3.3.1. The establishment of FFU antiviral assays for testing MON-DNJ against SARS-CoV-2 variants and HCoVs

The development of FFU assays for coronaviruses involves the selection of the most suitable cell lines, the culture and virus infection conditions, and the selection of primary and secondary antibodies to visualise and quantify virus foci efficiently. SARS-CoV-2 variants, as well as HCoVs OC43 and 229E, generated foci of variable sizes and numbers despite using the same initial m.o.i and incubation time (Figure 3.2). Adjustments were made to each FFU assay for each particular virus variant or strain to yield efficient foci counting; one such adjustment was the dilution factor of the original supernatant from the antiviral assay to generate a good FFU readout (Table 3.1).

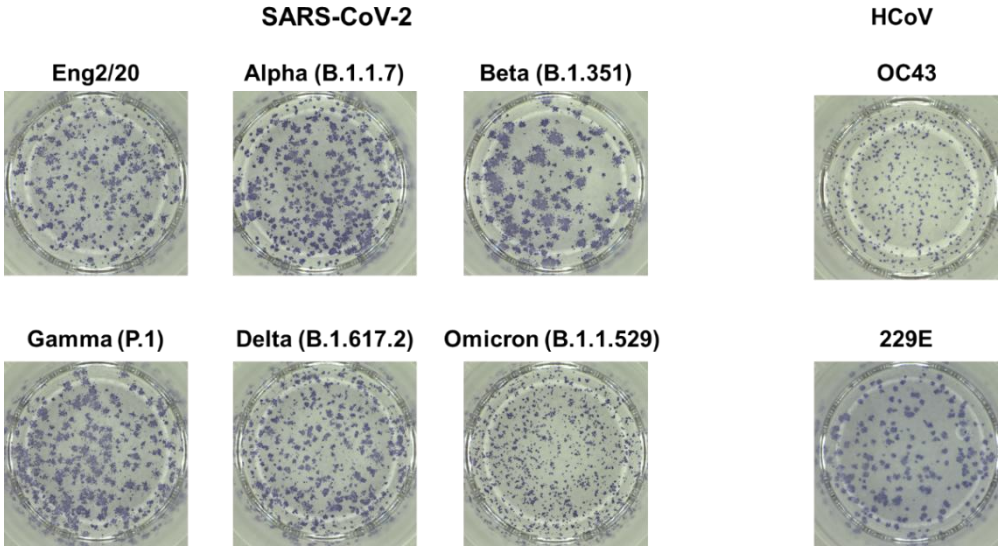

Figure 3.2. Focus morphology of different variants of SARS-CoV-2 and two HCoVs after an FFU assay visualisation in wells of a 96-well plate. The assay was performed using a m.o.i of 0.5 and 48 hours of incubation.

3.3.2. Cell cytotoxicity of MON-DNJ in different cell lines

The cell cytotoxicity of MON-DNJ was tested in the four different cell lines used in the study (Figure 3.3). The viability of the cell lines after treatment with MON-DNJ for 48 hours (mirroring the incubation time in the antiviral assay) was above the 50% cell death threshold. Approximately 30% of cell death was observed in both Vero E6 and Vero-TMPRSS2 cells post-MON-DNJ treatment at the highest concentration tested (1,000 µM). No significant reduction of cell viability was observed for both human Calu-3 and HuH-7 cells that are used in the SARS-CoV-2 and HCoV antiviral assays.

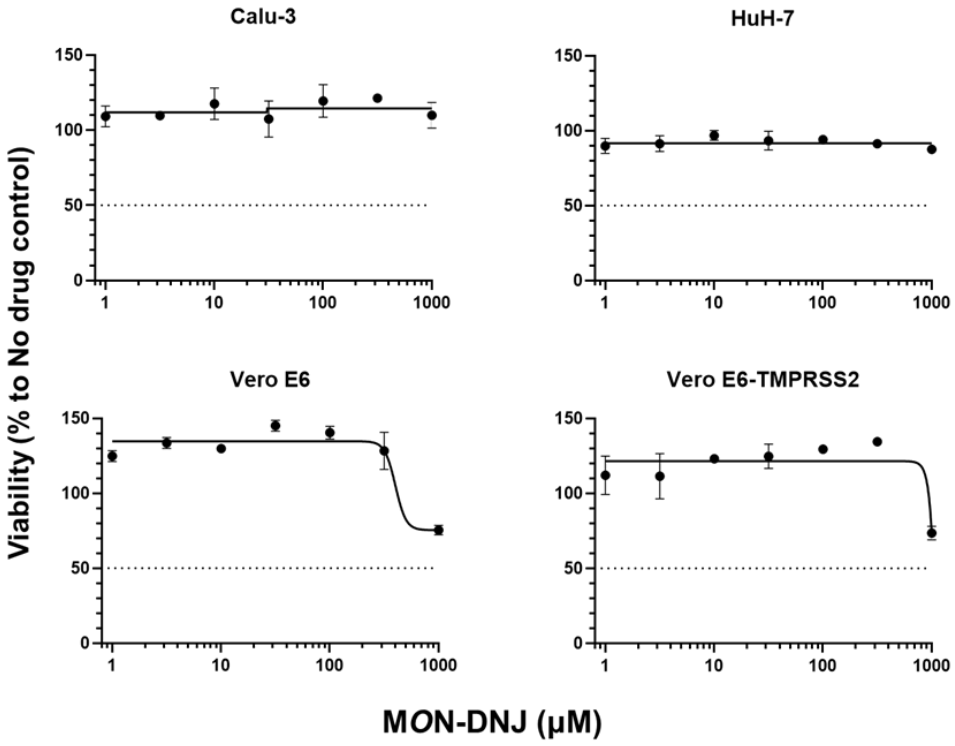

Figure 3.3. The CC_{50}s of MON-DNJ in four different cell lines. MON-DNJ treatment does not reach 50% inhibition of cell viability even at the highest dose tested (1,000 µM). Error bars showing the standard deviation of means from four replicates. The nonlinear regression curve fit was performed using the four-parameter logarithmic equation in GraphPad Prism v. 9.0.

3.3.3. The influence of virus multiplicity of infection (m.o.i) on the antiviral assay

In an attempt to determine the most suitable m.o.i for the antiviral assay and to check the influence of the number of viruses added to the experimental system, a comparison of different m.o.i.s (in Pfu/cell) was performed in the antiviral assay of SARS-CoV-2 alpha and Omicron variants. No significant differences were observed when comparing different m.o.i.s in both SARS-CoV-2 variants (Figure 3.4). Although different IC_{50} values were measured, similar pIC_{50} values were generated. The m.o.i of 0.5 was selected for the antiviral assay to allow sufficient virus particles to infect cells while ensuring the total amount of virus needed for the assay can be accommodated by preparing lower titer virus stocks.

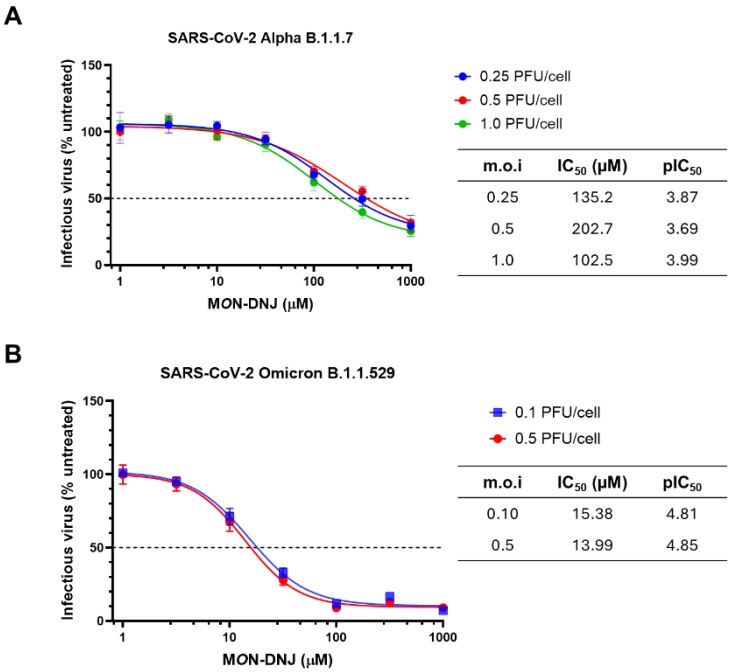

Figure 3.4. The effect of using different m.o.is on MON-DNJ antiviral activity. The comparison was performed using SARS-CoV-2 variants alpha (A) and Omicron (B). Error bars show the standard deviation of means from three biological replicates (N=3) and three technical replicates. The nonlinear regression curve fit was performed using the four-parameter logarithmic equation in GraphPad Prism v. 9.0.

3.3.4. Antiviral activity of MON-DNJ against coronaviruses

The iminosugar MON-DNJ was antiviral against all SARS-CoV-2 variants (Figure 3.5), though with varying efficacy. The IC_{50} values measured for the different SARS-CoV-2 variants are shown in Figure 3.5 and Table 3.2. MON-DNJ was most potent against the Omicron strain, with an IC_{50} of 14.1 μM. Higher IC_{50} values were observed for Eng2/20, beta, alpha, gamma, and delta variants, with IC_{50}s of 51.7, 88.1, 123.5, 186.0, and 219.2 μM, respectively.

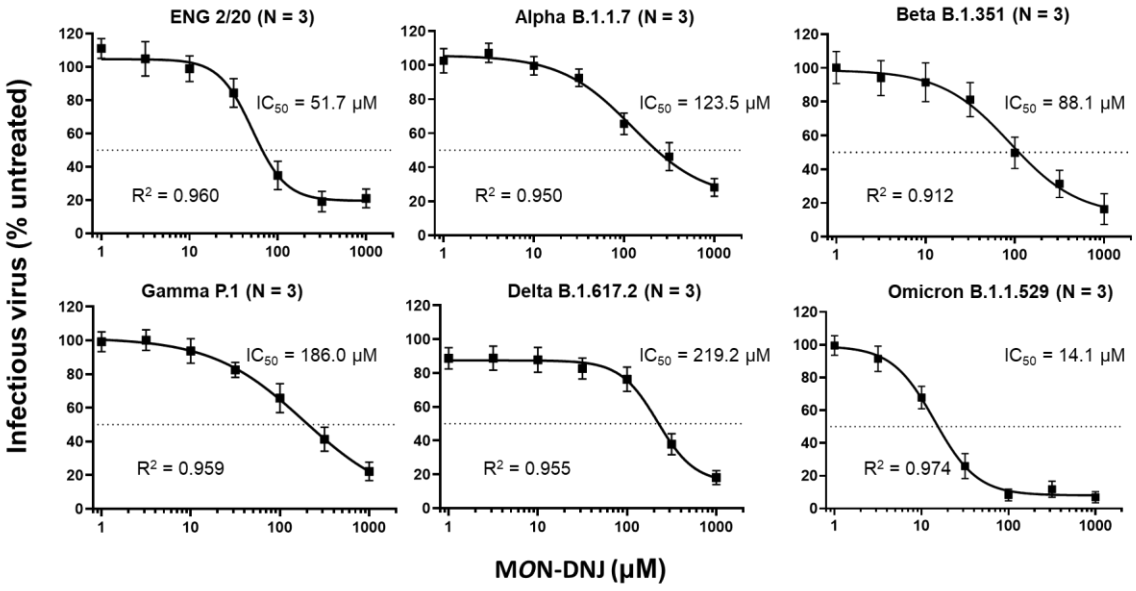

Figure 3.5. Antiviral activity of MON-DNJ against SARS-CoV-2 variants. The inhibitory curve against each SARS-CoV-2 strain is displayed as a measurement result of an FFU antiviral assay performed in three biological replicates (N=3) and three technical replicates, with error bars showing the standard deviation of the mean. The nonlinear regression curve fit was performed using the four-parameters logarithmic equation in GraphPad Prism v. 9.0. The R^2 value represents the goodness of fit of the curve.

Table 3.2. MON-DNJ antiviral activity against SARS-CoV-2 variants. The IC_{50}, 95% confidence interval/CI, and pIC_{50} are shown. Results were derived from three biological replicates (N = 3). Higher pIC_{50} values signify higher potency (68).

Virus strain/variant	MON-DNJ IC_{50} (μM)	MON-DNJ IC_{50} (μM, 95% CI)	pIC_{50} (μM)
ENG2/20	51.7	46.7 – 57.3	4.29
Alpha (B.1.1.7)	123.5	106.2 – 148.3	3.91
Beta (B.1.351)	88.1	70.7 – 117.8	4.06
Gamma (P.1)	186.0	142.2 – 279.4	3.73
Delta (B.1.617.2)	219.2	201.3 – 238.5	3.66
Omicron (B.1.1.529)	14.1	13.3 – 15.1	4.85

3.3.5. The replication rate of SARS-CoV-2 variants in relation to MON-DNJ potency

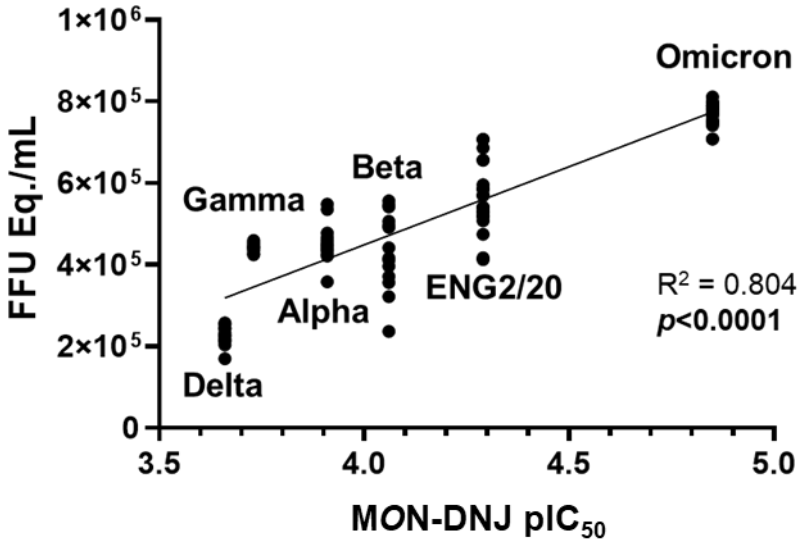

Figure 3.6. Linear regression analysis between the replication rates of SARS-CoV-2 variants and MON-DNJ antiviral potency. The infection levels were recorded after 48 hours post-infection with a m.o.i of 0.5 in untreated (no drug) Calu-3 cells. Results from three biological replicates (N=3) and four technical replicates are shown.

The replication rate of each SARS-CoV-2 variant in the untreated (virus only) control after incubation of 48 hrs in a 0.5 m.o.i antiviral assay system was plotted against the potency of MON-DNJ (shown as corresponding pIC_{50} values), revealing a significant correlation between both (Figure 3.6): MON-DNJ is more potent in SARS-CoV-2 strains/variants that have a higher replication rate.

3.3.6. MON-DNJ antiviral activities against human coronaviruses OC43 and 229E

When tested against human coronaviruses, MON-DNJ shows antiviral activity against HCoV OC43 but much less so against 229E (Figure 3.7). While the IC_{50} is 21.3 μM for HCoV OC43, for HCoV-229E, the IC_{50} was still not reached even at the highest MON-DNJ concentration tested (1,000 μM).

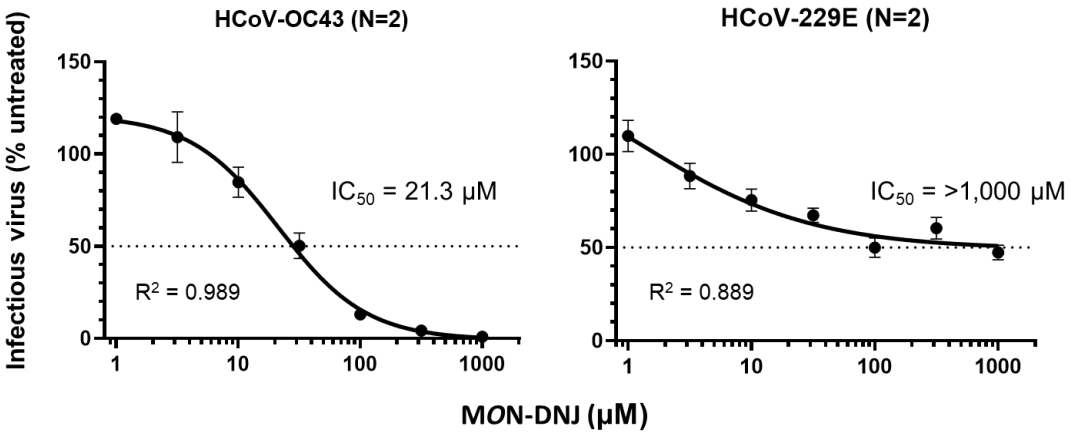

Figure 3.7. Antiviral activity of MON-DNJ against human betacoronavirus HCoV OC43 and alphacoronavirus HCoV 229E. Results are from FFU measurements performed in two biological replicates (N=2) and three technical replicates with error bars showing the standard deviation of the mean. The nonlinear regression curve fit was performed using the four-parameter logarithmic equation in GraphPad Prism v. 9.

3.4. Discussion

Conceptually, HTAs offer many advantages in a pandemic scenario, such as broad-spectrum antiviral activity and a high genetic barrier for viral escape mutants in comparison to DAAs.

Drug resistance has been one of the major challenges in antiviral drug discovery, and has been observed for DAAs targeting HCV, influenza, HIV, and coronaviruses (145,225–229). In addition, driven by the high error rate of the viral RdRp and selective immune pressure, circulating viruses constantly generate new variants, giving rise to recurrent COVID-19 waves (146,230).

On the other hand, viral variability is a challenge for the development of future vaccines and DAAs. One case report showed that a SARS-CoV-2 mutant bearing the NSP12 RdRp E802D mutation was detected in a patient experiencing recrudescence of viral shedding that occurred during and after remdesivir therapy (149). The effect of the mutation was confirmed in an *in vitro* replication kinetic study where SARS-CoV-2 mutant replicated to a higher titer than the parental virus, in the presence of a high concentration (5 μM) of remdesivir, resulting in an increased IC_{50} value (4.2 μM vs 0.7 μM or 6-fold) (149). The E802D mutation was also detected in another *in vitro* study, which selected drug-resistant viral populations by serially passaging SARS-CoV-2 in the presence of remdesivir (154). Case reports detected a V792I mutation, also in the NSP12 RdRp gene, developing in immunocompromised renal transplant recipients after remdesivir exposure (231,232).

In another serial passaging *in vitro* study, the V792I mutation conferred a 2.6-fold increase in EC_{50} compared to the DMSO-passaged virus (233). However, an *in vivo* RCT study (ACTT-1) in patients showed a similar rate of emergent mutations in NSP12

observed in participants treated with remdesivir or placebo, suggesting that NSP12 RdRp gene mutations were due to natural viral evolution for virus adaptation to evade the immune response, and not related to remdesivir (234). Further *in vitro* phenotyping showed a low change in susceptibility to remdesivir relative to the wild-type NSP12 reference for the V792I mutation (2.2-fold change in EC_{50}) (234).

The HTA approach is considered to be less prone to the emergence of drug resistance caused by virus mutations, and developing an HTA should become a priority for preventing future viral epidemics from turning into pandemics (59,60). *In vivo* studies in mice revealed that MON-DNJ exhibited low potential for the development of viral resistance when used against DENV (235) and influenza A virus (236,237), showing a high genetic barrier to the generation and selection of escape mutants following exposure to this iminosugar, making it a potential HTA (209,237).

For the most advanced antiviral iminosugar, MON-DNJ, I demonstrated no cellular toxicity when tested against Calu-3, HuH-7, Vero E6 and Vero-TMPRSS2 cells (Figure 3.3), with all cell lines showing acceptable viability up to the highest drug concentration tested (1,000 μM). These results are in accordance with previous data (238). MON-DNJ, which was developed for DENV, completed a phase I clinical study, with no serious adverse events at doses up to 1,000 mg in humans (63).

MON-DNJ displays antiviral activity against different betacoronavirus variants, including SARS-CoV-2 variants and HCoV OC43 in human Calu-3 and HuH-7 cells (Figures 3.5 and 3.7). This is in line with published data, where MON-DNJ was active against SARS-CoV-2-induced cell death and reduced viral replication after 24 hours of *in vitro* treatment of infected Vero E6 cells (215). Another study reported that UV-4B, the hydrochloride salt form of MON-DNJ, showed a potent *in vitro* antiviral activity against the wild type and beta variants of SARS-CoV-2 in A549 and Caco-2 cell lines expressing

ACE2 (239). Franco *et al*. also found different degrees of inhibition by MON-DNJ against the wild-type USA-WA1/2020 strain and the beta variant in A549 and Caco-2 cell lines, with higher EC_{50}s detected against wild-type strain (239). Further, in combination with EIDD-1931, the active form of molnupiravir, MON-DNJ exhibited potent cellular activity against SARS-CoV-2 *in vitro* at low micromolar IC_{50} concentrations (240).

A correlation between viral replication rate and the potency of MON-DNJ was observed, where MON-DNJ is more potent against SARS-CoV-2 variants with higher replication rates (Figure 3.6). An explanation for this observation is that the highly replicating SARS-CoV-2 virus variant may increase the load on the cell glycoprotein folding mechanism, through the calnexin/calreticulin cycle, to correctly fold the generated viral proteins. Hence, a smaller dose of MON-DNJ iminosugar is needed to further inhibit the overloaded CNX/CRT cycle and escalate the amount of misfolded proteins in the ER. This will result in a decreased amount of newly generated infectious virus.

In my hands, MON-DNJ was significantly less potent against HCoV 229E. In line with this data, strain-specific differences in iminosugar potency have been reported for other enveloped viruses such as Hazara (241), influenza (237), and vesicular stomatitis virus (242).

One of the drawbacks of the use of iminosugars is that, as glucose-mimetics, they may have several unitended off-target effects, including the inhibition of intestinal alpha-glucosidases (gut disaccharides) (243,244). Clinically, inhibition of intestinal alpha-glucosidases could lead to osmotic diarrhoea, however, this has not been reported as a side effect in the clinical trial for MON-DNJ (63).

I argue that, considering the antiviral effects of MON-DNJ, translational development into a clinical candidate for pandemic preparedness should be considered, in particular for viral families that rely on the CNX/CRT cycle for glycoprotein folding, such as influenza A, DENV, and coronaviruses. A potential next step in translational development would be testing MON-DNJ in human challenge models of either influenza A or SARS-CoV-2.

The results from iminosugar testing against SARS-CoV-2 variants presented here formed part of a paper published by the Zitzmann group and colleagues (122). Unfortunately, this part of my DPhil was impacted by the fact that the local CL-3 laboratory had to be closed down for over a year during my thesis, and I was therefore not able to pursue additional SARS-CoV-2 cellular assays. This prevented me from testing other iminosugars against different and newer variants of SARS-CoV-2.

In summary, the iminosugar MON-DNJ is an HTA that is active against different variants of SARS-CoV-2 and betacoronavirus HCoV OC43. Further preclinical and clinical studies are required to support the use of MON-DNJ as a therapeutic for pandemic preparedness.

Acknowledgement

I would like to acknowledge the work by and help from Michelle L. Hill and Juliane Brun, both ex-members of the Zitzmann group. I also acknowledge the help from Matteo N. Barbaglia (also an ex-member of the Zitzmann group) with the work related to HCoV replication rates, and for designing the calnexin/calreticulin cycle shown in Figure 3.1.

Publication arising from this chapter

The substance of this chapter has been published in the following paper:

Brun J[#], **Arman BY**[#], Hill ML[#], Kiappes JL[#], Alonzi DS, Makower LL, Witt KD, Gileadi C, Rangel V, Dwek RA, von Delft A, Zitzmann N. Assessment of repurposed compounds against coronaviruses highlights the antiviral broad-spectrum activity of host-targeting iminosugars and confirms the activity of potent directly acting antivirals. *Antiviral Res*. 2025 Feb 23;237:106123. doi: 10.1016/j.antiviral.2025.106123.

[#]Equal contributions

4

The development of matrix-assisted laser desorption ionisation – time of flight (MALDI-ToF) mass spectrometry methods to detect falsified vaccines

The rapid development of vaccines against COVID-19 was a remarkable success in biomedical research, marked by their supply and distribution worldwide, with billions of doses administered (13). However, while these vitally important vaccines were not distributed equitably around the globe, there were increasing concerns about the occurrence and impact of SF vaccines (14,68,69).

There are no readily available devices currently being used in the supply chain to screen for SF vaccines. Such devices are required to empower inspectors and enforcement agencies conducting risk-based post-marketing surveillance. The use of the devices could be integrated into the national regulatory standards and WHO's Prevent, Detect, and Respond strategy (14). Matrix-assisted laser desorption ionisation-time of flight (MALDI-ToF) MS is globally available for fast and accurate identification of

bacteria and fungi in patient samples (245), and this method could potentially be repurposed as an accessible solution to help identify SF vaccines. MALDI-ToF's low sample volume requirements and the high-throughput nature of the analysis provide significant benefits as a lower-cost MS platform that could be used for coordinated vaccine authenticity testing in local reference laboratories or central facilities (246).

4.1. Introduction

4.1.1. Substandard/falsified vaccines and medical products

According to the WHO, approximately 10% of medical products distributed in LMICs are either substandard or falsified (70,71). This concerning estimate suggests a significant but neglected risk, potentially leading to higher rates of illness, death, and economic harm, as well as eroding public trust in healthcare systems (71).

Substandard or 'out of specification' products are authorised medical products that fail to meet either their quality standards or specifications, or both (71). For example, if the vaccine cold chain is not maintained in the supply chain (*e.g.* if a vaccine is left at ambient temperature, which can be above 45°C in some countries), this is likely to result in a poor-quality substandard vaccine. In contrast, falsified products refer to products that deliberately or fraudulently misrepresent their identity, composition or source (70,71), as a result of criminal activities.

SF medical products pose a significant threat to health as they are of poor quality, unsafe and/or ineffective (73). Moreover, there is inadequate recognition of the scale of the problem or of the need to establish appropriate risk analysis, monitoring and intervention systems. Within a period of two years from 2020-2022, there were 184

reports of diverted and SF COVID-19 vaccines from 48 countries and most cases of vaccine falsification were in LMICs (74). In one of these 184 incidents alone, 2,500 people were wrongly injected with saline as a fake instead of the genuine COVID-19 vaccine in 12 fake vaccination drives in Mumbai, India, in 2021 (247). In another case in 2021, a member of the Indian parliament (along with a few hundred other individuals) was injected with falsified COVISHIELD in Kolkata, India, where they may have been injected with antibiotic amikacin instead (248). Other cases include 6,000 vials of falsified COVISHIELD COVID-19 vaccine (equivalent to 60,000 doses) seized in Varanasi, India in 2022 (249) and other falsified COVID-19 vaccines, including the Oxford AstraZeneca vaccine (in Iran in 2021) (250) and the Pfizer-BioNTech Comirnaty vaccine (in Poland, Mexico and Iran in 2021) (251,252). Before the pandemic, multiple non-COVID-19 vaccines had also been falsified, including vaccines for cholera (Dukoral in Bangladesh), rabies (Verorab in the Philippines) and meningitis (Mencevax in Niger) (253). In 2016 alone, around 5,000 children in Indonesia were injected with falsified vaccines (254).

Falsified COVISHIELD vaccine, a recombinant non-replicating chimpanzee adenovirus viral vector (ChAdOx1) vaccine encoding the SARS-CoV-2 S glycoprotein (255), has been identified in the WHO regions of Africa (Uganda), South Asia (India) and Southeast Asia (Myanmar) in 2021 (256). In these cases, the criminals had also changed the vial labels in the following ways: falsifying the expiry date (Uganda), stating an incorrect volume of 2 mL with 4 doses instead of 5 mL with 10 doses (India), and falsifying the batch number with an incorrect spelling of vaccine brand as COVISHELD (Myanmar). It is not in the public domain what materials the criminals used to make the falsified labels in the three countries. However, from the photos in the WHO Medical Product Alert (256), it appears as though the labels could have been self-adhesive office labels

with the label information printed using an office colour printer. Since falsified vaccines could sometimes be recognised by accompanying falsified vaccine vial labels, the analysis of labels is attractive for vaccine authenticity testing. In addition, it offers a non-invasive way to vaccine authenticity testing and therefore allows the tested vaccine vials to be retained in the supply chain.

4.1.2. Tools to detect SF vaccines

The world is at risk of a surge of SF medical products if the supply chains are not supported by appropriate quality assurance systems once these products leave the manufacturers' premises (14). This highlights the critical role of regulatory authorities to continuously prevent, detect, and remove SF medical products in the supply chains (75). The monitoring of SF medical products should always be an intrinsic part of disease surveillance programs since SF products can contribute to morbidity, mortality, and drug resistance, and lead to loss of confidence in health-care systems (76).

The risk of SF vaccines in the pandemic spawned increased interest, with the evaluation of near-infrared (257), spatially-offset Raman spectroscopy (SORS) (258) and lateral flow test devices (78). The VIE collaboration has been evaluating a diverse range of screening devices (78,258). MALDI-ToF MS is widely available throughout the world, including in some LMICs where they are used in clinical microbiology laboratories for the identification and speciation of microorganisms (259) and other specific purposes, *e.g.* to identify proteins in influenza virus vaccines (260). In terms of global distribution, an estimated 7,200 MALDI instruments were available worldwide in 2020 (261). As the devices are commonly used in hospital microbiology laboratories, they are potentially readily available for vaccine screening programs worldwide.

4.1.3. Principle of mass spectrometry

Mass spectrometry is an analytical technique that forms ions from atoms or molecules and measures their mass-to-charge ratio (*m/z*) using an instrument called a mass spectrometer (262). The instrument measures ions in gas phase and, unlike neutral atoms and molecules, ions can be accelerated, deflected, and decelerated in electric and magnetic fields (262,263). The process of MS sample analysis includes five basic components of a mass spectrometer, *i.e.* sample inlet, ionisation source, mass analyser, detector, and computer (262). A sample is introduced via an inlet system, and ions are formed in an ionisation source. The ions are then accelerated out of the ion source and guided to one or more mass analysers, which separate ions into the different *m/z* values present. Following separation, the ions hit the detector where their abundance is recorded, usually based on the amplification of the ion signal. The output is then digitised and transferred to a computer where the spectrum (plural spectra), which is a plot of ion abundance versus *m/z*, is displayed (262).

Different ionisation sources are available for mass spectrometers and six are routinely used, *i.e.* electron ionisation (EI), chemical ionisation (CI), electrospray ionisation (ESI), atmospheric chemical ionisation (APCI), inductively coupled plasma ionisation (ICP), and MALDI (described in more detail in Appendix 2). Among them, ESI and MALDI are the most commonly used (264). The ionisation sources differ in the physical mechanism of ion formation and their suitability for different sample types (polarity, volatility, and other chemical and physical properties). In general, protonated ($[M+H]^+$) or deprotonated ($[M-H]^-$ or radical cations ($M^{+\bullet}$)/anions ($M^{-\bullet}$) are the most common charged ion species formed in mass spectrometers (262).

A mass analyser is a device that separates ions according to their *m/z* ratios, making it the heart of every mass spectrometer instrument (262). Different analysers use different ways to manipulate ions for their *m/z* to be measured (265). Mass analysers can be divided into two main classes: beam analysers (magnetic sector, quadrupole, time of flight (ToF)) and trapping analysis (ion trap, ion cyclotron resonance, Orbitrap) (262). Among them, four basic types of mass analysers are widely used: the ion trap, ToF, quadrupole, and Fourier transform ion cyclotron, as a stand-alone or put together in tandem to take advantage of each analyser (263).

The detector generates an amplified signal, proportional to ion abundance, from ions that have been separated by the mass analyser (262) and displays it in a mass spectrum chart (266). There are different types of detectors, including Faraday cups (detect a current produced from ions captured by a metal surface), electron multipliers (generate an electron cascade that amplifies an electric current produced by the detected ions), and photomultipliers (produce a photon cascade from the detected ions) (262). The electron multiplier is the most common detection method used in MS (266).

4.1.4. MALDI-ToF mass spectrometer

MALDI is characterised by a photon-induced ionisation process that leads to energy and proton transfer via an intermediate crystalline matrix to yield desorbed ions (262). MALDI is considered a 'soft' ionisation process that tends to form singly charged ions, unlike other 'hard' ionisation techniques, such as is the case in EI, that can generate subsequent fragmentation of the radical cations. MALDI typically enable the analysis of non-volatile and thermally labile compounds via the formation of even electron, protonated or deprotonated molecules, such as ([M+H]+) and ([M-H]$^-$. MALDI is more

tolerant of salts, buffers, and ionic contaminants (262). However, the excess of the matrix (1,000 times more than the sample) results in the domination of the low mass region by matrix ions (300-400 Da, known as the matrix noise), making it less useful for analysis of molecules below 500 Da.

Time-of-flight mass analysers are popular due to their ability to deliver high-resolution and accurate mass measurements reliably at a relatively low cost (262). In ToF, ions of various *m/z* are accelerated to the same energy and achieve *m/z*-dependent velocities and thus will require different flight times to traverse a set distance before being detected by the detector (267). The travel time is in the order of microseconds, making scanning times very rapid (262,267).

In this chapter, I describe the development of methods to detect SF vaccines using the bioMérieux VITEK-MS instrument. In parallel, Rebecca Clarke and John Walsby-Tickle developed methods for the Bruker Biotyper Sirius in the Department of Chemistry, University of Oxford. These two instruments in particular were chosen as, between them, they are already available in most LMICs, in clinical laboratories for routine medical testing (261,268). The development and application of MALDI-ToF MS to distinguish genuine vaccines from a range of falsified vaccine surrogates is investigated by analysing MALDI spectral information from vaccine constituents as well as vaccine vial labels.

4.2. Materials and Methods

4.2.1. MALDI-ToF method development

4.2.1.1. Sample preparation

Genuine vaccines (Table 4.1) and constituents that have been reported in falsified vaccines (Table 4.2) were purchased from the Oxford University Hospitals Pharmacy and used in the development of MALDI-ToF detection methods using a VITEK-MS instrument.

Table 4.1. Genuine vaccines used in the development of MALDI-ToF methods to differentiate between genuine and fake vaccines

Vaccine/falsified surrogate	Target pathogen/disease	Manufacturer
Engerix B	Hepatitis B virus	GlaxoSmithKline, Brentford, UK
Flucelvax Tetra	Influenza virus strains[1]	Seqirus Ltd., Maidenhead, UK
Ixiaro	Japanese encephalitis virus	Valneva Ltd., Fleet, UK
Nimenrix	Meningococcal disease[2]	Pfizer Ltd, Sandwich, UK

[1]Sept/Oct 2021 to early 2022 season

[2]Caused by *Neisseria meningitidis* groups A, C, W-135 and Y

All samples were stored at 4°C prior to analysis in accordance with the manufacturers' storage recommendations and were in date (according to the 'use by' date on the label) at the time of sample preparation and data acquisition.

Table 4.2. Falsified vaccine surrogates used for MALDI-ToF MS analysis.

Vaccine surrogates	Manufacturer	Batch/part number	Composition	Remarks
0.9% *w/v* sodium chloride injection	Demo S.A Pharmaceutical Industry	24598/0002	0.9% *w/v* NaCl in water for injection	Surrogate for falsified COVID-19 vaccines intercepted in China and India (Mumbai) (74)
5.0% *w/v* D-glucose	B/Braun	03551/0059	D-glucose 5.0% *w/v* Glucose solution prepared in distilled water	Surrogate for falsified COVID-19 vaccines intercepted in the Philippines (74)
Amikacin, 250 mg/ml	Hospira (used for the Sirius Biotyper)	05015997122159	250 mg/ml amikacin sulphate, sodium citrate, sodium metabisulphite and water for injection	Surrogate for falsified COVID-19 vaccines intercepted in India (74,269)
	MA Holder Tillomed Laboratories Ltd. (used for the bioMérieux VITEK-MS)	11311/0604	250 mg/ml amikacin sulphate, sodium metabisulfite, sodium citrate dihydrate, sulfuric acid and water for injection	
Gentamicin, 40 mg/ml	Demo S.A.	05208063001339	40 mg/ml gentamicin sulphate, 1.60 mg/ml sodium metabisulfite, disodium edetate	Surrogate for falsified non-COVID vaccines intercepted in Indonesia (74)

Hyaluronic acid	Guangzhou Ailian Cosmetic Co Ltd.	QB/T 2660	Anti-wrinkle serum containing water, glycerine, propylene glycol, methylisothiazolinone, bis(hydroxmethyl) imidazolidinyl urea, iodopropynyl butylcarbamate, disodium EDTA, xanthan gum, sodium hyaluronate	Surrogate for falsified COVID-19 vaccines intercepted in Poland (74,270) (the precise formulation and form of intercepted hyaluronic product is unknown, apart from it being reported to contain an anti-wrinkle formulation)
Tap water	Biochemistry/ Chemistry Research Laboratory, Oxford	N/A	Tap water	Tap water from the building water facility
Milli-Q water	Merck Millipore	N/A	Water from a Milli-Q Direct 8 water purification system	Purified double-distilled water
Water for injection	Demo S.A Pharmaceutical Industry	24598/001	Sterile water for the preparation of a medicine intended for injection or infusion	Water for injection in plastic ampoules

N/A, not applicable

In the degradation study, vaccine samples were exposed to five different temperature conditions: (i) vaccine was stored at 4°C (as the recommended 2-8°C storage condition, (ii) at RT (recorded as 20 ± 1 °C), (iii) in an incubator oven set at 37°C, (iv) in an incubator oven set at 45°C, and (v) vaccine was exposed to three freeze-thaw cycles of 24 hours freezing at -70°C and one hour thawing at 4°C per cycle. The exposure to different temperature conditions (4°C, RT, 37°C and 45°C) was performed for seven days. All samples were stored at 4°C after completing each incubation period.

4.2.1.2. MALDI-ToF sample preparation

Samples were spotted onto MS-DS target slides (bioMérieux, Basingstoke, UK) and prepared for analysis using manual spotting by mixing 1 µL of sample with 1 µL of matrix or with the help of an ASSIST PLUS pipetting robot equipped with an 8-channel 12.5 µL VOYAGER adjustable tip spacing pipette and 12.5 µL GripTip pipette tips (INTEGRA Biosciences, Zizers, Switzerland), for an automated spotting of matrix and samples onto the MALDI target plates, performed at the Department of Chemistry.

The spotting involves a dual reservoir adaptor fitted with a 25 mL divided reservoir (INTEGRA Biosciences) that holds the prepared α-cyano-4-hydroxycinnamic acid (HCCA/CHCA) matrix (bioMérieux, Basingstoke, UK) in deck position A of the robot. Samples were pipetted manually into a 96-well plate (Sarstedt, Nümbrecht, Germany) and placed in deck position B and the MALDI target plates were placed into a custom-built holder in position C. A pipetting programme was designed and uploaded to the VOYAGER pipette using the INTEGRA VIALAB software (version 2.1.1.0).

For all sample preparations, the matrix and samples were mixed in a 1:1 *v/v* ratio, and four replicates of 2 µL spots of the mixture were pipetted onto the MALDI target

plates. The target plates were air-dried prior to MALDI-MS analysis. Although a pipetting robot was used for the preparation of samples, it should be noted that this is not mandatory and was used for efficiency rather than necessity.

4.2.1.3. MALDI-MS data acquisition

Raw MS spectra were acquired using a bioMérieux VITEK-MS. Each sample spot on the MALDI target plate was measured over three overlapping *m/z* mass ranges: low mass (0-900 *m/z*), mid mass (700-2,500 *m/z*) and high mass (2,000-20,000 *m/z*). Prior to sample analysis, the VITEK-MS instrument was calibrated with Bruker antibiotic calibration standard MBT Star-ACS, and Bruker bacterial test standard (both from Bruker, Coventry, UK).

VITEK-MS data were acquired using the Shimadzu Biotech Launchpad software version 2.9.5.6 (Kratos Analytical, Manchester, UK). Parameters were as follows: laser power, 48; profiles, 100 per sample; shots, five accumulated per profile; maximum laser rep rate, 50.0. Pulsed extraction was optimised at 450 Da for *m/z* 0–900, 1,600 Da for *m/z* 700–2,500 and 13,000 Da for *m/z* 2,000–20,000. The regular circle bioMérieux CHCA raster was used with a diameter of 2 mm, 180 µm spacing and 109 points per target. The 'Parent Data Export' in the 'Method Editor' was set as mzXML for the raw data file. SARAMIS Target Manager was used to create a list of samples with corresponding spot locations that was exported to 'Experiment Genie' as a *.txt file. The *.txt file was opened in Microsoft Excel, and the acquisition sequence was randomised. In the auto experiment, the 4 × 48 Fleximass DS plate configuration was chosen, and the *.txt file was set as a standard file in 'Import Experiment Genie' before running the randomised acquisition sequence.

4.2.1.4. Data processing

Manual inspection of the raw mass spectra was performed by uploading the data files into the Shimadzu Biotech Launchpad software (version 2.9.5.6) from the VITEK-MS instrument. Raw spectra in *.mzXML format were imported into R Studio and processed in R v4.1.3 using the MALDIquant (271), MALDIrppa, caret, lattice, factoextra, and dendextend packages. Baseline correction was performed using a "TopHat" algorithm, and intensity calibration was performed with probabilistic quotient normalisation (PQN). Spectral alignment was performed using a half window size, signal-to-noise ratio (SNR) and tolerance of 7, 1, and 0.2, respectively. A locally weighted scatterplot smoothing (LOWESS) warping method was used. Peak detection used the same SNR and half window size parameters as previously defined, and peak binning was used at a tolerance of 0.1. The resulting peak intensity matrices were exported as a *.csv file for further analysis.

4.2.1.5. Statistical analysis and data visualisation

Statistical analysis of the processed peak intensity matrices and visualisation of the data were performed using MetaboAnalyst (version 5.0, https://metaboanalyst.ca) online analysis (272). The resulting peak list from MALDIquant (Supplementary File, available on Oxford University Research Archive (ORA)) was then analysed using the 'Statistical Analysis (one factor)' module of the MetaboAnalyst online software. Experimental data were uploaded as peak intensities in 'Samples in columns (unpaired)' format. Data filtering was done using the interquartile range (IQR) statistical filter to identify and remove variables that are unlikely to be of use when modelling the data. The data were

normalised by 'sum and pareto' (mean-centred and divided by the square root of the standard deviation of each variable) scaling. Unsupervised principal component analysis (PCA) and supervised multivariate analysis, partial least squares-discriminant analysis (PLS-DA), were used to model the data. The PLS-DA cross-validation (CV) was performed using a 5-fold CV method and eight maximum components to search. The permutation testing uses the 'separation distance method' and 100 permutation numbers (246). Hierarchical dendrogram clustering was performed using Euclidean distance measure and Ward clustering algorithm methods. Two-way analysis of variance with Dunnett multiple comparisons test was performed in GraphPad Prism (GraphPad Software, Boston, MA, USA; version 9.4.1). Statistical analysis figures and graphical representations were created using both MetaboAnalyst and GraphPad Prism.

4.2.2. MALDI-ToF analysis of COVISHIELD COVID-19 vaccine

The developed MALDI-ToF protocol (section 4.2.1 above) was then used to distinguish between the genuine COVISHIELD COVID-19 vaccine and surrogates of falsified vaccines. The non-invasive analysis of vaccine vial labels without opening the vial and analyses of vaccine excipients were performed.

4.2.2.1. COVISHIELD COVID-19 vaccine samples

Vaccine samples were shipped in a temperature-controlled container and stored at 4°C upon arrival (within the 2-8°C manufacturer's recommended storage condition) and kept on ice prior to spotting onto the MALDI plate. All samples were analysed within their date of expiry.

Table 4.3. COVISHIELD vaccine samples from two factory sites in India, used in this study. Batches 1 – 5 were from the Hadapsar factory, while batch 6 was from the Manjari factory

Batch group	Batch number	Number of vials
Batch 1	4122Z001	20
Batch 2	4122Z002	5
Batch 3	4122Z003	5
Batch 4	4122Z004	5
Batch 5	4122Z005	5
Batch 6	4121MC180	5

A total of 45 vials of genuine COVISHIELD COVID-19 vaccine samples from Serum Institute of India were received for the study. The vials came from five production batches at the Hadapsar factory (Batch 1-5) and the Manjari factory (Batch 6), both located in Pune, Maharashtra, India (Table 4.3). Three vials per batch were used for batch-to-batch analysis by MALDI-ToF MS with four technical replicates (a total of 12 replicates per batch). COVISHIELD vaccine contains the excipients L-histidine, L-histidine hydrochloride monohydrate, magnesium chloride hexahydrate, polysorbate 80, ethanol, sucrose, sodium chloride, and disodium edetate dihydrate (EDTA) (273).

4.2.2.2. Analysis of excipients made up in water

For the comparative vaccine excipient measurements, the following solutions were used: L-histidine in water (<15 mM; Sigma-Aldrich) and polysorbate 80 in water (<1% *w/v* Tween 80; Sigma-Aldrich). Commercially available polysorbate 80 from two different online markets (www.thesoapery.co.uk, referred to as 'manufacturer A', and www.cosmeticsmadeeasy.com, referred to as 'manufacturer B') were also prepared at

the same <1% *w/v* concentration. Although not necessarily identical, these were in the same concentrations as those used in the authentic vaccines.

4.2.2.3. Surrogates of falsified vaccines

Falsified vaccine samples seized in supply chains were not accessible and not included in this study. Hence, to assess the capability of the techniques tested to detect falsified COVID-19 vaccine products, surrogates for potential and intercepted falsified products were used (Table 4.2). Falsified vaccine constituents were identified from reports available in the public domain, both in the scientific and lay literature (74).

4.2.2.4. MALDI-ToF MS processing of vaccine samples

MALDI-ToF sample preparation (section 4.2.1.3 above) was performed in three biological replicates (N=3) with four technical replicates for each N. All samples used were within their expiry dates at the time of the experimental work. The mass ranges analysed were low mass (0-900 *m/z*), mid mass (700-2,500 *m/z*) and high mass (2,000-20,000 *m/z*) ranges.

4.2.2.5. Degraded COVISHIELD samples

To study the effect of temperature on the stability of the COVISHIELD vaccine, the following temperature conditions were investigated: vaccine vials stored at 4°C, vials stored for seven days at RT (recorded as 20 ± 1°C) and at elevated temperature conditions of 37°C, 45°C; and exposed to 100°C (boiled), respectively. In addition, some

vials were exposed to three freeze-thaw cycles. The boiled vials were placed inside a beaker of boiling water on a 100°C hot plate for 10 minutes. All samples were stored at 4°C after undergoing the above temperature conditions.

4.2.3. Vaccine vial label analysis

A small piece of the vaccine vial label (approximately 2 × 2 mm) was cut, in duplicate, from different batches of the COVISHIELD vaccine vials (N=3, with four technical replicates for each N). Self-adhesive office stationery labels (Avery, Raunds, UK; N=2, with four technical replicates for each N) were used for comparison. Each piece of the label was then thoroughly vortex-mixed in 10 µL of CHCA matrix to help dissolve the adhesive into solution and then incubated for 10 minutes at RT. A volume of two µL of the extract was spotted in quadruplicate onto a MALDI plate and run to generate MS spectra at 0-900 *m/z*, 700-2,500 *m/z*, and 2,000-20,000 *m/z* mass ranges.

4.2.4. Data analysis

Raw spectra were visually analysed and plotted using Shimadzu LaunchPad software. VITEK-MS raw data files were also acquired in *.mzXML format for analysis using MetaboAnalyst. Spectra (four spectra from four technical replicates for each N) were analysed using a workflow that combined MALDI-ToF with MALDIquant and MetaboAnalyst analyses described above (section 4.2.1.4 and 4.2.1.5) (246).

4.2.5. PLS-DA external validation and confusion matrices

For each significant PLS-DA model generated, external validation was performed by randomly selecting 10% of the data to use as an external test set. Confusion matrices were produced as previously described elsewhere (274).

In brief, PLS-DA models were generated using either the entire data set or 90% of each class randomly selected as a training set, which was then used to predict both the training and test sets. The accuracy of the PLS-DA predictions relative to the true classification of each sample is then summarised in confusion matrices using R code generated in-house (275) and the ropls (276) package.

4.3. Results

4.3.1. Analysis of vaccines and surrogates of falsified constituents by MALDI-ToF-MS

Four different authentic commercially available vaccines (Table 4.1) and eight falsified surrogates previously reported in falsified vaccine products (Table 4.2) were used for MALDI-ToF analysis, and spectra were acquired over three different overlapping *m/z* ranges: 0–900; 700–2,500, and 2,000–20,000.

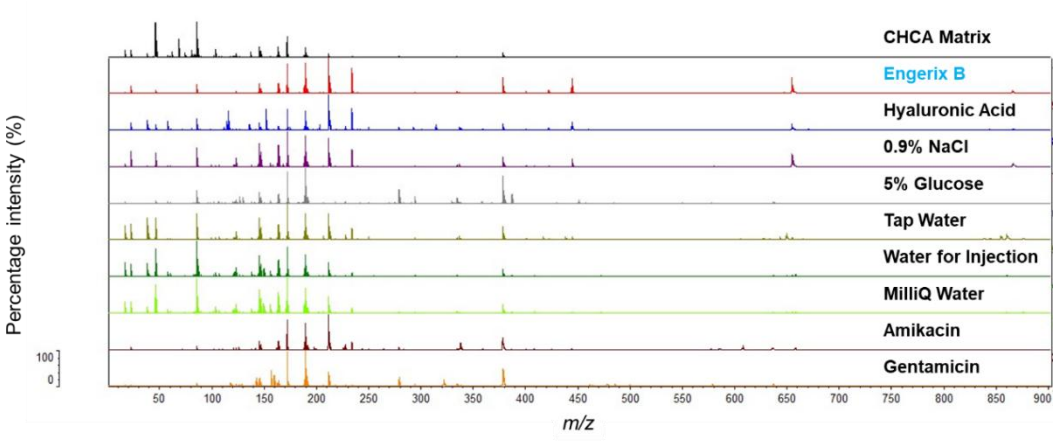

Figure 4.1. Representative VITEK-MS mass spectra for Engerix B vaccine (blue font) at 0-900 *m/z* compared to CHCA matrix and eight surrogates of falsified vaccine samples

Representative spectra for Engerix B and eight falsified constituent samples at 0-900 *m/z* mass ranges are shown in Figure 4.1. Visible peaks in the low mass range included CHCA matrix peaks (that were common to all samples and could be identified from matrix blanks), as well as analyte peaks related to the individual samples. Through the presence, absence and relative intensity ratios of peaks in the spectra, the genuine vaccine can be distinguished from the falsified constituents by manual inspection of the spectra.

Representative spectra for Ixiaro, Nimenrix, and Flucelvax, compared to the falsified constituent samples, are depicted in Figures 4.2, 4.3, and 4.4, respectively. Given the rich spectral data obtained in the 0-900 *m/z* range, where vaccine-specific excipients were found, we decided to focus on this *m/z* range for further analyses. Non-matrix peaks that were unique to either individual vaccines or falsified constituents were identified by manual inspection.

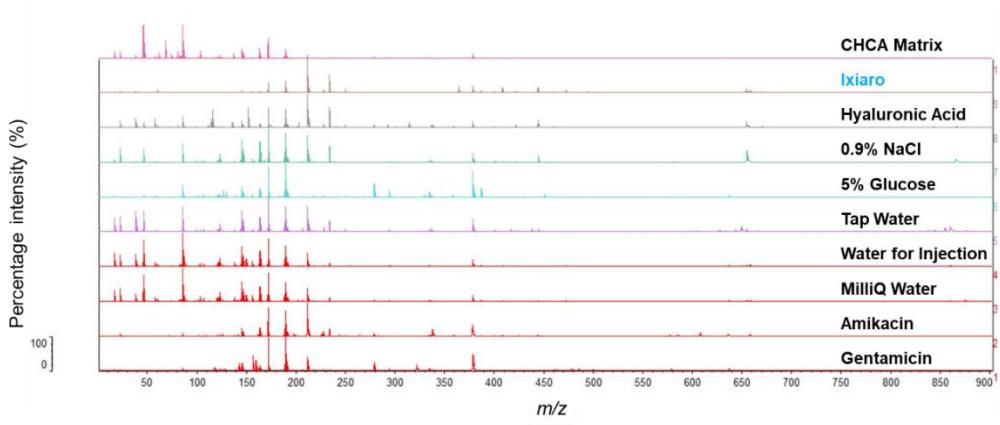

Figure 4.2. Representative VITEK-MS mass spectra for Ixiaro vaccine (blue font) at 0-900 *m/z* compared to CHCA matrix and eight surrogates of falsified vaccine samples

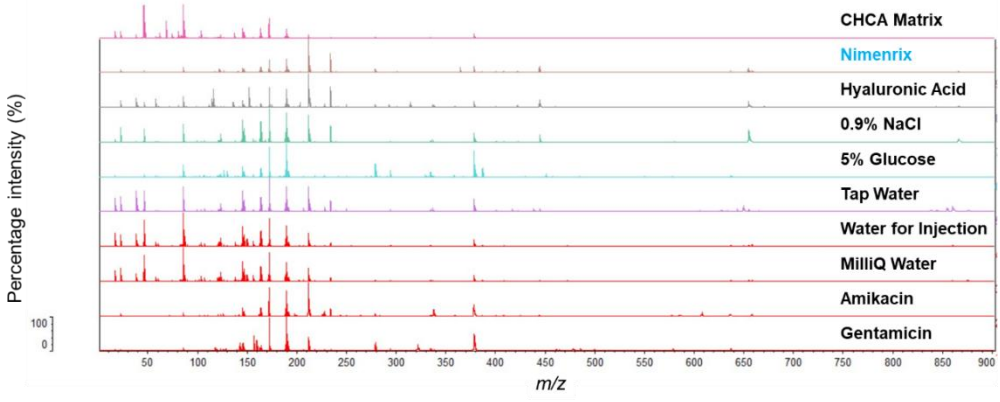

Figure 4.3. Representative VITEK-MS mass spectra for Nimenrix vaccine (blue font) at 0-900 *m/z* compared to CHCA matrix and eight surrogates of falsified vaccine samples

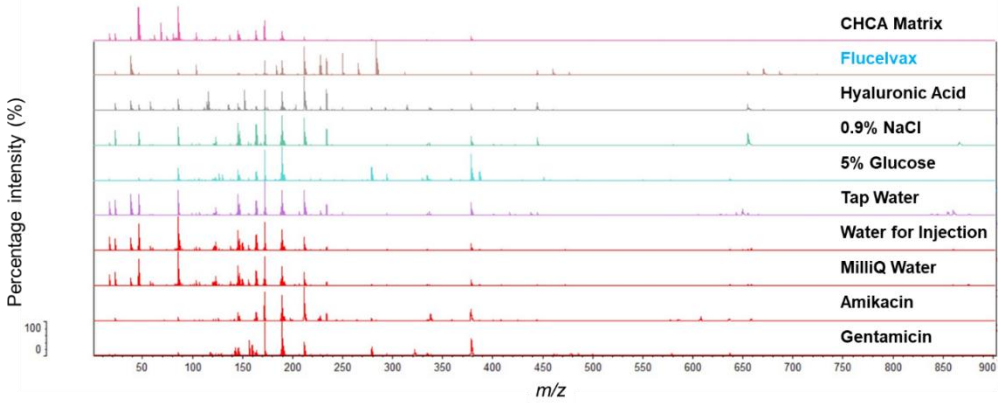

Figure 4.4. Representative VITEK-MS mass spectra for Flucelvax vaccine (blue font) at 0-900 *m/z* compared to CHCA matrix and eight surrogates of falsified vaccine samples

4.3.2. Analysis of MALDI-ToF spectra using multivariate analysis can differentiate between genuine vaccines and surrogates of falsified products

The hierarchical clustering reveals that each of the authentic vaccines and surrogate sample replicates were clustered together (Figure 4.5), except for water for injection and Milli-Q water, which grouped together. This result shows that the analysis workflow could differentiate between authentic and falsified vaccines.

To statistically model how well the data could distinguish the different sample groups, I compared each authentic vaccine with all the falsified vaccine samples using PLS-DA, commonly used in untargeted data modelling (277). To demonstrate that the PLS-DA models were reliable and not overfitting the datasets, CV, permutation testing and a modified external validation (confusion matrix) for each model were performed. The PLS-DA multivariate analysis could distinguish between authentic vaccines and surrogates of falsified constituents (Figure 4.6). Vaccine samples could be readily distinguished from the surrogates (Figure 4.6 A), with some overlap between Ixiaro and Nimenrix vaccines. The reliability test showed that the model was not overfitting (Figure 4.6 B-D). PLS-DA modelling demonstrates that the MALDI MS workflow was able to reliably tell apart each genuine vaccine from all the falsified constituents.

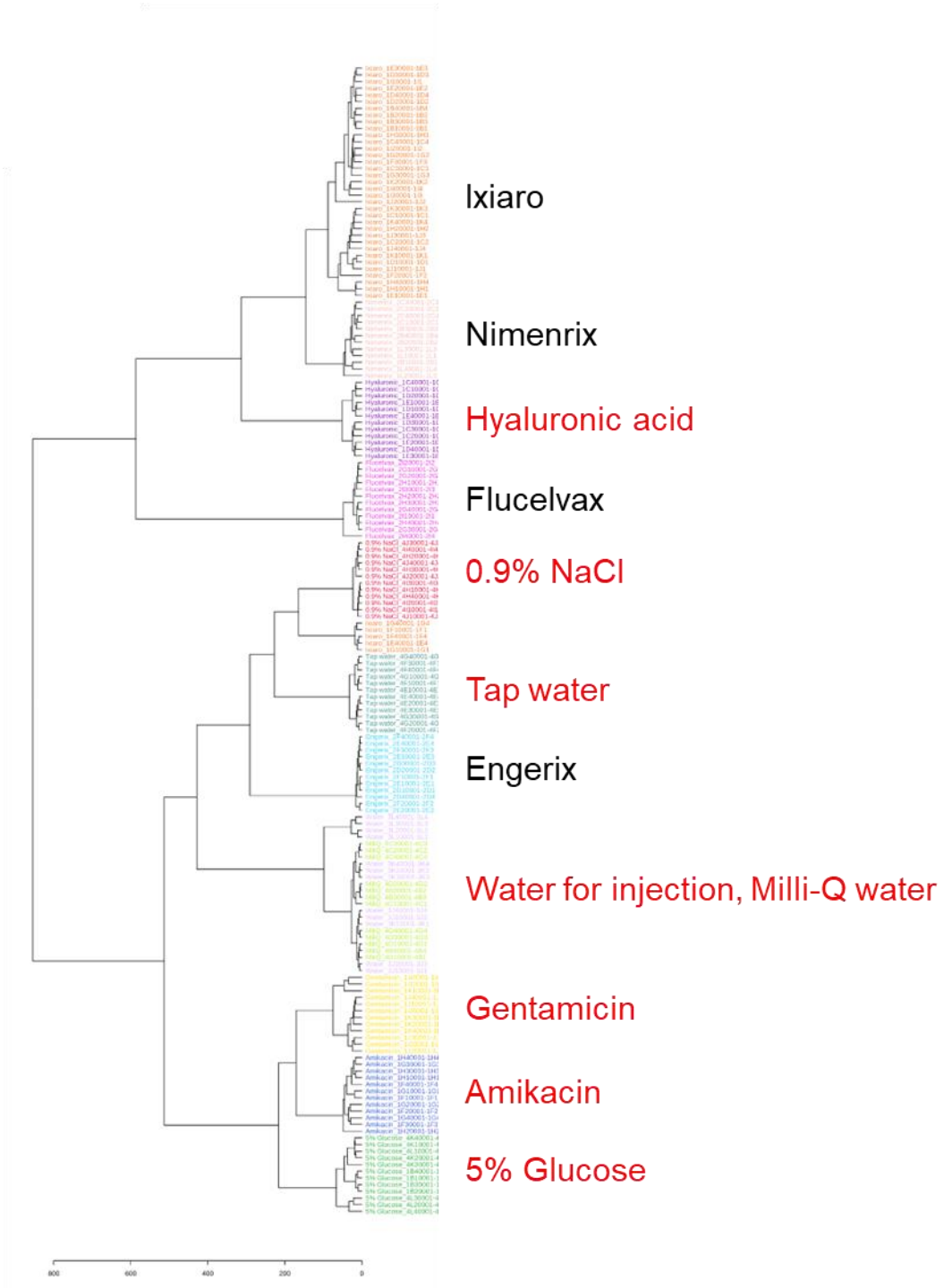

Figure 4.5. Multivariate statistical analysis and hierarchical clustering (Euclidean distance measure and a Ward clustering algorithm) of samples based on the analysis of MALDI-ToF spectra. Four authentic vaccines (black font) and eight surrogates of falsified vaccine samples (red font) show the clustering of each sample group into a single clade, except for water for injection and Milli-Q water.

A

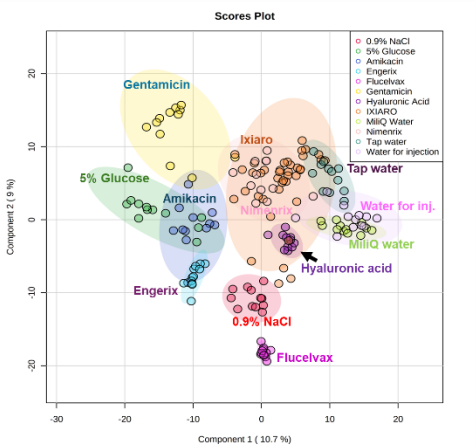

B

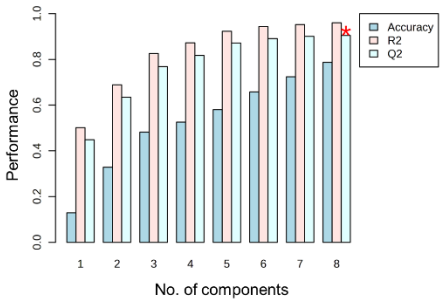

C

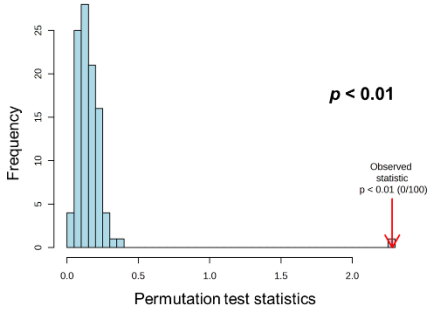

D

Measure	1 component	2 components	3 components	4 components	5 components	6 components	7 components	8 components
Accuracy	0.12838	0.32825	0.48147	0.52562	0.5799	0.65786	0.72407	0.78744
R2	0.501	0.68844	0.82577	0.87213	0.92265	0.94345	0.95248	0.96013
Q2	0.4488	0.63395	0.76854	0.81707	0.87174	0.89151	0.90106	0.90488

Figure 4.6. PLS-DA of peak list generated by the VITEK MS instrument from four genuine vaccines and eight falsified vaccine constituents. A. PLS-DA score plot shows sample group clustering, B. The cross-validation result shows a minimum of 8 components (mass spectral peaks) are required to differentiate the experimental groups for the best Q2 value (shown by *), C. Permutation testing shows the model is significant with a p-value of <0.01, D. R2, Q2, and accuracy values for the cross-validation

4.3.3. Confusion matrices of genuine vaccines versus surrogates of falsified products

External validation of genuine vaccines and surrogate spectra datasets was performed by generating tabulated values and presenting them as confusion matrices. The models were first created using the training set (90% of the data), and then the classifications were confirmed using the test set (an external test set, 10% of the data) which had not been seen by the model previously). The 'all data' matrices were then generated (Table 4.4 – 4.7).

Similar results were obtained when comparing the genuine vaccines with all falsified vaccine surrogates. Confusion matrices show that the authentic vaccines were identified correctly. Taken together, the PLS-DA modelling demonstrates that the MALDI-ToF MS analysis workflow was able to reliably tell apart each genuine vaccine from all falsified constituents tested in this study.

4.3.4. Inter- and intra-batch analyses of a COVID-19 vaccine

The inter- and intra-batch analyses were performed on genuine COVISHIELD vaccine vials. Using the generated peak list, PCA score plots of the first two most significant principal components showed no differences between batches (Figure 4.7 A) and between vials with the same batch number (Figure 4.7 B). These can be observed by the overlapping 95% confidence regions, shown as coloured elliptic areas.

Table 4.4. Confusion matrix of Engerix B vaccine (blue font) and surrogates of falsified vaccine using the 'all-data' dataset from spectra generated using MALDI-ToF mass spectrometry (N=12)

Vaccine and surrogates	Amikacin	Engerix B	Gentamicin	Glucose	Hyaluronic Acid	Milli-Q water	NaCl (0.9%)	Tap water	Water for injection
Amikacin	12	0	0	0	0	0	0	0	0
Engerix B	0	12	0	0	0	0	0	0	0
Gentamicin	0	0	12	0	0	0	0	0	0
Glucose	0	0	0	12	0	0	0	0	0
Hyaluronic Acid	0	0	0	0	12	0	0	0	0
Milli-Q water	0	0	0	0	0	12	0	0	0
NaCl (0.9%)	0	5	0	0	0	0	7	0	0
Tap water	0	0	0	0	0	0	0	12	0
Water for injection	0	0	0	0	0	8	0	1	3

Table 4.5. Confusion matrix of Flucelvax vaccine (blue font) using the 'all-data' dataset from spectra generated using MALDI-ToF mass spectrometry (N=12)

Vaccine and surrogates	Amikacin	Flucelvax	Gentamicin	Glucose	Hyaluronic Acid	Milli-Q water	NaCl (0.9%)	Tap water	Water for injection
Amikacin	12	0	0	0	0	0	0	0	0
Flucelvax	0	12	0	0	0	0	0	0	0
Gentamicin	0	0	12	0	0	0	0	0	0
Glucose	0	0	0	12	0	0	0	0	0
Hyaluronic Acid	0	0	0	0	12	0	0	0	0
Milli-Q water	0	0	0	0	0	12	0	0	0
NaCl (0.9%)	0	0	0	0	0	0	12	0	0
Tap water	0	0	0	0	0	0	0	12	0
Water for injection	0	1	0	0	0	8	0	0	3

Table 4.6. Confusion matrix of Nimenrix vaccine (blue font) and surrogates of falsified vaccine using the 'all-data' dataset from spectra generated using MALDI-ToF mass spectrometry (N=12)

Vaccine and surrogates	Amikacin	Gentamicin	Glucose	Hyaluronic Acid	Milli-Q water	NaCl (0.9%)	Nimenrix	Tap water	Water for injection
Amikacin	12	0	0	0	0	0	0	0	0
Gentamicin	0	12	0	0	0	0	0	0	0
Glucose	0	0	12	0	0	0	0	0	0
Hyaluronic Acid	0	0	0	12	0	0	0	0	0
Milli-Q water	0	0	0	0	12	0	0	0	0
NaCl (0.9%)	0	0	0	0	0	12	0	0	0
Nimenrix	0	0	0	0	0	0	12	0	0
Tap water	0	0	0	0	0	0	0	12	0
Water for injection	0	0	0	0	8	0	0	1	3

Table 4.7. Confusion matrix of Ixiaro vaccine (blue font) and surrogates of falsified vaccine using the 'all-data' dataset from spectra generated using MALDI-ToF mass spectrometry (N=12)

Vaccine and surrogates	Amikacin	Gentamicin	Glucose	Hyaluronic Acid	Ixiaro	Milli-Q water	NaCl (0.9%)	Tap water	Water for injection
Amikacin	12	0	0	0	0	0	0	0	0
Gentamicin	0	12	0	0	0	0	0	0	0
Glucose	0	0	12	0	0	0	0	0	0
Hyaluronic Acid	0	0	0	12	0	0	0	0	0
Ixiaro	0	0	0	0	12	0	0	0	0
Milli-Q water	0	0	0	0	0	12	0	0	0
NaCl (0.9%)	0	0	0	0	0	0	12	0	0
Tap water	0	0	0	0	0	0	0	12	0
Water for injection	0	0	0	0	0	8	0	0	4

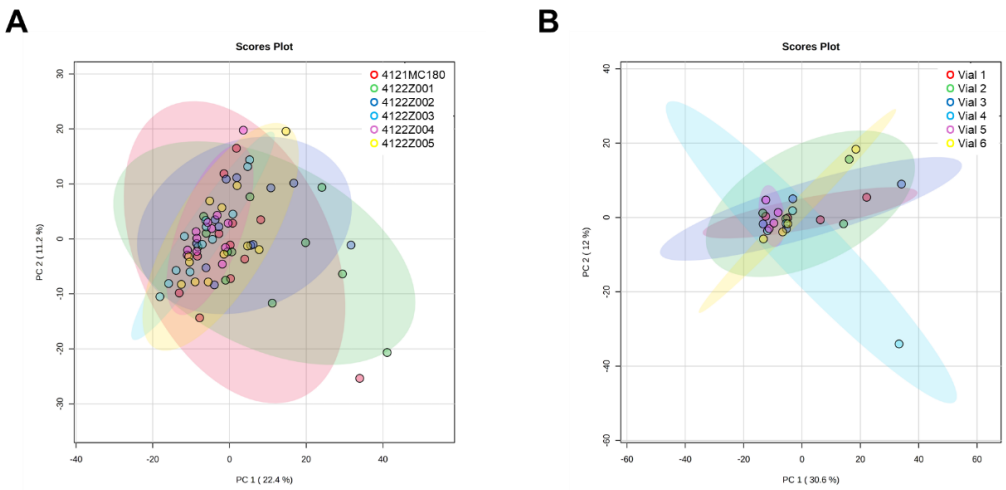

Figure 4.7. PCA analyses of the MALDI-ToF MS spectra generated from COVISHIELD COVID-19 vaccine batches. PCA score plots were generated for A. Six different batch numbers of COVISHIELD vaccine (inter-batch analysis, N=3 for each batch number, with four technical replicates for each N, generating a total of 12 spectra replicates); and B. Six vaccine vials of the same batch number 4122Z001 (intra-batch analysis, N=3, each vial has four technical replicates)

4.3.5. Detection of vaccine excipient masses using MALDI-ToF MS

In an attempt to identify COVISHIELD vaccine constituents using MALDI-ToF MS, visual inspection of the spectra at 0-900 *m/z* revealed the presence of a peak at 156 *m/z* which corresponded to the nominal mass for the excipient L-histidine (molecular weight 155.15 g/mol) in a protonated form ($[M+H]^+$) that was not detected in the matrix spectra (Figure 4.8 A). L-histidine was made up in water as a standard and analysed by MALDI-ToF MS. As expected, a peak at 156 *m/z* was observed, which aligned with the 156 *m/z* peak in the COVISHIELD vaccine.

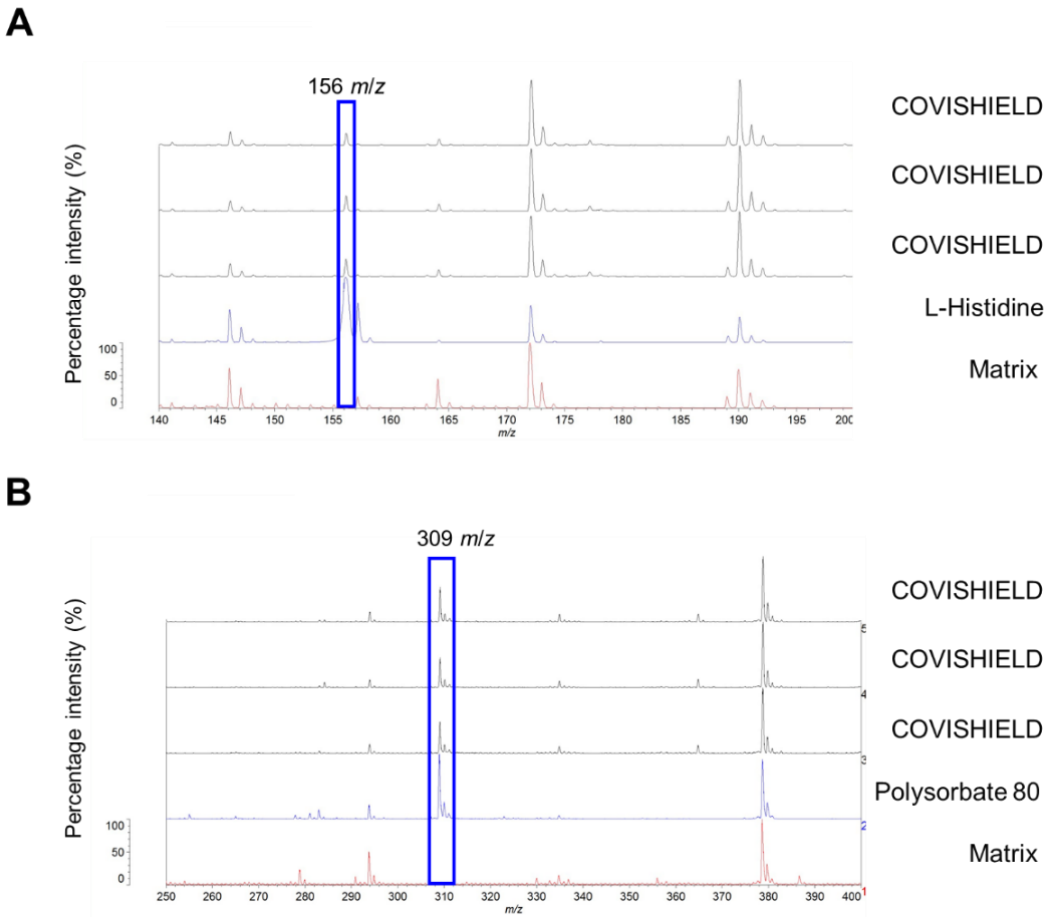

Figure 4.8. Identification of COVISHIELD COVID-19 vaccine constituents at 0-900 m/z using VITEK-MS. A. The presence of L-histidine was marked by a peak at 156 *m/z*, while a low mass peak of polysorbate 80 was detected at 309 *m/z*, B. The COVISHIELD spectra from three different vials of vaccine batch 4122Z001 are shown and compared to polysorbate 80 and matrix spectra.

The spectra for the excipient polysorbate 80, which was made up in water as a standard, showed a unique peak at 309 *m/z* (Figure 4.8 B) and as a series of evenly spaced peaks in the mid-mass range 700-2,500 *m/z* (Figure 4.9 B) and in the high mass range 2,000-20,000 *m/z* (Figure 4.10) that were not observed in the spectra of the surrogates but were seen in the genuine COVISHIELD vaccine. In the high mass range, most of these evenly spaced peaks for polysorbate 80 in COVISHIELD were seen from 2,000 to 4,000 *m/z* (Figure 4.11).

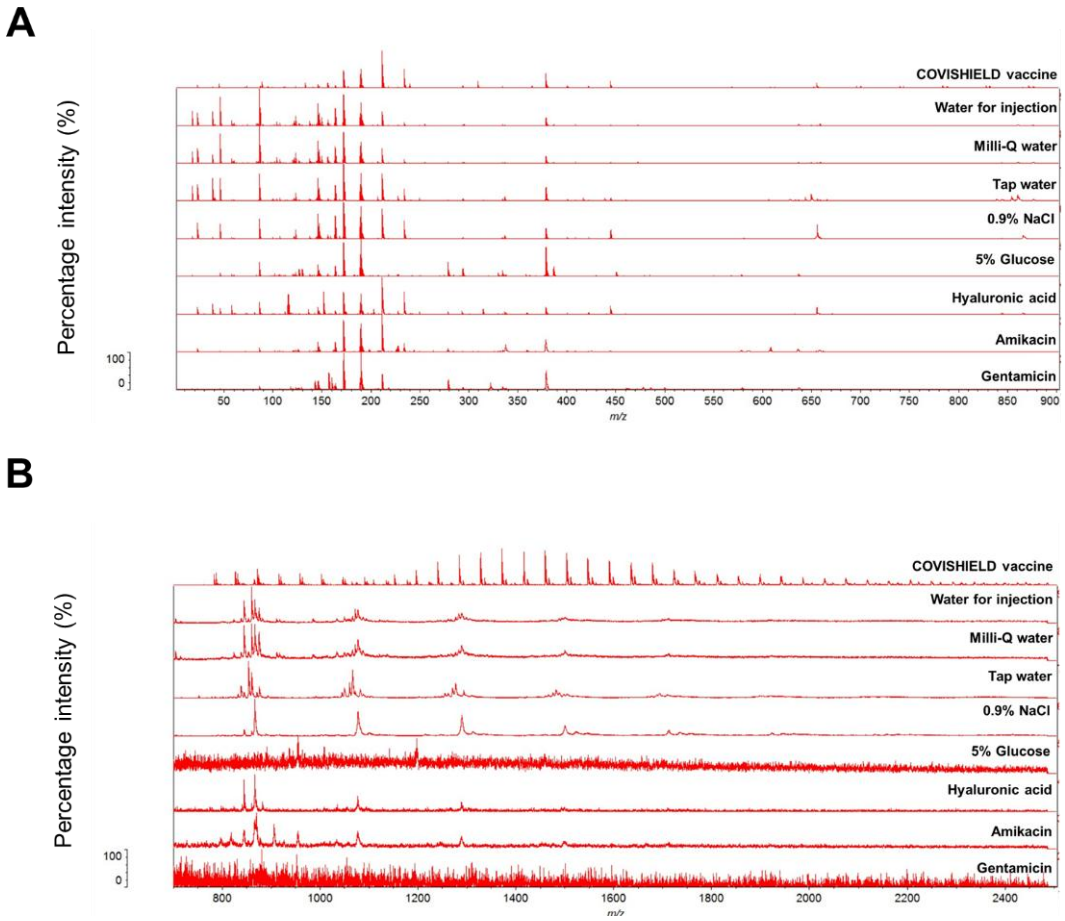

Figure 4.9. VITEK-MS spectra for COVISHIELD vaccine and eight falsified vaccine surrogates. Spectra were generated at A. 0-900 *m/z* and B. 700-2500 *m/z* mass ranges.

4.3.6. Differentiation of genuine COVISHIELD COVID-19 vaccine and surrogates of falsified vaccines

MALDI-ToF MS was used to differentiate between the genuine COVISHIELD vaccine and surrogates of falsified vaccines. Different spectral peaks could be visually observed in the low 0-900 (Figure 4.9 A) and mid 700-2,500 *m/z* (Figure 4.9 B) mass ranges when comparing the spectra of the genuine vaccine alongside eight surrogates. COVISHIELD vaccine could be readily distinguished from other surrogates of falsified products at the

2,000-4,000 *m/z* mass range (Figure 4.10), as well as at the 2,000-20,000 *m/z* mass range that is routinely used in microbial identification (Figure 4.11).

The spectral profile of polysorbate 80 was reproducible among the six batches of COVISHIELD vaccine (Figure 4.12 A). However, the peaks for polysorbate 80 from other manufacturers (Figure 4.12 B) were different and could be well separated by PCA analysis (Figure 4.12 C).

The PCA score plots showed a distinct separation of the COVISHIELD vaccine from all falsified vaccine surrogates (Figure 4.13 A), without any overlap in the 95% confidence regions. This was supported by the PLS-DA results with additional CV and permutation tests (Figure 4.13 C-E), which demonstrated perfect separation of all groups. To confirm the robustness of the PLS-DA model and investigate its potential to identify vaccine surrogates from previously unseen data, external validation was applied by splitting the data into training (90%) and test (10%) sets. This model was able to distinguish between COVISHIELD vaccine and all falsified vaccine surrogates with 100% accuracy in both the training and the external validation test sets with a 90/10 split (Table 4.9).

Amikacin has been used as a falsified COVISHIELD COVID-19 vaccine intercepted in India during the pandemic (74). When analysing only COVISHIELD and amikacin, the PCA score plots could differentiate between them (Figure 4.13 B). This was also supported by the PLS-DA score plot with good CV (high accuracy, R2, and Q2 scores) and significant permutation test ($p < 0.01$) results (Figure 4.13 C-E) and perfect accuracy of external validation confusion matrices (Table 4.8). Dendrogram analysis revealed the clustering of COVISHIELD samples into a monophyletic group (Figure 4.14). Other surrogates also clustered into separate groups in the dendrogram, except for the Milli-Q water and water for injection, since both are purified water and, as expected, had similar spectra (Figure 4.14).

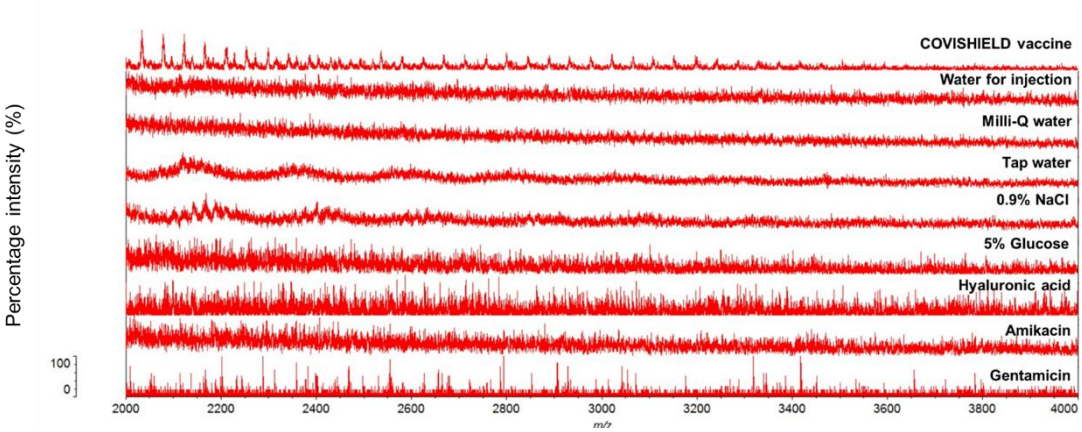

Figure 4.10. MALDI-ToF MS spectra for COVISHIELD vaccine and eight falsified vaccine surrogates at mid-mass range 2,000-4,000 *m/z*

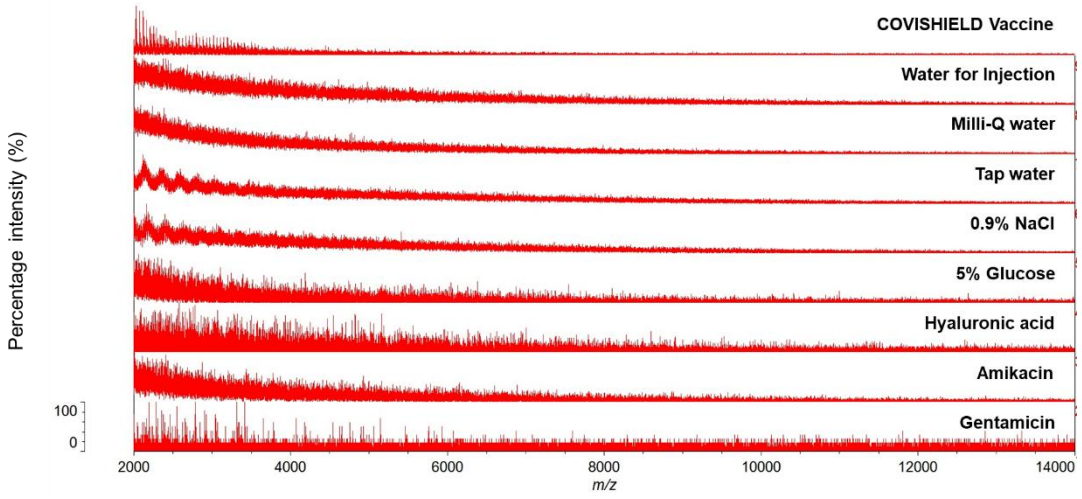

Figure 4.11. MALDI-ToF MS spectra for COVISHIELD vaccine and eight falsified vaccine surrogates at high mass range 2,000-20,000 *m/z* (shown up to 14,000 *m/z*)

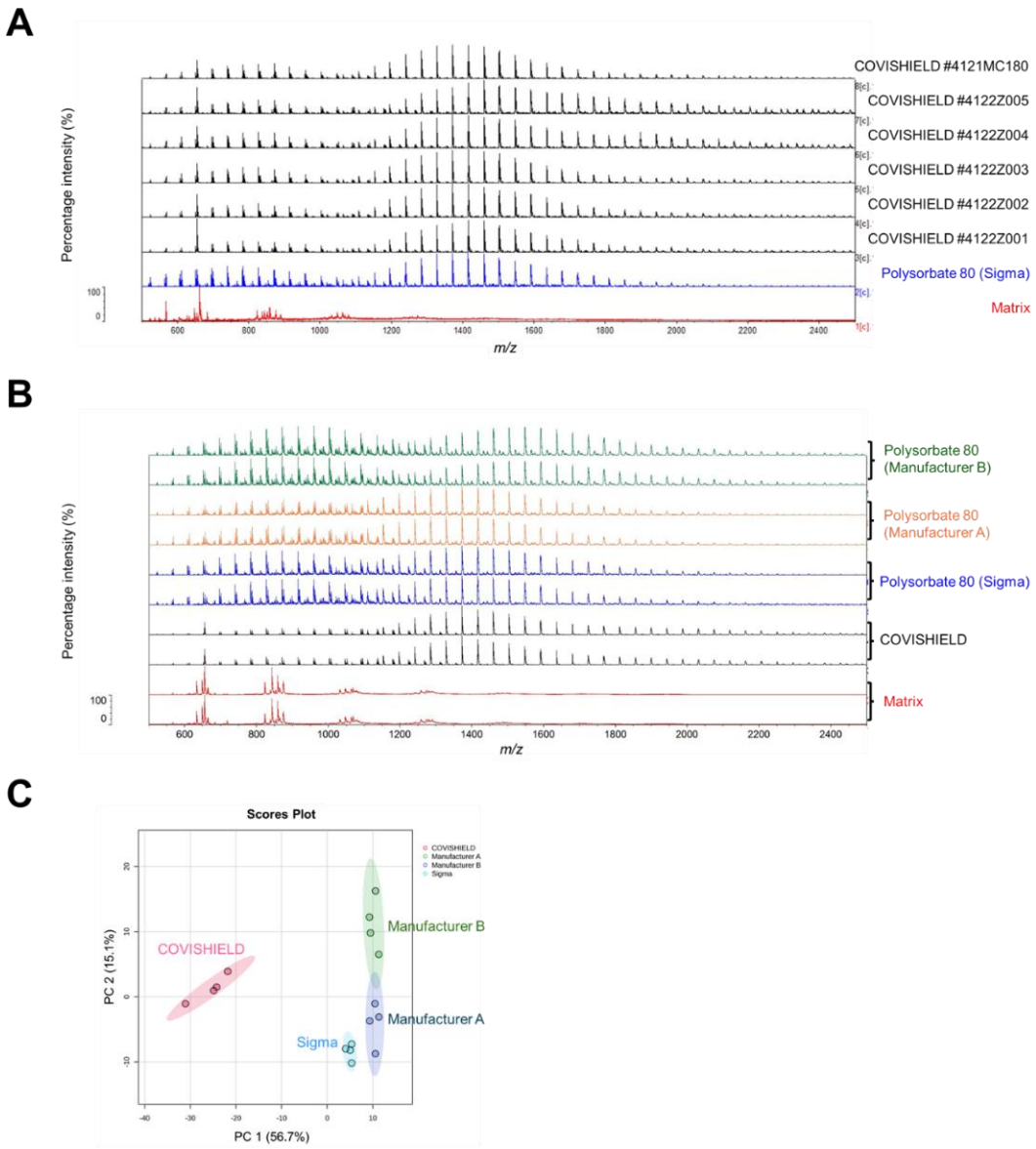

Figure 4.12. MALDI-ToF MS spectra (500-2,500 *m/z*) comparison between the COVISHIELD vaccine and commercially available polysorbate 80 samples. A. Spectra of six different batches of COVISHIELD vaccine and commercial research grade polysorbate 80 (Sigma-Aldrich). B. Spectra comparison between COVISHIELD and polysorbate 80 from three different manufacturers. C. PCA score plot showing the distinct grouping of COVISHIELD and polysorbate 80 from three different manufacturers. Samples were run with four technical replicates for each, and only two representative spectra are shown.

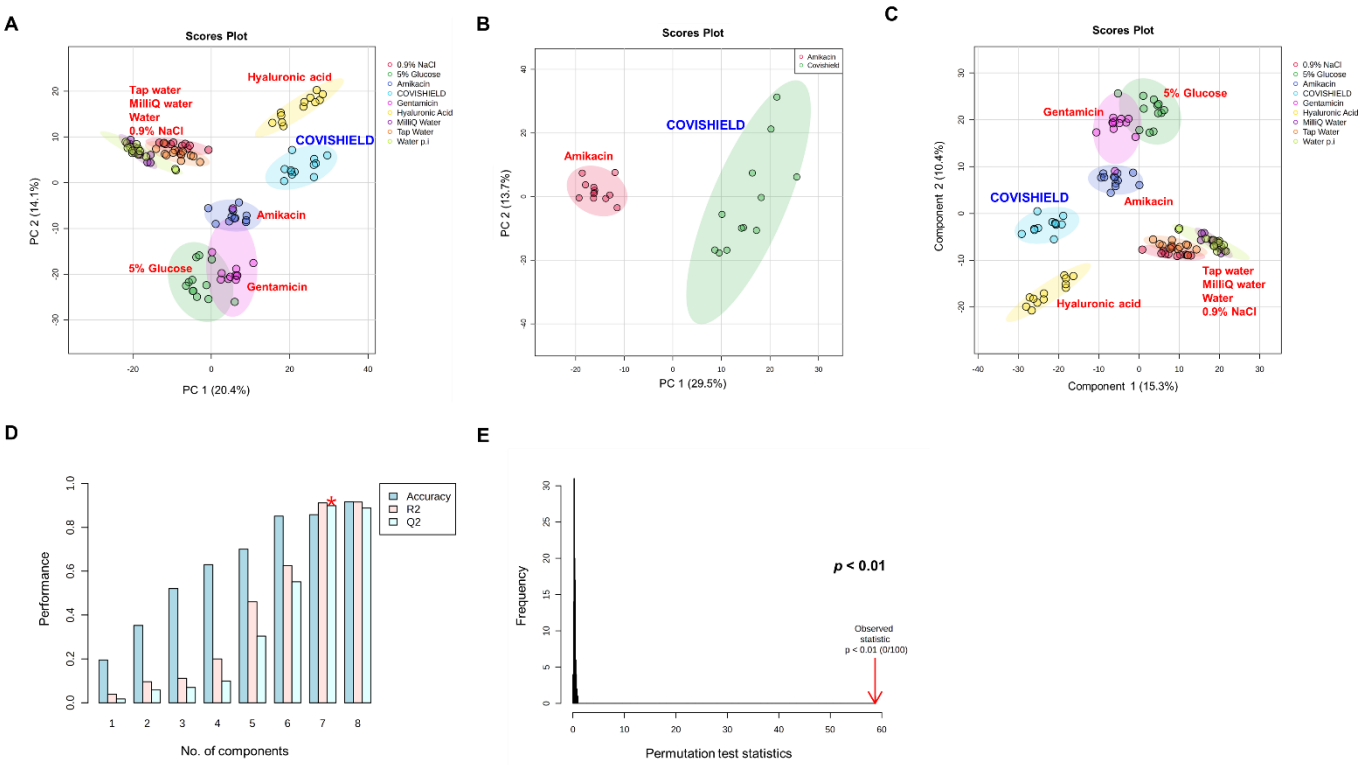

Figure 4.13. Multivariate analyses of the MALDI-ToF MS spectra generated from genuine COVISHIELD COVID-19 vaccine samples and eight surrogates of falsified vaccines. PCA score plots were generated from analysis of peak list data over the 0-900 *m/z* mass range (N = 3 with four technical replicates for each N) for A. COVISHIELD vaccine as compared to eight common falsified vaccine constituents and B. COVISHIELD compared to amikacin only, along with C. PLS-DA score plots, D. PLS-DA cross-validation results, and E. PLS-DA permutation analysis. The elliptical area reflects a region within the 95% confidence interval of the measurement.

Table 4.8. External validation and confusion matrix analysis results for PLS-DA data from Figure 4.13 comparing COVISHIELD (blue font) with surrogates of falsified vaccines using a 90/10 split of training/test parameters

Full dataset

	0.9% NaCl	5% Glucose	Amikacin	COVISHIELD	Gentamicin	Hyaluronic Acid	MilliQ Water	Tap Water	Water for injection
0.9% NaCl	12	0	0	0	0	0	0	0	0
5% Glucose	0	12	0	0	0	0	0	0	0
Amikacin	0	0	12	0	0	0	0	0	0
COVISHIELD	0	0	0	12	0	0	0	0	0
Gentamicin	0	0	0	0	12	0	0	0	0
Hyaluronic Acid	0	0	0	0	0	12	0	0	0
MilliQ Water	0	0	0	0	0	0	12	0	0
Tap Water	0	0	0	0	0	0	0	12	0
Water for injection	0	0	0	0	0	0	8	0	4

Test set

	0.9% NaCl	5% Glucose	Amikacin	COVISHIELD	Gentamicin	Hyaluronic Acid	MilliQ Water	Tap Water	Water for injection
0.9% NaCl	2	0	0	0	0	0	0	0	0
5% Glucose	0	2	0	0	0	0	0	0	0
Amikacin	0	0	2	0	0	0	0	0	0
COVISHIELD	0	0	0	2	0	0	0	0	0
Gentamicin	0	0	0	0	2	0	0	0	0
Hyaluronic Acid	0	0	0	0	0	2	0	0	0
MilliQ Water	0	0	0	0	0	0	2	0	0
Tap Water	0	0	0	0	0	0	0	2	0
Water for injection	0	0	0	0	0	0	0	0	2

Training set

	0.9% NaCl	5% Glucose	Amikacin	COVISHIELD	Gentamicin	Hyaluronic Acid	MilliQ Water	Tap Water	Water for injection
0.9% NaCl	10	0	0	0	0	0	0	0	0
5% Glucose	0	10	0	0	0	0	0	0	0
Amikacin	0	0	10	0	0	0	0	0	0
COVISHIELD	0	0	0	10	0	0	0	0	0
Gentamicin	0	0	0	0	10	0	0	0	0
Hyaluronic Acid	0	0	0	0	0	10	0	0	0
MilliQ Water	0	0	0	0	0	0	10	0	0
Tap Water	0	0	0	0	0	0	0	10	0
Water for injection	0	0	0	0	0	0	0	0	10

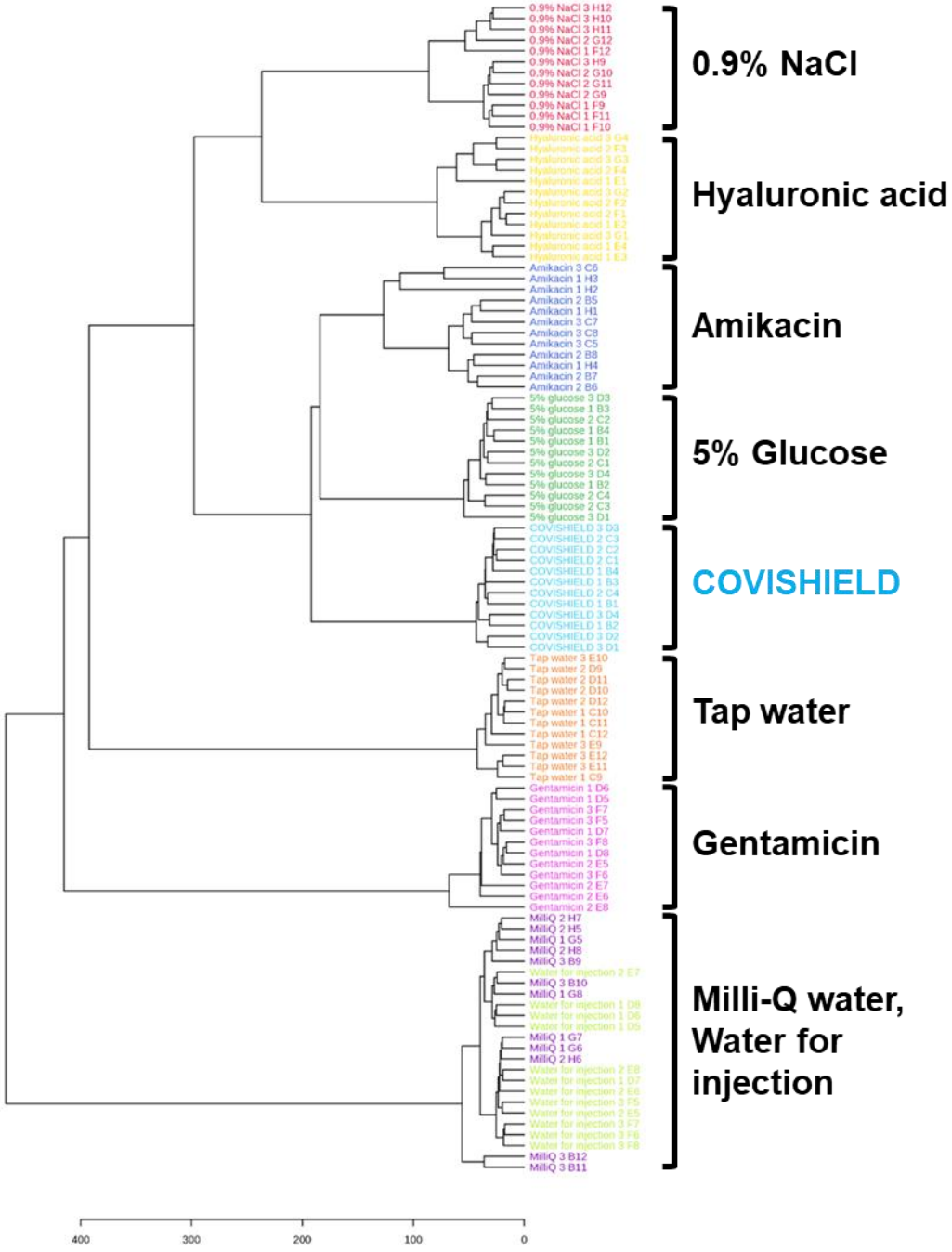

Figure 4.14. Dendrogram analysis of the MALDI-ToF MS spectra at 0-900 *m/z* for COVISHIELD vaccine compared to eight surrogates of falsified vaccine constituents (N = 3, with four technical replicates for each N).

4.3.7. Effect of altered temperature on the spectra

To explore vaccine degradation, vaccine samples were exposed to different temperature conditions, followed by comparison using MALDI-ToF analysis. Multivariate analysis of vaccine spectra showed no difference between degradation conditions, as depicted by the plotting of samples with overlapping 95% confidence regions of PCA (Figure 4.15 A). Further, PLS-DA resulted in a non-significant model (Figure 4.15 B) with low CV scores (Figure 4.15 C) and a non-significant permutation test (Figure 4.15 D). The high R2 of this model shows signs of overfitting. No significant differences were observed when analysing spectra from the mid-mass (700-2,500 *m/z*) and high-mass (2,000-20,000 *m/z*) ranges (Figure 4.16).

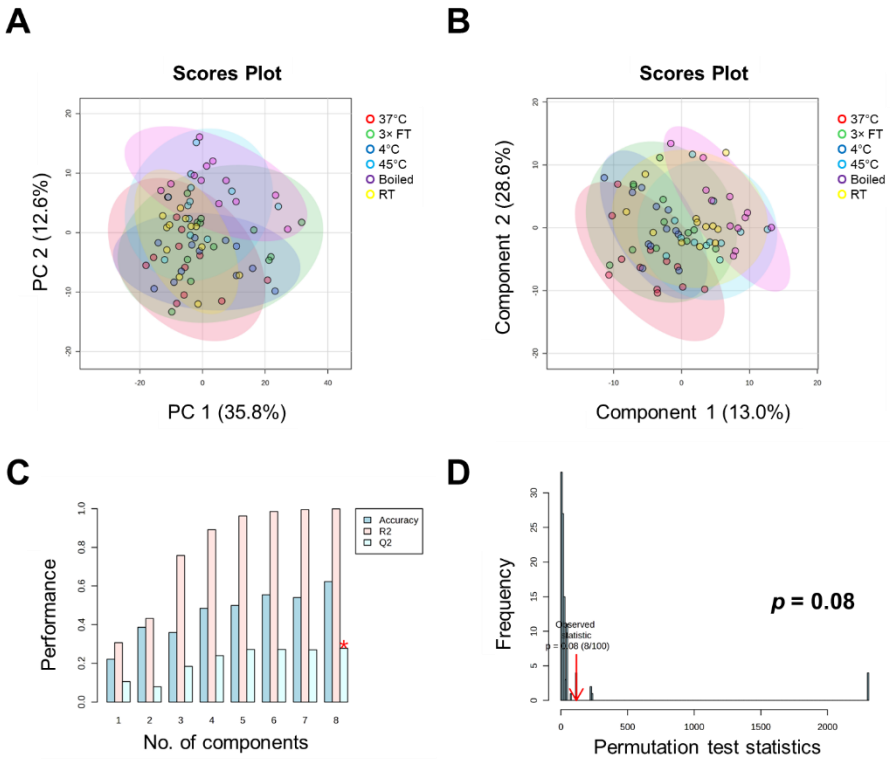

Figure 4.15. MALDI-ToF MS analysis at 0-900 *m/z* comparing COVISHIELD vaccine vials exposed to freeze-thaw cycles and different temperature conditions (three vials run (N=3, with four technical replicates for each N). A. PCA score plot, B. PLS-DA score plot, C. PLS-DA cross-validation results, and D. PLS-DA permutation analysis

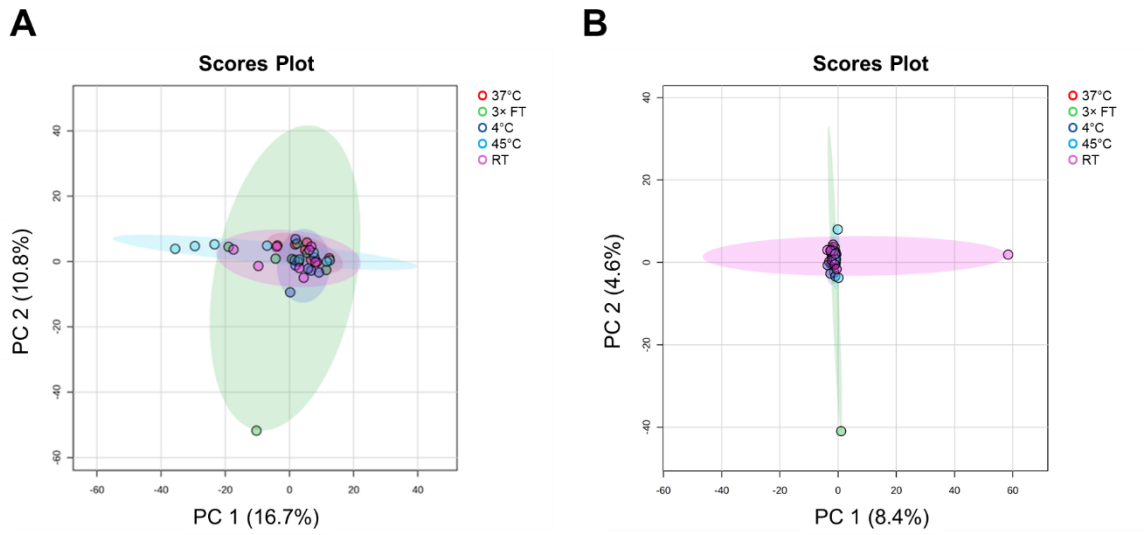

Figure 4.16. VITEK-MS PCA score plot analysis results comparing COVISHIELD vaccine vials exposed to freeze-thaw cycles and different temperature conditions (N=8). Score plots were generated from spectra data at A. 700-2,500 *m/z* and B. 2,000-20,000 *m/z*

4.3.8. Analysis of vaccine vial labels

For proof-of-concept, I investigated whether MALDI-ToF MS analysis could also be used to identify differences in the chemical composition between vaccine vial label extracts from genuine COVISHIELD labels and an office stationery label (Figure 4.17). The spectra for genuine COVISHIELD labels were found to be remarkably different from that of the office stationery label, and differences could easily be identified simply by visualising the spectra (Figure 4.17 A) and without needing to perform any statistical analysis of the spectral data. In addition, PCA (Figure 4.17 B) and PLS-DA (Figure 4.17 C) score plots of the genuine and stationery label spectra showed clear separation with no overlap of the 95% confidence regions and significant CV and permutation results (Figure 4.17 D-E). This was confirmed by external validation, which demonstrated that the PLS-DA model was able to distinguish between vaccine labels with 100% accuracy in the training and test sets using a 90/10 split

(Table 4.9). When comparing peaks derived from genuine COVISHIELD labels and the office stationery label, t-test statistical analysis revealed a total number of 395 significant (p<0.05) peaks with the peak at 534 *m/z* as the variable of importance in projection with the highest score based on PLS-DA analysis, shown as the base peak for the office stationery label (Figure 4.17 A). PCA could further distinguish between labels used in different batches of COVISHIELD vials produced in Hadapsar and Manjari factories, although some overlapping of the 95% confidence regions were observed (Figure 4.18 A). In addition, this was supported by a robust PLS-DA model, shown by high accuracy, R2, and Q2 scores and a significant permutation test (Figure 4.18 B-D) with perfect accuracy of the model on the training and test data sets using a 90/10 split (Table 4.10).

Table 4.9. External validation and confusion matrix analysis results for PLS-DA data from Figure 4.17 comparing genuine COVISHIELD vaccine vial label, office stationery label, and matrix using a 90/10 split of training/test parameters

Full dataset

	COVISHIELD	Matrix	Office label
COVISHIELD	48	0	0
Matrix	0	8	0
Office label	0	0	8

Test set

	COVISHIELD	Matrix	Office label
COVISHIELD	5	0	0
Matrix	0	1	0
Office label	0	0	1

Training set

	COVISHIELD	Matrix	Office label
COVISHIELD	43	0	0
Matrix	0	7	0
Office label	0	0	7

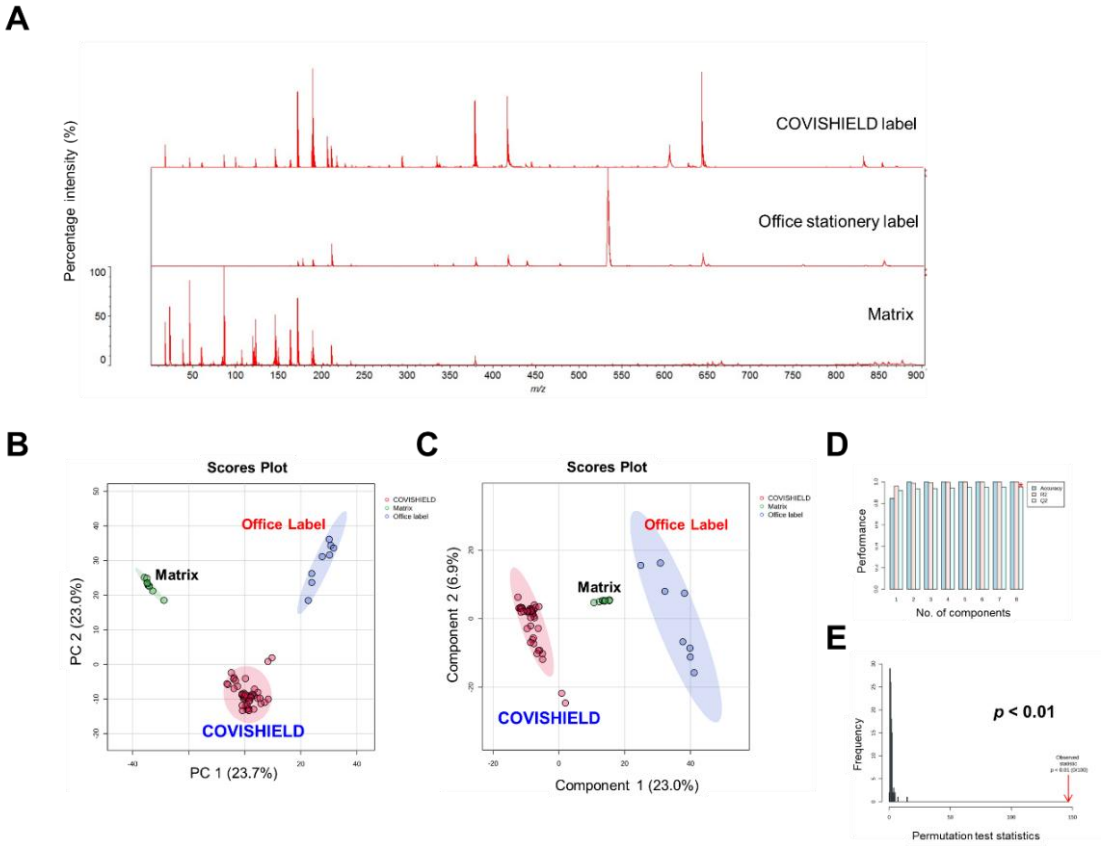

Figure 4.17. MALDI-ToF MS analysis of labels over the 0-900 *m/z* mass range comparing COVISHIELD label extracts from six batches (N=2), an office stationery label (N=2), and the CHCA matrix as a background control (N=2), with four technical replicates for each N. A. The 0-900 *m/z* representative spectra of label extracts and matrix, B. multi-variate analysis PCA score plot, C. PLS-DA score plot, D. PLS-DA cross-validation results, and E. PLS-DA permutation analysis

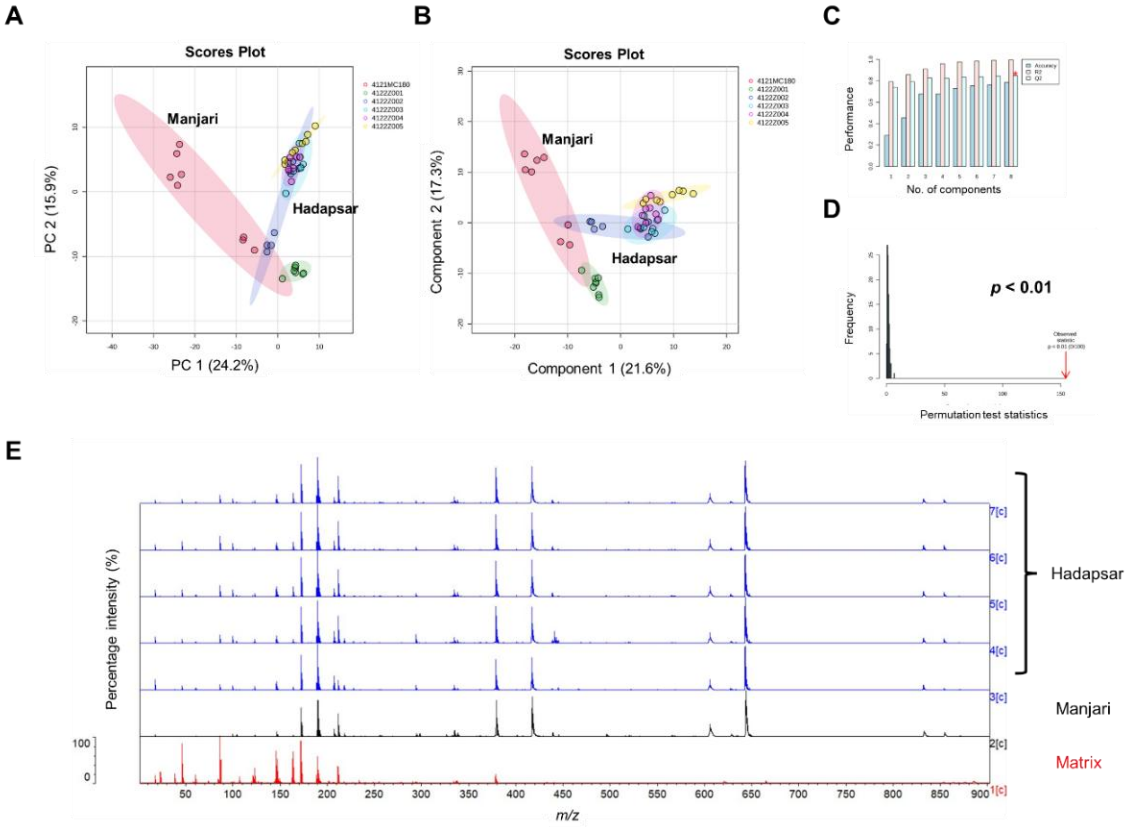

Figure 4.18. MALDI-ToF MS analysis over the 0-900 *m/z* mass range of COVISHIELD vial label extracts from six different batches (N=2, with four technical replicates) manufactured in Hadapsar and Manjari factories (Table 4.3). A. PCA score plot, B. PLS-DA score plot, C. PLS-DA cross-validation results, D. PLS-DA permutation analysis, and E. The 0-900 *m/z* representative spectra of label extracts from Hadapsar (five different batches) and Manjari (one batch), compared to the matrix

Table 4.10. External validation and confusion matrix analysis results for PLS-DA data from Figure 4.18 comparing vaccine vial labels from two different sites of vaccine manufacture using a 90/10 split of training/test parameters

Full dataset

	Hadapsar	Manjari
Hadapsar	40	0
Manjari	0	8

Test set

	Hadapsar	Manjari
Hadapsar	4	0
Manjari	0	1

Training set

	Hadapsar	Manjari
Hadapsar	36	0
Manjari	0	7

4.4. Discussion

Mass spectrometry has emerged as an important platform for molecular-level profiling, providing high sensitivity and high selectivity for the analysis of molecular composition in complex samples (262). Machine learning and additional statistical approaches are also used to classify samples and identify biomarkers (278–280). MALDI-ToF MS has been used in proteomics and more recently in MS imaging and molecular profiling applications such as metabolomics and small molecule pharmaceutical analysis (281–283). The principle behind the identification of microorganisms with MALDI “Biotyping” instruments is the comparison of the mass spectrum of an unknown organism against a library of reference mass spectra (284). For example, they are used in high-throughput microorganism identification where pathogenic bacteria and their antimicrobial resistance features can be rapidly identified at low cost (282). The speed and effectiveness of this approach have led

to worldwide deployment of MALDI-ToF MS instruments, mainly Bruker MALDI Biotyper Sirius and bioMérieux VITEK MS systems, in clinical laboratories for routine medical testing (261,268). This provides an attractive, low-cost MS platform with a global infrastructure that could also be used for coordinated vaccine authenticity testing.

A challenge in using MALDI-ToF MS is its potential variability in the mass spectral peak intensities. The MALDI-ToF method used in this study has been rigorously tested for analytical, experimental and vaccine vial reproducibility and demonstrated that post-acquisition data processing was effective at minimising these effects (246). Using the MALDIquant R package, the spectra data from all samples were analysed using a workflow that performs baseline correction, peak intensity normalisation and peak identification to reduce experimental and analytical variability in the dataset, and ultimately aligns peaks and compares their intensities between samples (246).

PLS-DA modelling is a supervised dimensionality reduction method that builds models based on input variables and identifies which of these variables maximises the separation between the groups. In MALDI-ToF MS analysis, PLS-DA provided proof of principle that an unbiased, machine learning approach was effective in falsification detection (246), as shown in Figure 4.6, where four genuine vaccines could be differentiated from surrogates of falsified products.

The MALDI-ToF MS methods are also useful in the QC process of vaccine production. MALDI-ToF MS of vaccines from vials of the same batch (intra-batch), different batches (inter-batch), and different manufacturing sites showed similar spectra with the same relative intensities among excipient peaks. Furthermore, the PCA analysis yielded no significant differences in both intra- and inter-batch analyses (Figure 4.7), reflecting the standard manufacturing quality implemented in both factories. MALDI-ToF and PCA

analysis could distinguish COVISHIELD vaccine from the falsified vaccine surrogates (Figures 4.9 – 4.11 and 4.13), which strongly suggests that they could be used to detect falsified vaccines in risk-based post-market surveillance. In addition, the dendrogram classification grouped COVISHIELD samples into a monophyletic group separated from other surrogates (Figure 4.14). According to an online news website, falsified COVISHIELD vaccines were found in a vaccination camp in Kolkata, India, where amikacin was used along with fake labels (269). Using the MALDI-ToF approach, amikacin could be readily differentiated from the genuine COVISHIELD vaccine (Figure 4.13 B).

MALDI-ToF MS can also be utilised to establish a molecular profile for a vaccine (246,260). Vaccine constituents such as polysorbate 80 (with evenly spaced peaks mainly between 500-2,500 *m/z*) and L-histidine (at 156 *m/z* corresponding to histidine $[M + H]^+$) are known to be observed by positive ionisation mass spectrometry (285,286), and their presence was confirmed in the COVISHIELD vaccine. Peaks corresponding to histidine (Figure 4.5) and polysorbate 80 (Figure 4.8 B) are therefore possible markers of the COVISHIELD vaccine. The 309 *m/z* peak, unique to the authentic COVISHIELD vaccine, could be the ions of C18:1 oleic acid ester of polysorbate as previously reported (287).

Polysorbate 80 consists of a population of ethoxylated structures with different masses seen in MALDI-ToF MS as evenly distributed peaks due to its random polymerisation process. The peaks are spaced apart in the spectra by 44 Da, equal to one ethylene oxide (C_2H_4O; 44.05 g/mol). These evenly spaced peaks were observed predominantly between 500-2,500 *m/z* (Figure 4.12 A). I analysed polysorbate 80 from a chemical manufacturer (Sigma) as well as two online stores, since criminals are likely to order excipients from publicly available sources. The peak intensity of distribution was found to differ when analysing polysorbate 80 from different manufacturers (Figure 4.12 B), suggesting that the

distribution of polysorbate 80 peaks in the COVISHIELD vaccine could act as an internal marker for authenticity and falsified vaccines manufactured by criminals. Polysorbate 80 stocks (either online or via a chemical supplier) could be detected due to their characteristic peak profiles (Figure 4.12).

While this study has focused on COVISHIELD vaccine, a very large number of medicines contain polysorbates, and these could also be used as an internal marker for authenticity in these cases. For example, anti-COVID-19 (Paxlovid; nirmatrelvir-ritonavir) (288), anti-malarial (Riamet; artemether-lumefantrine) (289), and cholesterol-lowering (Lipitor; atorvastatin) (290) drugs all contain polysorbate 80 and all have been falsified; fake atorvastatin caused the largest recall of counterfeit medicines in the United States. My methods can also be applied to drugs containing other polysorbates, such as polysorbate 20 and potentially could be used for other polymers commonly used as excipients in vaccines, such as PEGylated lipids (*e.g.* polyethylene glycol 2000 dimyristoyl glycerol in Spikevax, Moderna) or Triton X surfactants (*e.g.* octoxinol-9 in Quadrivalent Influenza vaccine, Sanofi).

As expected, MALDI-ToF MS could not detect the most dominant excipient sucrose, since it is not usually observed using positive ionisation mass spectrometry. Also, as expected, ethanol in the vaccine was not detected since it evaporated off the MALDI target. Both sucrose and ethanol are excipients that had previously been detected using SORS by scanning unopened COVISHIELD vaccine vials (258). However, SORS did not detect polysorbate 80 or L-histidine, highlighting the complementarity of the two techniques.

Analysis of vaccine vial labels is proven to be useful for authentication. Unique peaks were observed for the vial labels, which could be used as indicators of the genuine vaccine. Falsified COVISHIELD vaccine and vial labels have been identified in Uganda, India and

Myanmar (256). Since labels on the COVISHIELD vials have been falsified, I compared the extracts of a self-adhesive office label with those of genuine COVISHIELD labels. MALDI-ToF MS analysis of labels with their adhesives showed distinct spectral profiles (Figure 4.16 A). PCA and PLS-DA score plots showed distinct clustered groups for the genuine labels, the office stationery label, and the matrix background (Figures 4.16 B and C). Different score plots were observed between the two manufacturing sites (Figure 4.17), inferring the possibility of either slightly different label materials/adhesives between factories or that the same materials/adhesives were used, but MALDI-ToF MS is sensitive enough to detect a different batch of label material or adhesive. I have also analysed the label extracts of other COVID-19 vaccines (data not shown due to non-disclosure agreements in place), which showed unique spectra, different to the genuine COVISHIELD label, indicating that vaccine labels from different vaccine manufacturers have their own mass spectral fingerprints which could be used to non-invasively check authenticity. The criminal reuse of genuine vials filled with non-vaccine liquids would not be detected. However, these results illustrate a promising additional non-invasive method to detect falsification of vaccines, and the approach could be applied to analyse the labels or packaging of all medicines as well as other items. In this study, MALDI-ToF MS was capable of detecting even differences in the batches of adhesive used between the Manjari and Hadapsar sites (Figure 4.17). While it is required for vaccine manufacturers to disclose the list of excipients in vaccines, details for the label are proprietary information, making it almost impossible for criminals to reproduce a label with identical MALDI-ToF MS spectra without knowing the label material, label manufacturer and the exact composition (formulation) of the adhesive. Furthermore, they would need to know the precise concentration of ingredients used in the specific adhesive batch they are attempting to copy, since the technique was sensitive enough to

differentiate between adhesive batches (Figure 4.17). Many vaccine manufacturers also have security features on vaccine labels, which are usually difficult to replicate, but the unique MALDI-ToF spectra of the label extracts (molecular fingerprints) add a considerably higher level of security that cannot be replicated by falsifiers.

Crucially, thousands of these MS instruments are widely available (261,291) in hospital microbiology laboratories globally, for bacterial identification, and therefore provide a potential accessible analytical network for local vaccine analysis. Although the MALDI-ToF instruments used in hospitals are of low resolution in comparison to other mass spectrometers, they were capable of differentiating genuine vaccines from all falsified vaccine surrogates and genuine labels from an office stationery label, as reported in this chapter.

A limitation of some MALDI-ToF instruments in hospitals is that only the 2,000-20,000 *m/z* range is routinely used in microbial identification. Although this is a limited range, it does cover the mass range for the polysorbate 80 observed in this study (Figure 4.11). Peaks such as histidine at 156 *m/z* and polysorbate 80 at 309 *m/z* (Figure 4.8) would not be observed if only the routinely used mass range of 2,000-20,000 *m/z* is used. However, many MALDI-ToF mass spectrometers in hospitals are already capable of analysing a wide mass range (0-500 kDa), covering these peaks, and all other instruments currently set to analyse the 2,000-20,000 *m/z* can be upgraded to analyse the wider mass range.

The benefit of MALDI analysis for vaccine authentication is two-fold: first, the method involves globally distributed MALDI technology, already deployed in a health context, making it potentially feasible to develop a global vaccine screening system. Second, using open-source machine learning with the full MALDI mass spectrum would make it very difficult, if not impossible, to falsify vaccine surrogates that could pass through such a filter

effectively. Careful assessment of how best to deploy the approach in a real-world setting is required and may be context-dependent. One approach could be in combination with hand-held spectroscopic devices (*e.g.* SORS, as described in Mosca S, *et al.*, 2023 (258)) deployed for rapid 'on-site' analysis. Suspicious samples could then be sent for confirmatory analysis by MALDI-MS, potentially at a regional centre where MALDI-MS is already established for clinical testing applications.

In conclusion, I have developed methods that combine the VITEK MALDI-ToF processing of samples and data analysis of the generated spectra using multivariate analyses. The methods could be improved in the future, with the generation of a spectral data library of genuine vaccines and excipients that can be accessed freely. This is one way to automate matching and scoring multiple spectral peaks identified in experimental samples with a database containing multiple discriminatory *m/z* features previously collected and validated (246). This approach is analogous to that routinely used for bacterial strain identification by MALDI-MS in clinical laboratories worldwide.

Acknowledgement

Rebecca Clarke, Laura Gomez Fernandez, Bevin Gangadharan, and Tehmina Bharucha contributed to the initial development of the MALDI-ToF methods and testing of the preliminary samples. Tehmina Bharucha developed the MALDIquant R workflow for the analysis of MALDI-ToF spectra. Fay Probert contributed to the external cross-validation method using machine learning.

Publications arising from this chapter

The substance of this chapter has been published in the following papers:

1. Clarke R, Bharucha T, **Arman BY**, Gangadharan B, Gomez Fernandez L, Mosca S, et al. Using matrix assisted laser desorption ionisation mass spectrometry combined with machine learning for vaccine authenticity screening. *npj Vaccines*. 2024 Aug 28;9(1):1–14.
2. **Arman BY**, Clarke R, Bharucha T, Fernandez LG, Walsby-Tickle J, Deats M, et al. Identifying falsified COVID-19 vaccines by analysing vaccine vial label and excipient profiles using MALDI-ToF mass spectrometry. *npj Vaccines*. 2025 Jan 30;10(1):1–14.

5

A simple, rapid, low-cost method for detecting sucrose-containing vaccines exposed to elevated temperature

Vaccines are one of the most important contributions of biomedicine to global health. The global distribution of vaccines has prevented diseases and saved lives. The estimate that one in ten medical products are reported to be either substandard or falsified is worrying (71). Novel methods and tools are needed to detect these SF products and remove them from the supply chain. In general, it is easier to detect falsified products due to their chemical composition, which often differs grossly from the genuine product. On the other hand, since substandard products are originally authorised medical products, they typically resemble the genuine product, making them harder to detect.

Temperature is a dominant environmental factor contributing to the creation of 'out of specification' vaccines (292). It must be maintained within the prescribed limits to ensure vaccine stability and avoid degradation. Nevertheless, testing for degradation caused by elevated storage temperature is not routinely done due to the lack of tools to identify heat exposure, especially in countries with intemperate climates.

5.1. Introduction

The surge of SF vaccines, coupled with the unavailability of methods or tools for their detection in supply chains, has been a significant problem in recent times (74). Substandard products are genuine and authorised but fail to meet either their quality standards or specifications, or both (71). SF medical products have become significant health threats and potentially lead to higher rates of illness and death, as well as eroding public trust in the form of hesitancy, as they are of poor quality, unsafe and ineffective (73). When it affects antimicrobial drugs, SF products contribute to antimicrobial resistance and drug-resistant infections (293,294).

The WHO estimated that over half of vaccines are wasted globally each year due to temperature control failures, logistics challenges, and shipment-related issues (295). Environmental factors, such as temperature and light, should be examined in vaccine stability studies (292), with heat exposure being the greatest problem since light exposure can be more easily avoided by the packaging of vaccine vials and syringes. The cold chain system is a crucial aspect of protecting vaccines from deterioration, as improper temperature storage could affect vaccine stability and cause harmful effects of reduced efficacy and changes in the safety profile (296–298). Maintaining the cold chain is deemed expensive and contributes substantially to the total projected vaccine and distribution costs (299), with the pharmaceutical cold chain logistics market size of US$ 18.61 billion in 2024 and expected to reach $ 27.11 billion by 2033 (300). Successful formulation strategies are needed to generate stable and efficacious dosage forms; these include efforts to stabilise the antigen, selection of adjuvants, and development of methods to analytically detect vaccine stability (301).

Potency assays for vaccines and medical products rely on biological assays in the form of animal immunogenicity tests *in vivo* or cell-based or antibody-binding-based assays *in vitro* (302). However, these assays are complex, expensive and time-consuming, with the need for specialist laboratory instruments and trained personnel. To date, there is a lack of simple and low-cost methods to detect substandard heat-exposed vaccines that could be deployed in the supply chain.

Sugars, such as sucrose and lactose, are common ingredients in FDA-approved vaccines where they are used as stabilisers from natural sources (303,304), due to their antigen-stabilising and immunogenicity-maintaining properties (305–307). When sucrose is heated, it breaks down into glucose and fructose.

In this chapter, I investigated novel, simple, and sensitive methods to detect heat-exposed sucrose-containing vaccines based on the detection of the glucose formed as a product of degraded sucrose molecules. The approaches include simple, low-cost, and sensitive glucose assays based on bioluminescent and colorimetric assays and a clinical biochemical analyser for urine samples. The methods may be expanded to detect degradation in lactose-containing vaccines, as lactose breaks down into glucose and galactose when heated. Nevertheless, the methods are not intended to replace the standard vaccine potency assay. Ultimately, linking the results of this study to the outcome of the potency assays using the same samples has helped in understanding at what point a heat-exposed vaccine loses efficacy and is deemed ineffective.

5.2. Materials and Methods

5.2.1. Experimental settings

Different techniques were used to measure glucose concentrations in the vaccines exposed to different temperature conditions for seven days. After establishing which vaccines gave rise to measurable glucose levels upon heat treatment after a week, I looked at the sucrose degradation kinetics at 10 different time points over 7 days under the two temperature conditions (37°C and 45°C) that produced significant glucose changes in the previous tests, to determine when sucrose degradation could be first detected by the techniques under evaluation. For one human adenovirus type 5 (HAdV-5)-based vaccine, a potency assay was conducted in parallel to look at the correlation between glucose levels and potency loss due to heat exposure.

5.2.2. Vaccine samples

Five non-COVID-19 vaccines and two COVID-19 vaccines were used in this study (Table 5.1). Non-COVID-19 vaccines were purchased from the Oxford University Hospitals Pharmacy. The COVISHIELD and COMIRNATY (30 µg for adults and 10 µg for children) COVID-19 vaccines were received from the Serum Institute of India, Pvt. Ltd. and NHS England, respectively. COVID-19 vaccines were immediately stored in a refrigerator at 2-8°C when received and used within one month of receipt, according to the manufacturer's recommended use when the frozen vaccine is thawed and stored at 2-8°C. Vials and syringes were kept on wet ice when vaccines were used for tests.

Table 5.1. Sucrose-containing vaccines used in the study. Data were retrieved from the Electronic Medicine Compendium (EMC), available at https://www.medicines.org.uk/emc and other sources in the public domain.

Vaccine trade name	Description and usage	Manufacturer	Pharmaceutical form	Excipients including sucrose concentration in bold
Rotarix	Live attenuated rotavirus vaccine	GlaxoSmithKline (GSK)	Oral suspension in a squeezable tube, clear and colourless, viscous liquid	Sucrose (**715 mg/mL**), disodium adipate, Dulbecco's Modified Eagle Medium/DMEM (containing phenylalanine, sodium, glucose, and other substances), sterile water
Nimenrix	Meningococcal groups A, C, W-135 and Y conjugate vaccine	Pfizer	Powder and solvent for solution for injection in a pre-filled syringe	*Powder*: Sucrose (**56 mg/ml** after reconstitution), trometamol *Solvent*: Sodium chloride, water for injections
Rabipur	Rabies vaccine (inactivated, strain Flury LEP)	Bavarian Nordic A/S	Powder and solvent for solution for injection in a pre-filled syringe	*Powder*: Trometamol, sodium chloride, disodium edetate, potassium-L-glutamate, polygeline, sucrose (**60 mg/mL** after reconstitution[a]) *Solvent*: Water for injections
Bexsero	Meningococcal group-B vaccine (rDNA, component, adsorbed)	GSK	Suspension for injection in a pre-filled syringe	Sodium chloride, histidine, sucrose (**20 mg/mL**), water for injections, aluminium hydroxide (hydrated)

TicoVac Junior	Tick-Borne Encephalitis vaccine (whole virus, inactivated)	Pfizer	Suspension for injection in a pre-filled syringe	Human albumin, sodium chloride, disodium phosphate-dihydrate, potassium dihydrogen phosphate, water for Injections, sucrose (expected to be **≤30 mg/mL** as for TicoVac adult dose), aluminium hydroxide, hydrated.
COVISHIELD	COVID-19 vaccine; Recombinant, replication-deficient chimpanzee adenovirus vector encoding the SARS-CoV-2 S glycoprotein	Serum Institute of India	Solution for injection, colourless to slightly brown, clear to slightly opaque and particle-free, with a pH of 6.6	L-Histidine, L-Histidine hydrochloride monohydrate, magnesium chloride hexahydrate, polysorbate 80, ethanol, sodium chloride, disodium edetate dihydrate (EDTA), sucrose (**75 mg/mL**)[b]
COMIRNATY	COVID-19 vaccine; mRNA vaccine (nucleoside modified): 10 micrograms per dose (children 5 to 11 years) and 30 micrograms per dose (ages 12 years and older)	Pfizer	Concentrate for dispersion for injection	((4-hydroxybutyl)azanediyl)bis(hexane-6,1-diyl)bis(2-hexyldecanoate) (ALC-0315); 2-[(polyethylene glycol)-2000]-N,N-ditetradecylacetamide (ALC-0159); 1,2-Distearoyl-sn-glycero-3-phosphocholine (DSPC); cholesterol, trometamol; trometamol hydrochloride; water for injections; sucrose (**20 mg/mL** (308))

[a]Data obtained from https://www.medsafe.govt.nz/profs/datasheet/r/rabipurinj.pdf; [b]Data from https://www.seruminstitute.com/health_faq_covishield.php

A HAdV-5-based KC5 vaccine was generated by single-round infection with a m.o.i of 1 in a hyperflask containing approximately 1×10^8 human embryonic kidney HEK 293 cells. Cells were harvested 48 hours post-infection and pelleted at 200 × *g* for 30 minutes. Cell pellets were lysed in Cell Lysis Buffer (10 mM Tris, 135 mM sodium chloride, 1 mM magnesium chloride, all from Sigma) and freeze/thawed three times.

The cell lysate was treated with 250 Units/mL of Benzonase after the first thaw and incubated for 30 minutes at RT. The viral vector was then purified by double caesium chloride ultracentrifugation and dialysed three times in Formulation Buffer A438 (10 mM histidine, 7.5% sucrose, 35 mM sodium chloride, 1 mM magnesium chloride, 0.1% polysorbate 80, 0.1 mM ethylenediaminetetraacetic acid, 0.5% *v/v* ethanol, pH 6.6; all from Sigma) (309).

5.2.3. Substandard vaccine samples

In order to study how temperature affects the stability of vaccines leading to the generation of substandard samples, vaccine samples were exposed to five different temperature conditions: they were (i) stored at 4°C (as the recommended 2-8°C storage condition, (ii) stored at RT (recorded as 20 ± 1°C) for seven days, (iii) stored in an incubator oven set at 37°C for seven days, (iv) stored in an incubator oven set at 45°C for seven days, and (v) exposed to three freeze-thaw cycles of 24 hours freezing at -70°C and 1 hour thawing at 4°C per cycle. In a case of vaccines which had a separate vial containing lyophilised powder and a syringe filled with the solvent (Nimenrix and Rabipur), both the vial and syringe were exposed to the five conditions without prior mixing/reconstitution to resemble a real-life situation of how the vaccine could be exposed to altered temperature in the supply chain. The lyophilised vaccines were

reconstituted with their solvent just prior to analysis. All samples were stored at 4°C immediately after completing the incubation conditions.

A degradation test on HAdV-5 KC5 was performed by incubating glass vials containing 350 µL of the vaccine at RT (recorded as 20° ± 2°C), 4°C, 37°C and 45°C for 7 days. Vials were also exposed to the same freeze-thaw cycles as described above or stored at -80°C (as a reference control). All samples were stored at 4°C immediately after completing the incubation conditions. Each condition was tested in triplicate and tested using both the colorimetric and potency assays.

5.2.4. Bioluminescent-based glucose assay

The concentration of glucose, as a product of sucrose hydrolysis, was measured using the Glucose-Glo Assay (Promega, Madison, WI, USA) according to the manufacturer's protocol. Principally, glucose in the sample will be oxidised by glucose dehydrogenase concomitant with the reduction of NAD^+ to NADH. In the presence of NADH, the reductase enzyme catalyses the reduction of pro-luciferin to luciferin that generates light in an intensity that is proportional to the amount of glucose in the sample (Glucose-Glo Assay technical manual, version 3/17, Promega).

A volume of 50 µL of sample or glucose standard was transferred to the designated well of a white-bottom 96-well plate (Corning, NY, USA). The reagent buffer was included as a negative control (buffer only) to determine the assay background. Following sample addition, 50 µL of Glucose Detection Reagent (a mix of luciferin detection solution, reductase, reductase substrate, glucose dehydrogenase, and NAD) was added and the plate was shaken for 60 seconds. The reaction was then incubated for 60 minutes at RT. Luminescence was read using a plate-reading luminometer (Clariostar, BMG Labtech,

Germany). The concentration of glucose was interpolated into the glucose standard curve which is generated using a 4-parameter logistic statistic.

5.2.5. Sucrose in water exposed to an elevated temperature

Sucrose was made up in water at the following concentrations: 20, 87, 200, 350, 540 and 715 mg/ml. An aliquot of each sucrose sample was stored at 4°C while another aliquot was incubated at 45°C. These aliquots were 5 ml in volume and stored in the dark at various temperatures for 7 days. All samples were stored at 4°C immediately after completing the incubation period. Glucose levels were measured in each sample in duplicate using the bioluminescent glucose assay.

5.2.6. Time course for sucrose degradation after heat exposure

To evaluate the kinetics of vaccine degradation at increased temperatures, vaccine samples were distributed as 120 µL aliquots in microcentrifuge tubes and grouped into two incubation conditions (37 and 45°C). The tubes in each group were exposed to 37 and 45°C for 3, 6, 12, 24 (1 day), 48 (2 days), 72 (3 days), 96 (4 days), 120 (5 days), 144 (6 days), and 168 (7 days) hours. The tubes were stored at 4°C immediately after completing their respective incubation period. Aliquots of vaccines were also prepared in the same manner as the 2-8°C controls and stored at 4°C. Following the incubation period, 50 µL of vaccine sample from each aliquot was assayed, in duplicate, for its glucose content using the glucose assay mentioned above.

5.2.7. Colorimetric-based glucose assay

The glucose concentration in vaccine samples was measured using the Glucose Assay Kit (Colorimetric) (Cell Biolabs, San Diego, CA, USA), according to the manufacturer's protocol. The assay measures the amount of total glucose present in the sample in a 96-well microtiter plate format. Glucose is oxidized by glucose oxidase into D-gluconic acid and hydrogen peroxide. The hydrogen peroxide generated is detected with a highly specific colorimetric probe in a reaction catalysed by horseradish peroxidase (HRP).

A reaction mix consisting of the colorimetric probe, HRP, and glucose oxidase was prepared in 1x assay buffer. A mixture of 50 µL of glucose standard or sample and 50 µL of reaction mix was prepared in triplicate in a clear flat bottom 96-well microtiter plate (Corning). The mixture was mixed well and incubated for 30 minutes at 37°C, protected from light. The plate was read with a microplate reader (Clariostar) at 540 nm or documented visually using a mobile phone camera (type Oppo Reno 6, Oppo, Guangdong, People's Republic of China). The readouts were blanked to the assay buffer (0 µM), and Milli-Q water (Merck Millipore) was used as a negative control. The known concentrations of glucose are used to generate a standard curve that is used to calculate the amount of glucose in the sample tested using the 4-parameter logistic statistical model within the BMG MARS Data Analysis Software (BMG Labtech).

5.2.8. Potency determination for heat-exposed vaccines

Vaccine potency was determined by infectivity assay and expressed as infectious units per mL (Ifu/mL). Briefly, HEK-293 cells were seeded in 96-well plates at 5.8×10^4

cells/well and subsequently infected with serial dilutions of vaccine test samples. At 48 hours post-infection, cells were fixed with methanol, blocked with 1% *w/v* BSA, and stained with a mouse monoclonal anti-Hexon antibody (Abcam B025/AD51). Following the incubation with the secondary antibody, HRP-conjugated rabbit polyclonal anti-mouse IgG-H&L (Abcam ab6728), positive cells were visualised with DAB staining and enumerated using NyOne (Synentec). The term "potency" in the potency assay is defined as the number of virus infectious units still detectable using the immunostaining assay after exposure to different temperature conditions.

5.2.9. Vaccine analysis using an automated biochemical analyser

The Abbott Architect c16000 analyser (Abbott Laboratories, Maidenhead, UK) was used to analyse the heat-exposed vaccine samples. The degraded Bexsero, COMIRNATY, and COVISHIELD vaccine samples (after seven days of exposure to temperature-altered conditions), along with their correctly stored controls, were measured with eight separate runs on the instrument. The method optimised for urine specimens was used, and the following eight analytes were measured: calcium, chloride, glucose, magnesium, phosphate, potassium, protein and sodium.

5.2.10. Statistical analysis

Ordinary one-way ANOVA with Dunnett's multiple comparisons test was used to compare glucose levels between vaccine samples stored at the recommended 2-8°C and the other temperature-altered conditions. Statistical analysis was performed using

GraphPad Prism v.10.1.2 (GraphPad Software, Boston, MA, USA). The *p*-value of $p < 0.05$ is considered statistically significant.

5.3. Results

5.3.1. Glucose levels in sucrose-containing vaccines after seven days of exposure to temperature-altered conditions

Using a bioluminescent assay, the level of glucose was measured at a single seven-day time point and compared to vaccines stored at the manufacturer-recommended temperature of 2-8°C for the same time. Among the seven vaccines tested, four vaccines (Bexsero, COMIRNATY, COVISHIELD, and Nimenrix) showed an increase in glucose concentration after exposure to elevated temperatures of 37 and 45°C (Figure 5.1 A-D). A smaller increase was observed for Nimenrix, which was nevertheless significant at both 37°C and 45°C. The increase was recorded at 4.5-, 9.6-, 2.8-, and 1.1-fold in Bexsero, COMIRNATY, COVISHIELD, and Nimenrix, respectively, after seven days of incubation at 37°C compared to the properly stored samples. The increase was considerably higher after incubation at 45°C for seven days with a 9.2-, 27.6-, 6.3, and 1.2-fold change in Bexsero, COMIRNATY, COVISHIELD, and Nimenrix, respectively (Table 5.2). However, this increase in glucose levels after heat exposure was not observed for Rabipur, Rotarix, and Ticovac (Figure 5.1 E-G). Exposure to three freeze-thaw cycles and RT conditions after seven days did not result in significant changes in glucose levels in any of the vaccines tested.

Table 5.2. The concentration of glucose in samples and its fold-change increase after seven days of exposure to elevated temperatures

Vaccine	Glucose concentration* (µM)			Fold-change	
	2-8°C	37°C	45°C	37 vs 2-8°C	45 vs 2-8°C
Bexsero	5.63	25.49	51.59	4.5	9.2
COMIRNATY	2.34	22.13	64.08	9.6	27.6
COVISHIELD	26.21	73.46	164.85	2.8	6.3
Nimenrix	0.43	0.47	0.51	1.1	1.2

*Mean concentration, N=2

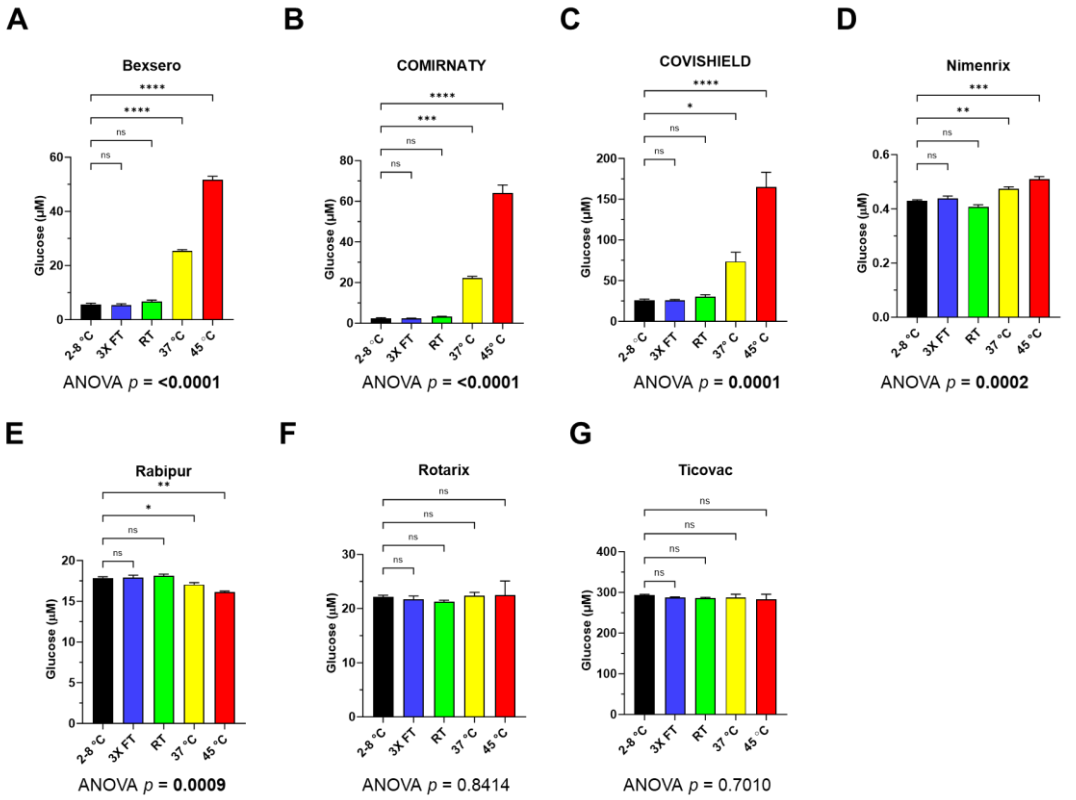

Figure 5.1. Glucose levels of seven sucrose-containing vaccines after exposure to different conditions for seven days (coloured bars) compared to the recommended 2-8°C (black bar) storage conditions, measured using a bioluminescent assay. Error bars show the standard deviations from two measurements for each temperature point. 3× FT, three freeze-thaw cycles, RT, room temperature. Ordinary one-way ANOVA with Dunnett's multiple comparisons test. ns, not significant; *p<0.05; **p<0.01; ***p<0.005; ****p<0.001

5.3.2. Using a bioluminescent glucose assay to monitor the thermal degradation of sucrose over time

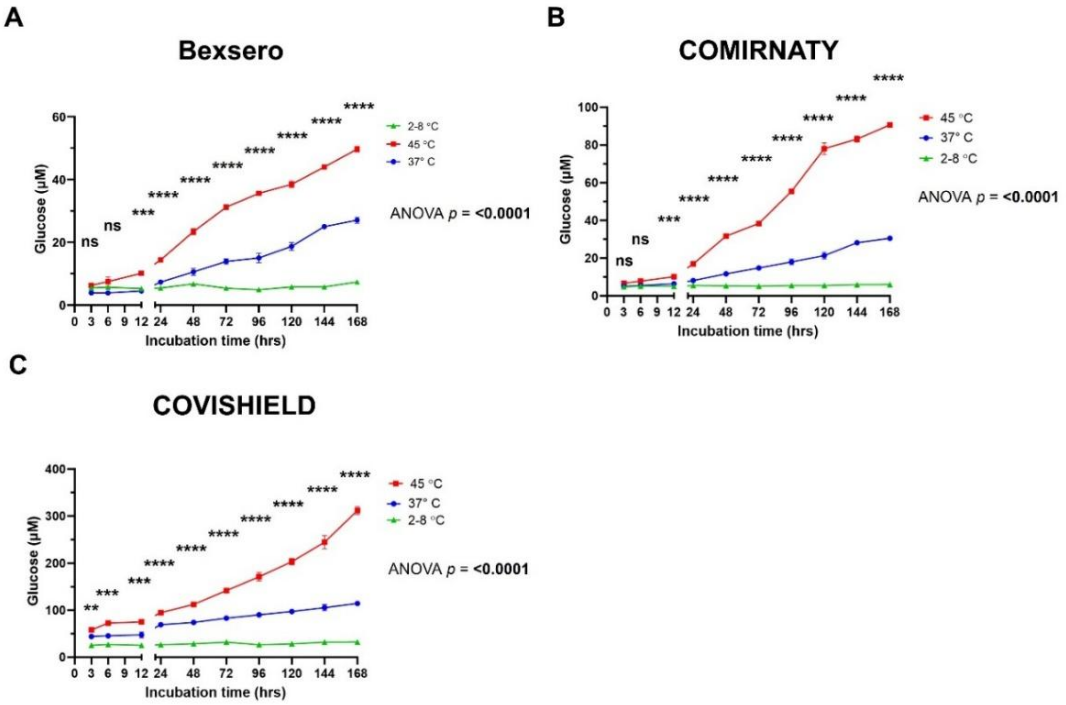

Figure 5.2. The kinetics of sucrose degradation measured as the increase in glucose levels after thermal degradation over seven days. The vaccines Bexsero (A), COVISHIELD (B), and COMIRNATY (C) exposed to 37°C (blue line) and 45°C (red line) conditions are compared to the recommended storage temperature of 2-8°C (green line). Error bars show the standard deviations from two measurements for each time point. Ordinary two-way ANOVA with Tukey's multiple comparisons test. ns, not significant; **p<0.01; ***p<0.005; ****p<0.001

After establishing which vaccines gave rise to measurable glucose levels upon heat treatment after a week, the kinetics of glucose generation were then measured for Bexsero, COMIRNATY, and COVISHIELD vaccines over a seven-day time course to determine when sucrose degradation could be first detected by the bioluminescent glucose assay. Thermal degradation of sucrose in all three vaccines was evident by increasing levels of glucose when exposed to 37 and 45°C, with a significant increase in

glucose levels detected after 12 hours (Figure 5.2), with COVISHIELD showing a significant increase already after 3 hours (Figure 5.2 C).

5.3.3. Using a colorimetric glucose assay to detect glucose levels in sucrose-containing vaccines

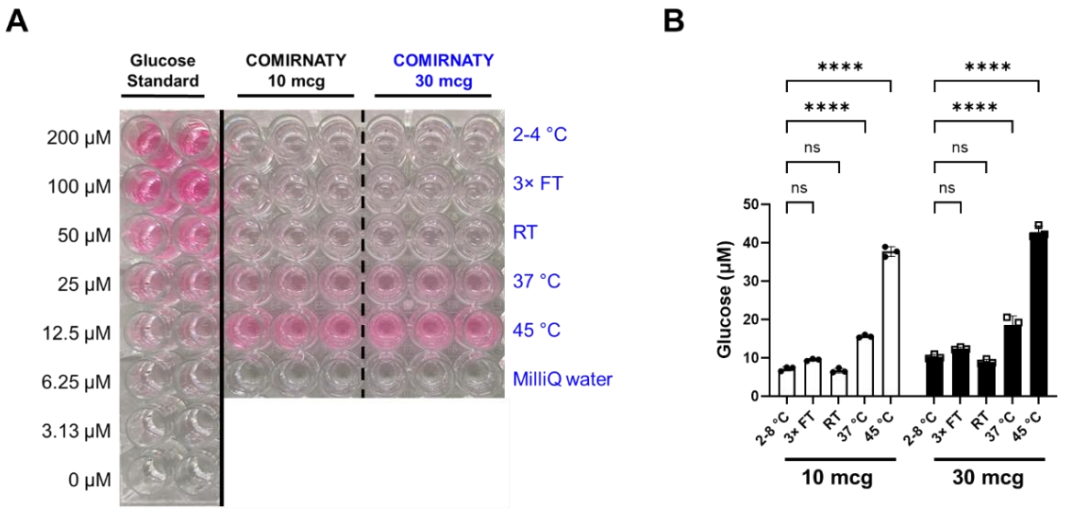

Figure 5.3. Glucose levels of COMIRNATY vaccines with two different amounts of active pharmaceutical ingredients after exposure to degradation conditions, measured using the colorimetric glucose assay. The increase in glucose levels can be visually observed (A) and monitored using the spectrophotometer at 540 nm, comparing the absorbance units to those of known glucose standards (B). The level of glucose in samples kept under degrading conditions was compared to that in samples kept at the recommended 2-8°C. Error bars show the standard deviations from three measurements for each temperature point. 3× FT, three freeze-thaw cycles; RT, room temperature. Ordinary one-way ANOVA with Dunnett's multiple comparisons test. ns, not significant; ****p<0.001

A simpler colorimetric glucose assay was used to determine the glucose levels in COMIRNATY vaccines with two different amounts of active pharmaceutical ingredients (API) present (Figure 5.3, Table 5.1). The development of colour intensity along with the increasing levels of glucose could be readily observed visually (Figure 3A). The assay

could significantly detect thermal degradation in vaccine vials exposed to elevated temperatures of 37°C and 45°C (Figure 5.3 B). Similar characteristics of glucose level changes were observed in both vaccines that contained either 10 or 30 micrograms of API, showing that the same amount of sucrose was used in the formulation of both vaccines.

5.3.4. Sucrose in water degradation

Sucrose in water samples showed low levels of glucose (below 10 µM) with a slight increase in glucose levels observed with the increasing sucrose concentration, after seven days of storage at 4°C (Figure 5.4, white bars). On the other hand, high glucose levels were observed for sucrose in water samples stored at 45°C (Figure 5.4, black bars).

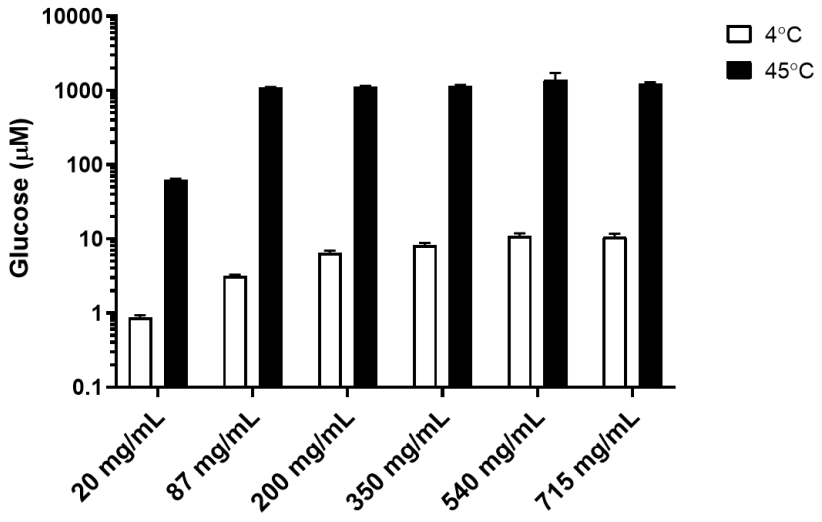

Figure 5.4. Sucrose samples were made up in water at various concentrations from 20 to 715 mg/ml and stored at both 4°C and 45°C for 7 days. Glucose concentrations were then measured using the bioluminescence assay. Error bars show the standard deviations from two measurements.

5.3.5. Correlation of potency with glucose for heat-exposed vaccines

To assess whether glucose levels correlate with vaccine potency, a HAdV-5-based KC5 vaccine formulated in a buffer containing 7.5% sucrose was exposed to various temperature-altered conditions. Storage at 4°C, RT, or exposure to three freeze-thaw cycles had no impact on adenoviral potency compared to the reference sample stored at -80°C (Figure 5.5 A). Conversely, the detected glucose levels showed no variation compared to the reference sample. Exposure of samples to higher temperatures (37°C and 45°C) resulted in reduced levels of potency, with a 2-log decrease for the 37°C incubation and a 3-log reduction for the 45°C storage. Glucose levels from those samples were elevated, between 5- and 11-fold (Figure 5.5 A). Furthermore, the correlation analysis confirmed that degradation-mediated glucose levels correlated significantly with vector infectivity, confirming that glucose levels generated are a good predictor for vaccine potency (Figure 5.5 B).

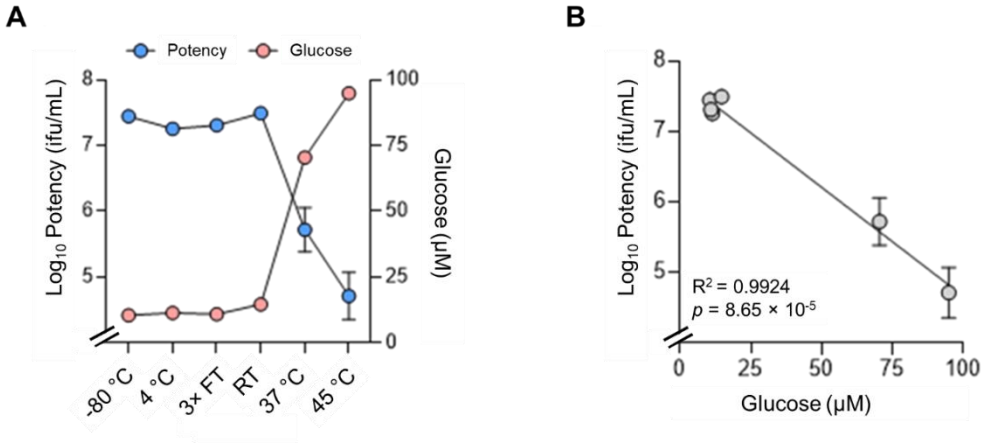

Figure 5.5. Assessment of the impact of degradation conditions on the potency of the HAdV-5 vaccine, indicated by virus infectivity, and the corresponding glucose levels measured. A. Correlation between vaccine potency and glucose levels, B. Pearson correlation of potency and glucose levels

Table 5.3. Concentrations of eight analytes measured in vaccine samples using a biochemical analyser after exposure to different altered temperature conditions. Values in bold indicate if the analytes could be detected and quantified showing their mean concentrations (± standard deviation) of eight measurements. All other values with the less than symbol (<) were below the limit of quantitation and the lower limit of quantitation is shown

Condition	Calcium (mM)	Chloride (mM)	Glucose (mM)	Magnesium (mM)	Phosphate (mM)	Potassium (mM)	Protein (mg/L)	Sodium (mM)
BEXSERO								
4°C	< 0.50	**110.92 ± 1.09**	< 0.06	< 0.74	< 1.50	**2.52 ± 0.04**	< 68	**107.30 ± 1.25**
3× FT	< 0.50	**110.10 ± 0.81**	< 0.06	< 0.74	< 1.50	**2.52 ± 0.04**	< 68	**106.93 ± 0.73**
RT	< 0.50	**110.17 ± 0.82**	< 0.06	< 0.74	< 1.50	**2.52 ± 0.04**	< 68	**106.73 ± 0.92**
37°C	< 0.50	**110.70 ± 0.95**	< 0.06	< 0.74	< 1.50	**2.52 ± 0.04**	< 68	**107.18 ± 0.94**
45°C	< 0.50	**110.95 ± 1.01**	< 0.06	< 0.74	< 1.50	**2.57 ± 0.07**	< 68	**107.68 ± 1.21**
COMIRNATY								
4 °C	< 0.50	< 20.0	< 0.06	< 0.74	< 1.50	< 1.0	**184.88 ± 13.41**	< 20.0
3× FT	< 0.50	< 20.0	< 0.06	< 0.74	< 1.50	< 1.0	**170.63 ± 7.19**	< 20.0
RT	< 0.50	< 20.0	< 0.06	< 0.74	< 1.50	< 1.0	**186.63 ± 5.24**	< 20.0
37°C	< 0.50	< 20.0	< 0.06	< 0.74	< 1.50	< 1.0	**190.88 ± 9.91**	< 20.0
45°C	< 0.50	< 20.0	< 0.06	< 0.74	< 1.50	< 1.0	**194.50 ± 10.24**	< 20.0
COVISHIELD								
4°C	< 0.50	**39.26 ± 0.26**	< 0.06	**1.04 ± 0.02**	< 1.50	< 1.0	< 68	**34.84 ± 0.67**
3× FT	< 0.50	**39.25 ± 0.29**	< 0.06	**1.04 ± 0.04**	< 1.50	< 1.0	< 68	**34.89 ± 1.12**
RT	< 0.50	**39.28 ± 0.24**	< 0.06	**1.03 ± 0.03**	< 1.50	< 1.0	< 68	**35.31 ± 1.39**
37°C	< 0.50	**39.44 ± 0.27**	**0.06 ± 0.01**	**1.04 ± 0.01**	< 1.50	< 1.0	< 68	**35.21 ± 1.21**
45°C	< 0.50	**39.33 ± 0.26**	**0.14 ± 0.01**	**1.03 ± 0.03**	< 1.50	< 1.0	< 68	**35.18 ± 0.65**

[a]Calculation based on six measurements due to the limited sample; 3× FT, three cycles of freeze-thaw; RT, room temperature (20 ± 1°C).

5.3.6. Analysis of vaccine excipients using an automated urine analyser

An automated urine analyser, widely available in diagnostic laboratories worldwide, could be repurposed to detect specific vaccine excipients and may be a potential means to distinguish a genuine vaccine from a falsified one. The urine analyser could detect the presence of sodium chloride and potassium excipients in Bexsero (Table 5.3). Magnesium was detected in COVISHIELD vaccine samples. The instrument could detect glucose only in COVISHIELD samples exposed to 37°C and 45°C temperatures. However, the instrument could not detect low levels of glucose with an LOD of 60 µM.

5.4. Discussion

Vaccine stability has always been an important factor in vaccine formulation development. Some forms of vaccine need a reliable cold-chain system and are more vulnerable to potency loss during storage and distribution due to increasing temperature (301). Vaccine potency becomes a critical quality determinant that is also a regulatory requirement for release on the market and further clinical use (310). However, the determination of vaccine potency is complex and requires specialised assays and instruments, and a good potency assay should reflect the structural integrity of the antigen (296,310–313).

There is a need for a faster and easier-to-use method that could be employed as an initial indicator for a potentially substandard vaccine, in particular, if it is caused by exposure to elevated temperature with loss of the cold chain, as one of the more common occurrences encountered by vaccines in supply chains. A potency assay will

be specific for each vaccine formulation from each vaccine manufacturer. In addition, it is too cumbersome to perform potency testing at all levels of the supply chain, including distributors and end users.

Sugars have been used as stabilisers in vaccine formulations. For example, sucrose is a commonly used stabilising agent in vaccine formulations and is effective in stabilising the API component (305–307). In addition, sucrose was also reported to maintain immunogenicity *in vivo* for viruses stored for 10 days at 37°C in an adenovirus-based vaccine (307). An increased stability for either HAdV-5 or other viruses at higher sucrose concentrations has been reported. Pelliccia *et al*. showed that sucrose was also able to protect both a double-stranded DNA virus as well as an RNA virus (307).

The results from this study demonstrate that glucose levels as a product of sucrose degradation could be used as a predictor of vaccine exposure to an elevated temperature. My data indicate that measuring glucose levels for such monitoring purposes could be applied to sucrose-containing vaccines in liquid suspension/dispersion form. A significant increase in glucose levels after seven days of exposure to elevated temperatures of 37°C and 45°C was detected (Figure 5.1 A-D). No significant change in glucose levels was observed when vaccines were exposed to freeze-thaw cycles and stored at RT for seven days (Figure 5.1 A-G). An increase in glucose levels was not observed in vaccines supplied in lyophilised form (Rabipur) or as a viscous liquid formulation (Rotarix) or with the addition of other excipients in the formulation (Ticovac) (Figure 5.1 E-G).

Lyophilised formulations have been routinely used in vaccine development and reported to increase stability at the higher temperature of 37°C for an extended time of up to one month (311). This suggests that sucrose degradation requires the presence of

an aqueous environment. At the temperature of 25°C or 298.15 K, sucrose hydrolysis has an enthalpy of -15.0 ± 0.071 kJ/mol, meaning that sucrose will spontaneously undergo hydrolysis to glucose and fructose in water at RT, and this will occur more rapidly at higher temperatures (314). Rotarix is formulated as a viscous liquid with the presence of a thickening agent, disodium adipate, that functions as a buffer to prevent gastric low pH inactivation after oral delivery (315). Ticovac contains excipient human serum albumin that functions as a sheer protection and thermal stability enhancer, but also as an inhibitor of fever-inducing cytokines (316). The presence of these additional excipients in a vaccine formulation may also protect sucrose from thermal degradation due to the substitution of water with more viscous materials.

Levels of glucose were measured in sucrose samples made up in water and stored at both 4°C and 45°C (Figure 5.4). Sucrose was made up at various concentrations from 20 to 715 mg/ml, reflecting the sucrose concentrations commonly used in vaccines, *e.g.* Bexsero (20 mg/ml), Spikevax (87 mg/ml), RotaTeq (540 mg/ml) and Rotarix (715 mg/ml). The sucrose solutions stored at 4°C contained very low levels of glucose (below 10 µM). However, for all solutions stored at 45°C, there was a large increase in glucose levels of around 100-fold (Figure 5.4), unlike the vaccine data with relatively small increases in glucose (Figure 5.1). This indicates that all concentrations of sucrose commonly used in vaccines could potentially show an increase in glucose with heat exposure. However, a relatively lower increase in glucose of 1.2 to 27.6-fold (Table 5.2, Figure 5.1 A-D) or no significant increase at all (Figure 5.1 E-G) was observed in the tested vaccines. The sucrose solutions made up in water did not have any other excipients, and therefore, the lower or no increase in glucose observed for the vaccines must be due to other excipients which are protecting sucrose from hydrolysis (Table 5.1).

Signs of sucrose degradation could be detected as early as 12 hours post-incubation (Figure 5.2), suggesting rapid hydrolysis into glucose and fructose at higher temperatures of 37°C and 45°C. This result proves that the bioluminescent-based glucose assay is sensitive enough to detect the smallest changes in glucose levels, down to 0.0031 µM (the lowest standard concentration used in the assay). Although a specific instrument is required to read the bioluminescence, the assay is relatively straightforward to do, and most reference laboratories worldwide will have the capacity to perform the assay.

Another rapid and simple tool to detect glucose in samples is the colorimetric glucose assay. I used it to detect sucrose in a COMIRNATY mRNA vaccine. The assay only requires a spectrophotometer (microplate reader) that is relatively widely available globally. Importantly, the changes in colour intensity along with the increased level of glucose can be observed visually (Figure 5.3 A). This will significantly aid the use of this assay in a field setting where instrumentation is lacking. However, the sensitivity of this assay is lower than the bioluminescent assay, with the capability to measure down to the limit of 6.25 µM of glucose.

The other analytes detected and quantified by the biochemical analyser helped to determine an analyte fingerprint for the vaccines, and we have shown how this is a low-cost way to distinguish genuine vaccines from falsified surrogates (317). The analytes identified and quantified for the three vaccines act as a fingerprint to confirm authenticity (Table 5.3). All vaccines tested contain sodium chloride, and as expected, both sodium and chloride ions were detected. Although Bexsero does not contain potassium, a positive result was seen, possibly due to interference from other excipients, which is not a problem since the result was consistent among all runs. Such

false positives may occur since the analyser is intended for urine samples instead of vaccines, which have a very different sample matrix. COMIRNATY tested positive for protein even though no protein is expected in this vaccine. An explanation for this false positive in mRNA vaccines could be due to benzethonium chloride used for the protein method, which interacts with lipids in the vaccine and disrupts the lipid nanoparticles (317). Magnesium chloride is present in COVISHIELD, and as expected, magnesium was detected. The Oxford COVID-19 ChAdOx1-S vaccine has the same excipient list as COVISHIELD, and we have shown that magnesium ions could also be detected in this vaccine (317).

Previous work assessing the stability of adenovirus-vectored vaccines at a temperature range from 4°C to 45°C using an *in vitro* infectivity assay reported a rapid loss of infectivity at higher temperatures of 30°C and 45°C in less than 10 days of exposure. On the other hand, only a small decrease in infectivity was observed when stored at ambient 22°C, and no loss of infectivity was detected over five freeze-thaw cycles (311). Therefore, while the glucose assays were not able to detect vaccines which had been exposed to freeze-thaw cycles, the potency may have been unaffected in the vaccines tested, and this was confirmed in the potency correlation data for the HAdV-5-based vaccine (Figure 5.5). This is consistent with a historical report that a rapid initial loss of vaccine potency occurs only on exposure to temperatures above ambient temperature (318). Furthermore, a case report assessing the stability of an adenovirus-vectored vaccine stored at ambient 21°C for 18 hours before vaccination reported the same safety profile and efficacy as the vaccines stored at the recommended temperature (302). mRNA vaccines are also vulnerable to degradation by elevated temperature (319). The decrease of mRNA integrity and the simultaneous increase of its fragmentation were observed after four days of incubation at the higher temperatures of

37, 45, and 60°C (319). The stability of mRNA (as of percentage of intact RNA) correlates with *in vitro* potency, as both rapidly decreased when exposed to an increasing temperature from 25 to 45°C (320).

Collectively, the pattern of sucrose degradation within seven days in this study correlates with the results of the vaccine potency assay (Figure 5.5). The detection of sucrose degradation could potentially be an endogenous indicator of vaccines having been exposed to elevated temperatures exposure and thus of cold chain failure. The proposed assays could detect heat exposure of vaccines by sensing the significant increase in glucose levels formed as a product of the heat degradation of sucrose molecules within the vaccine formulation. While monitoring the glucose levels at 37°C and 45°C incubation, the bioluminescent assay was able to detect an increase in glucose content as early as three hours of exposure to heat. The colorimetric assay offers the simplicity of glucose detection using a visual inspection, and the urine analyser offers the repurposing of instruments routinely used in clinical testing laboratories. The assay could be used as an early assessment by vaccine assessors to check the quality of the vaccine in the prevention of substandard vaccines.

In conclusion, although the proposed assays would not be able to replace the gold standard potency assays, they can be used as low-cost predictors of substandard sucrose-containing vaccines within the supply chain in the field. These lower-cost and more rapid assays could be used by medicine regulators, vaccine manufacturers, and NRA inspectors as an initial screening test to help prevent substandard vaccines from being used.

Acknowledgement

Jennifer Brook and Tim James at the Biochemistry Department, John Radcliffe Hospital, University of Oxford performed the vaccine analysis using the automated urine analyser. Matteo N. Barbaglia (former member of the Zitzmann group), Andrea Magri (Clinical BioManufacturing Facility (CBF), University of Oxford), and Lawrence Petherbridge (CBF, University of Oxford) performed the vaccine potency assay. Figure 5.5 was prepared by the CBF team.

Manuscript arising from this chapter

The substance of this chapter has been prepared as a manuscript and submitted for publication:

Arman BY, Magri A, Barbaglia MN, Petherbridge L, Brook J, Bharucha T, Legge I, Walsby-Tickle J, Deats M, Banerjee S, Mosca S, Chunekar SR, Patil KD, Gairola S, Merchant HA, Stokes R, Kuwana R, Maes A, James T, Green C, McCullagh J, Matousek P, Caillet C, Newton PN, Zitzmann N, and Gangadharan B. Ensuring vaccine cold chain integrity: A rapid and low-cost test for identifying heat-exposed sucrose-containing vaccines. 2025. *Manuscript submitted*.

6

Assays to investigate diethylene glycol and ethylene glycol contamination in raw materials and medical products

Toxic alcohol contaminations in medical products have been reported as sources of human intoxication (321) and may result from either the fraudulent act of changing the supposed ingredients in the pharmaceutical manufacturing process or failure to adhere to GMP QC procedures (322). The definitive diagnosis of DEG/EG contamination can be established using gas chromatography (GC), a method that is relatively costly, laborious, and often not available in many laboratories (323). Thin-layer chromatography (TLC) is of relatively lower cost and also portable, but requires time and trained personnel (324). Alternative rapid, low-cost and simple methods to detect DEG/EG contamination are desirable to provide simple, rapid and lower-cost determination of DEG and EG contamination and may be lifesaving.

6.1. Introduction

6.1.1. Toxic alcohol contamination in medical products

Substandard and falsified medical products have been found worldwide, although they are more prevalent in LMICs with often under-resourced NRAs (73,325,326). Substandard medical products do not meet their quality standards and/or quality specifications, and one of the causes is that the products originate from poor manufacturing practices (70,325).

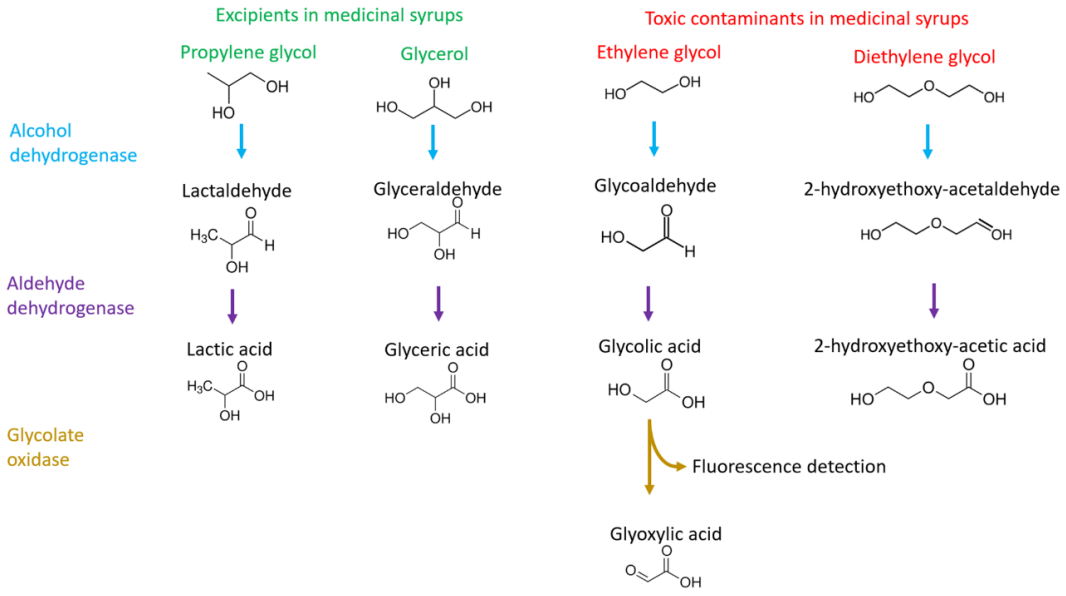

Figure 6.1. The metabolic pathways of propylene glycol and glycerol (used as excipients in syrups) and toxic alcohols DEG and EG. The pathways include the use of glycolate oxidase for the detection of glycolic acid. The pathway involves three enzymes: alcohol dehydrogenase, aldehyde dehydrogenase, and glycolate oxidase. Steps involving enzymatic reactions with NAD^+ and NADH have been omitted to simplify this pathway.

Medicinal syrups often contain excipients such as propylene glycol (PG) and glycerol as a base to sweeten and thicken the medicine, and these must be of pharmaceutical grade so that they meet stringent purity standards to be approved for human consumption. DEG and EG are industrial solvents often used in antifreeze and vehicle brake fluid and should never be used as an excipient in medicinal syrups since they are metabolised to the toxic acids 2-hydroxyethoxyacetic acid (HEAA), glycolic acid and calcium oxalate which can lead to neurological damage, renal failure, metabolic acidosis, hyperosmolality and an increased chance of death (Figure 6.1) (81). These toxic metabolites originate from enzymatic reactions involving alcohol dehydrogenase and aldehyde dehydrogenase (327).

DEG and EG contamination in medical products have been reported as sources of human intoxication (81,321) and may result from accidental mislabelling of barrels or deliberate criminal activity (322,328) since both industrial solvents are a fraction of the cost of pharmaceutical grade PG and glycerol. Both DEG and EG are colourless, odourless, and have a sweeter taste than PG and glycerol. Industrial-grade PG and glycerol are also cheaper than pharmaceutical-grade solvents, but should also not be used since they lack the required purity for oral consumption. DEG is an excellent solvent for water-insoluble chemicals with a sharp, slightly sweet taste and has been used as a component in a wide range of industrial products (329). The ingestion of DEG can lead to serious complications and can be fatal due to metabolic acidosis caused by the metabolite HEAA, which is the major contributor to renal and neurological toxicities (329). On the other hand, although EG is a non-toxic substance by itself (330), it is frequently considered an intoxicant in poisoned patients (331) due to its metabolic breakdown to oxalic and, to a greater extent, glycolic acids, which contribute to a significant metabolic acidosis (332,333). Haemodialysis is considered useful for EG-

poisoned patients (334) and is initiated when glycolic acid blood serum level exceeds 8 mmol/L (333).

The first reported case of contaminated syrup intoxication occurred in 1937 in the United States of America with the antibiotic product Elixir Sulfanilamide (335), and multiple outbreaks have occurred in different parts of the world since then (81). From October 2022 to March 2025, whilst this research was being carried out, over a dozen of global medical product alerts were issued by the WHO for over-the-counter (OTC) medicines contaminated with DEG/EG in The Gambia (336), Indonesia (337), Uzbekistan and Cambodia (338), the Federated States of Marshall Islands and Micronesia (339), Cameroon (340), the Republic of Iraq (341), The Maldives and Pakistan (20, 21), Thailand (328), India (322), Kenya, Nigeria, Rwanda, South Africa, Tanzania, and Zimbabwe (344). It has been estimated that there have been at least 300 fatalities in children worldwide (323). In The Gambia, as of 2022, adulteration of anti-histamine and cough-and-cold syrups has led to the death of 70 children, while in Indonesia, the fraudulent use of EG/DEG as a solvent in liquid medicine formulations was reported to be the cause of 324 cases of acute kidney injury leading to 199 child deaths, reported by the Indonesian Ministry of Health (79,80).

In 2022, the Indonesian Food and Drug Authority (Badan Pengawas Obat dan Makanan Republik Indonesia/BPOM RI) identified barrels labelled as PG that were contaminated with 4.69 - 99.09% weight per weight (% *w/w*) of EG (345). In another report, BPOM RI found cases of PG raw material contaminated with 33.46% EG and 5.94% DEG. In addition, 1.28 to 443.66 mg/mL (equivalent to 0.13 to 44.37%) of EG and DEG contamination was detected in finished syrup products (346).

The minimum lethal dose of DEG/EG intoxication in humans is uncertain, with a wide toxicity range (347). The maximum allowable level of DEG/EG is 0.1% *w/w* in raw materials or finished pharmaceutical products (324). Syrup manufacturers should test for DEG and EG in all barrels received labelled as PG or glycerol. However, syrup manufacturers may fail to adhere to manufacturing QC procedures (82).

6.1.2. Tools to detect DEG and EG contamination

The International Pharmacopoeia describes GC as the most suitable and widely used analytical technique to test pharmaceutical products precisely and accurately for DEG and EG, down to or below the minimum safe level for humans of 0.1% *w/w* (324). However, the method is costly, laborious, time-consuming and often not available in many LMICs (349,350). Another screening method for non-compliance is using TLC, which allows the detection of DEG or EG concentrations down to 0.2% *w/w* (324). However, these techniques are limited to national QC laboratories with access to the instruments, reagents, and competent human resources. TLC has failed to detect contaminants in cough expectorants (351) and, in the same way as GC, requires personnel with adequate laboratory skills (324,350). Although TLC is a lower-cost approach compared to GC, the method requires several consumables, including silica gel TLC plates, a chromatographic tank, a hairdryer, solvents (which are toxic, flammable, corrosive and hazardous), a visualisation solution containing potassium permanganate (which is very toxic, corrosive and harmful) and ideally a laboratory fume hood.

To the best of my knowledge, the only low-cost and portable device which can help to differentiate glycerol from DEG is by using a mbira, an ancient African musical

instrument (352), that was modified to contain the sample for analysis. The mbira's tines were replaced with bent steel tubing to be filled with a sample, and while plucking the tubing, the generated sound was then recorded using a mobile smartphone to measure the frequency of the sound using a free software tool and determine the density of the sample with a resolution of about 0.012 g/mL (352). Using this method, DEG and glycerol could be distinguished. However, the mbira has not been tested for PG, EG, or alcohol spiked into medicinal syrups. Furthermore, the limit of detecting DEG in glycerol using an mbira has not been investigated, and it is unlikely that it would be able to detect low levels of DEG or EG near the toxic and fatal threshold levels.

6.1.3. Alternative lower-cost methods to detect DEG/EG contamination

Alternative rapid, low-cost, portable and simpler methods to detect DEG/EG contamination are desirable. For the detection of DEG contamination, the use of polyethylene glycol (PEG) enzyme-linked immunosorbent assay (ELISA) and disposable breathalysers was evaluated. Enzymatic assays were tested based on the replication of EG metabolism in the body by converting it using alcohol dehydrogenase and aldehyde dehydrogenase to form glycolic acid, which could then be detected using glycolate oxidase and a substrate. These led to the evaluation of rapid diagnostic tests for alcohol detection in saliva and breast milk. In parallel, I investigated the expansion of the MALDI-ToF MS method for detecting EG and DEG contamination.

Mass spectrometry has been used to analyse glycols and glycerol by incorporating a benzoyl ester derivatisation method (353). I applied this approach and utilised a MALDI-ToF instrument to analyse DEG/EG contamination in raw materials and finished

products. The MALDI-ToF MS spectra profiles of EG and DEG were analysed, and additional multivariate analyses were used to specify the chemicals.

In this chapter, I investigated novel methods for detecting and preventing EG and DEG contamination that have the potential to be implemented in local settings and are beneficial for empowering the local NRA. The suitability of enzymatic assays and MALDI-ToF MS to detect DEG/EG contamination was evaluated. The low-cost enzymatic assays can be used as rapid screening tests in field settings without the need for a specialist to interpret the results. With an additional derivatisation protocol in a reference laboratory, MALDI-ToF MS may provide sensitive detection of EG and DEG in raw materials and medicinal syrups. Furthermore, the tests could also provide useful preliminary indicators of DEG and EG prior to further testing using more selective and sensitive techniques.

6.2. Materials and Methods

6.2.1. Chemicals and sample preparation

Ethylene glycol (≥99%, Sigma-Aldrich Cat. No. 102466), diethylene glycol (for synthesis, Sigma-Aldrich Cat. No. 8.03131), propylene glycol (Ph. Eur. grade, Sigma-Aldrich Cat. No. 16033), and glycerol (Ph. Eur. grade, Sigma-Aldrich Cat. No. 49779) were used in the study. A 5% *v/v* alcohol solution was prepared by volumetric measuring of 0.5 mL of alcohol and adding double-distilled water (Milli-Q, Millipore) up to 10 mL. EG-spiked PG samples were prepared by weighing EG in an amount to generate a percentage of 10.0, 5.0, 2.0, 1.0, 0.5, 0.1, and 0.05% *w/w* in PG.

6.2.2. Finished medical products

Eleven cough syrups and syrups containing paracetamol, ibuprofen and cetirizine were purchased OTC from local pharmacies in the UK and Indonesia (Table 6.1). EG-spiked samples of representative OTC syrups were prepared by gravimetrically adding EG to the syrup matrix, generating 10.0, 5.0, 2.0, 1.0, 0.5, 0.1, 0.05 and 0.01% *w/w* solutions. The syrups include products containing ethanol (Beechams, Covonia, and Benylin Chesty for adults) and paediatric syrups without ethanol (Calprofen, Dimetapp, Benylin Infant's, and Piriteze).

6.2.3. Ethanol assay

An ethanol assay was repurposed to qualitatively detect the presence of alcohol in the sample using the Ethanol Assay Kit (Megazyme Cat. No. K-ETOH, Wicklow, Ireland). In a clear-flat 96-well microplate (Greiner Bio-One, Stonehouse, UK), 10 µL of the sample was mixed with 200 µL of distilled water, 20 µL of buffer, 20 µL of NAD^+, and 5 µL of alcohol dehydrogenase enzyme. The reaction was mixed, incubated for 2 minutes at RT (recorded at 20 ± 1°C), and measured for the first absorbance (A1) at 340 nm on a Clariostar Plus microplate reader (BMG Labtech, Ortenberg, Germany). Without delay, 2 µL of aldehyde dehydrogenase enzyme was added to the reaction mix, incubated for 5 minutes at RT, and measured for the second absorbance at 340 nm (A2) in one-minute intervals for 15 minutes. The final absorbance was achieved from the subtraction of A2 and A1. The resulting absorbances were blank subtracted. The acids formed in the wells of the plate were used for the glycolic acid assay.

Table 6.1. The medicinal syrups used in the study which were bought commercially from registered pharmacies in the UK and Indonesia. The excipient ethanol is highlighted in bold.

Brand	Manufacturer	Intended use	Active Pharmaceutical Ingredients	Excipients
Beechams All in One	GlaxoSmithKline, Brentford, UK	Adults and children aged 16 years and over	Paracetamol, guaifenesin, phenylephrine hydrochloride	**Ethanol** (19% *v/v*), sodium propylene glycol, sorbitol, glycerol
Benylin Chesty Coughs non-drowsy	McNeil, High Wycombe, UK	Adults and children aged 12 years and over	Guaifenesin, levomenthol	Sucrose, liquid glucose, **ethanol**, glycerol, sodium citrate, saccharin sodium, citric acid monohydrate, sodium benzoate
Benylin Infant's Cough Syrup	McNeil, High Wycombe, UK	Children aged 3 months to 5 years	Glycerol	Maltitol liquid, hydroxyethylcellulose sodium citrate, sodium benzoate, citric acid monohydrate, propylene glycol
Bodrexin Flu & Batuk PE	PT. Tempo Scan Pacific, Tbk., Bekasi, Indonesia	Children below 12 years	Paracetamol, phenylephrine hydrochloride, guaifenesin, bromhexine hydrochloride, chlorphenamine maleate	No information
Calprofen	McNeil, UK	Babies and children aged 3 months to 12 years	Ibuprofen	Glycerol, xanthan gum, polysorbate 80, flavouring agent (contains propylene glycol and **ethanol**), maltitol, saccharin sodium, citric acid monohydrate, sodium methyl hydroxybenzoate, sodium propylhydroxybenzoate

Covonia	Thornton and Ross, Huddersfield, UK	Adults and children aged over 1 year	Honey, capsicum tincture, menthol, peppermint oil, anise oil, liquorice extract	Glycerol, **ethanol** (in capsicum tincture), citric acid, glucose, flavouring agent (contains ethanol), propylene glycol
Dimetapp Cold and cough	Foundation Consumer Brands, LLC., USA	Children 6 to under 12 years, children 12 years and older and adults	Brompheniramine maleate, dextromethorphan HBr, Phenylephrine HCl.	Anhydrous citric acid, glycerin, propylene glycol, sodium benzoate, sodium citrate, sorbitol solution, sucralose
OBH Combi Anak Batuk plus flu	Combiphar, Bandung, Indonesia	Children aged 2 to 12	Paracetamol, succus liquiritiae, ammonium chloride, pseudoephedrine hydrochloride, chlorphenamine maleate	No information
Paratusin	PT. Darya Varia Laboratories, Tbk., Bogor, Indonesia	Adults and children aged 2 to 12	Paracetamol, pseudoephedrine hydrochloride, noscapine, chlorphenamine maleate, guaifenesin, succus liquiritiae	**Ethanol** (10% *v/v*)
Piriteze Childrens' Hayfever & Allergy Syrup (GSL)	Haleon, Weybridge, Surrey, UK	Children 2 years and above	Cetirizine hydrochloride	Sorbitol
Termorex Plus Flu dan batuk	PT. Konimex, Sukoharjo, Indonesia	Children aged 2 to 12	Paracetamol, pseudoephedrine hydrochloride, guaifenesin, chlorphenamine maleate	No information

6.2.4. Glycolic acid assay

The presence of glycolic acid in samples was detected using the Glycolic Acid Assay Kit (Fluorometric) (Abcam Cat. No. 282915, Cambridge, UK), using the manufacturer's protocol. The samples analysed were the products of the ethanol assay kit (method described above) and diluted 10× in assay buffer. A volume of 50 µL of the prepared sample was added into a well of a 96-well black flat bottom plate (Corning, UK). A reaction mix was prepared consisting of 44 µL of assay buffer, 2 µL of detection reagent, 2 µL of enzyme mix (contains glycolate oxidase) and 2 µL of fluorogenic probe. A total of 50 µL of reaction mix was then added to the prepared sample, and the fluorescence was recorded at 30-second intervals for 90 minutes at RT with a setting of the microplate reader at Ex/Em = 535/587 nm. The fluorescence for the blank was subtracted from the fluorescence measurements for each sample.

6.2.5. Polyethylene glycol (PEG) Enzyme-linked Immunosorbent Assay (ELISA)

The PEG ELISA kit (Abcam Cat. No. ab215546, Cambridge, UK) was used according to the manufacturer's protocol. A competitive ELISA format was used, where a mixture of 50 µL sample and 50 µL of 1× PEG-HRP was prepared and 50 µL of the mixture was then added to the anti-PEG antibody-coated 96-well in a strip format. The reaction was incubated for 45 minutes at RT on a plate shaker set to 400 rpm. Following the incubation, the sample mix was aspirated, and the well was washed three times with 1× wash buffer. A volume of 100 µL of TMB substrate was then added to the well and

incubated for 15 minutes at RT in the dark with shaking, prior to the addition of 100 µL of stop solution and an absorbance reading at 450 nm.

6.2.6. Alcohol strip tests

Alcohol samples prepared in water were tested by adding 20 µL of sample onto the pad of the Alcohol Rapid Test Strip (Saliva) (Surescreen Diagnostics, Eagle Park, UK) or Frida mom Breast Milk Alcohol test (Frida, Miami, Florida, USA). Other strip tests evaluated include the One Step Saliva Alcohol Rapid Test Dipstick and AllTest Alcohol Rapid Test Dipstick (Saliva) (both from Hangzhou AllTest Biotech Co. Ltd., Hangzhou, P.R. China, distributed by Home Health, Bushey, UK), and Easy@ Home Breastmilk Alcohol test (Safecare Biotech, Hangzhou, P.R. China). Spiked PG samples and cough syrup samples were 5× diluted in Milli-Q water before being added to the pad. The reaction was allowed to proceed for 2 minutes at RT. The presence of blue colour qualitatively identifies the presence of alcohol in the sample. Additionally, a semi-quantitative interpretation of the alcohol range can be visually identified based on the intensity of the resultant blue colour.

6.2.7. Alcohol breathalyser

The One Step alcohol breathalyser (Test&Drive Sp. Z o.o., Ploty, Poland, distributed by Home Health Ltd, Bushey, UK) was repurposed by testing 1% *v/v* of diluted alcohol sample in water. The security seal of the test tube was broken by pressing firmly on both ends of the tube. An amount of 75 µL of diluted alcohol was added to the blowing end of the tube and flicked twice to ensure the liquid reached the crystal. The test was allowed

to incubate at room temperature for 2 minutes, with a manual recording of the time of colour change and visual observation of the resultant colour change in the crystal.

6.2.8. MALDI-ToF MS assay

6.2.8.1. Benzoyl chloride derivatisation

The derivatisation of glycol samples using benzoyl chloride (Figure 6.2) was performed by mixing 100 µL of alcohol sample with 100 µL of 4M NaOH (in distilled water) in a 2.0 mL centrifuge tube. To the mixture and under a chemical hood, an amount of 25 µL benzoyl chloride (ReagentPlus, 99%, Sigma Aldrich, UK) was added. The mixture was then vortex-mixed and incubated for 5 minutes at RT. An amount of 50 µL 10% glycine (*w/v* in distilled water) was added, vortex-mixed and incubated at RT for 3 minutes, followed by the addition of 1 mL of heptane (anhydrous, 99%, Sigma-Aldrich, UK). The tube was then vortex-mixed and centrifuged at 3,500 × *g* for 5 minutes at RT. A volume of 100 µL of the top organic layer was collected and moved to a fresh 1.5 mL centrifuge tube. The organic layer was dried using a Speed-Vac concentrator (Eppendorf, Germany) for 15 minutes at 40°C. The dried solution was reconstituted with 12 µL of CHCA matrix (bioMérieux, France), vortex-mixed, centrifuged briefly to pellet the content, and sonicated for 5 minutes. Another round of vortex and brief centrifugation was performed, and two µL of the derivatised sample was then spotted onto each of four MALDI slide wells (bioMérieux, France) (N=4). Samples were run on a VITEK-MS MALDI-ToF (bioMérieux, France) at 0-900 *m/z*.

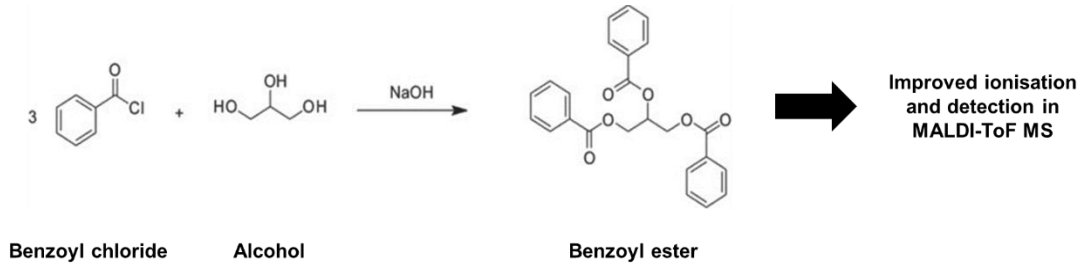

Figure 6.2. The schematic reaction of benzoyl chloride derivatisation of alcohol for MALDI-ToF MS sample preparation. Benzoyl chloride is reacted with alcohol (glycerol as an example) in a basic condition to generate a benzoyl ester form with a higher molecular weight and improved ionisation properties in MALDI-ToF MS. Image adapted from Nanco CR, *et al*. *J Anal Toxicol* 2019 (353)

6.2.8.2. MALDI-ToF mass spectrometry assay and spectral analysis

The MALDI-ToF MS assay and spectral analysis were performed according to the established method integrating MS spectral analysis and multivariate analysis (246) and are described in full in Chapter 4. Briefly, raw MS spectra were acquired at 0–900 *m/z* after instrument calibration with MBT Star-ACS (Bruker). Manual inspection of the raw mass spectra was performed by uploading the data files into the Shimadzu Biotech Launchpad software (version 2.9.5.6) from the VITEK-MS instrument. Raw spectra in *.mzXML format were imported into R Studio and processed in R v4.1.2 using the MALDIQuant package. The resulting peak intensity list (Supplementary file) was exported as a *.csv file for further analysis using MetaboAnalyst (version 5.0, https://metaboanalyst.ca). Statistical analysis figures and graphical representations were created using both MetaboAnalyst and GraphPad Prism (GraphPad Software, Boston, MA, USA; v.9.4.1).

6.3. Results

6.3.1. The detection of EG and DEG in raw materials using enzymatic assays

EG was successfully differentiated from the other alcohols (glycerol, PG and DEG) using alcohol dehydrogenase, aldehyde dehydrogenase and a plate reader to record the formation of NADH at 340 nm (Figure 6.3 A). By additionally using glycolate oxidase, a fluorogenic substrate, and recording the fluorescence with a plate reader, it was possible to more specifically determine EG and differentiate it from other alcohols by analysing the end-point absorbance (Figure 6.3 B) and relative fluorescence unit (RFU) (Figure 6.3 C).

More importantly, it was possible to successfully identify EG simply by visual observation of the oxidised fluorogenic substrate as a pink colour (Figure 6.3 D) without the need for a plate reader. The PEG ELISA showed that amongst the alcohols tested, there was some preferential binding to DEG, although this was very weak, and it is difficult to use this assay to discriminate DEG from the other alcohols (Figure 6.4).

6.3.2. The detection of EG in PG matrix using enzymatic assays

Alcohol and glycolic acid assays were used to test different concentrations of EG-spiked PG. The presence of EG in PG matrix could be confidently detected down to the percentage of 2% (Figure 6.5 A) and 1% (Figure 6.5 B), for alcohol assay and glycolic assay, respectively.

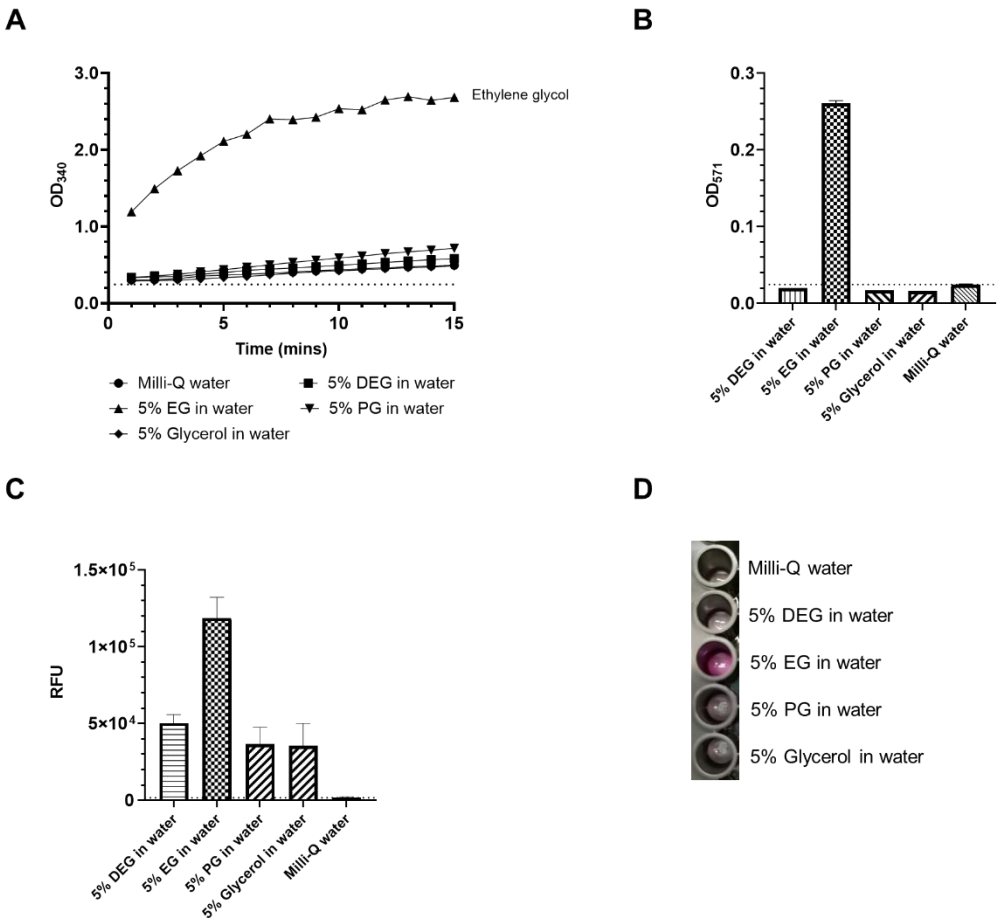

Figure 6.3. Determining EG using enzymatic assays. A. Using alcohol dehydrogenase and aldehyde dehydrogenase, EG was found to convert at a far higher rate than the other alcohols. NADH was measured at 340 nm over 15 minutes. The dotted line shows the blank absorbance limit. B. Further analysis using glycolate oxidase to detect glycolic acid, EG could be determined more specifically with endpoint absorbances measured at 571 nm. C. The detection of glycolic acid in alcohol samples, measured as the relative fluorescence unit (RFU). D. The identification of EG simply by visual observation of the oxidised fluorogenic substrate as a pink colour without the need for a plate reader. No pink colour was observed for the other alcohols. Error bars show the standard deviations of two replicates.

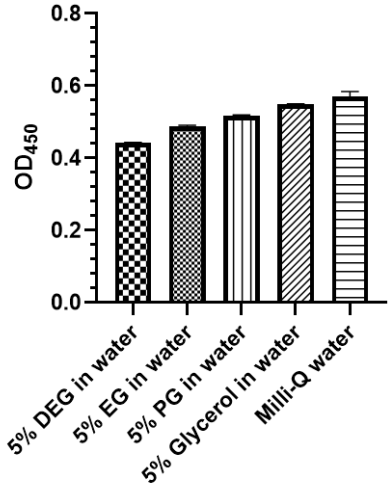

Figure 6.4. PEG ELISA results of the alcohol solutions show very weak preferential binding to DEG. Lower absorbances show greater binding due to this being a competitive ELISA. Error bars show the standard deviations of two replicates.

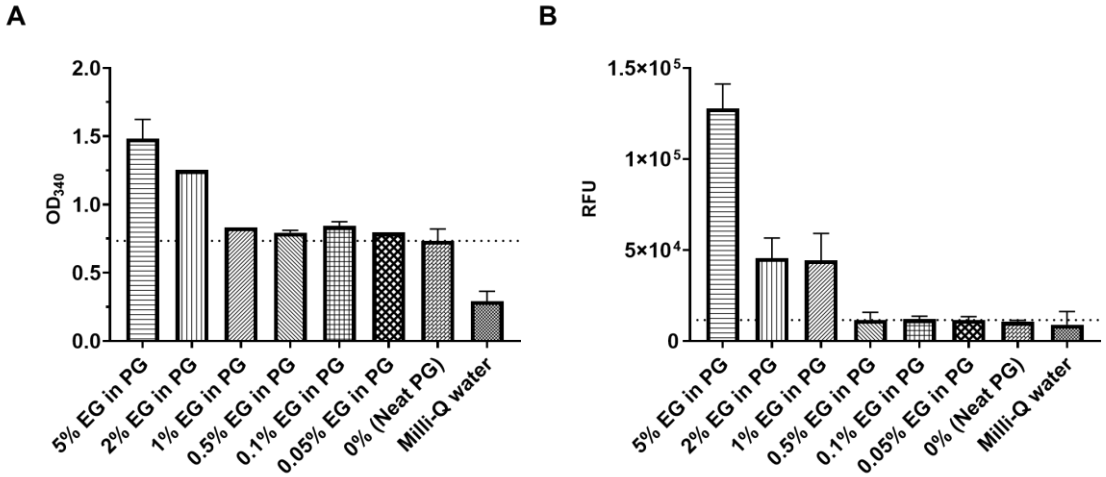

Figure 6.5. Determining EG in PG using enzymatic assays. PG was spiked with different percentages of EG. A. Endpoint 340 nm absorbance readings of NADH after using alcohol dehydrogenase and aldehyde dehydrogenase. B. Relative fluorescence unit (RFU) readings after additionally using glycolate oxidase in the glycolic acid assay. Milli-Q water was used as a no-matrix control. The dotted line shows the detection limit of neat PG. Error bars show the standard deviations of two replicates.

6.3.3. The detection of EG in medicinal syrups using an ethanol assay combined with a glycolic acid assay

EG-spiked syrups were prepared using both Calprofen and Dimetapp paediatric syrup matrices. The ethanol assay was able to detect EG as low as 0.1% and 0.5% *w/w* in Calprofen and Dimetapp, respectively (Figure 6.6 A). The glycolic acid assay was further able to detect EG at a percentage down to 0.01% *w/w* in both medicinal syrup matrices (Figure 6.6 B), although only small absorbance differences were observed in syrups spiked below 0.1% *w/w*, making it hard to distinguish whether the absorbance was due to the presence of EG or only noise. The assays, however, did not perform well for the detection of EG in other syrup matrices containing ethanol, *i.e.* Beechams, Benylin Chesty for adults, and Covonia (Figure 6.6 C and D). The detection limit of EG in syrups was therefore determined to be at 0.1% *w/w* for both ethanol and glycolic acid assays.

6.3.4. Alcohol strip tests in alcohol raw material testing

Five different brands of alcohol strip tests designed to detect alcohol in saliva and breast milk samples were tested initially in solutions of alcohol raw materials in water (Figure 6.7). All strips could successfully and rapidly (within 2 minutes) differentiate EG from glycerol and PG. The Surescreen alcohol saliva test kit detected EG with higher sensitivity and with minimal cross-reactivity to PG, compared to the One Step Saliva Alcohol Rapid Test Dipstick and AllTest Alcohol Rapid Test Dipstick (Saliva). On the other hand, the Frida mom Breast Milk Alcohol test showed a higher sensitivity to detect EG, compared to the Easy@ Home Breastmilk Alcohol test (Figure 6.7).

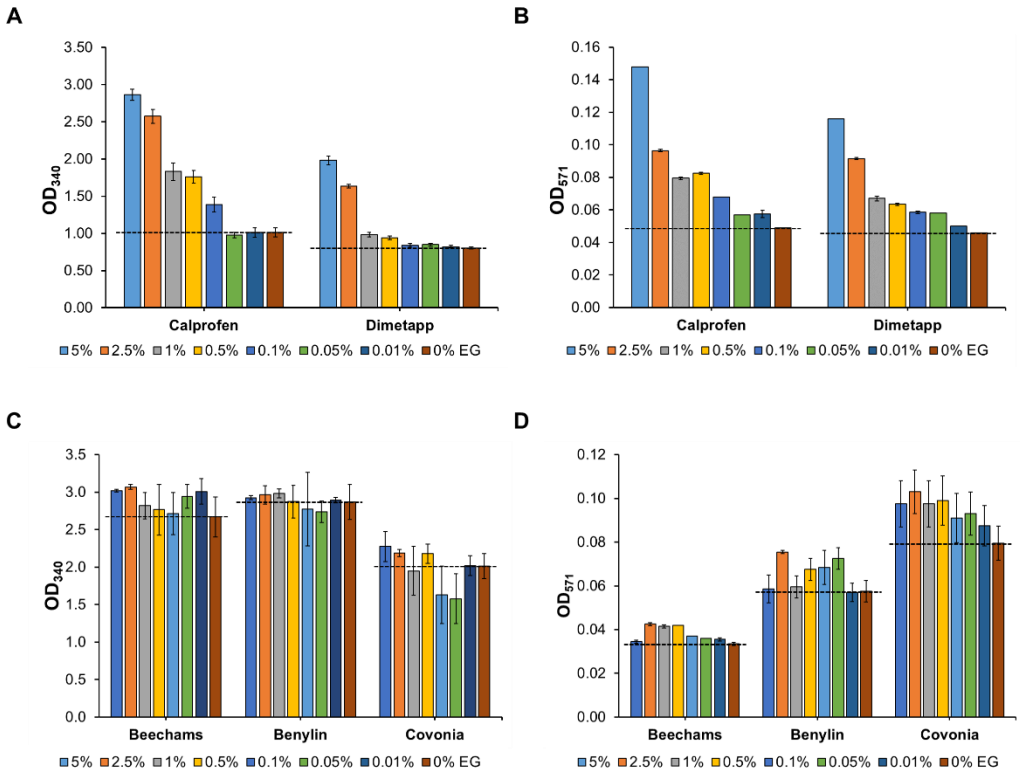

Figure 6.6. The enzymatic assay results of medicinal syrups spiked with different percentages of ethylene glycol. A. Ethanol assay results at end-point 340 nm absorbance reading after 15 minutes of incubation time for two paediatric syrups Calprofen and Dimetapp. B. Glycolic acid assay results at end-point 571 nm absorbance reading after 90 minutes of incubation time for two paediatric syrups. C. Ethanol assay results for three ethanol-containing syrups Beechams, Benylin Chesty, and Covonia. D. Glycolic acid assay results for three ethanol-containing syrups. Error bars show the standard deviations of two replicates. The measured absorbance values in panels A and C were out of the linear range.

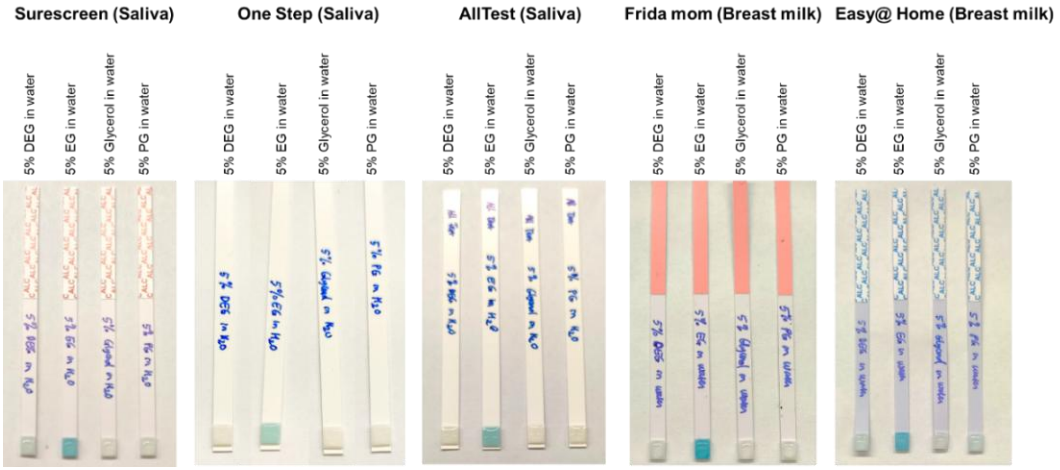

Figure 6.7. A comparison between five different brands of alcohol saliva and breast milk strip tests in detecting 5% *v/v* alcohol solutions in water

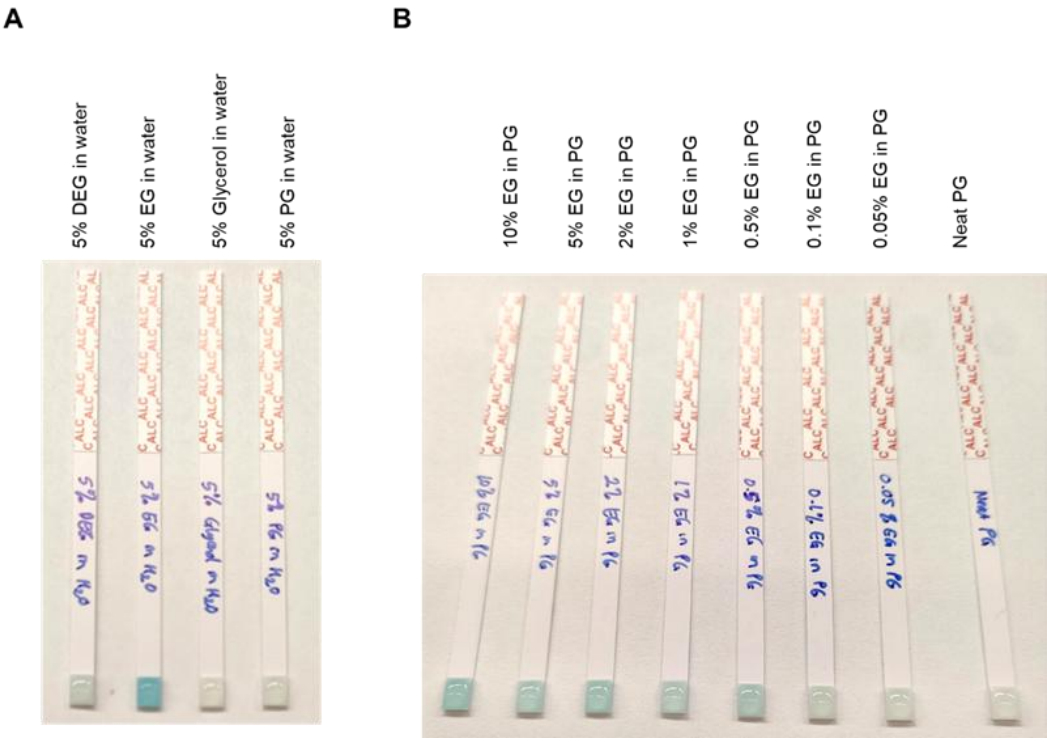

Figure 6.8. Alcohol saliva strip test results for glycols in water and PG. A. Alcohol saliva strip test results of 5% *v/v* alcohol in water and B. in different percentages of EG-spiked PG

The Surescreen alcohol saliva strip and Frida mom breast milk strip tests were then chosen as the rapid tests for EG detection. The Surescreen alcohol saliva strip could detect EG in both the 5% water solution and PG matrix (Figure 6.8). A slight colour change was observed for DEG, although it was not easily noticeable (Figure 6.8 A). The Surescreen alcohol saliva strip could also determine EG down to 0.5% *w/w* when spiked into PG (Figure 6.8 B).

6.3.5. Alcohol rapid strip tests to detect EG in medicinal syrups

The potential use of the alcohol saliva strip test was then tested in medicinal syrups. As expected, no change in the colour of the saliva strips was observed for the four non-alcohol-containing syrups (Figure 6.9 A and Table 6.1). Syrups that contain ethanol in the formulation generated a strong blue colour with the colorimetric substrate on the saliva strips. Visualisation of the blue colour change was more noticeable in colourless syrup samples (Figure 6.9 B).

Dimetapp, known to be free from ethanol, did not show a blue colour change, but the pad was slightly coloured due to the syrup colour. Calprofen and Covonia, both known to contain ethanol, showed no blue colour on the pad of the strips, although for Covonia, the pad was coloured due to the syrup colour. All other syrups known to contain ethanol (Beechams, Benylin Chesty and Paratusin) generated a blue colour on the pad of the strips.

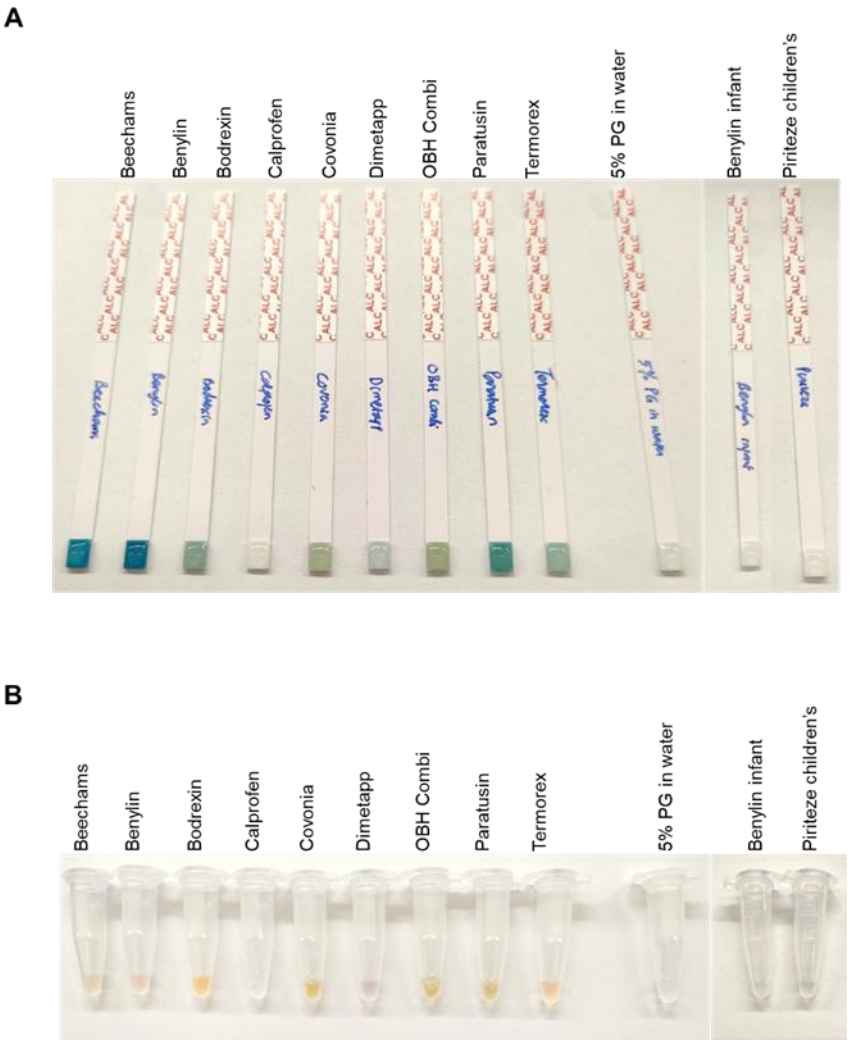

Figure 6.9. Alcohol saliva strip test results for neat medicinal syrups from 11 different manufacturers compared to 5% *v/v* PG in water. A. The visual of the alcohol saliva strip pad after the addition of the 5× diluted syrups. B. The colour of 5× diluted syrups in water before spotting onto the strip pad

6.3.6. Alcohol strip tests to determine EG spiked into infant medicinal syrups

Benylin infant and Piriteze syrups were spiked with various concentrations of EG. Both alcohol saliva and breast milk tests were able to detect EG, as shown in Figure 6.10. The

lowest detectable level of EG in the spiked syrups, for both alcohol strips, were 1% and 2% *w/w* in Benylin infant and Piriteze syrups, respectively.

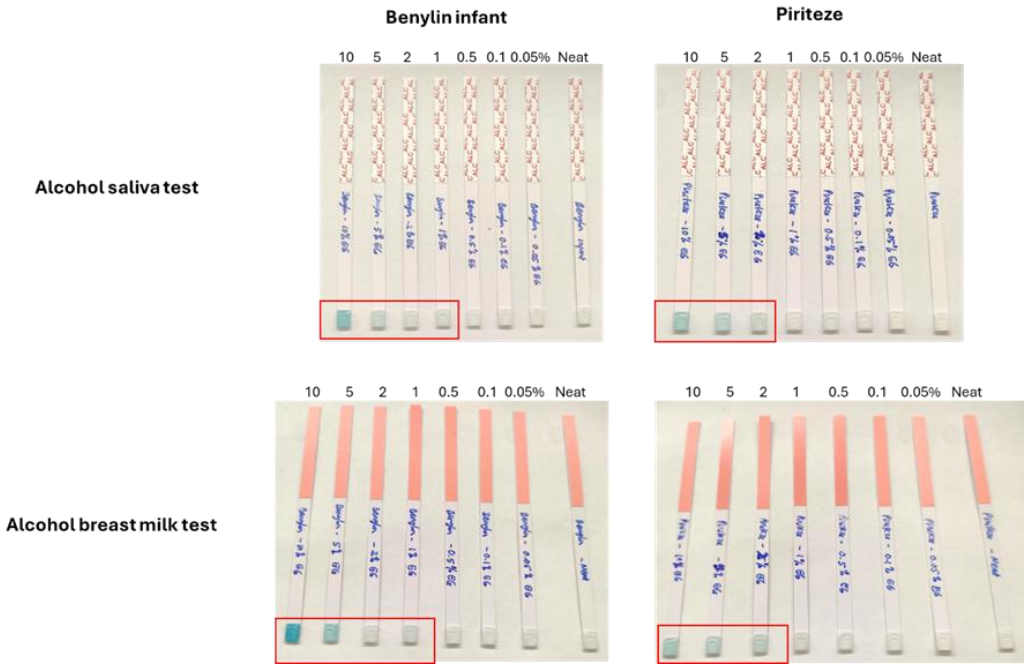

Figure 6.10. The detection of EG in spiked Benylin infant and Piriteze medicinal syrups using Surescreen alcohol saliva and Frida mom alcohol breast milk strip tests. The strips detect EG down to 1% and 2% *w/w* for Benylin infant and Piriteze, respectively (red boxes).

6.3.7. Alcohol breathalyser for the evaluation of toxic alcohols

Using the alcohol breathalyser, the detection of DEG could be established by observing the rate of crystal colour change after the addition of alcohol samples. Using a 1% *v/v* alcohol dilution in water, both glycerol and PG samples rapidly changed the colour of the crystals in test tubes from colourless to dark brown within seconds (Figure 6.11 A). The diluted EG had a lower rate of colour change, where a slight colour change for EG was observed at 10 seconds, and the crystals turned dark brown after two minutes (Figure 6.11 B). DEG did not change the crystal colour even after two minutes of incubation (Figure 6.11 B).

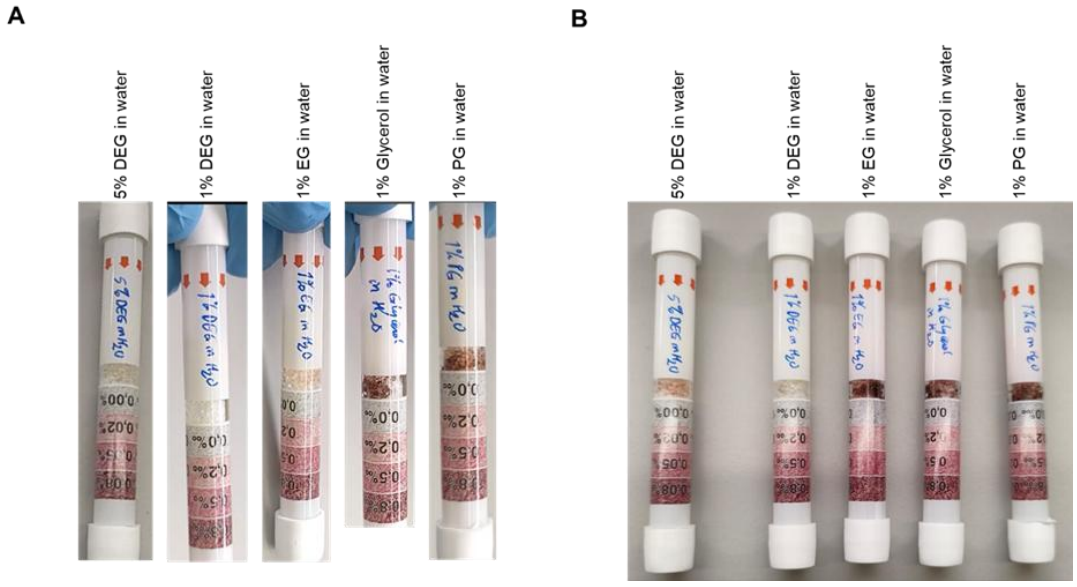

Figure 6.11. Alcohol breathalyser results from diluted alcohol in water. The results were recorded after incubation times of 10 seconds (A) and two minutes (B)

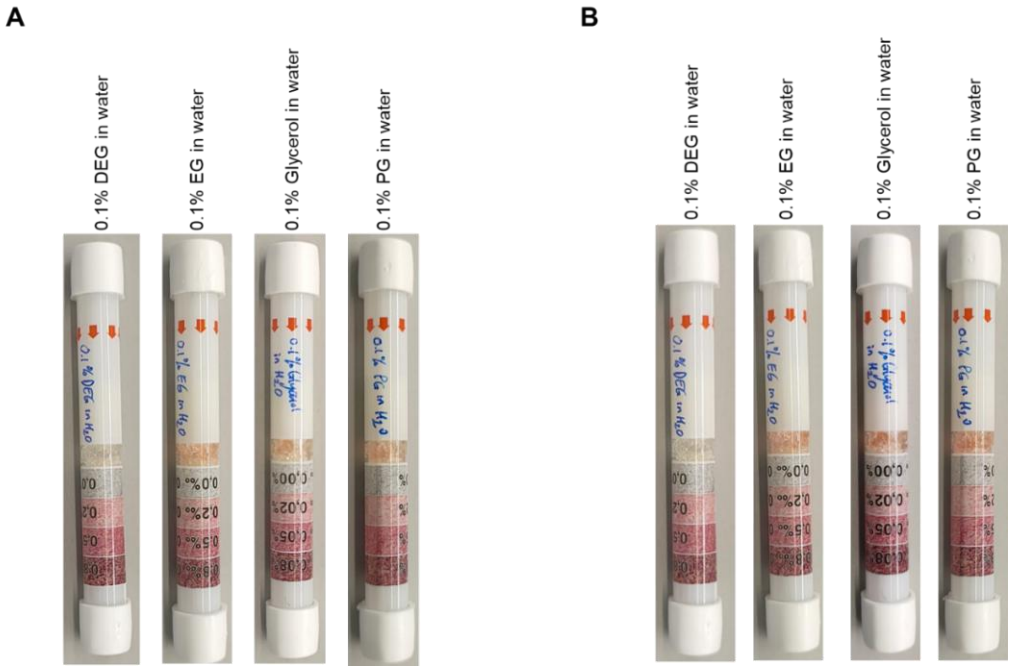

Figure 6.11. Alcohol breathalyser results of 0.1% *v/v* diluted alcohol in water. The results were recorded after incubation times of 10 seconds (A) and two minutes (B)

The best dilution of the alcohols in water was found to be 1% *v/v* in water when using the breathalysers. Testing a 5% *v/v* DEG dilution in water gave a slight colour change after two minutes (Figure 6.11 B), although the reaction was not rapid (Figure 6.11 A). Further testing of the alcohol breathalyser using the 0.1% *v/v* alcohol solution in water was able to distinguish between DEG and other alcohols (Figure 6.12). An optimum sample dilution of 1% *v/v* in water is recommended for the optimum sensitivity and specificity of this breathalyser tool.

6.3.8. The detection of EG and DEG using MALDI-ToF MS

DEG, EG, PG and glycerol were diluted to 5% *v/v* in water and analysed by MALDI-ToF MS. As expected, no additional peaks were observed for these alcohols when compared with the matrix spectrum (Figure 6.13) since the molecules are too small to be detected by MALDI-ToF MS.

Benzoyl chloride derivatisation of glycol samples in solution improved the ionisation and detection in MALDI-ToF MS with expected higher *m/z* peaks (Figure 6.14). DEG spectra could readily be distinguished by visual inspection by the presence of the 337 *m/z* peak (corresponding to the sodiated ion of DEG (DEG[M+Na]$^+$). A peak at 149 *m/z* was found in both EG and DEG samples, and fewer peaks were observed between 250 and 450 *m/z* compared to the other alcohols (Figure 6.14). Derivatisation allowed the differentiation of both EG and DEG spectra from PG and glycerol.

Multivariate analysis of derivatised samples' spectra could further group and differentiate EG and DEG from PG and glycerol (Figure 6.15). Both PCA and PLS-DA confidently separated toxic alcohols from non-toxic ones. Therefore, derivatisation allowed the differentiation of both EG and DEG spectra from PG and glycerol.

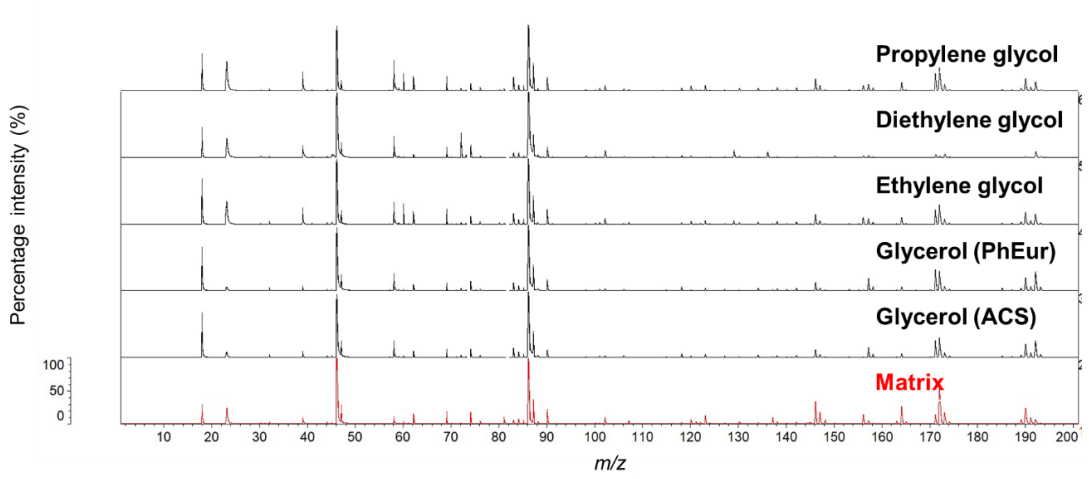

Figure 6.13. Spectra of non-derivatised alcohols in water solution generated by MALDI-ToF MS at 0-200 *m/z*

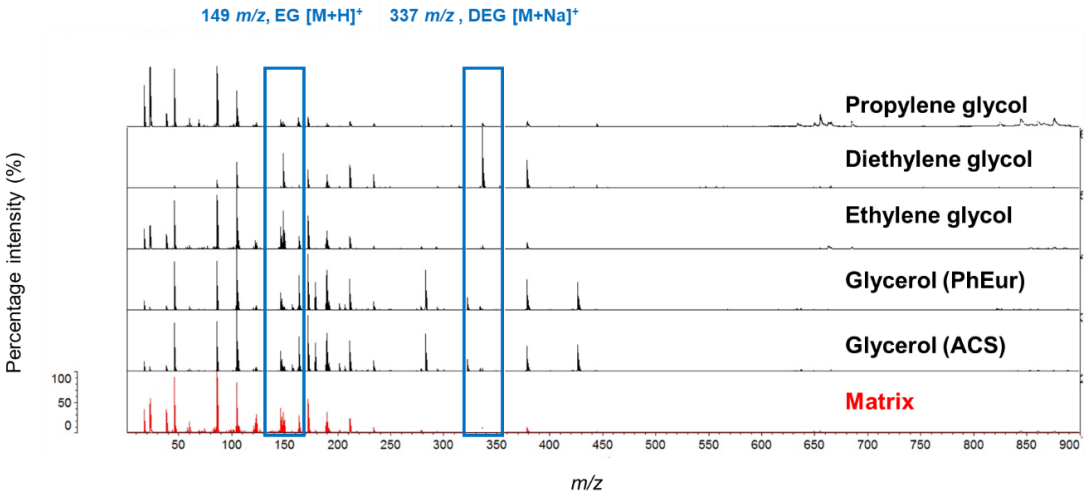

Figure 6.14. MALDI-ToF spectra of different alcohols after derivatisation using benzoyl chloride at 0-900 *m/z*. The spectra show signature peaks at 337 *m/z* for DEG and 149 *m/z* for both EG and DEG.

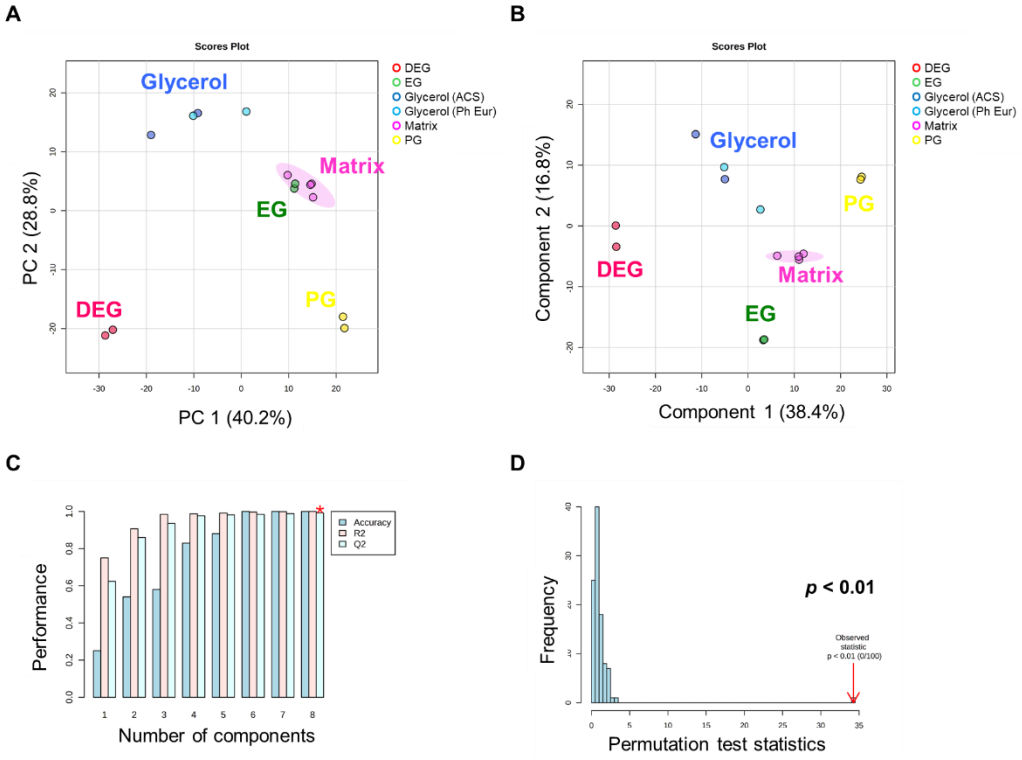

Figure 6.15. Multivariate analysis of 5% *v/v* alcohol solution in water after derivatisation using benzoyl chloride. Toxic alcohols EG and DEG could be differentiated from non-toxic alcohols PG and glycerol using A. PCA score plot result, B. PLS-DA score plot result and confirmed with C. cross-validation and D. permutation analysis results. The analysis was performed using four sample replicates (N=4).

When testing PG spiked with DEG or EG, MALDI-ToF was able to detect these same peaks corresponding to EG and DEG (Figure 6.16). EG could be detected at levels as low as 0.5% *w/w,* while DEG could be detected at only 0.05% *w/w*. For DEG, the *m/z* 337 peak helped in identifying contamination down to 0.05% *w/w* when spiked into PG. At 0.05% DEG, the peak intensity ratio of the peaks at *m/z* 337:335 was roughly 1:1, and if the peak intensity of the *m/z* 337 peak exceeded that of the *m/z* 335 peak, it helped to indicate more than 0.05% *w/w* DEG contamination. A peak at *m/z* 149 for DEG also helped in its identification, although the *m/z* 337 peak was of much greater intensity (Figure 6.14). For EG, the *m/z* 149 peak helped in identifying contamination down to 0.5% *w/w* when spiked

into PG. At 0.5% EG, the peak intensity ratio of the peaks at *m/z* 149:147 was roughly 1:1, and if the peak intensity of the *m/z* 149 peak exceeded that of the *m/z* 147 peak, it helped to indicate more than 0.5% *w/w* EG contamination.

In a more complex syrup matrix, spiked samples could be detected at levels as low as 1% for both EG and DEG (Figure 6.17). In a similar way to EG and DEG spiked into PG, this detection was achieved by analysing the peak intensity of the *m/z* 149 and 337 peaks relative to neighbouring peaks (*e.g.* the *m/z* 337 peak for DEG having a greater intensity than the *m/z* 336 peak indicated more than 1% *w/w* DEG contamination).

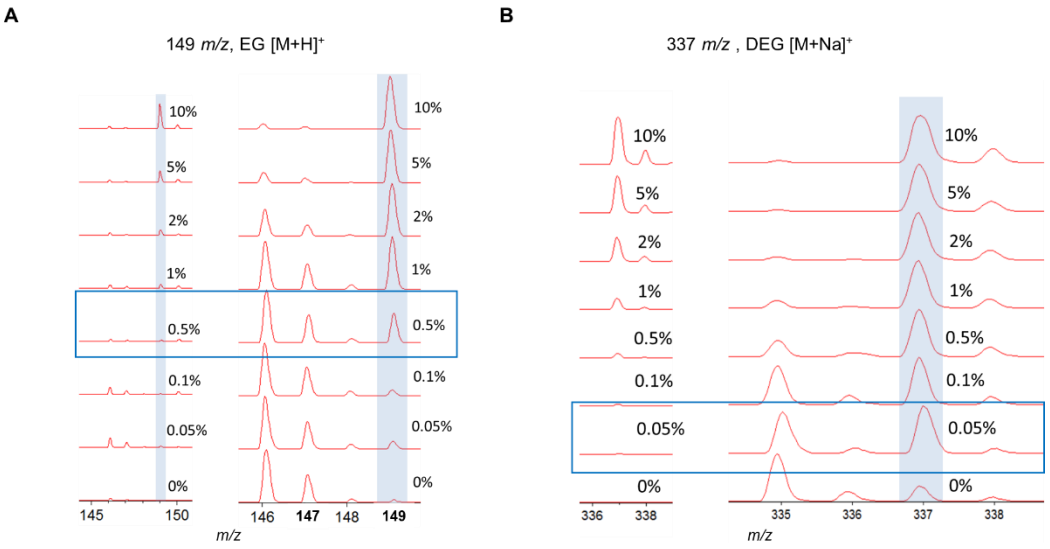

Figure 6.16. The sensitivity of MALDI-ToF MS in detecting the *m/z* 149 peak for EG (panel A) and the *m/z* 337 peak for DEG (panel B) in spiked into PG and derivatised with benzoyl chloride. The spectra on the left of each panel show the true relative intensities of the *m/z* 149 and 337 peaks. The spectra on the right of each panel show the same peaks but with the tallest peak in the mass range shown set at 100% height to allow neighbouring peaks to be seen more clearly. The panels were zoomed-in from the original 0-900 *m/z* spectra. MALDI-ToF MS was able to detect down to 0.5% and 0.05% *w/w* of EG and DEG, respectively (blue boxes).

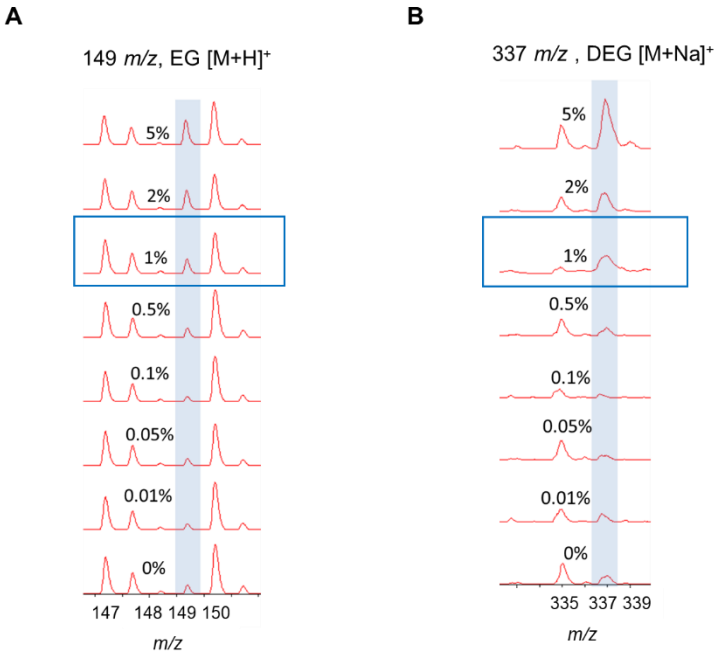

Figure 6.17. The sensitivity of MALDI-ToF MS in detecting EG (panel A) and DEG (panel B) in spiked Covonia syrup matrix, derivatised using benzoyl chloride. The panels were zoomed in from the original 0-900 *m/z* spectra. MALDI-ToF MS was able to detect down to 0.1% *w/w* of both EG and DEG (blue boxes).

6.4. Discussion

The alcohols, glycerol, and PG, used in syrups, are converted by alcohol dehydrogenase and aldehyde dehydrogenase to acids, which are safe. While DEG and EG themselves are not toxic, they are converted by the same two enzymes into very toxic metabolites (Figure 6.1). I used alcohol dehydrogenase and aldehyde dehydrogenase enzymes *in vitro* to copy the metabolism which occurs *in vivo* for individuals who have consumed these alcohols. In the case of EG, it is metabolised to glycolic acid for which an oxidase, glycolate oxidase, exists, allowing it to be detected simply with a chromogenic or fluorogenic substrate (Figure 6.3 B-D). I am unaware of an oxidase for HEAA or any other metabolites for DEG. Also, an oxidase for HEAA may not help since little conversion of

DEG with alcohol dehydrogenase and aldehyde dehydrogenase was observed (Figure 6.3 A). Therefore, further enzymatic assays for DEG were not explored.

Table 6.2. A summary of the assays repurposed to detect DEG/EG contamination, with their limit of detection and proposed use in raw material quality control or finished product analysis

Assay	Initial intended use	Repurposed for EG/DEG detection	LoD (% *w/w* in matrix)	Proposed use
Ethanol assay	Ethanol	EG	2.0% (in PG); 0.1-0.5% (in syrup)	Raw material and finished product testing
Glycolic acid assay	Glycolic acid	EG	1.0% (in PG); 0.1% (in syrup)	Raw material and finished product testing
Alcohol strip tests (saliva or breast milk)	Ethanol	EG	0.5% (in PG); 1.0-2.0% (in syrup)	Raw material testing
Alcohol breath test/breathalyser	Ethanol	DEG	1.0% *v/v* (in water)	Raw material testing
Polyethylene glycol (PEG) ELISA	PEG	DEG	Only 5.0% *v/v* tested (in water)	Custom antibody required
MALDI-ToF MS	Bacterial identification	EG, DEG	EG: 0.5% (in PG); 1.0% (in syrup) DEG: 0.05% (in PG); 1.0% (in syrup)	Raw material and finished product testing

DEG, diethylene glycol; EG, ethylene glycol; ELISA, enzyme-linked immunosorbent assay; LoD, limit of detection; PG, propylene glycol; PEG, polyethylene glycol

Alcohol dehydrogenase and aldehyde dehydrogenase could be used to determine EG and differentiate it from other alcohols (Table 6.2) and, when used in combination

with a glycolic acid assay, could determine EG as low as 1% *w/w* in PG (Figure 6.5) and down to <0.1% *w/w* in some medicinal syrups (Figure 6.6).

The glycolate oxidase used in this study was expected to be specific for glycolic acid, an alpha-hydroxy acid. Although the additional use of this enzyme did not work well with teenage/adult syrups containing ethanol, they did work successfully for ethanol-containing Covonia down to below 0.1% *w/w* (Figure 6.6 D). This is most likely due to Covonia having low levels of ethanol (Figure 6.9 and Table 6.1) since it is suitable for children over 1 year old, in addition to teenagers and adults. Ethanol was not expected to interfere with the assay since it would have been converted to acetaldehyde by alcohol dehydrogenase and then oxidised by aldehyde dehydrogenase to acetic acid, which is not an alpha-hydroxy acid and not an expected substrate for glycolate oxidase.

These assays could potentially be used in NRA laboratories, hospitals, or testing laboratories. Although a plate reader is required to measure the absorbance of NADH at 340 nm, EG could also be determined without the need for a plate reader since the reduced fluorescent substrate was seen visually by eye as a pink colour (Figure 6.3 D). It may be possible for this enzymatic test to be developed into a low-cost and rapid pad-based strip test using a cocktail of four enzymes (alcohol dehydrogenase, aldehyde dehydrogenase, glycolate oxidase and a peroxidase) and a chromogenic substrate such as tetramethylbenzidine to visualise a colour change. While this should work for raw materials, a potential problem is the testing of finished products since some syrups are coloured (Figure 6.9), which may hinder the visualisation of the colour change. To overcome this problem, a fluorogenic substrate could be used instead, since syrups are free from fluorescent excipients, and this approach potentially has the advantage of greater sensitivity. Rapid tests using fluorescence have successfully been visualised

simply using a low-cost UV torch (*e.g.* Hough COVID-19 Home test, Burleigh West, Australia). Due to the resource constraints of this study, I was unable to explore the possibility of developing such a rapid test.

The potential use of a PEG ELISA in detecting DEG is shown (Figure 6.4), although a more sensitive and specific assay is required to meet the regulatory limits. The PEG ELISA was designed to detect the polyether chains of PEG molecules. Since DEG has an ether chain (Figure 6.1), the PEG ELISA was tested to see if it would detect DEG, although the level of detection was not sensitive enough. While the binding with DEG was poor, it is still encouraging that at least there was some, although small, preferential binding to DEG. The antibody in the kit recognises the polyether chain of PEG and was tested to see if it could recognise the ether in DEG. There was some weak preferential binding to DEG (lowest absorbance) compared to the other alcohols, although the difference was so minor that it is hard to differentiate DEG from the other alcohols, and the breathalysers were considerably better at detecting DEG. The poor performance of the PEG ELISA was not surprising since it uses an antibody specific to PEG instead of DEG. A custom antibody or aptamer against DEG, due to its ether group and differences in branching/topology, may improve binding and DEG detection. While it is possible to develop custom antibodies and aptamers for small molecules, it may be challenging to develop them to be specific for DEG, especially when levels of other alcohols, such as glycerol and PG could be present as excipients in the syrups at much higher concentrations. But if a custom antibody can recognise DEG, then the antibody may not bind to glycerol and PG as well, due to minor differences in branching, and such an antibody could potentially be used in a rapid test. While such an antibody or aptamer could be used in a low-cost test, this was not investigated due to the initial expensive development costs.

Conversion of EG was far higher than the other alcohols when using only alcohol dehydrogenase and aldehyde dehydrogenase (Figure 6.3 A). Since EG is converted with these enzymes more like ethanol than the other alcohols, I hypothesised that EG may also convert faster than the other alcohols with alcohol oxidase. This led me to evaluate alcohol rapid test strips which use alcohol oxidase, a peroxidase and a chromogenic substrate which turns blue in the presence of alcohol. By repurposing these alcohol test strips, I show that EG could be rapidly and simply detected and easily differentiated from glycerol and PG, which yielded negative results (Figure 6.8 A). This successfully worked with three different brands of saliva strips and two brands of breast milk strips (Figure 6.7), suggesting that this approach may work with any brand of alcohol rapid test strips for testing raw materials. These rapid (2 minutes) and inexpensive (less than $1) strips do not require instrumentation and are easy to use with minimal training since they are designed for public use. The strips would be useful for syrup manufacturers for additional testing of incoming raw materials and checking for EG barrels, which have been mislabelled, such as the reported incidents in Indonesia (354) and Pakistan (343), where barrels containing pure EG were mislabelled as PG and used in the manufacturing without further raw material confirmation.

The rapid alcohol strips were able to determine levels as low as 0.5% *w/w* EG in PG (Figure 6.8 B). While this does not meet the 0.1% *w/w* WHO regulatory threshold, it may help to prevent deaths and/or toxicity. This is only the case if 0.5% *w/w* is below the fatal/toxic concentration limits, although there is no published evidence for these clinical limits. In a similar way as discussed earlier, it may be possible to improve the sensitivity down to 0.1% *w/w* if a more sensitive fluorogenic substrate is used, but it was not possible to investigate this further. The strips were less sensitive when testing EG spiked into syrups (Figure 6.10), where detection was down to around 1-2% EG. Again,

while this is above the regulatory limit, it would have helped to determine major EG contamination, such as in Indonesia and therefore could have prevented toxicity and/or deaths. These test strips were only tested with glycerol and PG as excipients used in syrups, since these alcohols are commonly used in relatively large amounts, and recent cases of contamination have been with PG (343,354). However, the US FDA additionally recommend testing maltitol and sorbitol solutions for DEG and EG (355). We show that the alcohol strips show no sign of blue colour change with the maltitol-containing syrups, Benylin Infant and Calprofen, and the sorbitol-containing syrup, Dimetapp (Table 6.1, Figure 6.9). This suggests that not only can these strips determine EG in PG and glycerol, but they could also be used to determine EG in both maltitol and sorbitol solutions received by syrup manufacturers. Furthermore, I show that the alcohol strips could successfully determine the presence of EG down to 1% *w/w* in a maltitol-containing syrup, Benylin Infant (Figure 6.10).

Disposable breathalysers were repurposed to determine DEG and EG (Figure 6.11). They contain a proprietary oxidiser which changes from white to pink/brown with alcohol. Some disposable breathalysers contain potassium dichromate, which is orange in colour and changes to green in the presence of alcohol. I did not test potassium dichromate since it is extremely toxic and harmful, and therefore not feasible to be used in the field to determine DEG or EG. The advantage of the disposable breathalysers used is that it is safe to use since the chemical oxidiser is contained inside the plastic case of the breathalyser and would not come into contact with an inspector using it to detect DEG/EG. DEG was less reactive to the oxidiser in the breathalyser compared to glycerol and PG, allowing DEG to be successfully determined. EG did oxidise, but at a lower rate, allowing EG to be detected. While the breathalysers are low-cost (around $1) and the reaction is rapid (10 seconds) since a positive result was observed with glycerol and PG

and the test relies on a negative result for DEG (and slower positive for EG), the breathalysers can only be used for testing raw materials testing and cannot be used in finished products. Glycerol and PG oxidise to result in a dark brown colour, whereas when the rate of colour change is lower or almost none, a suspicion of probable EG or DEG contamination, respectively, could be raised. This method may be beneficial to prevent cases of DEG and EG contamination in medical products. Substandard Naturcold cough syrup was contaminated with 28.6% DEG in Cameroon (340) and with such a high contamination, it is highly possible that the barrels of raw material used contained neat DEG, since typically 20-30% glycerol and/or PG are used in medicinal syrups. Furthermore, these breathalysers could have helped to determine EG in Indonesia and Pakistan for the barrels which contained 96-100% EG (337,354).

In terms of wider distribution of the methods, the alcohol strip tests and the alcohol breathalyser can potentially be incorporated into the inventory of non-sophisticated, low-cost screening methods, assembled as a self-contained kit for testing on the spot, *i.e.* the Minilab from the Global Pharma Health Fund. Recently, Minilab has expanded its method inventory with a TLC-based test for impurities in liquid preparations for oral use, *e.g.* in cough syrups (356).

MALDI-ToF mass spectrometers are widely available worldwide in most hospitals and diagnostic laboratories for microbial identification. I have recently used these devices to differentiate falsified vaccine surrogates from genuine vaccines (246,357), as described in Chapter 4. I investigated whether these instruments could also be used to detect DEG and EG contamination by evaluating the spectra profiles of raw materials or finished products.

By derivatising the alcohols in DEG/EG spiked PG and Covonia cough syrups using benzoyl chloride, I optimised a method that was able to detect peaks corresponding to

EG and DEG (Figure 6.14). The derivatisation method (Figure 6.2) increased the ionisation and detection of alcohols in MALDI-ToF (Figure 6.14). The 149 *m/z* peak corresponding to the EG peak (EG $[M+H]^+$) was detected in both EG and DEG spectra, while the specific 337 *m/z* peak of the sodiated DEG peak (DEG $[M+Na]^+$) was detected only in DEG spectra. In the PG matrix, the method was able to detect down to 0.5% and 0.05% of EG and DEG levels, respectively (Figure 6.16), the latter of which is lower than the regulatory limit of 0.1%.

Furthermore, in a more complex syrup matrix (Covonia cough syrup), the method was able to detect down to 1% for both EG and DEG (Figure 6.17). Although this detection limit of 1% is higher than the allowable regulatory limit of 0.1%, the method could save lives since it is unlikely that any contamination at 1% or lower would lead to deaths and toxicity. This novel approach can add to the currently available tests for EG and DEG contamination in LMICs, where GC-FID is not available but MALDI-ToF is already in place for microbial identification.

In conclusion, both enzymatic assays and MALDI-ToF MS can be useful in detecting DEG and EG contamination in both raw materials and finished products. The enzymatic tests are considerably easier and safer to carry out than TLC, and MALDI-ToF is more widely available than GC. Together, these methods may be lifesaving by preventing deaths and toxicity. Future collaborations with local NRAs are needed to test the ability of the methods to detect DEG/EG contamination in real-life situations.

Acknowledgement

I would like to thank Isabelle Legge for their help with the preparation of DEG- and EG-containing PG and syrup samples. Bevin Gangadharan helped in the interpretation of the enzymatic assays and MALDI-ToF spectra as a second test result reader and prepared Figure 6.1.

Manuscript arising from this chapter

The substance of this chapter has been prepared as a manuscript and submitted for publication:

Arman BY, Legge I, Walsby-Tickle J, Bharucha T, Gabel J, Gnegel G, Hauk C, Deats M, Banerjee S, Stokes R, Matousek M, McCullagh J, Caillet C, Newton PN, Zitzmann N, and Gangadharan B. Simple and rapid low-cost assays to investigate ethylene glycol and diethylene glycol contamination in raw materials and medical products. 2025. *Manuscript submitted*.

7

Conclusion and future directions

This thesis outlines the development and evaluation of both therapeutic and preventive strategies aimed at combating coronaviruses, including SARS-CoV-2. The therapeutic component of this thesis focused on the discovery and characterisation of antiviral compounds targeting SARS-CoV-2. Within the COVID Moonshot initiative, a collaborative effort to develop SARS-CoV-2 main protease inhibitors, I have identified three promising preclinical leads through compound screening using a robust antiviral assay in human Calu-3 cells. These candidates demonstrated efficacy against both the early SARS-CoV-2 strain (ENG2/20) and the Omicron variant, with high specificity and minimal cross-reactivity against other human coronaviruses. Ongoing studies are evaluating these compounds for preclinical toxicology and *in vivo* efficacy, with the goal of preparing for phase I clinical trials. Other future studies may include continued monitoring of efficacy against emerging variants as well as the development of potential drug resistance.

I also evaluated another therapeutic candidate, the iminosugar MON-DNJ, in the same cellular assay and showed it had a broad-spectrum antiviral activity with demonstrated efficacy against multiple SARS-CoV-2 variants as well as HCoV-OC43. This adds to the large body of knowledge on the use of iminosugars as host-targeting antivirals. MON-DNJ could either be given in a continuous low-dose treatment over

several days, where antiviral effects correlate with inhibition of the enzyme alpha-glucosidase II (59). In this context, MON-DNJ has successfully completed a phase I clinical trial in humans, where the aim had been to develop it as a therapeutic against DENV. In this phase I clinical study, MON-DNJ showed no serious adverse events or dose-dependent increases in adverse events at doses up to 1,000 mg (63), which suggests that therapeutically relevant drug levels can be safely administered. Some adverse events were recorded, however, during the trial and are likely due to off-target inhibition of gastrointestinal-resident disaccharidases leading to osmotic diarrhoea. In a separate approach, it is envisaged that MON-DNJ could be given in a single high dose. This is based on a 2020 study (211), where the Zitzmann group and others showed that a single dose of MON-DNJ prevents virally induced death in mice infected with lethal doses of influenza virus or DENV, even if administered days after infection. In this case, protection correlates with inhibition of the enzyme alpha-glucosidase I. This raises the exciting prospect that it might be possible to develop an oral drug that could be administered in a single dose even after infection. The proof of concept that alpha-glucosidase I plays an important part in the life cycle of some enveloped viruses comes from a study in the New England Journal of Medicine of two siblings, who were deficient in the target enzyme (alpha-glucosidase I) and whose cells were resistant to infection with certain viruses (358). The Zitzmann group is planning to develop MON-DNJ as a single-dose treatment in humans. Some phase I data are available (63). The next steps will be to repeat some of the preclinical toxicology and pharmacokinetics studies in animals, for those which so far were not done under good laboratory practices conditions, followed by a phase Ia safety study to determine the highest single ascending dose that can be safely achieved in humans. If this allows dose escalation up to 5 g administered in a single dose, it would be possible to safely inhibit ER alpha-glucosidase

I in humans, and the further plan would be to initially conduct a phase II influenza challenge study in humans. Should this prove successful, this approach could also be available in future for any newly emerging viruses with pandemic potential that depend on ER alpha-glucosidase I, including most likely coronaviruses. Such orally available host-targeting drugs might prevent an epidemic from turning into a pandemic and buy the time necessary to develop or identify and repurpose virus-specific DAAs.

For the preventive part of my DPhil project, I investigated novel techniques to verify the authenticity and quality of vaccines and other medical products. I repurposed MALDI-ToF MS, which is widely accessible in clinical laboratories globally, and was able to distinguish genuine vaccines from falsified ones. This was achieved by analysing chemical signatures from vial labels and excipients in the vaccine formulation. The use of multivariate analysis and machine learning enhanced the robustness of spectral data interpretation. This approach—especially the focus on ionisable vial labels and adhesive ingredients—represents a novel, non-invasive strategy for vaccine authentication. The developed methods have now been published and can be used by regulatory agencies or research laboratories worldwide.

Another problem encountered in the supply chain is the generation of substandard vaccines caused by environmental factors, such as exposure to high temperatures. In the absence of accessible tools and methods to detect this condition, I have proposed a simple, rapid, lower-cost assay to detect heat exposure by detecting the degradation of sucrose. In this thesis, I showed that sucrose degradation correlates inversely with vaccine potency, making it a promising novel indicator of vaccines being exposed to elevated temperatures and thus of cold chain failure. The method can be deployed and used by inspectors to check the quality of vaccines to prevent substandard vaccines.

Another major concern addressed in this study is the contamination of medicinal syrups with diethylene glycol and ethylene glycol, which has led to numerous fatalities worldwide. This research proposes the repurposing of existing breathalysers and alcohol enzymatic assays as low-cost and widely accessible methods for rapid DEG/EG detection. Both rapid alcohol strip tests and breathalysers proved effective in identifying contamination in raw materials and final products, offering a vital tool for resource-limited settings.

Collaborations with vaccine manufacturers and the WHO proved essential in this work and should be maintained to further refine and implement the developed methodologies. Engagement with NRAs, particularly in LMICs, will be key to evaluating the practical impact of these strategies in real-world settings.

In summary, this study presents novel and practical approaches for enhancing both therapeutic and preventive responses to corona- and other viruses. From the screening of antiviral compounds to the development of accessible analytical tools for identifying SF medical products, these strategies have the potential to significantly contribute to pandemic preparedness and global health security.

References

1. Son BWK. A Multipronged Approach to Combat COVID-19: Lessons from Previous Pandemics for the Future. In: Rezaei N, editor. Integrated Science of Global Epidemics. Cham: Springer International Publishing; 2023. p. 73–92. (Integrated Science).

2. Li G, Hilgenfeld R, Whitley R, De Clercq E. Therapeutic strategies for COVID-19: progress and lessons learned. Nat Rev Drug Discov. 2023 Jun;22(6):449–75.

3. Adamson CS, Chibale K, Goss RJM, Jaspars M, Newman DJ, Dorrington RA. Antiviral drug discovery: preparing for the next pandemic. Chem Soc Rev. 2021 Mar 21;50(6):3647–55.

4. Cheung YYH, Lau EHY, Yin G, Lin Y, Cowling BJ, Lam KF. Effectiveness of Vaccines and Antiviral Drugs in Preventing Severe and Fatal COVID-19, Hong Kong. Emerg Infect Dis. 2024 Jan;30(1):70–8.

5. Jonsson CB, Golden JE, Meibohm B. Time to "Mind the Gap" in novel small molecule drug discovery for direct-acting antivirals for SARS-CoV-2. Curr Opin Virol. 2021 Oct;50:1–7.

6. Dolgin E. The race for antiviral drugs to beat COVID - and the next pandemic. Nature. 2021 Apr;592(7854):340–3.

7. Harapan H, Itoh N, Yufika A, Winardi W, Keam S, Te H, et al. Coronavirus disease 2019 (COVID-19): A literature review. J Infect Public Health. 2020 May;13(5):667–73.

8. Mei M, Tan X. Current Strategies of Antiviral Drug Discovery for COVID-19. Front Mol Biosci. 2021;8:671263.

9. Arman BY, Brun J, Hill ML, Zitzmann N, von Delft A. An Update on SARS-CoV-2 Clinical Trial Results-What We Can Learn for the Next Pandemic. Int J Mol Sci. 2023 Dec 26;25(1):354.

10. National Institute for Health and Care Excellence. COVID-19 rapid guideline: managing COVID-19 [Internet]. 2021 [cited 2025 May 21]. Available from: https://www.nice.org.uk/guidance/ng191

11. COVID-19 Treatment Guidelines Panel. Coronavirus Disease 2019 (COVID-19) Treatment Guidelines. National Institutes of Health [Internet]. 2023 [cited 2023 Jul 14]. Available from: https://www.covid19treatmentguidelines.nih.gov/

12. World Health Organization. COVID-19 - Landscape of novel coronavirus candidate vaccine development worldwide [Internet]. 2022 [cited 2022 Sep 1]. Available from: https://www.who.int/publications/m/item/draft-landscape-of-covid-19-candidate-vaccines

13. Barouch DH. Covid-19 Vaccines - Immunity, Variants, Boosters. N Engl J Med. 2022 Sep 15;387(11):1011–20.

14. Newton PN, Bond KC, Adeyeye M, Antignac M, Ashenef A, Awab GR, et al. COVID-19 and risks to the supply and quality of tests, drugs, and vaccines. The Lancet Global Health. 2020 Jun 1;8(6):e754–5.

15. V'kovski P, Kratzel A, Steiner S, Stalder H, Thiel V. Coronavirus biology and replication: implications for SARS-CoV-2. Nat Rev Microbiol. 2021 Mar;19(3):155–70.

16. Artika IM, Dewantari AK, Wiyatno A. Molecular biology of coronaviruses: current knowledge. Heliyon. 2020 Aug;6(8):e04743.

17. Liu YC, Kuo RL, Shih SR. COVID-19: The first documented coronavirus pandemic in history. Biomed J. 2020 Aug;43(4):328–33.

18. Artese A, Svicher V, Costa G, Salpini R, Di Maio VC, Alkhatib M, et al. Current status of antivirals and druggable targets of SARS CoV-2 and other human pathogenic coronaviruses. Drug Resist Updat. 2020 Dec;53:100721.

19. Elrashdy F, Redwan EM, Uversky VN. Why COVID-19 Transmission Is More Efficient and Aggressive Than Viral Transmission in Previous Coronavirus Epidemics? Biomolecules. 2020 Sep 11;10(9):E1312.

20. Harrison AG, Lin T, Wang P. Mechanisms of SARS-CoV-2 Transmission and Pathogenesis. Trends Immunol. 2020 Dec;41(12):1100–15.

21. Hu B, Guo H, Zhou P, Shi ZL. Characteristics of SARS-CoV-2 and COVID-19. Nat Rev Microbiol. 2021 Mar;19(3):141–54.

22. Kirby T. New variant of SARS-CoV-2 in UK causes surge of COVID-19. Lancet Respir Med. 2021 Feb;9(2):e20–1.

23. Karim SSA, Karim QA. Omicron SARS-CoV-2 variant: a new chapter in the COVID-19 pandemic. Lancet. 2021 Dec 11;398(10317):2126–8.

24. Masters PS. The molecular biology of coronaviruses. Adv Virus Res. 2006;66:193–292.

25. Fehr AR, Perlman S. Coronaviruses: An Overview of Their Replication and Pathogenesis. Coronaviruses. 2015 Feb 12;1282:1–23.

26. Huang Y, Yang C, Xu XF, Xu W, Liu SW. Structural and functional properties of SARS-CoV-2 spike protein: potential antivirus drug development for COVID-19. Acta Pharmacol Sin. 2020 Sep;41(9):1141–9.

27. Pizzato M, Baraldi C, Boscato Sopetto G, Finozzi D, Gentile C, Gentile MD, et al. SARS-CoV-2 and the Host Cell: A Tale of Interactions. Frontiers in Virology. 2022;1.

28. Carpinteiro A, Edwards MJ, Hoffmann M, Kochs G, Gripp B, Weigang S, et al. Pharmacological Inhibition of Acid Sphingomyelinase Prevents Uptake of SARS-CoV-2 by Epithelial Cells. Cell Reports Medicine. 2020 Nov 17;1(8):100142.

29. Riggioni C, Comberiati P, Giovannini M, Agache I, Akdis M, Alves-Correia M, et al. A compendium answering 150 questions on COVID-19 and SARS-CoV-2. Allergy. 2020 Oct;75(10):2503–41.

30. von Delft F, Calmiano M, Chodera J, Griffen E, Lee A, London N, et al. A white-knuckle ride of open COVID drug discovery. Nature. 2021 Jun;594(7863):330–2.

31. DTB Drug Review. Two new oral antivirals for covid-19: ▼molnupiravir and ▼nirmatrelvir plus ritonavir. Drug Ther Bull. 2022 May 1;60(5):73.

32. Mukae H, Yotsuyanagi H, Ohmagari N, Doi Y, Imamura T, Sonoyama T, et al. A Randomized Phase 2/3 Study of Ensitrelvir, a Novel Oral SARS-CoV-2 3C-Like Protease Inhibitor, in Japanese Patients with Mild-to-Moderate COVID-19 or Asymptomatic SARS-CoV-2 Infection: Results of the Phase 2a Part. Antimicrob Agents Chemother. 2022 Oct 18;66(10):e0069722.

33. Gilead Sciences. Gilead Sciences Statement on Phase 3 Obeldesivir Clinical Trials in COVID-19: BIRCH Study to Stop Enrollment While OAKTREE Study Nears Full Enrollment [Internet]. 2023 [cited 2024 Jul 8]. Available from: https://www.gilead.com/news-and-press/company-statements/gilead-sciences-statement-on-phase-3-obeldesivir-clinical-trials-in-covid-19-birch-study-to-stop-enrollment-while-oaktree-study-nears-full-enrollment

34. Boby ML, Fearon D, Ferla M, Filep M, Koekemoer L, Robinson MC, et al. Open science discovery of potent noncovalent SARS-CoV-2 main protease inhibitors. Science. 2023 Nov 10;382(6671):eabo7201.

35. Cevik M, Kuppalli K, Kindrachuk J, Peiris M. Virology, transmission, and pathogenesis of SARS-CoV-2. BMJ. 2020 Oct 23;371:m3862.

36. Vegivinti CTR, Evanson KW, Lyons H, Akosman I, Barrett A, Hardy N, et al. Efficacy of antiviral therapies for COVID-19: a systematic review of randomized controlled trials. BMC Infectious Diseases. 2022 Jan 31;22(1):107.

37. Beigel JH, Tomashek KM, Dodd LE, Mehta AK, Zingman BS, Kalil AC, et al. Remdesivir for the Treatment of Covid-19 - Final Report. N Engl J Med. 2020 Nov 5;383(19):1813–26.

38. Gottlieb RL, Vaca CE, Paredes R, Mera J, Webb BJ, Perez G, et al. Early Remdesivir to Prevent Progression to Severe Covid-19 in Outpatients. N Engl J Med. 2022 Jan 27;386(4):305–15.

39. Schmidt P, Li Y, Popejoy M. Immunobridging for Pemivibart, a Monoclonal Antibody for Prevention of Covid-19. New England Journal of Medicine. 2024 Nov 13;391(19):1860–2.

40. Harris E. FDA Approves Vilobelimab for Emergency Use in Hospitalized Adults. JAMA. 2023 Apr 19;

41. Vlaar APJ, Witzenrath M, Paassen P van, Heunks LMA, Mourvillier B, Bruin S de, et al. Anti-C5a antibody (vilobelimab) therapy for critically ill, invasively mechanically ventilated patients with COVID-19 (PANAMO): a multicentre, double-blind, randomised, placebo-controlled, phase 3 trial. The Lancet Respiratory Medicine. 2022 Dec 1;10(12):1137–46.

42. Geng J, Wang F, Huang Z, Chen X, Wang Y. Perspectives on anti-IL-1 inhibitors as potential therapeutic interventions for severe COVID-19. Cytokine. 2021 Jul;143:155544.

43. Karakike E, Dalekos GN, Koutsodimitropoulos I, Saridaki M, Pourzitaki C, Papathanakos G, et al. ESCAPE: An Open-Label Trial of Personalized Immunotherapy in Critically lll COVID-19 Patients. J Innate Immun. 2021 Dec 1;1–11.

44. Jayk Bernal A, Gomes da Silva MM, Musungaie DB, Kovalchuk E, Gonzalez A, Delos Reyes V, et al. Molnupiravir for Oral Treatment of Covid-19 in Nonhospitalized Patients. N Engl J Med. 2022 Feb 10;386(6):509–20.

45. Lee CC, Hsieh CC, Ko WC. Molnupiravir-A Novel Oral Anti-SARS-CoV-2 Agent. Antibiotics (Basel). 2021 Oct 23;10(11):1294.

46. Hammond J, Leister-Tebbe H, Gardner A, Abreu P, Bao W, Wisemandle W, et al. Oral Nirmatrelvir for High-Risk, Nonhospitalized Adults with Covid-19. N Engl J Med. 2022 Apr 14;386(15):1397–408.

47. Owen DR, Allerton CMN, Anderson AS, Aschenbrenner L, Avery M, Berritt S, et al. An oral SARS-CoV-2 Mpro inhibitor clinical candidate for the treatment of COVID-19. Science. 2021 Dec 24;374(6575):1586–93.

48. Kalil AC, Patterson TF, Mehta AK, Tomashek KM, Wolfe CR, Ghazaryan V, et al. Baricitinib plus Remdesivir for Hospitalized Adults with Covid-19. N Engl J Med. 2021 Mar 4;384(9):795–807.

49. Lin Z, Niu J, Xu Y, Qin L, Ding J, Zhou L. Clinical efficacy and adverse events of baricitinib treatment for coronavirus disease-2019 (COVID-19): A systematic review and meta-analysis. J Med Virol. 2021 Nov 30;

50. Marconi VC, Ramanan AV, de Bono S, Kartman CE, Krishnan V, Liao R, et al. Efficacy and safety of baricitinib for the treatment of hospitalised adults with COVID-19 (COV-BARRIER): a randomised, double-blind, parallel-group, placebo-controlled phase 3 trial. Lancet Respir Med. 2021 Dec;9(12):1407–18.

51. Wolfe CR, Tomashek KM, Patterson TF, Gomez CA, Marconi VC, Jain MK, et al. Baricitinib versus dexamethasone for adults hospitalised with COVID-19 (ACTT-4): a randomised, double-blind, double placebo-controlled trial. Lancet Respir Med. 2022 Sep;10(9):888–99.

52. Abani O, Abbas A, Abbas F, Abbas M, Abbasi S, Abbass H, et al. Tocilizumab in patients admitted to hospital with COVID-19 (RECOVERY): a randomised, controlled, open-label, platform trial. The Lancet. 2021 May 1;397(10285):1637–45.

53. Antwi-Amoabeng D, Kanji Z, Ford B, Beutler BD, Riddle MS, Siddiqui F. Clinical outcomes in COVID-19 patients treated with tocilizumab: An individual patient data systematic review. Journal of Medical Virology. 2020;92(11):2516–22.

54. Wang D, Fu B, Peng Z, Yang D, Han M, Li M, et al. Tocilizumab in patients with moderate or severe COVID-19: a randomized, controlled, open-label, multicenter trial. Front Med. 2021 Jun;15(3):486–94.

55. Xu X, Han M, Li T, Sun W, Wang D, Fu B, et al. Effective treatment of severe COVID-19 patients with tocilizumab. Proc Natl Acad Sci U S A. 2020 May 19;117(20):10970–5.

56. Food and Drug Administration. Emergency Use Authorizations for Drugs and Non-Vaccine Biological Products [Internet]. 2024 [cited 2023 May 7]. Available from: https://www.fda.gov/drugs/emergency-preparedness-drugs/emergency-use-authorizations-drugs-and-non-vaccine-biological-products

57. Groaz E, De Clercq E, Herdewijn P. Anno 2021: Which antivirals for the coming decade? Annu Rep Med Chem. 2021 Nov 3;

58. Singh M, de Wit E. Antiviral agents for the treatment of COVID-19: Progress and challenges. Cell Rep Med. 2022 Mar 15;3(3):100549.

59. Dwek RA, Bell JI, Feldmann M, Zitzmann N. Host-targeting oral antiviral drugs to prevent pandemics. Lancet. 2022 Apr 9;399(10333):1381–2.

60. Robinson PC, Liew DFL, Tanner HL, Grainger JR, Dwek RA, Reisler RB, et al. COVID-19 therapeutics: Challenges and directions for the future. Proc Natl Acad Sci U S A. 2022 Apr 12;119(15):e2119893119.

61. Strasfeld L, Chou S. Antiviral Drug Resistance: Mechanisms and Clinical Implications. Infect Dis Clin North Am. 2010 Jun;24(2):413–37.

62. Bekerman E, Einav S. Infectious disease. Combating emerging viral threats. Science. 2015 Apr 17;348(6232):282–3.

63. Callahan M, Treston AM, Lin G, Smith M, Kaufman B, Khaliq M, et al. Randomized single oral dose phase 1 study of safety, tolerability, and pharmacokinetics of Iminosugar UV-4 Hydrochloride (UV-4B) in healthy subjects. PLoS Negl Trop Dis. 2022 Aug;16(8):e0010636.

64. Burrage DR, Koushesh S, Sofat N. Immunomodulatory Drugs in the Management of SARS-CoV-2. Front Immunol. 2020;11:1844.

65. Ferner RE, Aronson JK. Chloroquine and hydroxychloroquine in covid-19. BMJ. 2020 Apr 8;369:m1432.

66. Misra DP, Agarwal V, Gasparyan AY, Zimba O. Rheumatologists' perspective on coronavirus disease 19 (COVID-19) and potential therapeutic targets. Clin Rheumatol. 2020 Jul;39(7):2055–62.

67. RECOVERY Collaborative Group, Horby P, Lim WS, Emberson JR, Mafham M, Bell JL, et al. Dexamethasone in Hospitalized Patients with Covid-19. N Engl J Med. 2021 Feb 25;384(8):693–704.

68. Piranty S. Coronavirus fuels a surge in fake medicines. 2020 [cited 2024 Aug 14]. Coronavirus fuels a surge in fake medicines. Available from: https://www.bbc.co.uk/news/health-52201077

69. Srivastava K. Fake covid vaccines boost the black market for counterfeit medicines. BMJ. 2021 Nov 17;375:n2754.

70. World Health Organization. WHO Global Surveillance and Monitoring System for substandard and falsified medical products. Geneva: World Health Organization; 2017.

71. World Health Organization. Substandard and falsified medical products - Key facts [Internet]. 2024 [cited 2025 May 25]. Available from: https://www.who.int/news-room/fact-sheets/detail/substandard-and-falsified-medical-products

72. Nahum A, Drekonja DM, Alpern JD. The Erosion of Public Trust and SARS-CoV-2 Vaccines— More Action Is Needed. Open Forum Infect Dis. 2021 Jan 4;8(2):ofaa657.

73. Newton PN, Bond KC, Newton P, Bond K, Abiola V, Ade-Abolade K, et al. Global access to quality-assured medical products: the Oxford Statement and call to action. The Lancet Global Health. 2019 Dec 1;7(12):e1609–11.

74. Medicine Quality Research Group, University of Oxford. Medical Product Quality Report – COVID-19 Issues. Issue 15, January, February & March 2022 [Internet]. 2022 [cited 2023 Aug 29]. Available from: https://www.iddo.org/sites/default/files/publication/2022-09/Medical%20Product%20Quality%20Report_Covid-19_Issue15_January-March2022_V1.1.pdf

75. Vickers S, Bernier M, Zambrzycki S, Fernandez FM, Newton PN, Caillet C. Field detection devices for screening the quality of medicines: a systematic review. BMJ Glob Health. 2018;3(4):e000725.

76. Newton PN, Green MD, Fernández FM, Day NP, White NJ. Counterfeit anti-infective drugs. The Lancet Infectious Diseases. 2006 Sep 1;6(9):602–13.

77. Caillet C, Vickers S, Vidhamaly V, Boutsamay K, Boupha P, Zambrzycki S, et al. Evaluation of portable devices for medicine quality screening: Lessons learnt, recommendations for implementation, and future priorities. PLoS Med. 2021 Sep;18(9):e1003747.

78. Bharucha T, Gangadharan B, Clarke R, Fernandez LG, Arman BY, Walsby-Tickle J, et al. Repurposing rapid diagnostic tests to detect falsified vaccines in supply chains. Vaccine. 2024 Feb 13;S0264-410X(24)00019-7.

79. Umar TP, Jain N, Azis H. Endemic rise in cases of acute kidney injury in children in Indonesia and Gambia: what is the likely culprit and why? Kidney Int. 2023 Mar;103(3):444–7.

80. Fikri E, Firmansyah YW. A Case Report of Contamination and Toxicity of Ethylene Glycol and Diethylene Glycol on Drugs in Indonesia. Environment and Ecology Research. 2023 Apr;11(2):378–84.

81. Kraut JA, Kurtz I. Toxic alcohol ingestions: clinical features, diagnosis, and management. Clin J Am Soc Nephrol. 2008 Jan;3(1):208–25.

82. Schier JG, Rubin CS, Miller D, Barr D, McGeehin MA. Medication-associated diethylene glycol mass poisoning: a review and discussion on the origin of contamination. J Public Health Policy. 2009 Jul;30(2):127–43.

83. Waring WS. Poisoning by alcohols and glycols. Medicine. 2024 Jun 1;52(6):358–63.

84. Repurposed Antiviral Drugs for Covid-19 — Interim WHO Solidarity Trial Results. N Engl J Med. 2021 Feb 11;384(6):497–511.

85. Ader F, Bouscambert-Duchamp M, Hites M, Peiffer-Smadja N, Poissy J, Belhadi D, et al. Remdesivir plus standard of care versus standard of care alone for the treatment of patients admitted to hospital with COVID-19 (DisCoVeRy): a phase 3, randomised, controlled, open-label trial. Lancet Infect Dis. 2022 Feb;22(2):209–21.

86. Arshad U, Pertinez H, Box H, Tatham L, Rajoli RKR, Curley P, et al. Prioritization of Anti-SARS-Cov-2 Drug Repurposing Opportunities Based on Plasma and Target Site Concentrations Derived from their Established Human Pharmacokinetics. Clin Pharmacol Ther. 2020 Oct;108(4):775–90.

87. Teoh SL, Lim YH, Lai NM, Lee SWH. Directly Acting Antivirals for COVID-19: Where Do We Stand? Front Microbiol. 2020;11:1857.

88. Morris A, McCorkindale W, Consortium TCM, Drayman N, Chodera JD, Tay S, et al. Discovery of SARS-CoV-2 main protease inhibitors using a synthesis-directed de novo design model. Chem Commun (Camb). 2021 Jun 15;57(48):5909–12.

89. Pillaiyar T, Manickam M, Namasivayam V, Hayashi Y, Jung SH. An Overview of Severe Acute Respiratory Syndrome-Coronavirus (SARS-CoV) 3CL Protease Inhibitors: Peptidomimetics and Small Molecule Chemotherapy. J Med Chem. 2016 Jul 28;59(14):6595–628.

90. Cannalire R, Cerchia C, Beccari AR, Di Leva FS, Summa V. Targeting SARS-CoV-2 Proteases and Polymerase for COVID-19 Treatment: State of the Art and Future Opportunities. J Med Chem. 2022 Feb 24;65(4):2716–46.

91. Jin Z, Du X, Xu Y, Deng Y, Liu M, Zhao Y, et al. Structure of Mpro from SARS-CoV-2 and discovery of its inhibitors. Nature. 2020 Jun;582(7811):289–93.

92. Mody V, Ho J, Wills S, Mawri A, Lawson L, Ebert MCCJC, et al. Identification of 3-chymotrypsin like protease (3CLPro) inhibitors as potential anti-SARS-CoV-2 agents. Commun Biol. 2021 Jan 20;4(1):1–10.

93. Zagórska A, Czopek A, Fryc M, Jończyk J. Inhibitors of SARS-CoV-2 Main Protease (Mpro) as Anti-Coronavirus Agents. Biomolecules. 2024 Jul 4;14(7):797.

94. Yl N, Ck S, Jjh C. Drug repurposing for COVID-19: Approaches, challenges and promising candidates. Pharmacology & therapeutics. 2021 Dec;228.

95. Cattaneo D, Cattaneo D, Gervasoni C, Corbellino M, Galli M, Riva A, et al. Does lopinavir really inhibit SARS-CoV-2? Pharmacol Res. 2020 Aug;158:104898.

96. Choy KT, Wong AYL, Kaewpreedee P, Sia SF, Chen D, Hui KPY, et al. Remdesivir, lopinavir, emetine, and homoharringtonine inhibit SARS-CoV-2 replication in vitro. Antiviral Research. 2020 Jun 1;178:104786.

97. Kempf DJ, Marsh KC, Kumar G, Rodrigues AD, Denissen JF, McDonald E, et al. Pharmacokinetic enhancement of inhibitors of the human immunodeficiency virus protease by coadministration with ritonavir. Antimicrob Agents Chemother. 1997 Mar;41(3):654–60.

98. Lv Z, Chu Y, Wang Y. HIV protease inhibitors: a review of molecular selectivity and toxicity. HIV AIDS (Auckl). 2015 Apr 8;7:95–104.

99. Heskin J, Pallett SJC, Mughal N, Davies GW, Moore LSP, Rayment M, et al. Caution required with use of ritonavir-boosted PF-07321332 in COVID-19 management. Lancet. 2022 Jan 1;399(10319):21–2.

100. Lim S, Tignanelli CJ, Hoertel N, Boulware DR, Usher MG. Prevalence of Medical Contraindications to Nirmatrelvir/Ritonavir in a Cohort of Hospitalized and Nonhospitalized Patients With COVID-19. Open Forum Infect Dis. 2022 Aug;9(8):ofac389.

101. Cao B, Wang Y, Wen D, Liu W, Wang J, Fan G, et al. A Trial of Lopinavir-Ritonavir in Adults Hospitalized with Severe Covid-19. N Engl J Med. 2020 May 7;382(19):1787–99.

102. Di Castelnuovo A, Costanzo S, Antinori A, Berselli N, Blandi L, Bonaccio M, et al. Lopinavir/Ritonavir and Darunavir/Cobicistat in Hospitalized COVID-19 Patients: Findings From the Multicenter Italian CORIST Study. Front Med (Lausanne). 2021;8:639970.

103. Dorward J, Gbinigie O, Cai T, Roberts NW, Garrett N, Hayward G, et al. The protease inhibitor lopinavir, boosted with ritonavir, as treatment for COVID-19: a rapid review. Antivir Ther. 2020;25(7):365–76.

104. Patel TK, Patel PB, Barvaliya M, Saurabh MK, Bhalla HL, Khosla PP. Efficacy and safety of lopinavir-ritonavir in COVID-19: A systematic review of randomized controlled trials. Journal of Infection and Public Health. 2021 Jun 1;14(6):740–8.

105. Horby PW, Mafham M, Bell JL, Linsell L, Staplin N, Emberson J, et al. Lopinavir–ritonavir in patients admitted to hospital with COVID-19 (RECOVERY): a randomised, controlled, open-label, platform trial. The Lancet. 2020 Oct 24;396(10259):1345–52.

106. Tashima K, Crofoot G, Tomaka FL, Kakuda TN, Brochot A, Van de Casteele T, et al. Cobicistat-boosted darunavir in HIV-1-infected adults: week 48 results of a Phase IIIb, open-label single-arm trial. AIDS Research and Therapy. 2014 Dec 1;11(1):39.

107. De Meyer S, Bojkova D, Cinatl J, Van Damme E, Buyck C, Van Loock M, et al. Lack of antiviral activity of darunavir against SARS-CoV-2. International Journal of Infectious Diseases. 2020 Aug 1;97:7–10.

108. Chen H, Zhang Z, Wang L, Huang Z, Gong F, Li X, et al. First clinical study using HCV protease inhibitor danoprevir to treat COVID-19 patients. Medicine (Baltimore). 2020 Nov 25;99(48):e23357.

109. Gammeltoft KA, Zhou Y, Duarte Hernandez CR, Galli A, Offersgaard A, Costa R, et al. Hepatitis C Virus Protease Inhibitors Show Differential Efficacy and Interactions with Remdesivir for Treatment of SARS-CoV-2 In Vitro. Antimicrob Agents Chemother. 2021 Aug 17;65(9):e0268020.

110. Zhang Z, Wang S, Tu X, Peng X, Huang Y, Wang L, et al. A comparative study on the time to achieve negative nucleic acid testing and hospital stays between danoprevir and lopinavir/ritonavir in the treatment of patients with COVID-19. J Med Virol. 2020 Nov;92(11):2631–6.

111. Fillmore N, Bell S, Shen C, Nguyen V, La J, Dubreuil M, et al. Disulfiram use is associated with lower risk of COVID-19: A retrospective cohort study. PLoS One. 2021;16(10):e0259061.

112. Tamburin S, Mantovani E, De Bernardis E, Zipeto D, Lugoboni F, Agostoni C, et al. COVID-19 and related symptoms in patients under disulfiram for alcohol use disorder. Intern Emerg Med. 2021 Sep 1;16(6):1729–31.

113. Lin MH, Moses DC, Hsieh CH, Cheng SC, Chen YH, Sun CY, et al. Disulfiram can inhibit MERS and SARS coronavirus papain-like proteases via different modes. Antiviral Res. 2018 Feb;150:155–63.

114. Ma C, Hu Y, Townsend JA, Lagarias PI, Marty MT, Kolocouris A, et al. Ebselen, Disulfiram, Carmofur, PX-12, Tideglusib, and Shikonin Are Nonspecific Promiscuous SARS-CoV-2 Main Protease Inhibitors. ACS Pharmacol Transl Sci. 2020 Dec 11;3(6):1265–77.

115. Unoh Y, Uehara S, Nakahara K, Nobori H, Yamatsu Y, Yamamoto S, et al. Discovery of S-217622, a Noncovalent Oral SARS-CoV-2 3CL Protease Inhibitor Clinical Candidate for Treating COVID-19. J Med Chem. 2022 May 12;65(9):6499–512.

116. Tyndall JDA. S-217622, a 3CL Protease Inhibitor and Clinical Candidate for SARS-CoV-2. J Med Chem. 2022 May 12;65(9):6496–8.

117. Sasaki M, Tabata K, Kishimoto M, Itakura Y, Kobayashi H, Ariizumi T, et al. Oral administration of S-217622, a SARS-CoV-2 main protease inhibitor, decreases viral load and accelerates recovery from clinical aspects of COVID-19. 2022. p. 2022.02.14.480338.

118. Shionogi. Shionogi Announces Global Phase 3 Trial Demonstrates Post-Exposure Prophylactic Use of Ensitrelvir Prevents Symptomatic COVID-19 [Internet]. 2024 [cited 2025 Apr 9]. Available from: https://www.shionogi.com/global/en/news/2024/10/20241029.html

119. Shionogi. Late-Breaking at CROI 2025: SCORPIO-PEP Phase 3 Trial: Ensitrelvir is the First and Only COVID-19 Oral Antiviral to Demonstrate Prevention of COVID-19 as Post Exposure Prophylaxis [Internet]. 2025 [cited 2025 May 19]. Available from: https://www.shionogi.com/global/en/news/2025/03/20250313.html

120. Antonopoulou I, Sapountzaki E, Rova U, Christakopoulos P. Inhibition of the main protease of SARS-CoV-2 (Mpro) by repurposing/designing drug-like substances and utilizing nature's toolbox of bioactive compounds. Computational and Structural Biotechnology Journal. 2022 Jan 1;20:1306–44.

121. Zaidman D, Gehrtz P, Filep M, Fearon D, Gabizon R, Douangamath A, et al. An automatic pipeline for the design of irreversible derivatives identifies a potent SARS-CoV-2 Mpro inhibitor. Cell Chem Biol. 2021 Jun 22;S2451-9456(21)00263-4.

122. Brun J, Arman BY, Hill ML, Kiappes JL, Alonzi DS, Makower LL, et al. Assessment of repurposed compounds against coronaviruses highlights the antiviral broad-spectrum activity of host-targeting iminosugars and confirms the activity of potent directly acting antivirals. Antiviral Res. 2025 Feb 23;237:106123.

123. Hendrickx R, Lamm Bergström E, Janzén DLI, Fridén M, Eriksson U, Grime K, et al. Translational model to predict pulmonary pharmacokinetics and efficacy in man for inhaled bronchodilators. CPT Pharmacometrics Syst Pharmacol. 2018 Mar;7(3):147–57.

124. Li P, Wang Y, Lavrijsen M, Lamers MM, de Vries AC, Rottier RJ, et al. SARS-CoV-2 Omicron variant is highly sensitive to molnupiravir, nirmatrelvir, and the combination. Cell Res. 2022 Mar;32(3):322–4.

125. Kawashima S, Matsui Y, Adachi T, Morikawa Y, Inoue K, Takebayashi S, et al. Ensitrelvir is effective against SARS-CoV-2 3CL protease mutants circulating globally. Biochem Biophys Res Commun. 2023 Feb 19;645:132–6.

126. Pruijssers AJ, George AS, Schäfer A, Leist SR, Gralinksi LE, Dinnon KH, et al. Remdesivir Inhibits SARS-CoV-2 in Human Lung Cells and Chimeric SARS-CoV Expressing the SARS-CoV-2 RNA Polymerase in Mice. Cell Rep. 2020 Jul 21;32(3):107940.

127. Lin HXJ, Cho S, Meyyur Aravamudan V, Sanda HY, Palraj R, Molton JS, et al. Remdesivir in Coronavirus Disease 2019 (COVID-19) treatment: a review of evidence. Infection. 2021;49(3):401–10.

128. Alipoor R, Ranjbar R. Small-molecule metabolites in SARS-CoV-2 treatment: a comprehensive review. Biol Chem. 2023 May 25;404(6):569–84.

129. Aboul-Fotouh S, Mahmoud AN, Elnahas EM, Habib MZ, Abdelraouf SM. What are the current anti-COVID-19 drugs? From traditional to smart molecular mechanisms. Virol J. 2023 Oct 24;20:241.

130. Rasool G, Khan WA, Khan AM, Riaz M, Abbas M, Rehman AU, et al. COVID-19: A threat to the respiratory system. Int J Immunopathol Pharmacol. 2024;38:3946320241310307.

131. Ravindra NG, Alfajaro MM, Gasque V, Huston NC, Wan H, Szigeti-Buck K, et al. Single-cell longitudinal analysis of SARS-CoV-2 infection in human airway epithelium identifies target cells, alterations in gene expression, and cell state changes. PLoS Biol. 2021 Mar 17;19(3):e3001143.

132. Lamers MM, Mykytyn AZ, Breugem TI, Wang Y, Wu DC, Riesebosch S, et al. Human airway cells prevent SARS-CoV-2 multibasic cleavage site cell culture adaptation. Elife. 2021 Apr 9;10:e66815.

133. Meinhardt J, Radke J, Dittmayer C, Franz J, Thomas C, Mothes R, et al. Olfactory transmucosal SARS-CoV-2 invasion as a port of central nervous system entry in individuals with COVID-19. Nat Neurosci. 2021 Feb;24(2):168–75.

134. Puelles VG, Lütgehetmann M, Lindenmeyer MT, Sperhake JP, Wong MN, Allweiss L, et al. Multiorgan and Renal Tropism of SARS-CoV-2. N Engl J Med. 2020 Aug 6;383(6):590–2.

135. Schaefer IM, Padera RF, Solomon IH, Kanjilal S, Hammer MM, Hornick JL, et al. In situ detection of SARS-CoV-2 in lungs and airways of patients with COVID-19. Modern Pathology. 2020 Nov 1;33(11):2104–14.

136. Dittmar M, Lee JS, Whig K, Segrist E, Li M, Kamalia B, et al. Drug repurposing screens reveal cell-type-specific entry pathways and FDA-approved drugs active against SARS-Cov-2. Cell Rep. 2021 Apr 6;35(1):108959.

137. Grossegesse M, Bourquain D, Neumann M, Schaade L, Schulze J, Mache C, et al. Deep Time Course Proteomics of SARS-CoV- and SARS-CoV-2-Infected Human Lung Epithelial Cells (Calu-3) Reveals Strong Induction of Interferon-Stimulated Gene Expression by SARS-CoV-2 in Contrast to SARS-CoV. J Proteome Res. 2022 Feb 4;21(2):459–69.

138. Chen R, Fulton KM, Tran A, Duque D, Kovalchik K, Caron E, et al. Integrated Immunopeptidomics and Proteomics Study of SARS-CoV-2–Infected Calu-3 Cells Reveals Dynamic Changes in Allele-specific HLA Abundance and Antigen Presentation. Mol Cell Proteomics. 2023 Sep 13;22(10):100645.

139. Murigneux E, Softic L, Aubé C, Grandi C, Judith D, Bruce J, et al. Proteomic analysis of SARS-CoV-2 particles unveils a key role of G3BP proteins in viral assembly. Nat Commun. 2024 Jan 20;15:640.

140. Huang KYA, Tan TK, Chen TH, Huang CG, Harvey R, Hussain S, et al. Breadth and function of antibody response to acute SARS-CoV-2 infection in humans. PLoS Pathog. 2021 Feb;17(2):e1009352.

141. Skelly DT, Harding AC, Gilbert-Jaramillo J, Knight ML, Longet S, Brown A, et al. Two doses of SARS-CoV-2 vaccination induce robust immune responses to emerging SARS-CoV-2 variants of concern. Nat Commun. 2021 Aug 17;12:5061.

142. Mortezavi M, Sloan A, Singh RSP, Chen LF, Kim JH, Shojaee N, et al. Virologic Response and Safety of Ibuzatrelvir, A Novel SARS-CoV-2 Antiviral, in Adults With COVID-19. Clin Infect Dis. 2025 Mar 17;80(3):673–80.

143. Zhu W, Chen CZ, Gorshkov K, Xu M, Lo DC, Zheng W. RNA-Dependent RNA Polymerase as a Target for COVID-19 Drug Discovery. SLAS Discov. 2020 Dec;25(10):1141–51.

144. Yazdani S, De Maio N, Ding Y, Shahani V, Goldman N, Schapira M. Genetic Variability of the SARS-CoV-2 Pocketome. J Proteome Res. 2021 Aug 6;20(8):4212–5.

145. Ledford H. COVID antiviral pills: what scientists still want to know. Nature. 2021 Nov;599(7885):358–9.

146. Korber B, Fischer WM, Gnanakaran S, Yoon H, Theiler J, Abfalterer W, et al. Tracking Changes in SARS-CoV-2 Spike: Evidence that D614G Increases Infectivity of the COVID-19 Virus. Cell. 2020 Aug 20;182(4):812-827.e19.

147. Goldman JD, Wang K, Röltgen K, Nielsen SCA, Roach JC, Naccache SN, et al. Reinfection with SARS-CoV-2 and Waning Humoral Immunity: A Case Report. Vaccines (Basel). 2022 Dec 20;11(1):5.

148. Tut G, Lancaster T, Krutikov M, Sylla P, Bone D, Spalkova E, et al. Strong peak immunogenicity but rapid antibody waning following third vaccine dose in older residents of care homes. Nat Aging. 2023 Jan;3(1):93–104.

149. Gandhi S, Klein J, Robertson AJ, Peña-Hernández MA, Lin MJ, Roychoudhury P, et al. De novo emergence of a remdesivir resistance mutation during treatment of persistent SARS-CoV-2 infection in an immunocompromised patient: a case report. Nat Commun. 2022 Mar 17;13(1):1547.

150. Yang S, Multani A, Garrigues JM, Oh MS, Hemarajata P, Burleson T, et al. Transient SARS-CoV-2 RNA-Dependent RNA Polymerase Mutations after Remdesivir Treatment for Chronic COVID-19 in Two Transplant Recipients: Case Report and Intra-Host Viral Genomic Investigation. Microorganisms. 2023 Aug;11(8):2096.

151. Ip JD, Chu AWH, Chan WM, Leung RCY, Abdullah SMU, Sun Y, et al. Global prevalence of SARS-CoV-2 3CL protease mutations associated with nirmatrelvir or ensitrelvir resistance. eBioMedicine. 2023 May 1;91.

152. Uehara T, Yotsuyanagi H, Ohmagari N, Doi Y, Yamato M, Imamura T, et al. Ensitrelvir treatment–emergent amino acid substitutions in SARS-CoV-2 3CLpro detected in the SCORPIO-SR phase 3 trial. Antiviral Research. 2025 Apr 1;236:106097.

153. Heyer A, Günther T, Robitaille A, Lütgehetmann M, Addo MM, Jarczak D, et al. Remdesivir-induced emergence of SARS-CoV2 variants in patients with prolonged infection. Cell Rep Med. 2022 Aug 16;3(9):100735.

154. Szemiel AM, Merits A, Orton RJ, MacLean OA, Pinto RM, Wickenhagen A, et al. In vitro selection of Remdesivir resistance suggests evolutionary predictability of SARS-CoV-2. PLoS Pathog. 2021 Sep;17(9):e1009929.

155. Pepperrell T, Ellis L, Wang J, Hill A. Barriers to Worldwide Access for Paxlovid, a New Treatment for COVID-19. Open Forum Infect Dis. 2022 Apr 7;9(9):ofac174.

156. Schreiber A, Ludwig S. Host-targeted antivirals against SARS-CoV-2 in clinical development - Prospect or disappointment? Antiviral Res. 2025 Mar;235:106101.

157. Pawlotsky JM. What are the pros and cons of the use of host-targeted agents against hepatitis C? Antiviral Res. 2014 May;105:22–5.

158. Tripathi N, Goel B, Bhardwaj N, Vishwakarma RA, Jain SK. Exploring the Potential of Chemical Inhibitors for Targeting Post-translational Glycosylation of Coronavirus (SARS-CoV-2). ACS Omega. 2022 Aug 9;7(31):27038–51.

159. He Y, Zhou J, Gao H, Liu C, Zhan P, Liu X. Broad-spectrum antiviral strategy: Host-targeting antivirals against emerging and re-emerging viruses. Eur J Med Chem. 2024 Feb 5;265:116069.

160. Mazzon M, Marsh M. Targeting viral entry as a strategy for broad-spectrum antivirals. F1000Res. 2019 Sep 12;8:F1000 Faculty Rev-1628.

161. Majdoul S, Compton AA. Lessons in self-defence: inhibition of virus entry by intrinsic immunity. Nat Rev Immunol. 2022 Jun;22(6):339–52.

162. Wilkin TJ, Gulick RM. CCR5 antagonism in HIV infection: current concepts and future opportunities. Annu Rev Med. 2012;63:81–93.

163. Beyerstedt S, Casaro EB, Rangel ÉB. COVID-19: angiotensin-converting enzyme 2 (ACE2) expression and tissue susceptibility to SARS-CoV-2 infection. Eur J Clin Microbiol Infect Dis. 2021;40(5):905–19.

164. Jackson CB, Farzan M, Chen B, Choe H. Mechanisms of SARS-CoV-2 entry into cells. Nat Rev Mol Cell Biol. 2022 Jan;23(1):3–20.

165. Hoffmann M, Kleine-Weber H, Schroeder S, Krüger N, Herrler T, Erichsen S, et al. SARS-CoV-2 Cell Entry Depends on ACE2 and TMPRSS2 and Is Blocked by a Clinically Proven Protease Inhibitor. Cell. 2020 Apr 16;181(2):271-280.e8.

166. Vu MN, Menachery VD. Binding and entering: COVID finds a new home. PLoS Pathog. 2021 Aug;17(8):e1009857.

167. Sheng X, Zhu F, Peng H, Yang F, Yang Y, Yang C, et al. Host cyclophilin A facilitates SARS-CoV-2 infection by binding and stabilizing spike on virions. Sig Transduct Target Ther. 2023 Dec 14;8(1):1–4.

168. Liu C, von Brunn A, Zhu D. Cyclophilin A and CD147: novel therapeutic targets for the treatment of COVID-19. Med Drug Discov. 2020 Sep;7:100056.

169. Pfefferle S, Schöpf J, Kögl M, Friedel CC, Müller MA, Carbajo-Lozoya J, et al. The SARS-coronavirus-host interactome: identification of cyclophilins as target for pan-coronavirus inhibitors. PLoS Pathog. 2011 Oct;7(10):e1002331.

170. Softic L, Brillet R, Berry F, Ahnou N, Nevers Q, Morin-Dewaele M, et al. Inhibition of SARS-CoV-2 Infection by the Cyclophilin Inhibitor Alisporivir (Debio 025). Antimicrob Agents Chemother. 2020 Jun 23;64(7):e00876-20.

171. Oroojalian F, Haghbin A, Baradaran B, Hemmat N, Shahbazi MA, Baghi HB, et al. Novel insights into the treatment of SARS-CoV-2 infection: An overview of current clinical trials. Int J Biol Macromol. 2020 Dec 15;165(Pt A):18–43.

172. Bian H, Chen L, Zheng ZH, Sun XX, Geng JJ, Chen R, et al. Meplazumab in hospitalized adults with severe COVID-19 (DEFLECT): a multicenter, seamless phase 2/3, randomized, third-party double-blind clinical trial. Sig Transduct Target Ther. 2023 Jan 30;8(1):1–9.

173. Villalaín J. Membranotropic effects of arbidol, a broad anti-viral molecule, on phospholipid model membranes. J Phys Chem B. 2010 Jul 1;114(25):8544–54.

174. Haviernik J, Štefánik M, Fojtíková M, Kali S, Tordo N, Rudolf I, et al. Arbidol (Umifenovir): A Broad-Spectrum Antiviral Drug That Inhibits Medically Important Arthropod-Borne Flaviviruses. Viruses. 2018 Apr 10;10(4):184.

175. Deng L, Li C, Zeng Q, Liu X, Li X, Zhang H, et al. Arbidol combined with LPV/r versus LPV/r alone against Corona Virus Disease 2019: A retrospective cohort study. J Infect. 2020 Jul;81(1):e1–5.

176. Wang X, Cao R, Zhang H, Liu J, Xu M, Hu H, et al. The anti-influenza virus drug, arbidol is an efficient inhibitor of SARS-CoV-2 in vitro. Cell Discov. 2020 May 2;6(1):28.

177. Li Y, Xie Z, Lin W, Cai W, Wen C, Guan Y, et al. Efficacy and Safety of Lopinavir/Ritonavir or Arbidol in Adult Patients with Mild/Moderate COVID-19: An Exploratory Randomized Controlled Trial. Med (N Y). 2020 Dec 18;1(1):105-113.e4.

178. Alkafaas SS, Abdallah AM, Ghosh S, Loutfy SA, Elkafas SS, Abdel Fattah NF, et al. Insight into the role of clathrin-mediated endocytosis inhibitors in SARS-CoV-2 infection. Reviews in Medical Virology. 2023;33(1):e2403.

179. Prichard KL, O'Brien NS, Murcia SR, Baker JR, McCluskey A. Role of Clathrin and Dynamin in Clathrin Mediated Endocytosis/Synaptic Vesicle Recycling and Implications in Neurological Diseases. Front Cell Neurosci. 2022 Jan 18;15.

180. Hessien M, Donia T, Tabll AA, Adly E, Abdelhafez TH, Attia A, et al. Mechanistic-Based Classification of Endocytosis-Related Inhibitors: Does It Aid in Assigning Drugs against SARS-CoV-2? Viruses. 2023 Apr 23;15(5):1040.

181. de Wilde AH, Jochmans D, Posthuma CC, Zevenhoven-Dobbe JC, van Nieuwkoop S, Bestebroer TM, et al. Screening of an FDA-Approved Compound Library Identifies Four Small-Molecule Inhibitors of Middle East Respiratory Syndrome Coronavirus Replication in Cell Culture. Antimicrob Agents Chemother. 2014 Aug;58(8):4875–84.

182. Muric NN, Arsenijevic NN, Borovcanin MM. Chlorpromazine as a Potential Antipsychotic Choice in COVID-19 Treatment. Front Psychiatry. 2020 Dec 23;11.

183. Plaze M, Attali D, Petit AC, Blatzer M, Simon-Loriere E, Vinckier F, et al. Repurposing chlorpromazine to treat COVID-19: The reCoVery study. Encephale. 2020 Jun;46(3):169–72.

184. Zumla A, Chan JFW, Azhar EI, Hui DSC, Yuen KY. Coronaviruses - drug discovery and therapeutic options. Nat Rev Drug Discov. 2016 May;15(5):327–47.

185. Savan R, Gale M. Innate immunity and interferon in SARS-CoV-2 infection outcome. Immunity. 2023 Jul 11;56(7):1443–50.

186. Samuel CE. Interferon at the crossroads of SARS-CoV-2 infection and COVID-19 disease. J Biol Chem. 2023 Jun 24;299(8):104960.

187. Park A, Iwasaki A. Type I and Type III Interferons - Induction, Signaling, Evasion, and Application to Combat COVID-19. Cell Host Microbe. 2020 Jun 10;27(6):870–8.

188. Znaidia M, Demeret C, van der Werf S, Komarova AV. Characterization of SARS-CoV-2 Evasion: Interferon Pathway and Therapeutic Options. Viruses. 2022 Jun 8;14(6):1247.

189. Tilmanis D, van Baalen C, Oh DY, Rossignol JF, Hurt AC. The susceptibility of circulating human influenza viruses to tizoxanide, the active metabolite of nitazoxanide. Antiviral Res. 2017 Nov;147:142–8.

190. Jasenosky LD, Cadena C, Mire CE, Borisevich V, Haridas V, Ranjbar S, et al. The FDA-Approved Oral Drug Nitazoxanide Amplifies Host Antiviral Responses and Inhibits Ebola Virus. iScience. 2019 Sep 27;19:1279–90.

191. Haffizulla J, Hartman A, Hoppers M, Resnick H, Samudrala S, Ginocchio C, et al. Effect of nitazoxanide in adults and adolescents with acute uncomplicated influenza: a double-blind, randomised, placebo-controlled, phase 2b/3 trial. Lancet Infect Dis. 2014 Jul;14(7):609–18.

192. Lokhande AS, Devarajan PV. A review on possible mechanistic insights of Nitazoxanide for repurposing in COVID-19. Eur J Pharmacol. 2021 Jan 15;891:173748.

193. Stewart DD. Can Nitazoxanide and/or other anti-viral medications be a solution to long COVID? Case report with a brief literature review. Clin Case Rep. 2023 Nov 17;11(11):e8162.

194. Blum VF, Cimerman S, Hunter JR, Tierno P, Lacerda A, Soeiro A, et al. Nitazoxanide superiority to placebo to treat moderate COVID-19 – A Pilot prove of concept randomized double-blind clinical trial. eClinicalMedicine. 2021 Jul 1;37:100981.

195. Rossignol JF, Bardin MC, Fulgencio J, Mogelnicki D, Bréchot C. A randomized double-blind placebo-controlled clinical trial of nitazoxanide for treatment of mild or moderate COVID-19. eClinicalMedicine [Internet]. 2022 Mar 1 [cited 2025 May 18];45. Available from: https://www.thelancet.com/journals/eclinm/article/PIIS2589-5370(22)00040-2/fulltext

196. Alketbi EH, Hamdy R, El-Kabalawy A, Juric V, Pignitter M, A. Mosa K, et al. Lipid-based therapies against SARS-CoV-2 infection. Rev Med Virol. 2021 Sep;31(5):e2214.

197. Kornhuber J, Tripal P, Reichel M, Mühle C, Rhein C, Muehlbacher M, et al. Functional Inhibitors of Acid Sphingomyelinase (FIASMAs): a novel pharmacological group of drugs with broad clinical applications. Cell Physiol Biochem. 2010;26(1):9–20.

198. Oskotsky T, Maric I, Tang A, Oskotsky B, Wong RJ, Aghaeepour N, et al. Mortality Risk Among Patients With COVID-19 Prescribed Selective Serotonin Reuptake Inhibitor Antidepressants. JAMA Netw Open. 2021 Nov 1;4(11):e2133090.

199. Prasad V, Bartenschlager R. A snapshot of protein trafficking in SARS-CoV-2 infection. Biol Cell. 2022 Nov 14;10.1111/boc.202200073.

200. Schoberer J, Shin YJ, Vavra U, Veit C, Strasser R. Protein glycosylation in the ER. Methods Mol Biol. 2018 Jan 1;1691:205–22.

201. Chang J, Warren TK, Zhao X, Gill T, Guo F, Wang L, et al. Small molecule inhibitors of ER α-glucosidases are active against multiple hemorrhagic fever viruses. Antiviral Res. 2013 Jun;98(3):432–40.

202. Caramelo JJ, Parodi AJ. A sweet code for glycoprotein folding. FEBS Lett. 2015 Nov 14;589(22):3379–87.

203. Fregno I, Fasana E, Soldà T, Galli C, Molinari M. N-glycan processing selects ERAD-resistant misfolded proteins for ER-to-lysosome-associated degradation. EMBO J. 2021 Aug 2;40(15):e107240.

204. Krshnan L, van de Weijer ML, Carvalho P. Endoplasmic Reticulum-Associated Protein Degradation. Cold Spring Harb Perspect Biol. 2022 Dec 1;14(12):a041247.

205. Alonzi DS, Scott KA, Dwek RA, Zitzmann N. Iminosugar antivirals: the therapeutic sweet spot. Biochem Soc Trans. 2017 Apr 15;45(2):571–82.

206. Dwek RA, Butters TD, Platt FM, Zitzmann N. Targeting glycosylation as a therapeutic approach. Nat Rev Drug Discov. 2002 Jan;1(1):65–75.

207. Mehta A, Zitzmann N, Rudd PM, Block TM, Dwek RA. Alpha-glucosidase inhibitors as potential broad based anti-viral agents. FEBS Lett. 1998 Jun 23;430(1–2):17–22.

208. Zitzmann N, Block T, Methta A, Rudd P, Burton D, Wilson I, et al. Glycosylation: disease targets and therapy. Adv Exp Med Biol. 2005;564:1–2.

209. Miller JL, Tyrrell BE, Zitzmann N. Mechanisms of Antiviral Activity of Iminosugars Against Dengue Virus. Adv Exp Med Biol. 2018;1062:277–301.

210. Perera N, Miller JL, Zitzmann N. The role of the unfolded protein response in dengue virus pathogenesis. Cell Microbiol. 2017 May;19(5).

211. Warfield KL, Alonzi DS, Hill JC, Caputo AT, Roversi P, Kiappes JL, et al. Targeting Endoplasmic Reticulum α-Glucosidase I with a Single-Dose Iminosugar Treatment Protects against Lethal Influenza and Dengue Virus Infections. J Med Chem. 2020 Apr 23;63(8):4205–14.

212. Wu SF, Lee CJ, Liao CL, Dwek RA, Zitzmann N, Lin YL. Antiviral effects of an iminosugar derivative on flavivirus infections. J Virol. 2002 Apr;76(8):3596–604.

213. Jacob JR, Mansfield K, You JE, Tennant BC, Kim YH. Natural iminosugar derivatives of 1-deoxynojirimycin inhibit glycosylation of hepatitis viral envelope proteins. J Microbiol. 2007 Oct;45(5):431–40.

214. Chang J, Guo JT, Du Y, Block T. Imino sugar glucosidase inhibitors as broadly active anti-filovirus agents. Emerg Microbes Infect. 2013 Nov;2(11):e77.

215. Clarke EC, Nofchissey RA, Ye C, Bradfute SB. The iminosugars celgosivir, castanospermine and UV-4 inhibit SARS-CoV-2 replication. Glycobiology. 2021 May 3;31(4):378–84.

216. Fukushi M, Yoshinaka Y, Matsuoka Y, Hatakeyama S, Ishizaka Y, Kirikae T, et al. Monitoring of S Protein Maturation in the Endoplasmic Reticulum by Calnexin Is Important for the Infectivity of Severe Acute Respiratory Syndrome Coronavirus. Journal of Virology. 2012 Nov;86(21):11745–53.

217. Casas-Sanchez A, Romero-Ramirez A, Hargreaves E, Ellis CC, Grajeda BI, Estevao IL, et al. Inhibition of Protein N-Glycosylation Blocks SARS-CoV-2 Infection. mBio. 2021 Feb 22;13(1):e0371821.

218. Rajasekharan S, Milan Bonotto R, Nascimento Alves L, Kazungu Y, Poggianella M, Martinez-Orellana P, et al. Inhibitors of Protein Glycosylation Are Active against the Coronavirus Severe Acute Respiratory Syndrome Coronavirus SARS-CoV-2. Viruses. 2021 Apr 30;13(5):808.

219. Karade SS, Franco EJ, Rojas AC, Hanrahan KC, Kolesnikov A, Yu W, et al. Structure-Based Design of Potent Iminosugar Inhibitors of Endoplasmic Reticulum α-Glucosidase I with Anti-SARS-CoV-2 Activity. J Med Chem. 2023 Feb 23;66(4):2744–60.

220. Caramelo JJ, Parodi AJ. Getting in and out from calnexin/calreticulin cycles. J Biol Chem. 2008 Apr 18;283(16):10221–5.

221. Iftikhar M, Lu Y, Zhou M. An overview of therapeutic potential of N-alkylated 1-deoxynojirimycin congeners. Carbohydr Res. 2021 Jun;504:108317.

222. Mehta A, Ouzounov S, Jordan R, Simsek E, Lu X, Moriarty RM, et al. Imino Sugars That are Less Toxic but More Potent as Antivirals, In Vitro, Compared with N-n-Nonyl DNJ. Antivir Chem Chemother. 2002 Oct 1;13(5):299–304.

223. Alonzi DS, Kukushkin NV, Allman SA, Hakki Z, Williams SJ, Pierce L, et al. Glycoprotein misfolding in the endoplasmic reticulum: identification of released oligosaccharides reveals a second ER-associated degradation pathway for Golgi-retrieved proteins. Cell Mol Life Sci. 2013 Aug;70(15):2799–814.

224. Alonzi DS, Neville DCA, Lachmann RH, Dwek RA, Butters TD. Glucosylated free oligosaccharides are biomarkers of endoplasmic- reticulum alpha-glucosidase inhibition. Biochem J. 2008 Jan 15;409(2):571–80.

225. Iyidogan P, Anderson KS. Current perspectives on HIV-1 antiretroviral drug resistance. Viruses. 2014 Oct 24;6(10):4095–139.

226. Ahmed A, Felmlee DJ. Mechanisms of Hepatitis C Viral Resistance to Direct Acting Antivirals. Viruses. 2015 Dec 18;7(12):6716–29.

227. Pawlotsky JM. Retreatment of Hepatitis C Virus-Infected Patients with Direct-Acting Antiviral Failures. Semin Liver Dis. 2019 Jul;39(3):354–68.

228. Collier DA, Monit C, Gupta RK. The Impact of HIV-1 Drug Escape on the Global Treatment Landscape. Cell Host Microbe. 2019 Jul 10;26(1):48–60.

229. Smyk JM, Szydłowska N, Szulc W, Majewska A. Evolution of Influenza Viruses-Drug Resistance, Treatment Options, and Prospects. Int J Mol Sci. 2022 Oct 13;23(20):12244.

230. Afshinnekoo E, Bhattacharya C, Burguete-García A, Castro-Nallar E, Deng Y, Desnues C, et al. COVID-19 drug practices risk antimicrobial resistance evolution. Lancet Microbe. 2021 Apr;2(4):e135–6.

231. Hogan JI, Duerr R, Dimartino D, Marier C, Hochman SE, Mehta S, et al. Remdesivir Resistance in Transplant Recipients With Persistent Coronavirus Disease 2019. Clin Infect Dis. 2023 Jan 13;76(2):342–5.

232. Tanino Y, Nishioka K, Yamamoto C, Watanabe Y, Daidoji T, Kawamoto M, et al. Emergence of SARS-CoV-2 with Dual-Drug Resistant Mutations During a Long-Term Infection in a Kidney Transplant Recipient. Infect Drug Resist. 2024;17:531–41.

233. Stevens LJ, Pruijssers AJ, Lee HW, Gordon CJ, Tchesnokov EP, Gribble J, et al. Mutations in the SARS-CoV-2 RNA-dependent RNA polymerase confer resistance to remdesivir by distinct mechanisms. Sci Transl Med. 2022 Aug 3;14(656):eabo0718.

234. Hedskog C, Rodriguez L, Roychoudhury P, Huang ML, Jerome KR, Hao L, et al. Viral Resistance Analyses From the Remdesivir Phase 3 Adaptive COVID-19 Treatment Trial-1 (ACTT-1). J Infect Dis. 2023 Nov 2;228(9):1263–73.

235. Plummer E, Buck MD, Sanchez M, Greenbaum JA, Turner J, Grewal R, et al. Dengue Virus Evolution under a Host-Targeted Antiviral. Journal of Virology. 2015 Apr 21;89(10):5592–601.

236. Warfield KL, Schaaf KR, DeWald LE, Spurgers KB, Wang W, Stavale E, et al. Lack of selective resistance of influenza A virus in presence of host-targeted antiviral, UV-4B. Sci Rep. 2019 May 16;9(1):7484.

237. Tyrrell BE, Sayce AC, Warfield KL, Miller JL, Zitzmann N. Iminosugars: Promising therapeutics for influenza infection. Crit Rev Microbiol. 2017 Sep 3;43(5):521–45.

238. Evans DeWald L, Starr C, Butters T, Treston A, Warfield KL. Iminosugars: A host-targeted approach to combat *Flaviviridae* infections. Antiviral Research. 2020 Dec 1;184:104881.

239. Franco EJ, Warfield KL, Brown AN. UV-4B potently inhibits replication of multiple SARS-CoV-2 strains in clinically relevant human cell lines. Front Biosci (Landmark Ed). 2022 Jan 5;27(1):3.

240. Franco EJ, Drusano GL, Hanrahan KC, Warfield KL, Brown AN. Combination Therapy with UV-4B and Molnupiravir Enhances SARS-CoV-2 Suppression. Viruses. 2023 May 16;15(5):1175.

241. Tyrrell BE, Kumar A, Gangadharan B, Alonzi D, Brun J, Hill M, et al. Exploring the Potential of Iminosugars as Antivirals for Crimean-Congo Haemorrhagic Fever Virus, Using the Surrogate Hazara Virus: Liquid-Chromatography-Based Mapping of Viral N-Glycosylation and In Vitro Antiviral Assays. Pathogens. 2023 Mar 1;12(3):399.

242. Schlesinger S, Malfer C, Schlesinger MJ. The formation of vesicular stomatitis virus (San Juan strain) becomes temperature-sensitive when glucose residues are retained on the oligosaccharides of the glycoprotein. J Biol Chem. 1984 Jun 25;259(12):7597–601.

243. Butters TD, van den Broek LAGM, Fleet GWJ, Krulle TM, Wormald MR, Dwek RA, et al. Molecular requirements of imino sugars for the selective control of N-linked glycosylation and glycosphingolipid biosynthesis. Tetrahedron: Asymmetry. 2000 Jan 28;11(1):113–24.

244. Fischl MA, Resnick L, Coombs R, Kremer AB, Pottage JC, Fass RJ, et al. The safety and efficacy of combination N-butyl-deoxynojirimycin (SC-48334) and zidovudine in patients with HIV-1 infection and 200-500 CD4 cells/mm3. J Acquir Immune Defic Syndr (1988). 1994 Feb;7(2):139–47.

245. Singhal N, Kumar M, Kanaujia PK, Virdi JS. MALDI-TOF mass spectrometry: an emerging technology for microbial identification and diagnosis. Front Microbiol. 2015 Aug 5;6:791.

246. Clarke R, Bharucha T, Arman BY, Gangadharan B, Gomez Fernandez L, Mosca S, et al. Using matrix assisted laser desorption ionisation mass spectrometry combined with machine learning for vaccine authenticity screening. npj Vaccines. 2024 Aug 28;9(1):155.

247. Gupta S, Yeung J. Thousands thought they were getting the Covid vaccine. They were injected with salt water instead [Internet]. 2021 [cited 2024 Mar 10]. Available from: https://edition.cnn.com/2021/07/05/india/india-fake-covid-vaccine-scam-intl-hnk/index.html

248. Hindustan Times. Hindustan Times. 2021 [cited 2024 Aug 14]. People may have got antibiotics at fake jab camp in Kolkata: Cops. Available from: https://www.hindustantimes.com/india-news/people-may-have-got-antibiotics-at-fake-jab-camp-in-kolkata-cops-101624561190596.html

249. Kaur B. The Wire. 2022 [cited 2024 Aug 14]. Officials seize large cache of fake COVID vaccines, drugs, test kits in Varanasi. Available from: https://science.thewire.in/health/up-fda-officials-seize-fake-covid-vaccines-drugs-test-kits-varanasi/

250. World Health Organization. WHO. 2021 [cited 2024 Aug 15]. Medical Product Alert N°7/2021: Falsified COVID-19 Vaccine AstraZeneca. Available from: https://www.who.int/news/item/04-11-2021-medical-product-alert-n-7-2021-falsified-covid-19-vaccine-astrazeneca

251. BBC. BBC. 2021 [cited 2024 Aug 15]. Coronavirus: Pfizer confirms fake versions of vaccine in Poland and Mexico. Available from: https://www.bbc.co.uk/news/world-56844149

252. World Health Organization. WHO. 2021 [cited 2024 Aug 15]. Medical Product Alert N°6/2021: Falsified Pfizer-BioNTech COVID-19 Vaccine. Available from:

https://www.who.int/news/item/04-11-2021-medical-product-alert-n-6-2021-falsified-pfizer-biontech-covid-19-vaccine

253. World Health Organization. Full List of WHO Medical Product Alerts [Internet]. 2024 [cited 2024 Aug 14]. Available from: https://www.who.int/teams/regulation-prequalification/incidents-and-SF/full-list-of-who-medical-product-alerts

254. The Washington Times. Vaccine scandal highlights Indonesian health system woes [Internet]. 2016 [cited 2025 May 30]. Available from: https://www.washingtontimes.com/news/2016/jul/22/vaccine-scandal-highlights-indonesian-health-syste/

255. World Health Organization. WHO lists two additional COVID-19 vaccines for emergency use and COVAX roll-out [Internet]. 2021 [cited 2023 Sep 6]. Available from: https://www.who.int/news/item/15-02-2021-who-lists-two-additional-covid-19-vaccines-for-emergency-use-and-covax-roll-out

256. World Health Organization. Medical Product Alert N°5/2021: Falsified COVISHIELD vaccine (Update) [Internet]. 2021 [cited 2023 Aug 31]. Available from: https://www.who.int/news/item/31-08-2021-medical-product-alert-n-5-2021-falsified-covishield-vaccine

257. Assi S, Arafat B, Abbas I, Evans K. Evaluation of portable near-infrared spectroscopy for authentication of mRNA based COVID-19 vaccines. PLoS One. 2022;17(5):e0267214.

258. Mosca S, Lin Q, Stokes R, Bharucha T, Gangadharan B, Clarke R, et al. Innovative method for rapid detection of falsified COVID-19 vaccines through unopened vials using handheld Spatially Offset Raman Spectroscopy (SORS). Vaccine. 2023;41(47):6960–8.

259. Tsuchida S, Umemura H, Nakayama T. Current Status of Matrix-Assisted Laser Desorption/Ionization-Time-of-Flight Mass Spectrometry (MALDI-TOF MS) in Clinical Diagnostic Microbiology. Molecules. 2020 Oct 17;25(20):E4775.

260. Garcia-Cañas V, Lorbetskie B, Cyr TD, Hefford MA, Smith S, Girard M. Approach to the profiling and characterization of influenza vaccine constituents by the combined use of size-exclusion chromatography, gel electrophoresis and mass spectrometry. Biologicals. 2010 Mar;38(2):294–302.

261. Manchester Metropolitan University. MALDI-TOF MS for microbe identification: the gold standard for clinical microbiologists worldwide [Internet]. REF2021; [cited 2025 May 22]. Available from: https://results2021.ref.ac.uk/impact/3739b960-033f-4a1a-9142-e4d31e0d306f?page=1

262. McCullagh JSO, Oldham NJ. Mass Spectrometry. Oxford University Press; 2019.

263. Aebersold R, Mann M. Mass spectrometry-based proteomics. Nature. 2003 Mar;422(6928):198–207.

264. Awad H, Khamis ,Mona M., and El-Aneed A. Mass Spectrometry, Review of the Basics: Ionization. Applied Spectroscopy Reviews. 2015 Feb 7;50(2):158–75.

265. Haag AM. Mass Analyzers and Mass Spectrometers. Adv Exp Med Biol. 2016;919:157–69.

266. Garg E, Zubair M. Mass Spectrometer. In: StatPearls [Internet]. Treasure Island (FL): StatPearls Publishing; 2025 [cited 2025 May 25]. Available from: http://www.ncbi.nlm.nih.gov/books/NBK589702/

267. Brais CJ, Ibañez JO, Schwartz AJ, Ray SJ. Recent advances in instrumental approaches to time-of-flight mass spectrometry. Mass Spectrom Rev. 2021 Sep;40(5):647–69.

268. Lévesque S, Dufresne PJ, Soualhine H, Domingo MC, Bekal S, Lefebvre B, et al. A Side by Side Comparison of Bruker Biotyper and VITEK MS: Utility of MALDI-TOF MS Technology for Microorganism Identification in a Public Health Reference Laboratory. PLoS One. 2015;10(12):e0144878.

269. Hindustan Times. Amikacin may have been used at fake Covid-19 vaccination camp in Kolkata [Internet]. 2021 [cited 2023 Sep 2]. Available from: https://www.hindustantimes.com/india-news/amikacin-may-have-been-used-at-fake-covid-19-vaccination-camp-in-kolkata-101624564851378.html

270. The Wall Street Journal. Pfizer identifies fake covid-19 shots abroad as criminals exploit vaccine demand [Internet]. 2021 [cited 2023 Aug 29]. Available from: https://www.livemint.com/companies/news/pfizer-identifies-fake-covid-19-shots-abroad-as-criminals-exploit-vaccine-demand-11619024998051.html

271. Gibb S, Strimmer K. MALDIquant: a versatile R package for the analysis of mass spectrometry data. Bioinformatics. 2012 Sep 1;28(17):2270–1.

272. Pang Z, Zhou G, Ewald J, Chang L, Hacariz O, Basu N, et al. Using MetaboAnalyst 5.0 for LC–HRMS spectra processing, multi-omics integration and covariate adjustment of global metabolomics data. Nat Protoc. 2022 Aug;17(8):1735–61.

273. Serum Institute of India. COVISHIELD FAQs [Internet]. 2021 [cited 2023 Nov 21]. Available from: https://www.seruminstitute.com/health_faq_covishield.php#faq1

274. Ralbovsky NM, Smith JP. Machine Learning for Prediction, Classification, and Identification of Immobilized Enzymes for Biocatalysis. Pharm Res. 2023 Jun;40(6):1479–90.

275. R Core Team. R: A language and environment for statistical computing. R Foundation for Statistical Computing, Vienna, Austria. [Internet]. 2021. Available from: URL https://www.R-project.org/

276. Thévenot EA, Roux A, Xu Y, Ezan E, Junot C. Analysis of the Human Adult Urinary Metabolome Variations with Age, Body Mass Index, and Gender by Implementing a Comprehensive Workflow for Univariate and OPLS Statistical Analyses. J Proteome Res. 2015 Aug 7;14(8):3322–35.

277. Worley B, Powers R. Multivariate Analysis in Metabolomics. Curr Metabolomics. 2013;1(1):92–107.

278. Pomyen Y, Wanichthanarak K, Poungsombat P, Fahrmann J, Grapov D, Khoomrung S. Deep metabolome: Applications of deep learning in metabolomics. Comput Struct Biotechnol J. 2020 Oct 1;18:2818–25.

279. Blaise BJ, Correia GDS, Haggart GA, Surowiec I, Sands C, Lewis MR, et al. Statistical analysis in metabolic phenotyping. Nat Protoc. 2021 Sep;16(9):4299–326.

280. Galal A, Talal M, Moustafa A. Applications of machine learning in metabolomics: Disease modeling and classification. Front Genet. 2022;13:1017340.

281. van Oosten LN, Klein CD. Machine Learning in Mass Spectrometry: A MALDI-TOF MS Approach to Phenotypic Antibacterial Screening. J Med Chem. 2020 Aug 27;63(16):8849–56.

282. Feucherolles M, Nennig M, Becker SL, Martiny D, Losch S, Penny C, et al. Combination of MALDI-TOF Mass Spectrometry and Machine Learning for Rapid Antimicrobial Resistance Screening: The Case of Campylobacter spp. Front Microbiol. 2021;12:804484.

283. Lazari LC, Rosa-Fernandes L, Palmisano G. Machine Learning Approaches to Analyze MALDI-TOF Mass Spectrometry Protein Profiles. Methods Mol Biol. 2022;2511:375–94.

284. Asare PT, Lee CH, Hürlimann V, Teo Y, Cuénod A, Akduman N, et al. A MALDI-TOF MS library for rapid identification of human commensal gut bacteria from the class Clostridia. Front Microbiol. 2023;14:1104707.

285. Nilsson EJ, Lind TK, Scherer D, Skansberger T, Mortensen K, Engblom J, et al. Mechanisms of crystallisation in polysorbates and sorbitan esters. CrystEngComm. 2020 Jun 8;22(22):3840–53.

286. Bellina B, Merthe DJ, Kresin VV. Proton transfer in histidine-tryptophan heterodimers embedded in helium droplets. The Journal of Chemical Physics. 2015 Mar 18;142(11):114306.

287. Hvattum E, Yip WL, Grace D, Dyrstad K. Characterization of polysorbate 80 with liquid chromatography mass spectrometry and nuclear magnetic resonance spectroscopy: Specific determination of oxidation products of thermally oxidized polysorbate 80. Journal of Pharmaceutical and Biomedical Analysis. 2012 Mar 25;62:7–16.

288. Yang Z. MIT Technology Review. 2023 [cited 2024 Feb 23]. China's Paxlovid cyber scams are everywhere. Available from: https://www.technologyreview.com/2023/01/11/1066605/chinas-paxlovid-cyber-scams/

289. Frosch T, Wyrwich E, Yan D, Domes C, Domes R, Popp J, et al. Counterfeit and Substandard Test of the Antimalarial Tablet Riamet® by Means of Raman Hyperspectral Multicomponent Analysis. Molecules. 2019 Sep 5;24(18):3229.

290. Korcok M. Counterfeit drugs latest public health hazard in US. CMAJ. 2003 Aug 5;169(3):223.

291. Elbehiry A, Aldubaib M, Abalkhail A, Marzouk E, ALbeloushi A, Moussa I, et al. How MALDI-TOF Mass Spectrometry Technology Contributes to Microbial Infection Control in Healthcare Settings. Vaccines. 2022 Nov;10(11):1881.

292. Dobbelaer R, Pfleiderer M, Haase M, Griffiths E, Knezevic I, Merkle A, et al. Guidelines on stability evaluation of vaccines. Biologicals. 2009 Nov;37(6):424–34; discussion 421-423.

293. Gulumbe BH, Adesola RO. Revisiting the blind spot of substandard and fake drugs as drivers of antimicrobial resistance in LMICs. Ann Med Surg (Lond). 2023 Feb 7;85(2):122–3.

294. Cavany S, Nanyonga S, Hauk C, Lim C, Tarning J, Sartorius B, et al. The uncertain role of substandard and falsified medicines in the emergence and spread of antimicrobial resistance. Nat Commun. 2023 Oct 3;14(1):6153.

295. World Health Organization. Monitoring vaccine wastage at country level Guidelines for programme managers [Internet]. Department of Immunization, Vaccines and Biologicals; 2005 [cited 2025 May 2]. Available from: https://iris.who.int/handle/10665/68463

296. Crommelin DJA, Anchordoquy TJ, Volkin DB, Jiskoot W, Mastrobattista E. Addressing the Cold Reality of mRNA Vaccine Stability. Journal of Pharmaceutical Sciences. 2021 Mar 1;110(3):997–1001.

297. Holm MR, Poland GA. Critical aspects of packaging, storage, preparation, and administration of mRNA and adenovirus-vectored COVID-19 vaccines for optimal efficacy. Vaccine. 2021 Jan 15;39(3):457–9.

298. Wang J, Peng Y, Xu H, Cui Z, Williams RO. The COVID-19 Vaccine Race: Challenges and Opportunities in Vaccine Formulation. AAPS PharmSciTech. 2020 Aug 5;21(6):225.

299. Wolfson LJ, Gasse F, Lee-Martin SP, Lydon P, Magan A, Tibouti A, et al. Estimating the costs of achieving the WHO-UNICEF Global Immunization Vision and Strategy, 2006-2015. Bull World Health Organ. 2008 Jan;86(1):27–39.

300. DataM Intelligence. Pharmaceutical cold chain logistics market size, share analysis, growth trends, and forecast 2025-2033 [Internet]. 2025 [cited 2025 May 23]. Available from: https://www.datamintelligence.com/research-report/pharmaceutical-cold-chain-logistics-market

301. Kumru OS, Joshi SB, Smith DE, Middaugh CR, Prusik T, Volkin DB. Vaccine instability in the cold chain: mechanisms, analysis and formulation strategies. Biologicals. 2014 Sep;42(5):237–59.

302. Mikołajczyk M, Lewandowski RA, Goncharuk AG. Impact of Improper Storage of ChAdOx1-S (AstraZeneca) Vaccine on Its Efficacy and Safety. Vaccines (Basel). 2022 Dec 30;11(1):93.

303. Food and Drug Administration. Common Ingredients in FDA-Approved Vaccines [Internet]. 2024 [cited 2024 Mar 3]. Available from: https://www.fda.gov/vaccines-blood-biologics/safety-availability-biologics/common-ingredients-fda-approved-vaccines

304. Centers for Disease Control and Prevention. Pinkbook Course Book: Epidemiology of Vaccine Preventable Diseases - 14th Ed. 2021.

305. Croyle MA, Cheng X, Wilson JM. Development of formulations that enhance physical stability of viral vectors for gene therapy. Gene Ther. 2001 Sep;8(17):1281–90.

306. Gupta CK, Leszczynski J, Gupta RK, Siber GR. Stabilization of respiratory syncytial virus (RSV) against thermal inactivation and freeze-thaw cycles for development and control of RSV vaccines and immune globulin. Vaccine. 1996 Oct;14(15):1417–20.

307. Pelliccia M, Andreozzi P, Paulose J, D'Alicarnasso M, Cagno V, Donalisio M, et al. Additives for vaccine storage to improve thermal stability of adenoviruses from hours to months. Nat Commun. 2016 Nov 30;7:13520.

308. Urru SAM, Maines E, Campomori A, Soffiati M. Safety of Sars-Cov-2 vaccines administration for adult patients with hereditary fructose intolerance. Hum Vaccin Immunother. 17(11):4112–4.

309. Colloca S, Barnes E, Folgori A, Ammendola V, Capone S, Cirillo A, et al. Vaccine vectors derived from a large collection of simian adenoviruses induce potent cellular immunity across multiple species. Sci Transl Med. 2012 Jan 4;4(115):115ra2.

310. Sanyal G. Development of functionally relevant potency assays for monovalent and multivalent vaccines delivered by evolving technologies. npj Vaccines. 2022 May 5;7(1):1–10.

311. Berg A, Wright D, Dulal P, Stedman A, Fedosyuk S, Francis MJ, et al. Stability of Chimpanzee Adenovirus Vectored Vaccines (ChAdOx1 and ChAdOx2) in Liquid and Lyophilised Formulations. Vaccines (Basel). 2021 Oct 28;9(11):1249.

312. Kis Z. Stability Modelling of mRNA Vaccine Quality Based on Temperature Monitoring throughout the Distribution Chain. Pharmaceutics. 2022 Feb 17;14(2):430.

313. Uddin MN, Roni MA. Challenges of Storage and Stability of mRNA-Based COVID-19 Vaccines. Vaccines (Basel). 2021 Sep 17;9(9):1033.

314. Goldberg RN, Tewari YB, Ahluwalia JC. Thermodynamics of the hydrolysis of sucrose. Journal of Biological Chemistry. 1989 Jun 15;264(17):9901–4.

315. Kumar P, Pullagurla SR, Patel A, Shukla RS, Bird C, Kumru OS, et al. Effect of Formulation Variables on the Stability of a Live, Rotavirus (RV3-BB) Vaccine Candidate using in vitro Gastric Digestion Models to Mimic Oral Delivery. J Pharm Sci. 2021 Feb;110(2):760–70.

316. Orellana C. Albumin put back in encephalitis vaccine. The Lancet Infectious Diseases. 2002 Aug 1;2(8):456.

317. Brook J, Bharucha T, Caillet C, Morris S, Taylor-Siddons M, Gomez Fernandez L, et al. Detection of falsified vaccines and insulin using simple biochemical profiling – an accessible and inexpensive method. Submitted. 2025;

318. Mann GF, Allison LM, Lloyd JS, Tam P, Zuckerman AJ, Perkins FT. Stability of further-attenuated measles vaccines. Rev Infect Dis. 1983;5(3):482–6.

319. Raffaele J, Loughney JW, Rustandi RR. Development of a microchip capillary electrophoresis method for determination of the purity and integrity of mRNA in lipid nanoparticle vaccines. Electrophoresis. 2022 May;43(9–10):1101–6.

320. Tong X, Raffaele J, Feller K, Dornadula G, Devlin J, Boyd D, et al. Correlating Stability-Indicating Biochemical and Biophysical Characteristics with In Vitro Cell Potency in mRNA LNP Vaccine. Vaccines. 2024 Feb;12(2):169.

321. Gallagher N, Edwards FJ. The Diagnosis and Management of Toxic Alcohol Poisoning in the Emergency Department: A Review Article. Adv J Emerg Med. 2019 May 22;3(3):e28.

322. Singh R. Over 100 Indian cough syrup samples fail quality tests, linked to deaths [Internet]. Business Standard; 2024 [cited 2025 Apr 2]. Available from: https://www.business-standard.com/india-news/over-100-indian-cough-syrup-samples-fail-quality-tests-linked-to-deaths-124072300262_1.html

323. World Health Organization. Diethylene Glycol (DEG) and Ethylene Glycol (EG) contamination - analytical methods developed for testing paediatric medicines [Internet]. 2023 [cited 2024 Sep 16]. Available from: https://www.who.int/news/item/01-12-2023-diethylene-glycol-(deg)-and-ethylene-glycol-(eg)-contamination---analytical-methods-developed-for-testing-paediatric-medicines

324. World Health Organization. Tests for diethylene glycol and ethylene glycol in liquid preparations for oral use. Chapter for inclusion in The International Pharmacopoeia [Internet]. 2023 [cited 2024 Sep 16]. Available from: https://cdn.who.int/media/docs/default-source/medicines/pharmacopoeia/2023-11-16-deg-eg-inliquidoraldosageforms-qas22-922rev3.pdf?sfvrsn=284f645d_1

325. Pyzik OZ, Abubakar I. Fighting the fakes: tackling substandard and falsified medicines. Nat Rev Dis Primers. 2022 Aug 18;8(1):1–2.

326. Medicine Quality Research Group, University of Oxford. Oxford Statement following the MQPH 2018 Conference [Internet]. [cited 2024 Sep 19]. Available from: https://www.tropicalmedicine.ox.ac.uk/events/medicine-quality/mqph2018/oxford-statement

327. Winek CL, Shingleton DP, Shanor SP. Ethylene and Diethylene Glycol Toxicity. Clinical Toxicology. 1978 Jan 1;13(2):297–324.

328. Bangkok Post. Toxin found in 15 syrup products for children [Internet]. 2024 [cited 2025 Apr 2]. Available from: https://www.bangkokpost.com/thailand/general/2807819/toxin-found-in-15-syrup-products-for-children

329. Schep LJ, Slaughter RJ, Temple WA, Beasley DMG. Diethylene glycol poisoning. Clinical Toxicology. 2009 Jul 1;47(6):525–35.

330. Wu AHB, McKay C, Broussard LA, Hoffman RS, Kwong TC, Moyer TP, et al. National academy of clinical biochemistry laboratory medicine practice guidelines: recommendations for the use of laboratory tests to support poisoned patients who present to the emergency department. Clin Chem. 2003 Mar;49(3):357–79.

331. Filip AB, Farnsworth CW, Mullins ME, Crews BO, Kraut JA. Accuracy of a Glycerol Dehydrogenase Assay for Ethylene Glycol Detection. J Med Toxicol. 2023 Oct;19(4):362–7.

332. Jacobsen D, Hewlett TP, Webb R, Brown ST, Ordinario AT, McMartin KE. Ethylene glycol intoxication: evaluation of kinetics and crystalluria. Am J Med. 1988 Jan;84(1):145–52.

333. Porter WH, Rutter PW, Bush BA, Pappas AA, Dunnington JE. Ethylene glycol toxicity: the role of serum glycolic acid in hemodialysis. J Toxicol Clin Toxicol. 2001;39(6):607–15.

334. Moreau CL, Kerns W, Tomaszewski CA, McMartin KE, Rose SR, Ford MD, et al. Glycolate kinetics and hemodialysis clearance in ethylene glycol poisoning. META Study Group. J Toxicol Clin Toxicol. 1998;36(7):659–66.

335. Sharfstein JM. Elixir Sulfanilamide. In: Sharfstein JM, editor. The Public Health Crisis Survival Guide: Leadership and Management in Trying Times [Internet]. Oxford University Press; 2018 [cited 2024 Sep 17]. p. 0. Available from: https://doi.org/10.1093/oso/9780190697211.003.0002

336. World Health Organization. Medical Product Alert N°6/2022: Substandard (contaminated) paediatric medicines [Internet]. 2022 [cited 2024 Sep 16]. Available from: https://www.who.int/news/item/05-10-2022-medical-product-alert-n-6-2022-substandard-(contaminated)-paediatric-medicines

337. World Health Organization. Medical Product Alert N°7/2022: Substandard (contaminated) paediatric liquid dosage medicines [Internet]. 2022 [cited 2024 Sep 16]. Available from: https://www.who.int/news/item/02-11-2022-medical-product-alert-n-7-2022-substandard-(contaminated)-paediatric-liquid-dosage-medicines

338. World Health Organization. Medical Product Alert N°1/2023: Substandard (contaminated) liquid dosage medicines [Internet]. 2023 [cited 2024 Sep 16]. Available from: https://www.who.int/news/item/11-01-2023-medical-product-alert-n-1-2023-substandard-(contaminated)-liquid-dosage-medicines

339. World Health Organization. Medical Product Alert N°4/2023: Substandard (contaminated) syrup medicines [Internet]. 2023 [cited 2024 Sep 16]. Available from: https://www.who.int/news/item/25-04-2023-medical-product-alert-n-4-2023--substandard-(contaminated)-syrup-medicines

340. World Health Organization. Medical Product Alert N°5/2023: Substandard (contaminated) syrup medicines [Internet]. 2023 [cited 2024 Sep 16]. Available from: https://www.who.int/news/item/19-07-2023-medical-product-alert-n-5-2023--substandard-(contaminated)-syrup-medicines

341. World Health Organization. Medical Product Alert N°6/2023: Substandard (contaminated) syrup medicines [Internet]. 2023 [cited 2024 Sep 16]. Available from: https://www.who.int/news/item/07-08-2023-medical-product-alert-n-6-2023--substandard-(contaminated)-syrup-medicines

342. World Health Organization. Medical Product Alert N°8/2023: Substandard (contaminated) syrup and suspension medicines [Internet]. 2023 [cited 2024 Sep 16]. Available from: https://www.who.int/news/item/07-12-2023-medical-product-alert-n-8-2023--substandard-(contaminated)-syrup-and-suspension-medicines

343. World Health Organization. Medical Product Alert N°1/2024: Falsified (contaminated) USP/EP PROPYLENE GLYCOL [Internet]. 2024 [cited 2024 Sep 16]. Available from: https://www.who.int/news/item/15-04-2024-medical-product-alert-n-1-2024--falsified-(contaminated)-usp-ep-propylene-glycol

344. Wasswa H. African countries recall batch of Johnson and Johnson cough syrup because of toxicity concerns. BMJ. 2024 Apr 22;385:q923.

345. BPOM RI. Penjelasan BPOM RI Nomor HM.01.1.2.11.22.178 Tanggal 9 November 2022 tentang perkembangan hasil pengawasan sirup obat dan penindakan bahan baku propilen glikol yang mengandung cemaran EG dan DEG melebihi ambang batas. [Internet]. 2022 [cited 2024 Sep 17]. Available from: https://www.pom.go.id/penjelasan-publik/penjelasan-bpom-ri-nomor-hm-01-1-2-11-22-178-tanggal-9-november-2022-tentang-perkembangan-hasil-pengawasan-sirup-obat-dan-penindakan-bahan-baku-propilen-glikol-yang-mengandung-cemaran-eg-dan-deg-melebihi-ambang-batas

346. BPOM RI. Penjelasan BPOM RI NOMOR HM.01.1.2.12.22.186 Tanggal 7 Desember 2022 Tentang pencabutan izin edar sirup obat produksi PT. Rama Emerald Multi Sukses (PT REMS) [Internet]. 2022 [cited 2024 Sep 17]. Available from: https://www.pom.go.id/penjelasan-publik/penjelasan-bpom-ri-nomor-hm-01-1-2-12-22-186-tanggal-7-desember-2022-tentang-pencabutan-izin-edar-sirup-obat-produksi-pt-rama-emerald-multi-sukses-pt-rems

347. Alkahtani S, Sammons H, Choonara I. Epidemics of acute renal failure in children (diethylene glycol toxicity). Arch Dis Child. 2010 Dec;95(12):1062–4.

348. Kraut JA. Diagnosis of toxic alcohols: limitations of present methods. Clin Toxicol (Phila). 2015;53(7):589–95.

349. Shin JM, Sachs G, Kraut JA. Simple diagnostic tests to detect toxic alcohol intoxications. Transl Res. 2008 Oct;152(4):194–201.

350. Altamimy MA, Alshehri YM, Aldawsari FS, Altalyan NH, AlShmmari SK, Alzaid SF, et al. A Selective Gas Chromatography–Tandem Mass Spectrometry Method for Quantitation of Ethylene and Diethylene Glycol in Paediatric Syrups. Heliyon. 2024 Mar 15;10(7):e27559.

351. Singh J, Dutta AK, Khare S, Dubey NK, Harit AK, Jain NK, et al. Diethylene glycol poisoning in Gurgaon, India, 1998. Bull World Health Organ. 2001;79(2):88–95.

352. Bhakta HC, Choday VK, Grover WH. Musical Instruments As Sensors. ACS Omega. 2018 Sep 30;3(9):11026–32.

353. Nanco CR, Poklis JL, Hiler MM, Breland AB, Eissenberg T, Wolf CE. An Ultra-High-Pressure Liquid Chromatographic Tandem Mass Spectrometry Method for the Analysis of Benzoyl Ester Derivatized Glycols and Glycerol. J Anal Toxicol. 2019 Aug 21;43(9):720–5.

354. Widianto S. Deadly Indonesian cough syrup was almost pure toxin, court papers show [Internet]. 2023. Available from: https://www.reuters.com/business/healthcare-pharmaceuticals/deadly-indonesian-cough-syrup-was-almost-pure-toxin-court-papers-show-2023-10-13/

355. Food and Drug Administration. Testing of Glycerin, Propylene Glycol, Maltitol Solution, Hydrogenated Starch Hydrolysate, Sorbitol Solution, and other High-Risk Drug Components for Diethylene Glycol and Ethylene Glycol Guidance for Industry [Internet]. 2023 [cited 2025 Mar 26]. Available from: https://www.fda.gov/media/167974/download

356. Jähnke RWO, Dwornik K. A Concise Quality Control Guide on Essential Drugs and other Medicines: Special edition 2024 for the testing of toxic impurities in liquids for oral use [Internet]. Global Pharma Health Fund; 2024 [cited 2024 Sep 17]. Available from: https://www.gphf.org/images/downloads/Manual_2024_English_Special.pdf

357. Arman BY, Clarke R, Bharucha T, Fernandez LG, Walsby-Tickle J, Deats M, et al. Identifying falsified COVID-19 vaccines by analysing vaccine vial label and excipient profiles using MALDI-ToF mass spectrometry. npj Vaccines. 2025 Jan 30;10(1):19.

358. Sadat MA, Moir S, Chun TW, Lusso P, Kaplan G, Wolfe L, et al. Glycosylation, hypogammaglobulinemia, and resistance to viral infections. N Engl J Med. 2014 Apr 24;370(17):1615–25.

Appendix

Appendix 1. A summary of small molecule directly acting antivirals tested in clinical trials for COVID-19, as published in Arman BY, *et al.* 2023.

Drug name	Initial development target	Mechanism	Trial attributes	Clinical trial settings	Readout	Reference
Lopinavir/ritonavir	HIV	Protease inhibitor	Prospective	An exploratory randomised controlled trial in patients with mild/moderate COVID-19 (n=86), in Guangzhou in 2020.	Little benefit in improving the clinical outcome of patients compared to no antiviral control.	(Li et al. 2020)
Lopinavir/ritonavir	HIV	Protease inhibitor	Prospective	A randomised, controlled, open-label, platform trial in patients with COVID-19, admitted to 176 hospitals (n=1,616) in the United Kingdom in 2020 (RECOVERY trial).	Treatment was not associated with reductions in 28-day mortality, the duration of hospital stays, or the risk of progressing to invasive mechanical ventilation or death.	(Horby et al. 2020)
Lopinavir/ritonavir	HIV	Protease inhibitor	Prospective	A randomised, controlled, open-label trial in hospitalised adult patients (n=199) with confirmed SARS-CoV-2 infection in Hubei, China in 2020 (Lopinavir Trial for Suppression of SARS-CoV-2 in China/ LOTUS China).	No benefit was observed with treatment compared to standard care.	(Cao et al. 2020)

Lopinavir, ritonavir, ribavirin, and interferon beta-1b combination	HIV	Protease inhibitor	Prospective	A multi-centre, prospective, open-label, randomised, phase 2 trial in adults (n=127) with COVID-19 at 6 hospitals in Hong Kong in 2020, comparing lopinavir, ritonavir, ribavirin, and interferon beta-1b combination group and lopinavir and ritonavir control group.	The combination group was safe and superior to lopinavir-ritonavir alone in alleviating symptoms and shortening the duration of viral shedding and hospital stay in patients with mild to moderate COVID-19.	(Hung et al. 2020)
Lopinavir (without interferon)	HIV	Protease inhibitor	Prospective	A randomised trial with intention to treat primary analysis in hospitalised patients with COVID-19. The study was conducted at 405 hospitals in 30 countries (n=11,330) in 2020 (WHO SOLIDARITY trial).	Little or no effect marked by no reduction in mortality, initiation of ventilation or hospitalisation duration.	(WHO Solidarity Trial Consortium et al. 2021)
Lopinavir/ritonavir	HIV	Protease inhibitor	Retrospective observational study	A multi-centre study to test the association of risk factors and therapies with in-hospital COVID-19 mortality (n=3,451) in Italy in 2020 (CORIST study).	No change in death rate after treatment with lopinavir-ritonavir.	(Di Castelnuovo et al. 2021)
Lopinavir/ritonavir	HIV	Protease inhibitor	Prospective	A randomised trial in critically ill patients from different countries (n=694) in 2020 (REMAP-CAP study).	Worsened outcomes compared to no antiviral therapy.	(Arabi et al. 2021)

Lopinavir/ritonavir, lopinavir/ritonavir-interferon (IFN)-β-1a	HIV	Protease inhibitor	Prospective	Multi-centre, open-label, randomised, adaptive, controlled trial in COVID-19 inpatients (n=603) requiring oxygen and/or ventilatory support, conducted at 30 sites in France and Luxembourg in 2020 (DisCoVeRy trial).	No improvement in clinical status at day 15 or SARS-CoV-2 clearance in respiratory tract specimens compared to the standard care.	(Ader et al. 2021)
Danoprevir with ritonavir booster	HCV	Protease inhibitor	Prospective	An open-label, single-arm study on the treatment of naïve and experienced COVID-19 patients (n=11, China, 2020) for the first time, with the rate of composite adverse outcomes as the primary endpoint.	No composite adverse outcomes.	(H. Chen et al. 2020)
Danoprevir	HCV	Protease inhibitor	Prospective	A comparative study between two treatment groups, danoprevir and lopinavir/ritonavir treatment (n=33) in Nanchang, China in 2020.	Shorter duration of the time to achieve negative nucleic acid testing and hospital stay compared to the lopinavir/ritonavir group.	(Zhang et al. 2020)
Darunavir/cobicistat	HIV	Protease inhibitor	Prospective	A single-centre, randomised, and open-label trial in mild patients with PCR-confirmed COVID-19 (n=30) in Shanghai, China in 2020.	No increase in the proportion of conversion compared to the interferon alpha 2b and standard care control group.	(J. Chen et al. 2020)

Darunavir/cobicistat	HIV	Protease inhibitor	Retrospective observational study	A multi-centre study aimed at testing the association of risk factors and therapies with in-hospital COVID-19 mortality (n=3,451) in Italy in 2020 (CORIST study).	No benefit was observed with treatment compared to standard care.	(Di Castelnuovo et al. 2021)
Darunavir/ritonavir in combination with hydroxychloroquine	HIV	Protease inhibitor	Prospective	Open-labelled, randomised controlled trial with an intention to treat protocol (n=113) in Thailand from Dec 2020 to Apr 2021.	No virological or clinical benefit observed.	(Nimitvilai et al. 2022)
Darunavir/cobicistat	HIV	Protease inhibitor	Retrospective	Multi-centre observational study in Qatar in 2020 on adult patients (n=400) hospitalised due to COVID-19.	Less time to clinical improvement compared to treatment with lopinavir-ritonavir.	(Elmekaty et al. 2022)
Nirmatrelvir/ritonavir	SARS-CoV-2/COVID-19	Protease inhibitor	Prospective	A phase 2-3 double-blind, randomised, controlled multi-centre trial in 21 countries, in symptomatic, unvaccinated, non-hospitalised adults (n=2,246) at high risk for progression to severe COVID-19, conducted in 2021 in 21 countries.	Lower risk of progression to severe COVID-19 compared to the placebo control.	(Hammond et al. 2022)
Nirmatrelvir/ritonavir	SARS-CoV-2/COVID-19	Protease inhibitor	Retrospective	A multi-centre (11 hospitals and 55 clinics in Minnesota, USA), retrospective review of patients evaluated for a diagnosis of COVID-19 (n=66,007) in 2020-2022.	Prevalent medical contraindications to nirmatrelvir/ritonavir.	(Lim et al. 2022)

Nirmatrelvir/ritonavir	SARS-CoV-2/COVID-19	Protease inhibitor	Retrospective	An accelerated, randomised, double-blind, placebo-controlled, phase I study, conducted in a Japanese cohort in 2021.	Significant decrease in SARS-CoV-2 viral load in patients and prevention of severe disease, hospitalisation, and death.	(Singh et al. 2022)
Nirmatrelvir/ritonavir	SARS-CoV-2/COVID-19	Protease inhibitor	Prospective	An open-label, multi-centre, randomised controlled trial in hospitalised adult patients (n=264) with severe COVID-19 comorbidities at 5 hospitals in Shanghai, China in 2022.	No significant reduction in the risk of all-cause mortality on day 28 and the duration of SARS-CoV-2 RNA clearance.	(Liu et al. 2023)
Nirmatrelvir/ritonavir	SARS-CoV-2/COVID-19	Protease inhibitor	Prospective	An open-label, multi-centre, randomised, controlled, phase 2 adaptive pharmacometric platform trial in adult patients (n=383) with early symptomatic COVID-19 in Thailand, Brazil, Pakistan, and Laos in 2022 (PLATCOV study).	Ritonavir-boosted nirmatrelvir accelerated oropharyngeal SARS-CoV-2 viral clearance with significantly greater effect than molnupiravir.	(Schilling et al. 2023)
Ensitrelvir	SARS-CoV-2/COVID-19	Protease inhibitor	Prospective	A multi-centre, double-blind, phase 2a part of a phase 2/3 study in mild to moderate patients with COVID-19 (n=69), conducted in Japan from Sep 2021 to Jan 2022.	Reduction of SARS-CoV-2 RNA on day 4 and a decrease in the median time to infectious viral clearance compared to placebo.	(Mukae et al. 2022)

Ensitrelvir	SARS-CoV-2/COVID-19	Protease inhibitor	Prospective	A multi-centre, double-blind, phase 2b part of a phase 2/3 study in mild to moderate patients with COVID-19 (n=341) in Japan and South Korea in 2022.	Favourable antiviral efficacy (as change from baseline in SARS-CoV-2 titer on day 4) and potential clinical benefit with an acceptable safety profile compared to placebo.	(Mukae et al. 2023)
Ensitrelvir	SARS-CoV-2/COVID-19	Protease inhibitor	Prospective	A multi-centre, randomised, double-blind, placebo-controlled, phase 3 study in mild to moderate patients with COVID-19 (Phase 3 part) in Japan, Korea, Singapore, and Vietnam started in 2022.	Reduced time to the resolution of 5 symptoms in patients with mild-to-moderate COVID-19 compared to placebo.	(Yotsuyanagi et al. 2023)
Ensitrelvir	SARS-CoV-2/COVID-19	Protease inhibitor	Prospective	A phase 1, multi-centre, single-arm, open-label study in healthy Japanese adult participants (n=42) in 2022 to investigate the effect of ensitrelvir on the pharmacokinetics of CYP3A substrates and assess the pharmacokinetics, safety, and tolerability following multiple-dose administration.	Ensitrelvir at the clinical dose was well tolerated with no additional safety signal and can be co-administered with several CYP3A substrates likely to be used in COVID-19 patients.	(Shimizu et al. 2023)
Favipiravir	Influenza virus	RdRp inhibitor	Prospective	A randomised, open-label trial of early versus late therapy in adolescent and adult patients with COVID-19 (n=89) at 25 hospitals in Japan in 2020.	No improvement of viral clearance by day 6, although there was a numerical reduction in time to defervescence.	(Doi et al. 2020)

Favipiravir	Influenza virus	RdRp inhibitor	Prospective	An adaptive, multi-centre, open-label, randomised, Phase 2/3 clinical trial compared to the standard of care in hospitalised patients with moderate COVID-19 pneumonia (n=60) at 6 sites in Russia in 2020.	Rapid antiviral response against SARS-CoV-2, shown by the higher proportion of patients who achieved negative PCR on Day 5 when treated using favipiravir compared to the control group.	(Ivashchenko et al. 2021)
Favipiravir	Influenza virus	RdRp inhibitor	Prospective	A randomised, open-label, parallel-arm, multi-centre, phase 3 trial in adults (18-75 years) patients with RT-PCR confirmed COVID-19 and mild-to-moderate symptoms (including asymptomatic) (n=150) in India in 2020.	No statistically significant result on the primary endpoint of time to RT-PCR negativity.	(Udwadia et al. 2021)
Favipiravir combined with inhaled interferon beta-1β	Influenza virus	RdRp inhibitor	Prospective	A randomised, open-label controlled trial in adults hospitalised with moderate to severe COVID-19 pneumonia (n=89) in Oman in 2020.	No difference in clinical outcome compared to the standard arm hydroxychloroquine.	(Khamis et al. 2021)
Favipiravir	Influenza virus	RdRp inhibitor	Prospective	A randomised exploratory trial in hospitalised adult patients with COVID-19 (n=30) in Zhejiang, China in 2020.	No clinical improvement compared to the standard care.	(Lou et al. 2021)

Favipiravir	Influenza virus	RdRp inhibitor	Prospective	A phase 2, double-blind, randomised, controlled outpatient trial in asymptomatic or mildly symptomatic adults with a positive SARS-CoV-2 RT-PCR within 72 hours of enrolment (n=149) in California, USA, in Jul 2020 – Mar 2021.	No clinical benefit shown as no difference in shedding cessation time, and time to symptom resolution, compared to placebo.	(Holubar et al. 2022)
Favipiravir	Influenza virus	RdRp inhibitor	Prospective	A phase 2, randomised placebo-controlled phase 2 trial of favipiravir versus matched placebo in individuals infected with COVID-19 and 5 days or less of symptoms (n=199) in Australia in Jul 2020 – Sep 2021.	No improvement on the time to virological cure or clinical outcomes, and no evidence of an antiviral effect in early symptomatic COVID-19 infection.	(McMahon et al. 2022)
Favipiravir	Influenza virus	RdRp inhibitor	Prospective	A phase 3, multi-centre, open-label, randomised controlled trial of oral favipiravir in adult patients (n=499) who were newly admitted to hospital with proven or suspected COVID-19 across 5 sites in the UK, Brazil, and Mexico in 2020-2021 (PIONEER trial).	No significant difference in time to recovery and serious adverse events.	(Shah et al. 2023)
Favipiravir	Influenza virus	RdRp inhibitor	Prospective	A triple-blind, randomised, placebo-controlled trial in mild to moderate adult patients in an outpatient setting (n=77) in Iran in Dec 2020 – Mar 2021.	No reduction in hospitalisation rate.	(Vaezi et al. 2023)

Remdesivir	EBOV	RdRp inhibitor	Prospective	A double-blind, randomised, placebo-controlled trial in adults who were hospitalised with Covid-19 and had evidence of lower respiratory tract infection (n=1,062) in the United States, Denmark, UK, Greece, Germany, Korea, Mexico, Spain, Japan, and Singapore in 2020 (ACTT-1 study).	A shorter time to recovery was observed in patients treated with remdesivir compared to placebo.	(Beigel et al. 2020)
Remdesivir	EBOV	RdRp inhibitor	Prospective	A randomised, open-label, phase 3 trial involving hospitalised patients with severe COVID-19 (n=397) at 55 hospitals in the United States, Italy, Spain, Germany, Hong Kong, Singapore, South Korea, and Taiwan in 2020.	No significant difference between a 5-day and 10-day course, and no clinical benefit compared to placebo control.	(Goldman et al. 2020)
Remdesivir	EBOV	RdRp inhibitor	Prospective	A randomised, open-label trial in hospitalised patients (n=596) with moderate COVID-19 in the United States, Europe, and Asia in 2020.	No significant clinical status difference at 11 days compared to the standard care.	(Spinner et al. 2020)
Remdesivir	EBOV	RdRp inhibitor	Prospective	A randomised, double-blind, placebo-controlled, multi-centre trial in hospitalised adults with severe COVID-19 (n=237) in Wuhan, Hubei, China in 2020.	No significant difference in time to clinical improvement compared to placebo.	(Wang et al. 2020)

Remdesivir	EBOV	RdRp inhibitor	Prospective	A randomised, multi-centre, open control, in hospitalised adult patients with a diagnosis of COVID-19 (n=11,330) at 405 hospitals in 30 countries in 2020 (WHO Solidarity trial).	Little or no effect marked by no reduction in mortality before or after day 28, initiation of ventilation or hospitalisation duration.	(WHO Solidarity Trial Consortium et al. 2021)
Remdesivir	EBOV	RdRp inhibitor	Prospective	A randomised, double-blind, placebo-controlled trial involving non-hospitalised patients with COVID-19 who had symptom onset within the previous 7 days and who had at least one risk factor for disease progression (age ≥60 years, obesity, or certain coexisting medical conditions) (n=562), at 64 sites in the United States, Spain, Denmark, and the United Kingdom, Sep 2020 – Apr 2021 (PINETREE study).	Remdesivir, given in a 3-day course, showed an acceptable safety profile and resulted in an 87% lower risk of hospitalisation or death compared to placebo.	(Gottlieb et al. 2022)
Remdesivir-dexamethasone	EBOV	RdRp inhibitor	Prospective	A controlled non-randomised study in COVID-19 patients requiring supplemental oxygen therapy (n=151) in Italy in 2021.	Significant reduction in mortality, length of hospitalisation, and faster SARS-CoV-2 clearance, compared to dexamethasone alone.	(Marrone et al. 2022)

Molnupiravir	VEEV	RdRp inhibitor	Prospective	A phase Ib/IIa, dose-escalating, open-label, randomised, controlled trial in adult outpatients with PCR-confirmed SARS-CoV-2 infection within 5 days of symptom onset (n=18) in the United Kingdom in 2020.	Molnupiravir is safe and well-tolerated.	(Khoo et al. 2021)
Molnupiravir	VEEV	RdRp inhibitor	Prospective	A randomised, controlled trial in patients with mild or moderate COVID-19 (n=116) in Shenzhen, China in Mar 2022.	Acceleration of SARS-CoV-2 Omicron variant RNA clearance in patients, compared to the standard of care.	(Zou et al. 2022)
Molnupiravir	VEEV	RdRp inhibitor	Prospective	A phase 2a double-blind, placebo-controlled, randomised, multi-centre clinical trial in unvaccinated participants with confirmed SARS-CoV-2 infection and symptom duration of less than 7 days (n=204) in the United States from Jun 2020 – Jan 2021.	Acceleration of viral RNA and infectious virus clearance, compared to placebo control.	(Fischer et al. 2022)
Molnupiravir	VEEV	RdRp inhibitor	Prospective	A randomised, double-blind, placebo-controlled, multi-centre phase 3 trial in non-hospitalised adults with mild to moderate COVID-19 (n=1,433) at 107 sites globally in 2020 - 2022 (MOVe-OUT study).	Reduction of hospitalisation duration and death compared to the placebo control group.	(Johnson et al. 2022)

Molnupiravir	VEEV	RdRp inhibitor	Prospective	A phase 3, double-blind, randomised, placebo-controlled trial in non-hospitalised, unvaccinated adults with mild-to-moderate, laboratory-confirmed COVID-19 and at least one risk factor for severe COVID-19 (n=1,433) in 2021, globally (MOVe-OUT study).	Reduction of the risk of hospitalisation or death compared to the placebo group.	(Jayk Bernal et al. 2022)
Molnupiravir	VEEV	RdRp inhibitor	Prospective	A randomised, placebo-controlled, double-blind, phase 2 trial in adult (aged ≥18 years) outpatients with PCR-confirmed, mild-to-moderate SARS-CoV-2 infection (n=180) in the United Kingdom in 2020 (AGILE CST-2 study).	Inconclusive evidence of antiviral activity in vaccinated and unvaccinated patients.	(Khoo et al. 2023)
Molnupiravir	VEEV	RdRp inhibitor	Prospective	A multi-centre, open-label, multigroup, platform adaptive randomised controlled trial involving 26,411 participants in the community in the United Kingdom from Dec 2021 – Apr 2022 (PANORAMIC trial study).	No reduction in the frequency of COVID-19-associated hospitalisations or deaths among high-risk vaccinated adults.	(Butler et al. 2023)
Molnupiravir	VEEV	RdRp inhibitor	Prospective	A phase 3, randomised, placebo-controlled trial in non-hospitalised at-risk adults with mild-to-moderate COVID-19 and immunocompromised status (n=55) in 2021, globally (MOVe-OUT study).	Increased clearance of infectious virus compared to the placebo control, efficacious in immunocompromised patients.	(Johnson et al. 2023)

Azvudine/FNC	HIV	RdRp inhibitor	Prospective	A randomised, open-label, controlled trial comparing azvudine and symptomatic treatment (FNC group, n=10) to standard antiviral and symptomatic treatment (control group, n=10) in mild COVID-19 patients in Guangshan, China in 2020.	Shorter duration of the mean times of the first nucleic acid negative conversion.	(Ren et al. 2020)
Azvudine/FNC	HIV	RdRp inhibitor	Retrospective	A single-centre, retrospective cohort study in hospitalised patients (n=245 for each Azvudine and matched control groups) from Dec 2022 to Jan 2023 in Hunan, China.	Substantial clinical benefits in the composite disease progression outcome of hospitalised patients with COVID-19 and pre-existing conditions.	(Sun et al. 2023)
Azvudine/FNC	HIV	RdRp inhibitor	Retrospective	A retrospective, real-world clinical study in hospitalised COVID-19 patients comparing azvudine (n=281) with nirmatrelvir-ritonavir (n=281) from Dec 2022 to Jan 2023 in Hunan, China.	A lower crude incidence rate of composite disease progression outcome compared to the nirmatrelvir-ritonavir group.	(Deng et al. 2023)
Sofosbufir/daclatasvir and ribavirin	HCV	RdRp inhibitor	Prospective	A single-centre randomised controlled trial in adults with moderate COVID-19 (n=48) in Iran in 2020.	No difference between the experimental group compared to the standard care control.	(Abbaspour Kasgari et al. 2020)

Sofosbuvir/daclatasvir	HCV	RdRp inhibitor	Prospective	A single-centre, open-label, parallel trial in hospitalised patients (n=62) with severe COVID-19 in Iran in 2020.	No decrease in mortality compared to the ribavirin control group.	(Eslami et al. 2020)
Sofosbuvir/daclatasvir	HCV	RdRp inhibitor	Prospective	An open-label, multi-centre, randomised, controlled clinical trial in adults with moderate or severe COVID-19 (n=66) in Iran in 2020.	A reduced duration of hospital stay compared to standard care.	(Sadeghi et al. 2020)
Sofosbuvir/ledipasvir	HCV	RdRp inhibitor	Prospective	A single-centre, open-label, randomised clinical trial in patients with mild to moderate COVID-19 (n=82) in Iran in 2020.	No difference in clinical response, duration of hospital and ICU stay, or 14-day mortality compared to the standard care control.	(Khalili et al. 2020)
Sofosbuvir/daclatasvir with hydroxychloroquine	HCV	RdRp inhibitor	Prospective	A randomised, controlled, single-centre clinical trial in outpatients with mild COVID-19 (n=55) in Iran in 2020.	No clinical symptoms alleviation compared to the hydroxychloroquine-only control group.	(Roozbeh et al. 2021)
Sofosbuvir/daclatasvir	HCV	RdRp inhibitor	Prospective	A placebo-controlled, double-blind, randomised clinical trial in adults hospitalised with COVID-19 (n=1,083) at 19 hospitals in Iran in 2020.	No effect on patients' hospital discharge or survival compared to the placebo control.	(Mobarak et al. 2022)

Sofosbuvir/ledipasvir	HCV	RdRp inhibitor	Prospective	A single-blinded parallel-randomised controlled trial of patients (n=250) treated with sofosbuvir/ledipasvir in the intervention group and oseltamivir, hydroxychloroquine, and azithromycin (OCH group) in the control group, conducted in Egypt in 2020.	Reduced time to patients' recovery and time of hospital stay compared to the control group.	(Elgohary et al. 2022)

FNC, 2 -deoxy-2 -β-fluoro-4 -azidocytidine; EBOV, Ebola virus; HIV, human immunodeficiency virus; HCV, hepatitis C virus; RdRp, RNA-dependent RNA polymerase; VEEV, Venezuelan equine encephalitis virus

References (Appendix 1)

Abbaspour Kasgari, Hamideh, Siavash Moradi, Amir Mohammad Shabani, Farhang Babamahmoodi, Ali Reza Davoudi Badabi, Lotfollah Davoudi, Ahmad Alikhani, et al. 2020. "Evaluation of the Efficacy of Sofosbuvir plus Daclatasvir in Combination with Ribavirin for Hospitalized COVID-19 Patients with Moderate Disease Compared with Standard Care: A Single-Centre, Randomized Controlled Trial." *The Journal of Antimicrobial Chemotherapy* 75 (11): 3373–78. https://doi.org/10.1093/jac/dkaa332.

Ader, Florence, Nathan Peiffer-Smadja, Julien Poissy, Maude Bouscambert-Duchamp, Drifa Belhadi, Alpha Diallo, Christelle Delmas, et al. 2021. "An Open-Label Randomized Controlled Trial of the Effect of Lopinavir/Ritonavir, Lopinavir/Ritonavir plus IFN-β-1a and Hydroxychloroquine in Hospitalized Patients with COVID-19." *Clinical Microbiology and Infection: The Official Publication of the European Society of Clinical Microbiology and Infectious Diseases* 27 (12): 1826–37. https://doi.org/10.1016/j.cmi.2021.05.020.

Arabi, Yaseen M., Anthony C. Gordon, Lennie P. G. Derde, Alistair D. Nichol, Srinivas Murthy, Farah Al Beidh, Djillali Annane, et al. 2021. "Lopinavir-Ritonavir and Hydroxychloroquine for Critically Ill Patients with COVID-19: REMAP-CAP Randomized Controlled Trial." *Intensive Care Medicine* 47 (8): 867–86. https://doi.org/10.1007/s00134-021-06448-5.

Beigel, John H., Kay M. Tomashek, Lori E. Dodd, Aneesh K. Mehta, Barry S. Zingman, Andre C. Kalil, Elizabeth Hohmann, et al. 2020. “Remdesivir for the Treatment of COVID-19 - Final Report.” *The New England Journal of Medicine* 383 (19): 1813–26. https://doi.org/10.1056/NEJMoa2007764.

Butler, Christopher C., F. D. Richard Hobbs, Oghenekome A. Gbinigie, Najib M. Rahman, Gail Hayward, Duncan B. Richards, Jienchi Dorward, et al. 2023. “Molnupiravir plus Usual Care versus Usual Care Alone as Early Treatment for Adults with COVID-19 at Increased Risk of Adverse Outcomes (PANORAMIC): An Open-Label, Platform-Adaptive Randomised Controlled Trial.” *Lancet (London, England)* 401 (10373): 281–93. https://doi.org/10.1016/S0140-6736(22)02597-1.

Cao, Bin, Yeming Wang, Danning Wen, Wen Liu, Jingli Wang, Guohui Fan, Lianguo Ruan, et al. 2020. “A Trial of Lopinavir-Ritonavir in Adults Hospitalized with Severe Covid-19.” *The New England Journal of Medicine* 382 (19): 1787–99. https://doi.org/10.1056/NEJMoa2001282.

Chen, Hongyi, Zhicheng Zhang, Li Wang, Zhihua Huang, Fanghua Gong, Xiaodong Li, Yahong Chen, and Jinzi J. Wu. 2020. “First Clinical Study Using HCV Protease Inhibitor Danoprevir to Treat COVID-19 Patients.” *Medicine* 99 (48): e23357. https://doi.org/10.1097/MD.0000000000023357.

Chen, Jun, Lu Xia, Li Liu, Qingnian Xu, Yun Ling, Dan Huang, Wei Huang, et al. 2020. “Antiviral Activity and Safety of Darunavir/Cobicistat for the Treatment of COVID-19.” *Open Forum Infectious Diseases* 7 (7): ofaa241. https://doi.org/10.1093/ofid/ofaa241.

Deng, Guangtong, Daishi Li, Yuming Sun, Liping Jin, Qian Zhou, Chenggen Xiao, Qingrong Wu, et al. 2023. “Real-World Effectiveness of Azvudine versus Nirmatrelvir-Ritonavir in Hospitalized Patients with COVID-19: A Retrospective Cohort Study.” *Journal of Medical Virology* 95 (4): e28756. https://doi.org/10.1002/jmv.28756.

Di Castelnuovo, Augusto, Simona Costanzo, Andrea Antinori, Nausicaa Berselli, Lorenzo Blandi, Marialaura Bonaccio, Raffaele Bruno, et al. 2021. “Lopinavir/Ritonavir and Darunavir/Cobicistat in Hospitalized COVID-19 Patients: Findings From the Multicenter Italian CORIST Study.” *Frontiers in Medicine* 8:639970. https://doi.org/10.3389/fmed.2021.639970.

Doi, Yohei, Masaya Hibino, Ryota Hase, Michiko Yamamoto, Yu Kasamatsu, Masahiro Hirose, Yoshikazu Mutoh, et al. 2020. “A Prospective, Randomized, Open-Label Trial of Early versus Late Favipiravir Therapy in Hospitalized Patients with COVID-19.” *Antimicrobial Agents and Chemotherapy* 64 (12): e01897-20. https://doi.org/10.1128/AAC.01897-20.

Elgohary, Mohamed Abdel-Salam, Eman Medhat Hasan, Amany Ahmad Ibrahim, Mohamed Farouk Ahmed Abdelsalam, Raafat Zaher Abdel-Rahman, Ashraf Ibrahim Zaki, Mohamed Bakr Elaatar, et al. 2022. "Efficacy of Sofosbuvir plus Ledipasvir in Egyptian Patients with COVID-19 Compared to Standard Treatment: A Randomized Controlled Trial." *Journal of Medicine and Life* 15 (3): 350–58. https://doi.org/10.25122/jml-2021-0175.

Elmekaty, Eman Zeyad I., Rim Alibrahim, Rania Hassanin, Sitelbanat Eltaib, Ahmed Elsayed, Fatima Rustom, Mohamed Izham Mohamed Ibrahim, et al. 2022. "Darunavir-Cobicistat versus Lopinavir-Ritonavir in the Treatment of COVID-19 Infection (DOLCI): A Multicenter Observational Study." *PloS One* 17 (5): e0267884. https://doi.org/10.1371/journal.pone.0267884.

Eslami, Gholamali, Sajedeh Mousaviasl, Esmat Radmanesh, Saeed Jelvay, Saeid Bitaraf, Bryony Simmons, Hannah Wentzel, et al. 2020. "The Impact of Sofosbuvir/Daclatasvir or Ribavirin in Patients with Severe COVID-19." *The Journal of Antimicrobial Chemotherapy* 75 (11): 3366–72. https://doi.org/10.1093/jac/dkaa331.

Fischer, William A., Joseph J. Eron, Wayne Holman, Myron S. Cohen, Lei Fang, Laura J. Szewczyk, Timothy P. Sheahan, et al. 2022. "A Phase 2a Clinical Trial of Molnupiravir in Patients with COVID-19 Shows Accelerated SARS-CoV-2 RNA Clearance and Elimination of Infectious Virus." *Science Translational Medicine* 14 (628): eabl7430. https://doi.org/10.1126/scitranslmed.abl7430.

Goldman, Jason D., David C. B. Lye, David S. Hui, Kristen M. Marks, Raffaele Bruno, Rocio Montejano, Christoph D. Spinner, et al. 2020. "Remdesivir for 5 or 10 Days in Patients with Severe Covid-19." *The New England Journal of Medicine* 383 (19): 1827–37. https://doi.org/10.1056/NEJMoa2015301.

Gottlieb, Robert L., Carlos E. Vaca, Roger Paredes, Jorge Mera, Brandon J. Webb, Gilberto Perez, Godson Oguchi, et al. 2022. "Early Remdesivir to Prevent Progression to Severe Covid-19 in Outpatients." *The New England Journal of Medicine* 386 (4): 305–15. https://doi.org/10.1056/NEJMoa2116846.

Hammond, Jennifer, Heidi Leister-Tebbe, Annie Gardner, Paula Abreu, Weihang Bao, Wayne Wisemandle, MaryLynn Baniecki, et al. 2022. "Oral Nirmatrelvir for High-Risk, Nonhospitalized Adults with Covid-19." *New England Journal of Medicine* 386 (15): 1397–1408. https://doi.org/10.1056/NEJMoa2118542.

Holubar, Marisa, Aruna Subramanian, Natasha Purington, Haley Hedlin, Bryan Bunning, Katharine S. Walter, Hector Bonilla, et al. 2022. "Favipiravir for Treatment of Outpatients With Asymptomatic or Uncomplicated Coronavirus Disease 2019: A Double-Blind, Randomized, Placebo-Controlled, Phase 2 Trial." *Clinical Infectious Diseases: An Official Publication of the Infectious Diseases Society of America* 75 (11): 1883–92. https://doi.org/10.1093/cid/ciac312.

Horby, Peter W., Marion Mafham, Jennifer L. Bell, Louise Linsell, Natalie Staplin, Jonathan Emberson, Adrian Palfreeman, et al. 2020. “Lopinavir–Ritonavir in Patients Admitted to Hospital with COVID-19 (RECOVERY): A Randomised, Controlled, Open-Label, Platform Trial.” *The Lancet* 396 (10259): 1345–52. https://doi.org/10.1016/S0140-6736(20)32013-4.

Hung, Ivan Fan-Ngai, Kwok-Cheung Lung, Eugene Yuk-Keung Tso, Raymond Liu, Tom Wai-Hin Chung, Man-Yee Chu, Yuk-Yung Ng, et al. 2020. “Triple Combination of Interferon Beta-1b, Lopinavir-Ritonavir, and Ribavirin in the Treatment of Patients Admitted to Hospital with COVID-19: An Open-Label, Randomised, Phase 2 Trial.” *Lancet (London, England)* 395 (10238): 1695–1704. https://doi.org/10.1016/S0140-6736(20)31042-4.

Ivashchenko, Andrey A., Kirill A. Dmitriev, Natalia V. Vostokova, Valeria N. Azarova, Andrew A. Blinow, Alina N. Egorova, Ivan G. Gordeev, et al. 2021. “AVIFAVIR for Treatment of Patients With Moderate Coronavirus Disease 2019 (COVID-19): Interim Results of a Phase II/III Multicenter Randomized Clinical Trial.” *Clinical Infectious Diseases: An Official Publication of the Infectious Diseases Society of America* 73 (3): 531–34. https://doi.org/10.1093/cid/ciaa1176.

Jayk Bernal, Angélica, Monica M. Gomes da Silva, Dany B. Musungaie, Evgeniy Kovalchuk, Antonio Gonzalez, Virginia Delos Reyes, Alejandro Martín-Quirós, et al. 2022. “Molnupiravir for Oral Treatment of Covid-19 in Nonhospitalized Patients.” *New England Journal of Medicine* 386 (6): 509–20. https://doi.org/10.1056/NEJMoa2116044.

Johnson, Matthew G., Amy Puenpatom, Pablo Andrés Moncada, Lesley Burgess, Elizabeth R. Duke, Norio Ohmagari, Timo Wolf, et al. 2022. “Effect of Molnupiravir on Biomarkers, Respiratory Interventions, and Medical Services in COVID-19 : A Randomized, Placebo-Controlled Trial.” *Annals of Internal Medicine* 175 (8): 1126–34. https://doi.org/10.7326/M22-0729.

Johnson, Matthew G., Julie M. Strizki, Michelle L. Brown, Hong Wan, Hala H. Shamsuddin, Moti Ramgopal, Diana F. Florescu, et al. 2023. “Molnupiravir for the Treatment of COVID-19 in Immunocompromised Participants: Efficacy, Safety, and Virology Results from the Phase 3 Randomized, Placebo-Controlled MOVe-OUT Trial.” *Infection*, January, 1–12. https://doi.org/10.1007/s15010-022-01959-9.

Khalili, Hossein, Anahid Nourian, Zahra Ahmadinejad, Hamid Emadi Kouchak, Sirous Jafari, Sayed Ali Dehghan Manshadi, Mehrnaz Rasolinejad, and Abbas Kebriaeezadeh. 2020. “Efficacy and Safety of Sofosbuvir/ Ledipasvir in Treatment of Patients with COVID-19; A Randomized Clinical Trial.” *Acta Bio-Medica: Atenei Parmensis* 91 (4): e2020102. https://doi.org/10.23750/abm.v91i4.10877.

Khamis, Faryal, Hanan Al Naabi, Adil Al Lawati, Zaiyana Ambusaidi, Mariam Al Sharji, Umkulthum Al Barwani, Nenad Pandak, et al. 2021. “Randomized Controlled Open Label Trial on the Use of Favipiravir Combined with Inhaled Interferon Beta-1b in Hospitalized Patients with Moderate to Severe

COVID-19 Pneumonia." *International Journal of Infectious Diseases: IJID: Official Publication of the International Society for Infectious Diseases* 102 (January):538–43. https://doi.org/10.1016/j.ijid.2020.11.008.

Khoo, Saye H., Richard Fitzgerald, Thomas Fletcher, Sean Ewings, Thomas Jaki, Rebecca Lyon, Nichola Downs, et al. 2021. "Optimal Dose and Safety of Molnupiravir in Patients with Early SARS-CoV-2: A Phase I, Open-Label, Dose-Escalating, Randomized Controlled Study." *The Journal of Antimicrobial Chemotherapy* 76 (12): 3286–95. https://doi.org/10.1093/jac/dkab318.

Khoo, Saye H., Richard FitzGerald, Geoffrey Saunders, Calley Middleton, Shazaad Ahmad, Christopher J. Edwards, Dennis Hadjiyiannakis, et al. 2023. "Molnupiravir versus Placebo in Unvaccinated and Vaccinated Patients with Early SARS-CoV-2 Infection in the UK (AGILE CST-2): A Randomised, Placebo-Controlled, Double-Blind, Phase 2 Trial." *The Lancet. Infectious Diseases* 23 (2): 183–95. https://doi.org/10.1016/S1473-3099(22)00644-2.

Li, Yueping, Zhiwei Xie, Weiyin Lin, Weiping Cai, Chunyan Wen, Yujuan Guan, Xiaoneng Mo, et al. 2020. "Efficacy and Safety of Lopinavir/Ritonavir or Arbidol in Adult Patients with Mild/Moderate COVID-19: An Exploratory Randomized Controlled Trial." *Med (New York, N.Y.)* 1 (1): 105-113.e4. https://doi.org/10.1016/j.medj.2020.04.001.

Lim, Sarah, Christopher J. Tignanelli, Nicolas Hoertel, David R. Boulware, and Michael G. Usher. 2022. "Prevalence of Medical Contraindications to Nirmatrelvir/Ritonavir in a Cohort of Hospitalized and Nonhospitalized Patients With COVID-19." *Open Forum Infectious Diseases* 9 (8): ofac389. https://doi.org/10.1093/ofid/ofac389.

Liu, Jiao, Xiaojun Pan, Sheng Zhang, Ming Li, Ke Ma, Cunyi Fan, Ying Lv, et al. 2023. "Efficacy and Safety of Paxlovid in Severe Adult Patients with SARS-Cov-2 Infection: A Multicenter Randomized Controlled Study." *The Lancet Regional Health. Western Pacific*, February, 100694. https://doi.org/10.1016/j.lanwpc.2023.100694.

Lou, Yan, Lin Liu, Hangping Yao, Xingjiang Hu, Junwei Su, Kaijin Xu, Rui Luo, et al. 2021. "Clinical Outcomes and Plasma Concentrations of Baloxavir Marboxil and Favipiravir in COVID-19 Patients: An Exploratory Randomized, Controlled Trial." *European Journal of Pharmaceutical Sciences: Official Journal of the European Federation for Pharmaceutical Sciences* 157 (February):105631. https://doi.org/10.1016/j.ejps.2020.105631.

Marrone, Aldo, Riccardo Nevola, Ausilia Sellitto, Domenico Cozzolino, Ciro Romano, Giovanna Cuomo, Concetta Aprea, et al. 2022. "Remdesivir Plus Dexamethasone Versus Dexamethasone Alone for the Treatment of Coronavirus Disease 2019 (COVID-19) Patients Requiring Supplemental O2

Therapy: A Prospective Controlled Nonrandomized Study." *Clinical Infectious Diseases: An Official Publication of the Infectious Diseases Society of America* 75 (1): e403–9. https://doi.org/10.1093/cid/ciac014.

McMahon, James H., Jillian S. Y. Lau, Anna Coldham, Janine Roney, Michelle Hagenauer, Sally Price, Mellissa Bryant, et al. 2022. "Favipiravir in Early Symptomatic COVID-19, a Randomised Placebo-Controlled Trial." *EClinicalMedicine* 54 (December):101703. https://doi.org/10.1016/j.eclinm.2022.101703.

Mobarak, Sara, Mehdi Salasi, Ahmad Hormati, Javad Khodadadi, Masood Ziaee, Farshid Abedi, Azadeh Ebrahimzadeh, et al. 2022. "Evaluation of the Effect of Sofosbuvir and Daclatasvir in Hospitalized COVID-19 Patients: A Randomized Double-Blind Clinical Trial (DISCOVER)." *The Journal of Antimicrobial Chemotherapy* 77 (3): 758–66. https://doi.org/10.1093/jac/dkab433.

Mukae, Hiroshi, Hiroshi Yotsuyanagi, Norio Ohmagari, Yohei Doi, Takumi Imamura, Takuhiro Sonoyama, Takahiro Fukuhara, et al. 2022. "A Randomized Phase 2/3 Study of Ensitrelvir, a Novel Oral SARS-CoV-2 3C-Like Protease Inhibitor, in Japanese Patients with Mild-to-Moderate COVID-19 or Asymptomatic SARS-CoV-2 Infection: Results of the Phase 2a Part." *Antimicrobial Agents and Chemotherapy* 66 (10): e0069722. https://doi.org/10.1128/aac.00697-22.

Mukae, Hiroshi, Hiroshi Yotsuyanagi, Norio Ohmagari, Yohei Doi, Hiroki Sakaguchi, Takuhiro Sonoyama, Genki Ichihashi, et al. 2023. "Efficacy and Safety of Ensitrelvir in Patients With Mild-to-Moderate Coronavirus Disease 2019: The Phase 2b Part of a Randomized, Placebo-Controlled, Phase 2/3 Study." *Clinical Infectious Diseases: An Official Publication of the Infectious Diseases Society of America* 76 (8): 1403–11. https://doi.org/10.1093/cid/ciac933.

Nimitvilai, Sireethorn, Yupin Suputtamongkol, Ussanee Poolvivatchaikarn, Dechatorn Rassamekulthana, Nuttawut Rongkiettechakorn, Anek Mungaomklang, Susan Assanasaen, Ekkarat Wongsawat, Chompunuch Boonarkart, and Waritta Sawaengdee. 2022. "A Randomized Controlled Trial of Combined Ivermectin and Zinc Sulfate versus Combined Hydroxychloroquine, Darunavir/Ritonavir, and Zinc Sulfate among Adult Patients with Asymptomatic or Mild Coronavirus-19 Infection." *Journal of Global Infectious Diseases* 14 (2): 69–74. https://doi.org/10.4103/jgid.jgid_281_21.

Ren, Zhigang, Hong Luo, Zujiang Yu, Jingchao Song, Lan Liang, Ling Wang, Haiyu Wang, et al. 2020. "A Randomized, Open-Label, Controlled Clinical Trial of Azvudine Tablets in the Treatment of Mild and Common COVID-19, A Pilot Study." *Advanced Science (Weinheim, Baden-Wurttemberg, Germany)*, July, 2001435. https://doi.org/10.1002/advs.202001435.

Roozbeh, Fatemeh, Majid Saeedi, Reza Alizadeh-Navaei, Akbar Hedayatizadeh-Omran, Shahin Merat, Hannah Wentzel, Jacob Levi, Andrew Hill, and Amir Shamshirian. 2021. “Sofosbuvir and Daclatasvir for the Treatment of COVID-19 Outpatients: A Double-Blind, Randomized Controlled Trial.” *Journal of Antimicrobial Chemotherapy* 76 (3): 753–57. https://doi.org/10.1093/jac/dkaa501.

Sadeghi, Anahita, Ali Ali Asgari, Alireza Norouzi, Zahedin Kheiri, Amir Anushirvani, Mahnaz Montazeri, Hadiseh Hosamirudsai, et al. 2020. “Sofosbuvir and Daclatasvir Compared with Standard of Care in the Treatment of Patients Admitted to Hospital with Moderate or Severe Coronavirus Infection (COVID-19): A Randomized Controlled Trial.” *The Journal of Antimicrobial Chemotherapy* 75 (11): 3379–85. https://doi.org/10.1093/jac/dkaa334.

Schilling, William H. K., Podjanee Jittamala, James A. Watson, Simon Boyd, Viravarn Luvira, Tanaya Siripoon, Thundon Ngamprasertchai, et al. 2023. “Antiviral Efficacy of Molnupiravir versus Ritonavir-Boosted Nirmatrelvir in Patients with Early Symptomatic COVID-19 (PLATCOV): An Open-Label, Phase 2, Randomised, Controlled, Adaptive Trial.” *The Lancet Infectious Diseases* 0 (0). https://doi.org/10.1016/S1473-3099(23)00493-0.

Shah, Pallav L., Christopher M. Orton, Beatriz Grinsztejn, Gavin C. Donaldson, Brenda Crabtree Ramírez, James Tonkin, Breno R. Santos, et al. 2023. “Favipiravir in Patients Hospitalised with COVID-19 (PIONEER Trial): A Multicentre, Open-Label, Phase 3, Randomised Controlled Trial of Early Intervention versus Standard Care.” *The Lancet. Respiratory Medicine* 11 (5): 415–24. https://doi.org/10.1016/S2213-2600(22)00412-X.

Shimizu, Ryosuke, Takuhiro Sonoyama, Takahiro Fukuhara, Aya Kuwata, Takanobu Matsuzaki, Yumiko Matsuo, and Ryuji Kubota. 2023. “Evaluation of the Drug-Drug Interaction Potential of Ensitrelvir Fumaric Acid with Cytochrome P450 3A Substrates in Healthy Japanese Adults.” *Clinical Drug Investigation* 43 (5): 335–46. https://doi.org/10.1007/s40261-023-01265-8.

Singh, Ravi Shankar P., Sima S. Toussi, Frances Hackman, Phylinda L. Chan, Rohit Rao, Richard Allen, Lien Van Eyck, et al. 2022. “Innovative Randomized Phase I Study and Dosing Regimen Selection to Accelerate and Inform Pivotal COVID-19 Trial of Nirmatrelvir.” *Clinical Pharmacology and Therapeutics* 112 (1): 101–11. https://doi.org/10.1002/cpt.2603.

Spinner, Christoph D., Robert L. Gottlieb, Gerard J. Criner, José Ramón Arribas López, Anna Maria Cattelan, Alex Soriano Viladomiu, Onyema Ogbuagu, et al. 2020. “Effect of Remdesivir vs Standard Care on Clinical Status at 11 Days in Patients With Moderate COVID-19: A Randomized Clinical Trial.” *JAMA* 324 (11): 1048–57. https://doi.org/10.1001/jama.2020.16349.

Sun, Yuming, Liping Jin, Yating Dian, Minxue Shen, Furong Zeng, Xiang Chen, and Guangtong Deng. 2023. “Oral Azvudine for Hospitalised Patients with COVID-19 and Pre-Existing Conditions: A Retrospective Cohort Study.” *eClinicalMedicine* 59 (May). https://doi.org/10.1016/j.eclinm.2023.101981.

Udwadia, Zarir F., Pawan Singh, Hanmant Barkate, Saiprasad Patil, Shabbir Rangwala, Amol Pendse, Jatin Kadam, Wen Wu, Cynthia F. Caracta, and Monika Tandon. 2021. “Efficacy and Safety of Favipiravir, an Oral RNA-Dependent RNA Polymerase Inhibitor, in Mild-to-Moderate COVID-19: A Randomized, Comparative, Open-Label, Multicenter, Phase 3 Clinical Trial.” *International Journal of Infectious Diseases: IJID: Official Publication of the International Society for Infectious Diseases* 103 (February):62–71. https://doi.org/10.1016/j.ijid.2020.11.142.

Vaezi, Atefeh, Mehrzad Salmasi, Forogh Soltaninejad, Mehrdad Salahi, Shaghayegh Haghjooy Javanmard, and Babak Amra. 2023. “Favipiravir in the Treatment of Outpatient COVID-19: A Multicenter, Randomized, Triple-Blind, Placebo-Controlled Clinical Trial.” *Advances in Respiratory Medicine* 91 (1): 18–25. https://doi.org/10.3390/arm91010004.

Wang, Yeming, Dingyu Zhang, Guanhua Du, Ronghui Du, Jianping Zhao, Yang Jin, Shouzhi Fu, et al. 2020. “Remdesivir in Adults with Severe COVID-19: A Randomised, Double-Blind, Placebo-Controlled, Multicentre Trial.” *Lancet (London, England)* 395 (10236): 1569–78. https://doi.org/10.1016/S0140-6736(20)31022-9.

WHO Solidarity Trial Consortium, Hongchao Pan, Richard Peto, Ana-Maria Henao-Restrepo, Marie-Pierre Preziosi, Vasee Sathiyamoorthy, Quarraisha Abdool Karim, et al. 2021. “Repurposed Antiviral Drugs for Covid-19 - Interim WHO Solidarity Trial Results.” *The New England Journal of Medicine* 384 (6): 497–511. https://doi.org/10.1056/NEJMoa2023184.

Yotsuyanagi, Hiroshi, Norio Ohmagari, Yohei Doi, Takumi Imamura, Takuhiro Sonoyama, Genki Ichihashi, Takao Sanaki, Yuko Tsuge, Takeki Uehara, and Hiroshi Mukae. 2023. “A Phase 2/3 Study of S-217622 in Participants with SARS-CoV-2 Infection (Phase 3 Part).” *Medicine* 102 (8): e33024. https://doi.org/10.1097/MD.0000000000033024.

Zhang, Zhicheng, Shumei Wang, Xianglin Tu, Xuping Peng, Yanxia Huang, Li Wang, Weihua Ju, et al. 2020. “A Comparative Study on the Time to Achieve Negative Nucleic Acid Testing and Hospital Stays between Danoprevir and Lopinavir/Ritonavir in the Treatment of Patients with COVID-19.” *Journal of Medical Virology* 92 (11): 2631–36. https://doi.org/10.1002/jmv.26141.

Zou, Rongrong, Ling Peng, Dan Shu, Lei Zhao, Jianfeng Lan, Guoyu Tan, Jinghan Peng, et al. 2022. “Antiviral Efficacy and Safety of Molnupiravir Against Omicron Variant Infection: A Randomized Controlled Clinical Trial.” *Frontiers in Pharmacology* 13:939573. https://doi.org/10.3389/fphar.2022.939573.

Appendix 2. A summary of ionisation methods used in mass spectrometry. Extracted and summarised from McCullagh JSO and Oldham NJ. 2019. Mass Spectrometry. Oxford University Press.

Ionisation Method	Principle of ion formation	Application	Optimal mass range	Field of use	Instrument modification/interface
1. Ionisation of vaporised samples					
Electron ionisation (EI)	Interaction between a high-energy electron (70 eV) and a neutral analyte	Analysis of organic compounds in the gas phase and volatile, thermally-stable compounds	< 1000 Da	Metabolomic and environmental residue analysis	Gas chromatography (GC)-EI-Orbitrap
Chemical ionisation (CI)	Electron beam is used to ionise reagent gas molecules (methane, ammonia), forming reagent-gas radical cations. There is also a possibility for negative ion formation	Analysis of small organic compounds, including amines, alcohols, nitriles, nitro-containing compounds, and acidic compounds (via negative ion formation)	< 1000 Da	Organic compound analysis	

Inductively coupled plasma ionisation (ICP)	The process of electron removal from analyte atoms, where a sample in gaseous or aerosol form is introduced into an argon plasma	Analysis of metals		Geochemistry, geochronology, archaeology	With GC-MS and liquid chromatography (LC)-MS
Field ionisation (FI)	Localised electric field to form radical cations and anions, and sometimes secondary, protonated, or deprotonated molecules	Volatile, thermally-stable compounds			Superseded by MALDI
2. Desorption ionisation					
Matrix-assisted laser desorption ionisation (MALDI)	A pulsed transfer of laser energy (CO_2 (IR) or nitrogen (UV)) to a co-crystallised mixture of analyte and a matrix (small organic aromatic acid which is strongly absorbing at the wavelength of the laser). This leads to a rapid local heating, expansion, and vaporisation of the mixture, forming a small local gas plume.	Higher molecular weight compounds	Up to 500 kDa	Proteomics, metabolomics (protein, peptide, lipid, nucleotide, oligonucleotide, oligosaccharide	

Secondary ion mass spectrometry (SIMS)	Secondary ions are produced from a high-energy primary ion beam (caesium ions) which bombard the surface of a sample material	Surface analysis on solids, semiconductors, glass, stainless steel, meteorites, fuel cells, museum artefacts, alloys, and biomaterials	300 – 13,000 Da	Material science and surface chemistry	
Fast atom bombardment (FAB)	Secondary ions bombardment from a neutral atom beam (xenon or neon)	Analysis of liquid matrix in a low-volatility solvent in which the sample is dissolved and ionisation occurs at the surface of the matrix	Similar to SIMS	Protein, biological molecule	Superseded by electrospray ionisation and MALDI
Field desorption	Similar to FI, however, the sample is coated onto a needle electrode and allowed to dry				

3. Atmospheric pressure ionisation					
Electrospray ionisation (ESI)	Rapid evaporation of solvent droplets containing dissolved analyte molecules, in a strong electric field (Taylor cone formation)	Wide range of organic and biological compounds	Wide range	Environmental analysis, toxicology, drugs of abuse and doping control, pesticide analysis, biologicals (metabolites, protein, peptides, oligonucleotides)	Interfaced with LC
Atmospheric pressure chemical ionisation (APCI)	A heated nebuliser converts a liquid eluent stream into gas-phase molecules by rapid heating. A neutral, rather than charged, spray is produced from the probe				Interfaced with high-performance or ultra-high-performance liquid chromatography (HPLC or UPLC)

Atmospheric pressure photoionisation (APPI)	The use of a high-energy photon irradiation (from UV light) to ionise molecules in the gas phase.	Pharmaceutical, clinical, and environmental monitoring applications	Steroids, sterols, other hydrophobic compounds
4. Hybrid ambient ionisation			
Desorption electrospray ionisation (DESI), direct analysis in real-time (DART), atmospheric pressure solids analysis probe (ASAP), etc	Direct analysis of the sample with little or no sample preparation, ionisation occurring at atmospheric pressure, desorption of ions from the surface of samples, hybrid or multiple mechanisms of ion formation		
	DESI: The process resembles ESI, but rather than the analyte being dissolved in the solvent spray, the charged droplets of solvent are directed at the surface of the sample		

	DART: A dry stream of electronically excited neutral gas atoms (He) which are heated and directed at the sample	DART: Forensic, environmental, food analysis applications	Non-polar, neutral molecules, explosives, cosmetics, soils, food
	ASAP: Rapid heating of solids or liquids transferred or evaporated onto an inert surface, ionisation by a coronal discharge in a similar way to APCI	ASAP: Forensic, environmental, biological, and pharmaceutical applications	

"Credo ut intelligam"

I believe so that I may understand

(St. Anselm of Canterbury, 1033-1109)